The molecular mechanism of tumour budding and its relationship with tumour microenvironment in colorectal cancer

Phimmada Hatthakarnkul

BSc, MSc

Submitted in fulfilment of the requirements for the degree of PhD

School of Cancer Science

College of Medical, Veterinary and Life Sciences

May 2024

The work presented in this thesis was performed by the author except where acknowledged. This thesis has not been submitted for a degree or diploma at this or any other institution.

Phimmada Hatthakarnkul
May 2024

Acknowledgement

I would like to express my deepest appreciation to my PhD supervisor Joanne Edwards. I couldn't ask for the best supervisor. Thanks for taking me after that afternoon meeting in your office in 2020. Even though my PhD started during the end of covid-19, Joanne made sure I had all the support I need. She gave me a lot of opportunities that I wouldn't think I will be given anywhere else. I always doubt myself, but Joanne always makes me feel like I'm in the right path and made a right choice to pursue my career in cancer research. Words cannot express my gratitude to Jean Quinn my second supervisor, thank you very much for all your generous support great and helped me in every single one of my reports. My English writing is better because of Jean, you're an icon. Thank you for all the morning coffee and thank you for teaching me how to do IHC, without Jean I wouldn't know how to work with tissue samples. Thanks for all your great support and advice, I'm very grateful and can't imagine my PhD would be like without them.

Thanks should also go to Aj.Chanitra, thank you very much for all your supervised and support in Thailand. Without your advertisement on Facebook 4 years ago, I wouldn't be here and become the person I am right now. I am also thankful for Hester, thanks for teaching me how to count tumour budding in CRC tissue, without you I wouldn't be able to do this project. Your patience with my absolute zero experience in tissue pathology made me feel welcome and encouraged me to be more confident and continue working on this project.

This endeavor would not have been possible without having Kathryn sit next to me. Kathryn you're the best of the best, thank you for noticing me and making me feel better when I'm down, without you, I can't imagine what I would do. Thank you for taking me for a hike, teaching me to balance myself on the paddle board, and all the other things we did together. It was so much fun and made my life here easier than I thought it would be. I would like to extend my sincere thanks to Assya and Holly for that 8pm late night pizza running GeoMx. Despite

the problem we had, you guys made me feel like I'm not in this alone. Thank Holly, for all the GeoMx support. I wouldn't be able to learn this much and finish it without you. Thanks, Assya, my PGR buddy, you're the babe. Thank you for all the de-stress talks session, I owe you a bottle of red wine for the rest of your life.

I would like to thank M19 lab members for all the very interesting topics during lunches and all the social drinks we had together. Special thanks to Gerard, thanks for reading my thesis and giving me an insightful comment. I will miss your full page red highlighted. I am also grateful for Aula who supervised me for my multiplex study, thanks for all those first 6 months in my PhD at QE. I learned a lot from you. Thank should also go to people from the GTRF who took me in when I first started my PhD and scanned all my multiplex tissue slides. Thanks Sara and Molly for all the funny stories and all your lovely supportive texts. Thank Amna for teaching me how to do western blot and your mental support, I am really appreciated.

I would like to thank all my friends from Thailand who made my life easier when I'm back in Thailand to continue my PhD. Special thanks to Pin for every last-minute dinner called after work. Thanks SCMU cheerleader group for the great trip, the stay up all night talks and the tarot reading. Thanks Swagger group for coming with me on one-day Pattaya trip and literally everywhere I wanted to go. Thank you all for your companion every weekend. It was one of the stressful years of my life, but it's way easier than I thought with you all and I'm grateful for that. Thanks people at Siriraj for making me feel welcome especially Aon for all my annoying talks and still sit next to me for 1 year.

Lastly, I would like to express my gratitude to my parents who always support me throughout my career. Thank you very much for supporting me to do this PhD. I'm grateful for Dad who always looks after me and for all the life skills you gave me. I'm also grateful for Mom, thanks for all your time listening to my problem and all your suggestions. Thanks for believing in me and provided me throughout these years. As promised, I will pay you back. I

also would like to take this opportunity to thank myself for deciding to do a PhD. For all these years, through good and bad times, I've learned a lot and that made me become the person I am right now. I wouldn't change anything if I needed to, best decision ever.

Summary

Colorectal cancer (CRC) is the third most diagnosed cancer and the second lethal disease worldwide (1). CRC development has recently been well-documented, and the screening program has been shown to improve patient outcomes and survival due to the early detection of the disease (2, 3). However, some patients still experienced disease metastasis with a 5 year survival of only 12% (4). Recent studies have focused on identifying prognostic biomarkers that can predict the adverse outcomes in CRC patients (5).

One promising factor that has recently been reported is tumour budding (TB). TB, the single or up to four tumour cells found at the invasive tumour area, is now a well-known prognostic independent biomarker in many solid cancers including CRC (6). Patients with high TB phenotype experienced a poor outcome with an incidence of disease recurrence and metastasis (7). In 2016, the international tumour budding consensus conference (ITBCC) was held and agreed to set up the criteria for TB assessment and suggested to include TB status in a routine clinical report (8). Since then, multiple studies have investigated the prognostic role of TB not only in CRC but also in other solid cancers such as pancreatic (9), breast (10, 11), head and neck (12) and lung (13) cancer.

Although TB has a strong prognostic value, few studies investigated its underlying mechanism and how it may relate to adverse features and disease metastasis in CRC. It has been hypothesised that TB could undergo epithelial-mesenchymal transition (EMT), thereby, allowing cells to escape from the main tumour and promote metastasis (14, 15). However, some studies argued that TB may only undergo partial EMT and there is another tumour-related signalling involved in its formation and induction of the metastasis (16, 17). Moreover, some studies have reported an inverse correlation between TB and cytotoxic T cells which could suggested an immunosuppressive role of TB leading to disease metastasis in CRC (18-20).

Until now, there has been little understanding of the underlying mechanism of TB and its relationship with the tumour microenvironment in CRC (21). This thesis aims to unravel the molecular mechanism of TB to identify the potential tumour signalling that drives TB formation and how TB is associated with the immune profile at the invasive edge of the tumour. To investigate this, TB status in CRC patients has been identified according to the TB assessment criteria from ITBCC. After that, bulk transcriptomic RNA (n=787) was used to identify tumour-related signalling expressed in tumours with high TB phenotype compared to low TB group. In addition, regional bulk spatial transcriptomic (GeoMx) (n=12) was performed to identify gene expression within the region of interested (ROI), the classification of tumour and stromal areas using specific protein mask (PanCK+/-) was done. This allows the identification of the potential genes related to both budding tumour cells and the surrounded tumour microenvironment between tumours with low and high TB profile as well as the different area of interest (AOI); tumour core, invasive edge, distant stromal area, within the same tumours. The results from GeoMx were later validated in a TMA of the full CRC cohort (n=787), using immunohistochemistry, to verify the translation from RNA to protein. Of these, cyclinD1 expression within TB was identified as a promising prognostic value in CRC patients. Additionally, multiplex immunofluorescence (mIF) using immune panels (lymphocytes and myeloid cells) were also performed to investigate the immune profile within the invasive budding area. Results showed a high density of regulatory and low cytotoxic T cells within the invasive compared to further stromal area of tumours with high TB. Nearest neighbour analysis also showed that TB tend to have a closer distant to regulatory cells as well as pan-macrophages. This finding suggested that TB may have a possible interaction with the surrounding immune cells leading to an alteration of the microenvironment to help it thrive and invade other parts of the body.

To investigate if TB formation can be observed within an *in vitro* setting, CRC spheroids were cultured. The induction of TNF-α and TGF-β were shown to stimulate more TB formation in CRC spheroids and that cyclinD1 expression within the TB was higher in treated spheroids compared to control groups. Moreover, mouse AKPT organoids showed an increased in roundness, which indicates disruption in the formation of TB, in treated compared to control groups. These results suggested that cyclinD1 expressed within TB could have a potential role as a prognostic marker and may be used as a biomarker for TB formation.

In summary, data from this thesis have demonstrated potential biomarkers of TB and the relationship with tumour microenvironment in CRC. This will help understand the underlying mechanism of TB, and how they might interact with the surrounding microenvironment and could also pave the way for a future target therapeutic approach in CRC.

Graphical abstract

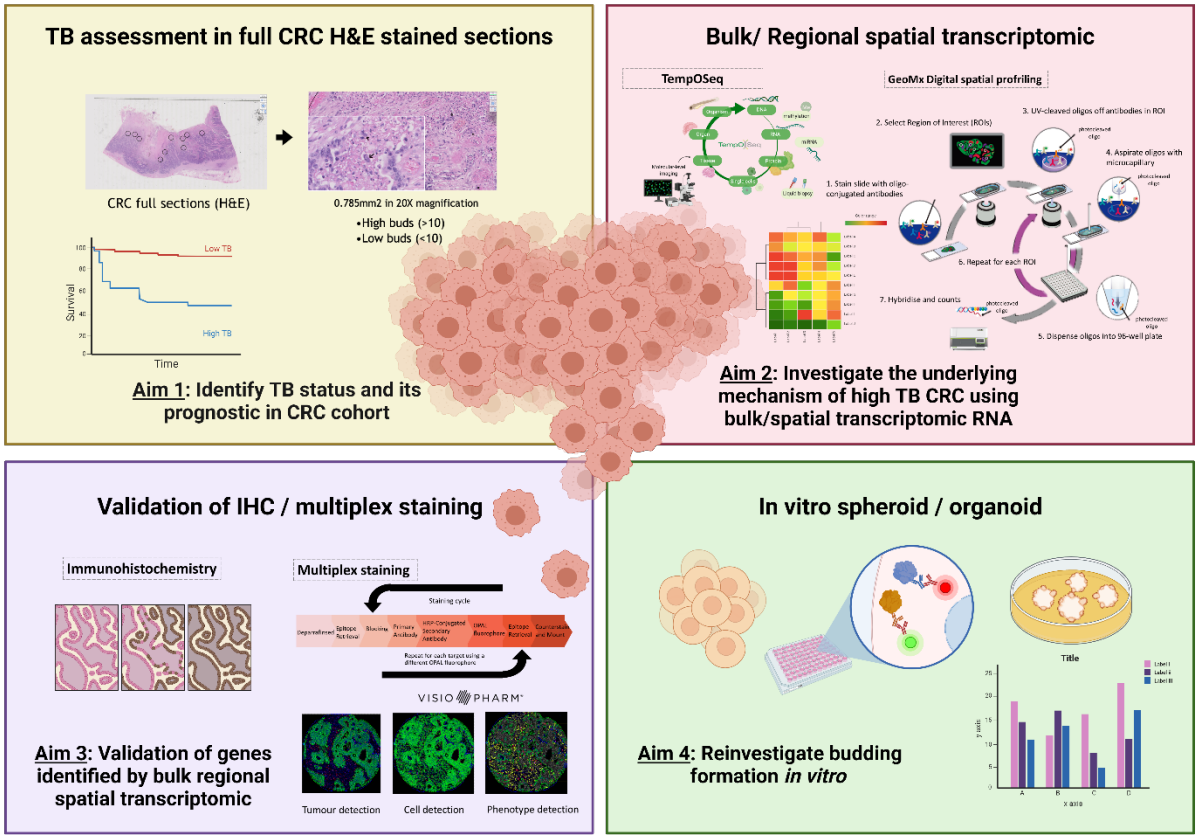

Publication and presentations

Publication relating to this thesis

P. Hatthakarnkul, J. A. Quinn, A. A. M. Matly, A. Ammar, H. C. van Wyk, D. C. McMillan, et al. Systematic review of tumour budding and association with common mutations in patients with colorectal cancer. Crit Rev Oncol Hematol 2021 Vol. 167 Pages 103490

P. Hatthakarnkul, J. A. Quinn, A. Ammar, G. Lynch, H. Van Wyk, D. C. McMillan, et al. Molecular mechanisms of tumour budding and its association with microenvironment in colorectal cancer. Clin Sci (Lond) 2022 Vol. 136 Issue 8 Pages 521-535

P. Hatthakarnkul, A. Ammar, K. A. F. Pennel, L. Officer-Jones, S. Cusumano, J. A. Quinn, et al. Protein expression of S100A2 reveals it association with patient prognosis and immune infiltration profile in colorectal cancer. J Cancer 2023 Vol. 14 Issue 10 Pages 1837-1847

K. A. F. Pennel, **P. Hatthakarnkul**, C. S. Wood, G. Y. Lian, S. S. F. Al-Badran, J. A. Quinn, et al. JAK/STAT3 represents a therapeutic target for colorectal cancer patients with stromal-rich tumors. J Exp Clin Cancer Res 2024 Vol. 43 Issue 1 Pages 64

P. Hatthakarnkul, K. Pennel, P. Alexander, H. van Wyk, A. Roseweir, J. Inthagard, et al. Histopathological tumour microenvironment score independently predicts outcome in primary operable colorectal cancer. J Pathol Clin Res 2024 Vol. 10 Issue 3 Pages e12374

In preparation - **P. Hatthakarnkul,** H. Leslie, A. Legrini, K. A. F. Pennel, L. A. Ammar, et al. Understanding the underly mechanism of tumour budding and its correlation with tumour microenvironment in colorectal cancer.

Oral presentations

Understanding the molecular mechanism of tumour budding and its relationship with tumour microenvironment in colorectal cancer. CRUK Scotland Centre Colorectal Theme Day, The Institute of Genetics & Cancer, University of Edinburgh, Scotland, UK.

The mechanism of tumour budding and its correlation with tumour microenvironment in colorectal cancer. Siriraj International Conference in Medicine and Public Health (SIMPH) 2023, Bangkok, Thailand.

Poster presentations

The mechanism of tumour budding and its correlation with tumour microenvironment in colorectal cancer. American Cancer Association (AACR) annual meeting 2023. Florida, US.

The mechanism of tumour budding and its correlation with tumour microenvironment in colorectal cancer. The 17th International Symposium of the protein society of Thailand (PST2022), Chiang Mai University, Thailand.

Understanding the mechanism of tumour budding and its relationship with tumour microenvironment in colorectal cancer. The British Association for Cancer Research

(BACR) 60th anniversary meeting poster presentation, University of Nottingham, Nothingham, UK.

Table of contents

List of figures

List of tables

Abbreviations

APC Adenomatous polyposis coli

α-SMA Alpha smooth muscle actin

BRAF v-raf murine sarcoma viral oncogene homolog B1

BME Basement membrane extract

CI Confidence interval

CIMP CpG Island methylation

CIN Chromosomal instability

CMS Consensus molecular subtypes

CRC Colorectal cancer

CRIS Cancer cell intrinsic subtype

CSS Cancer specific survival

CXCL9 Chemokine (C-X-C motif) ligand 9

CXCL10 Chemokine (C-X-C motif) ligand 10

DAB 3,3'-diaminobenzidine

DEG Differentially expressed genes

DNA Deoxyribonucleic acid

DSP Digital Spatial Profiler

ER Epitope retrieval

FAP Familial adenomatous polyposis

FBS Fetal bovine serum

FC Fold change

FFPE Formalin fixed paraffin embedded

FDR False Discovery Rate

FOV Field of view

GMS Glasgow Microenvironment Score

GPOL Glasgow precision oncology laboratory

GPS Glasgow prognostic score

GTRF Glasgow tissue research facility

GRI Glasgow royal infirmary

GSEA Gene set enrichment analysis

HCl Hydrogen chloride

H&E Haematoxylin and Eosin

HIER Heat Induced Epitope Retrieval

HNPCC Hereditary nonpolyposis cancer

H2O2 Hydrogen peroxide

HK House keeping

HR Hazard ratio

HRP Horse radish peroxidase

IF Immunofluorescence

IHC Immunohistochemistry

IL6 Interleukin 6

IL6R Interleukin 6 receptor

ITBCC International Tumor Budding Consensus Conference

KM Klintrup-Mäkinen

KRAS Ki-ras2 Kirsten rat sarcoma viral oncogene homolog

LNM Linear mix model

mCRC metastatic colorectal cancer

mGPS modified Glasgow prognostic score

mIF Multiplex immunofluorescence

dMMR Deficient mismatch repair

pMMR Proficient mismatch repair

MMR Mismatch repair

MSI Microsatellite instability

MSS Microsatellite stability

NES Normalized Enrichment Score

Padj Adjusted p value

PanCK Pan-cytokeratin

PBS Phosphate buffered saline

PVF Polyvinylidene fluoride

RAS Rat sarcoma

RNA Ribonucleic acid

ROI Region of interest

SDS Sodium dodecyl sulfate

STAT3 Signal transducer and activator of transcription 3

ssGSEA Single sample gene set enrichment analysis

TAMs Tumour associated macrophage

TANs Tumour associated neutrophil

TB Tumour budding

TBST Tris buffer saline solution plus tween

TGFβ Transforming growth factor beta

TMA Tissue microarray

TNM Tumour node metastases

TNFα Tumour necrosis factor alpha

TP53 tumour protein (EC :2.7.1.37)

TRIS Tris buffered saline

TSP Tumour stroma percentage

QC Quality control

WNT Wingless-related integration site

WST-1 Water-soluble tetrazolium salt 1

Chapter 1. Introduction

1.1. Colorectal cancer and its incidence

Colorectal cancer (CRC), comprising of both the colon and rectum, develops from the epithelial cells or stem cells at the base of the crypt which acquire genetic or epigenetic mutations to induce tumour formation. CRC is the third most diagnosed cancer and the second most lethal malignancy worldwide. In 2018, nearly 2 million CRC cases were registered, and the global trend is likely to increase in the coming decades (1).

The development of CRC is reported to be associated with 1) nonmodifiable risk factors such as age and heredity factors and 2) modifiable factors including environmental and lifestyle. It is known that the difference in sex is one of the most significant factors in cancer epidemiology. In the UK, men are more likely to develop CRC and have a higher mortality rate than women (22). The development of CRC mainly occurs in people aged 50 and above, however an increasing incidence of CRC in younger people has been observed. In the UK, 43% of CRC cases were reported in people aged 75 and over, with the highest rate reported in those between ages 85-89. Dietary choices are also a risk factor. A meta-analysis reported an increased overall risk of red and processed meat consumption in CRC development (23). Obesity, lack of exercise, and smoking have also been reported as contributing factors in CRC (1).

1.2. Colorectal pathology

1.2.1. Anatomy

The colon or large intestine is a long hollow tube divided into three different parts: colon, rectum and anus. Its main function is to absorb water and nutrients, and the formation of stool. The entry point of the colon is called the cecum which is six inches long. This enters the ascending colon leading to transverse colon then the descending colon and finally the sigmoid colon which joins to the rectum. The rectum is the terminal portion of the large intestine which functions as the temporary storage for stool and connects to the anus (Figure 1.1).

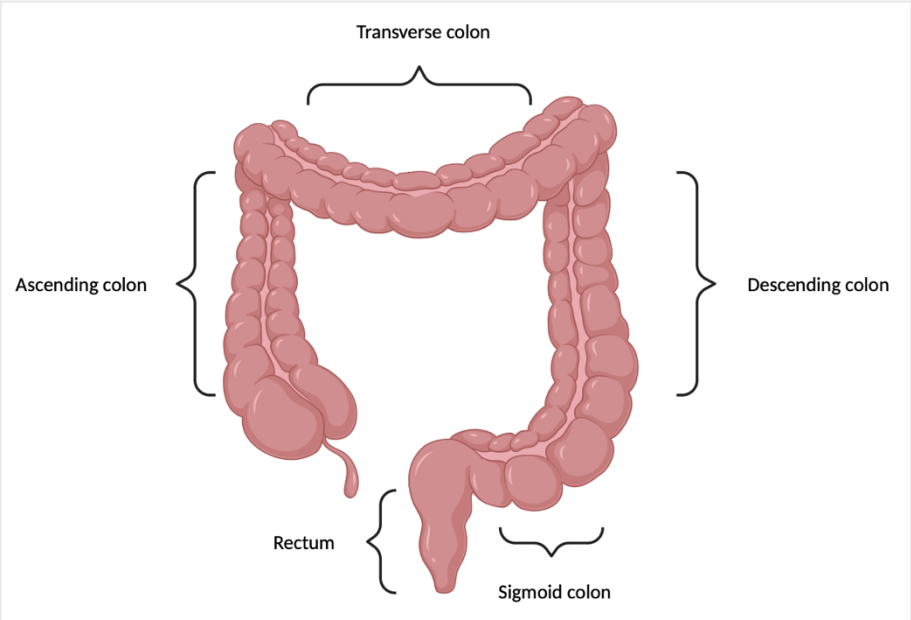

Figure 1.1 *Illustration of colorectal anatomy made from BioRender*

The colon is covered by a sheet of epithelial cells that form long glands known to produce mucin which aids movement through the digestive tract. The glands form in a thin layer inside the colon surface called the mucosa (Figure 1.2) (24). Below this layer is the submucosa layer where all the vessels and lymph nodes are located. This is covered by an outside layer consisting of fat and a layer of tissue called serosa.

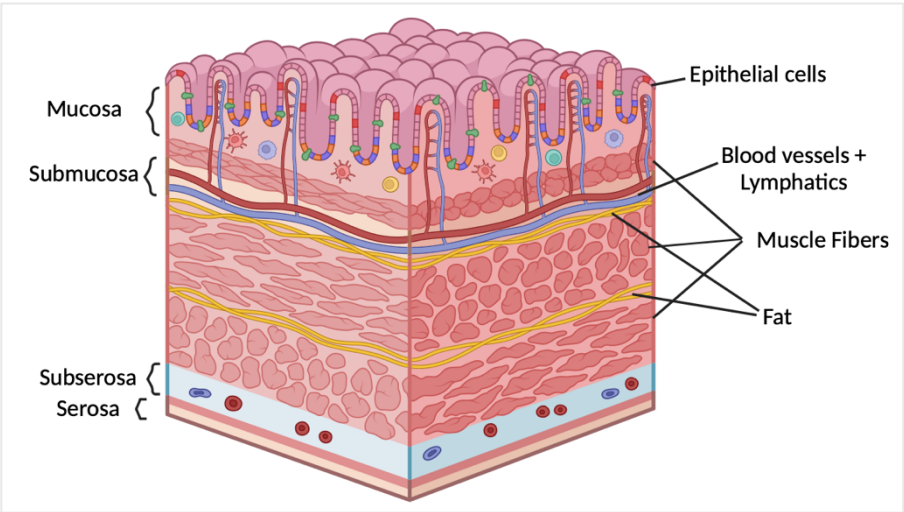

Figure 1.2 *Representative image inside of the colon made from BioRender*

1.2.2. Histopathology of CRC

1.2.2.1. Adenocarcinoma

Ninety percent of colorectal carcinomas are adenocarcinomas derived from epithelial cells in the mucosa tissue layer (25). Tumour differentiation is characterised by glandular

formation, the higher gland formation the more well-differentiated the tumours are. 70% of CRCs were found to be moderately differentiated while 20% were poorly differentiated and 10% were well-differentiated (26). Most CRCs are diagnosed by endoscopic biopsy or polypectomy. Tumour invasion is usually determined by the presence of tumour cells that have invaded from the mucosa through the submucosa tissue layer.

1.2.2.2. Signet ring cell carcinoma (SRCC)

Signet ring cell carcinoma (SRCC) is rarely observed in CRC with only 1-2% cases reported. SRCC is defined by tumour being composed of more than 50% signet ring cells (27). This subtype has been reported to be associated with younger age with advance tumour stage, lymph node metastasis and has a poorer prognostic outcome when compared to the most common adenocarcinoma (28-31).

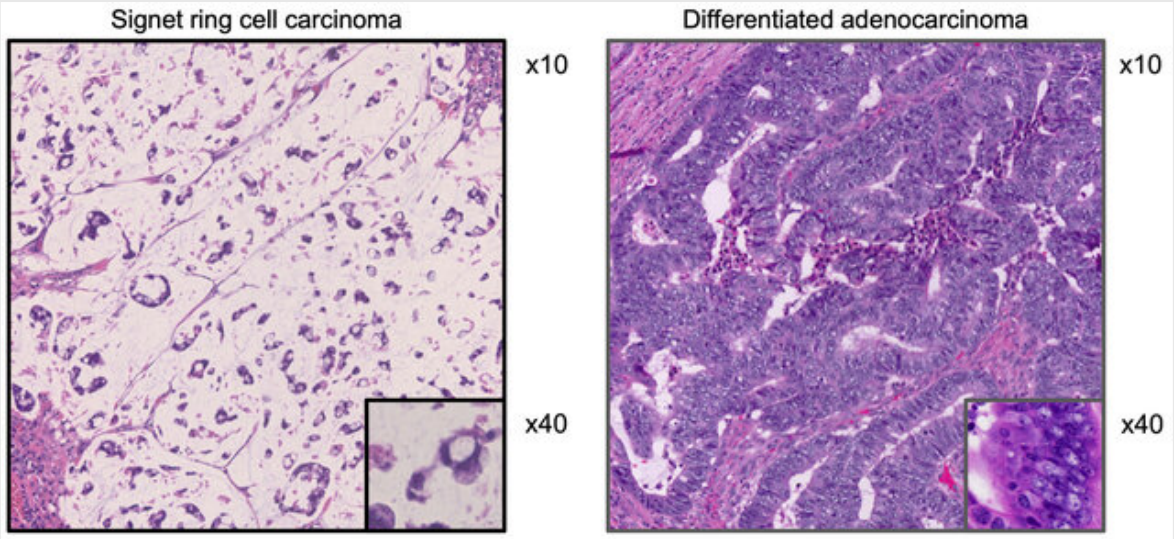

Figure 1.3 *Representative image compared between signet ring cell carcinoma and adenocarcinoma in colorectal cancer (31).*

1.3. Development of the disease

Genome instability is known to be one of the factors that can promote the accumulation of mutations, therefore, leading to a rapid evolution and growth of cancer cells (32). There are three types of CRC: Sporadic, Hereditary, and Colitis Associated.

1.3.1. Sporadic CRC

Approximately 75% of CRCs are sporadic, and there is no known genetic predisposition or family history. Most sporadic CRCs occur by chromosomal instability (CIN) which is characterised by chromosome abnormalities, loss of heterozygosity, and chromosomal rearrangements (33). CIN is reported to be initiated by adenomatous polyposis coli (APC*)* gene mutation. Accumulation of *APC* mutations is found in 50-83% of sporadic CRCs and initiates cancer progression by promoting β-catenin accumulation leading to sustained activation of *WNT* signalling (34, 35). Loss of the tumour-suppressor gene *APC* results in the formation of an early adenoma (36, 37). This is followed by *KRAS, BRAF*, *PIK3CA*, *SMAD4* mutations*,* loss of heterozygosity of chromosome 18 *(*LOH18q*),* and *TP53* mutations (38-40). *KRAS* and *BRAF* mutations are reported in tumour development, progression, and drug resistance in CRC (41, 42). There are two pathways involved in development of CRC, conventional and serrated (43). While most CRC cases developed from conventional adenoma, CRC developing from serrated polyps has been reported (44). At a molecular level, the serrated pathway is thought to involve mutations of either *KRAS* or *BRAF* and has recently been reported to be a precursor for CRC (45) (Figure 1.4).

Mutated *KRAS* and *BRAF* lead to disease metastasis and a significantly worse outcome in CRC patients (46). Additionally, microsatellite instability (MSI), found in 15% of CRC cases, is reported to arise through the dysfunction of DNA mismatch repair (MMR). MSI is observed in the early stage of disease development along with progression and metastasis (47). Deficiency in MMR (dMMR), characterised by hypermutation leading to a high level of mutations, is considered a prognostic and therapeutic factor in CRC (48). dMMR in tumours has been reported to play an important role in patient survival when compared to normal state proficient MMR (pMMR), leading to an investigation into its association with tumour progression and development in CRC (49-51).

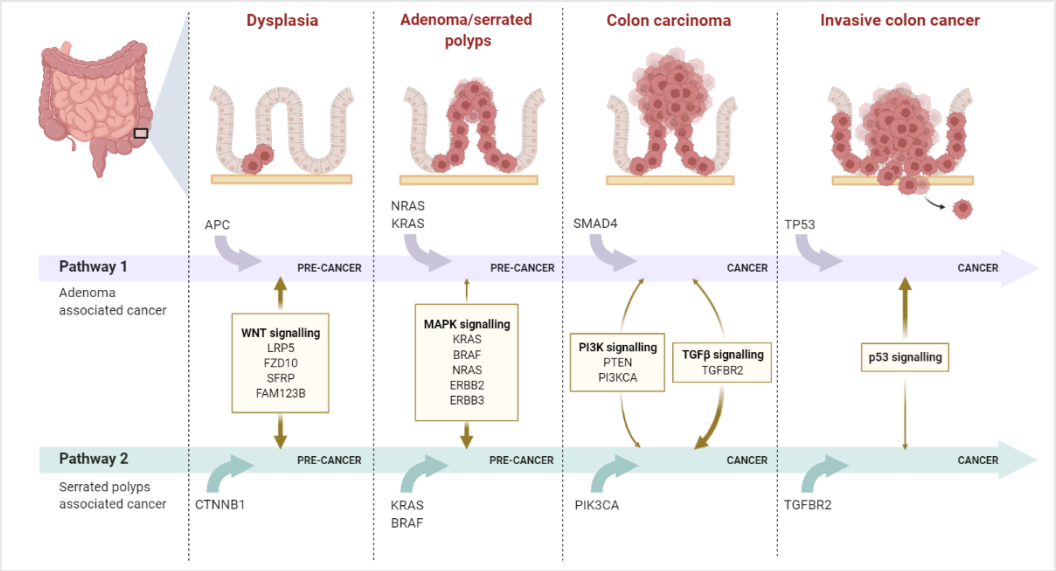

Figure 1.4 *The development of colorectal cancer cited from BioRender (2020). Colon Cancer Progression. https://app.biorender.com/biorender-templates/t-5efa094aaab8e100ae9b361b-colon-cancer-progression.*

1.3.2. Hereditary CRC

This type of CRC has been associated with a predisposition to hereditary CRC or polyposis. There are two well-known types, hereditary non-polyposis colorectal cancer (HNPCC) and hereditary polyposis colorectal cancer (HPCC). HNPCC is an autosomal dominant cancer that accounts for up to 4.2% of CRC patients (52, 53). Lynch syndrome (LS), which presents with flat polyps located in the right colon, is the most common type in this group. LS is associated with mutations of DNA MMR; *MLH1* (76%), *MSH6, PMS2, MSH2* (40%) (54). HPCC accounts for approximately 5% of all CRC cases (55). This group is mainly affected by germline mutation of the *APC* gene; Familial Adenomatous Polyposis (FAP) and characterised by multiple precancerous adenomatous polyps (56).

1.3.3. Colitis associated colorectal cancer (CAC)

Approximately only 1-2% of CRCs are CAC. It is a specific type of CRC that develops from a long-standing colitis in inflammatory bowel disease (IBD) patients. Chronic inflammation is a major factor hypothesised to play an important role in the development of this type of disease (57).

1.4. TNM classification system

Tumour-Nodes-Metastasis (TNM) staging is the classification system that has been used to define the stages of cancer (58). It is the most widely used tool for the staging of many cancers including colorectal (Table 1.1).

The t stage is determined by the size of the tumour and its level of spread through the bowel. T1 is the stage when tumour is only located in the inner layer of the bowel where T2 has grown to the muscle layer. T3 is the stage where tumour spreads into the outer lining of the bowel wall. T4 has 2 substages; T4a is the stage where tumour has grown through the outer lining of the bowel wall and spread into the tissue layer and T4b means tumour has grown and spread to other organs.

N stages are based on the level of spread into lymph nodes. N0 means there are no cancer cells in the nodes. N1 is when cancer cells are found in 1-3 lymph nodes. N2 is when there are cancer cells in more than 4 lymph nodes.

M stages are described when cancer has spread to another part of the body. M0 means there is no spread of the cells. M1 means cancer cells have been spread to nearby organs such as liver and lung. Overall TNM stage ranges from I-IV. TNMI patients T1N0M0 or T2N0M0 and TNM II are either T3N0M0 or T4N0M0. TNM stage III patients are classified as any t-stage, N1M0 or N2M0. Any tumour with metastases will classify as TNM IV with any T N and M1.

Although it is a useful tool for staging CRC patients and selecting them for specific treatment, many patients experience various outcomes. For example, a predictive biomarker to classify tumours with stages II and III is required as similar outcomes are found between these two stages (59). Additionally, adjuvant therapy be required to be modified in clinical practice to improve patient outcomes.

Table 1.1 *TNM Staging Classification of Colorectal Cancer adapted from Puccini et al. (60).*

Stage	***Characteristics***
Tumour	
T0	No evidence of primary tumour
T1	Tumour invades mucosa or submucosa T1a size <1cm T1b size 1-2cm
T2	Tumour invades muscularis propria or size >2cm
T3	Tumour invades subserosa/pericolic/perirectal fat
T4	Tumour directly invades other organs
Nodal metastasis	
NX	Regional lymph nodes cannot be assessed
N0	No nodal metastasis
N1	Metastasis in one to three nodes
N2	Metastasis in four to more nodes
Distant metastasis	
MX	Distance metastasis cannot be assessed
M0	No distant metastasis
M1	Distant metastasis

1.5. The consensus molecular subtypes (CMS)

In addition to the TNM classification system, the classification of CRC using molecular features has been proposed. Using sequencing data, CRC has been classified, according to Guinney and colleagues, into 4 subgroups (Figure 1.5) (61).

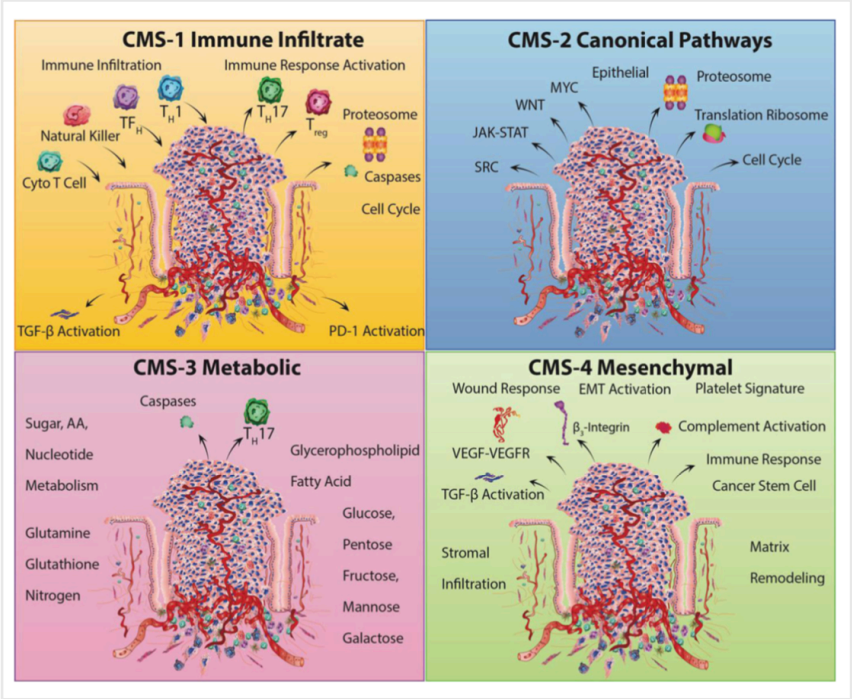

Figure 1.5 *The illustration of 4 groups of consensus molecular subtypes (CMS) in CRC cited from Menter et al. (62)*

CMS1 represents the immune subtype characterised by hypermutation and low somatic copy number alterations (SCNAs). This group comprises mostly of microsatellite instability (MSI) tumours with an overexpression of proteins involved in DNA damage repair; defective DNA mismatch repair (dMMR). Additionally, an increase in immune cell infiltration was also found in this group. Conversely, other subtypes (CMS2-4) were shown to have a higher chromosomal instability (CIN). The frequent observation of an increase in oncogenes together with the loss of tumour suppressor genes was found in CMS2, the canonical pathways subtype. This subgroup was shown to have epithelial differentiation with activation of oncogenic pathways such as WNT and MYC downstream targets. The dysregulation of the metabolic pathway has been reported in the CMS3 subtype along with an occurrence of KRAS-activating mutations. Lastly, there is a unique upregulation of epithelial-mesenchymal transition (EMT) in CMS4 mesenchymal subtype. An association with transforming growth factor (TGF)-β signalling, angiogenesis, and immune suppression was reported in this group. These characteristics are summarised in Table 1.2. CMS characterisation has been consistently reported to indicate efficacy of chemotherapy and be predictive of

metastasis disease (63). For example, in local disease, CMS4 was associated with the worst outcomes while the worst survival was reported in CMS1 when metastasis developed (64).

Table 1.2 *Table outlining the characteristics of the consensus molecular subtypes of colorectal cancer and relative survival prediction. Modified from Buikhuisen et al, 2020 (65).*

	CMS1 Immune	**CMS2 Canonical**	**CMS3 Metabolic**	**CMS4 Mesenchymal**
Characteristic	MSI-H *BRAF*^{V600E} Strong immune	*TP53*^{mut} Wnt, Myc, Src	*KRAS*^{mut} Dysregulated metabolism	EMT, TGF-β
Prognosis	Best	Intermediate	Intermediate	Worst

Moreover, tumours with CMS4 characteristics were reported as stromal in origin (66, 67) and it maybe that stromal traits dominate those of the cancer cells. Therefore, a recent study proposed a new classification based on a large collection of patient-derived xenografts tumours to access the human cancer cell transcriptomic profile (Table 1.3). Colorectal cancer intrinsic subtype (CRIS) was suggested and its prognostic value in CRC has been reported (68).

Table 1.3 *Table outlining the characteristics of the colorectal cancer intrinsic subtypes and relative survival prediction. Modified from Buikhuisen et al, 2020 (65).*

	CRIS-A	**CRIS-B**	**CRIS-C**	**CRIS-D**	**CRIS-E**
Characteristic	MSI-H *BRAF*^{V600E} --- MSS *KRAS*^{mut}	EMT, TGF-*β*	*TP53*^{mut} EGFR	IGFR, Wnt Lgr5	*KRAS*^{mut} *TP53*^{mut} Wnt
Prognosis	Intermediate	Worst	Intermediate	Best	Intermediate

A recent report has proposed a pathway-derived classification system; pathway-derived subtypes (PDS). In this classification, *KRAS* mutant CRC tumours were used to identify the biological differences between subtypes (69). The prognostic value of PDS to stratify CMS subtypes has been reported and its clinical relevance in CRC confirmed (Table 1.4).

Overall, these studies have created a useful tool for personalised and classified CRC treatment groups. The developing of new technologies has made an important impact on the identification of specific biomarkers in CRC regarding disease's plasticity and its unique

characteristic. Different classification subtypes based on different approaches, together will help unravel the underlying molecular mechanism of CRC leading to the right therapy to patients.

Table 1.4 *Table outlining the characteristics of the colorectal cancer intrinsic subtypes and relative survival prediction. Modified from Malla et al.(69).*

	PDS1	**PDS2**	**PDS3**
Characteristic	LGR5+ stem-rich Proliferative E2F2	ANXA+ stem-rich Inflammatory $BRAF^{V600E}$	Less stemness Differentiated
Prognosis	Best	Intermediate	Worst

1.6. Inflammation and tumour microenvironment in CRC

The biology of metastatic CRC has been shown to have distinct characteristics when compared to local disease which is challenging to target (70). In addition to tumour-based classification, the interaction between cancer cells and their microenvironment is also considered a crucial factor for tumour progression and metastasis.

1.6.1. Systematic inflammatory

Inflammation is associated with the development of cancer, which either promotes or suppresses tumour progression (71, 72). Systemic inflammation contributes to an increase in pro-inflammatory cytokines and chronic activation leading to an increase in protein breakdown (C-reactive protein; CRP), progressive nutritional decline (hypoalbuminaemia), and poorer survival (73, 74). This led to the establishment of a prognostic score, the Glasgow prognostic score (GPS), which combined serum CRP and albumin concentrations (75-77). However, studies have shown that hypoalbuminaemia alone may not be associated with reduced survival in patients (78-80). Therefore, a modified GPS (mGPS) has been introduced and reported as a strong prognostic factor and could be potentially implemented in routine clinical practice in CRC patients (77, 81-83).

The mGPS score aside, the link between inflammation and cancer is consistently reported (84, 85). The relationship between the cancer cell and its surrounding inflammatory-related cells could influence tumour biology such as cell proliferation, angiogenesis, invasion, and migration (86, 87). Inflammatory cells in the peritumoral stroma have been studied (88) and peritumoral inflammation is associated with outcomes in CRC (89). A combination of peritumoral inflammation (Klintrup–Mäkinen; KM) and tumour stroma percentage (TSP) scores have been accessed to identify the relationship between the tumour and its local TME - Glasgow microenvironment score (GMS) (90) (Figure 1.6). GMS has been described as an independent factor for disease recurrence, and patients with a higher GMS may benefit from additional CRC treatment (77, 81) (Table 1.5).

Table 1.5 *Table outlining the components of Glasgow Microenvironment Scoring and relative prognosis of each subgroup.*

KM Grade (Immune Infiltrate)	TSP (Stromal Invasion)	GMS	Prognosis
High (2-3)	Any	0	Good
Low (0-1)	<50%	1	Intermediate
Low (0-1)	>50%	2	Worst

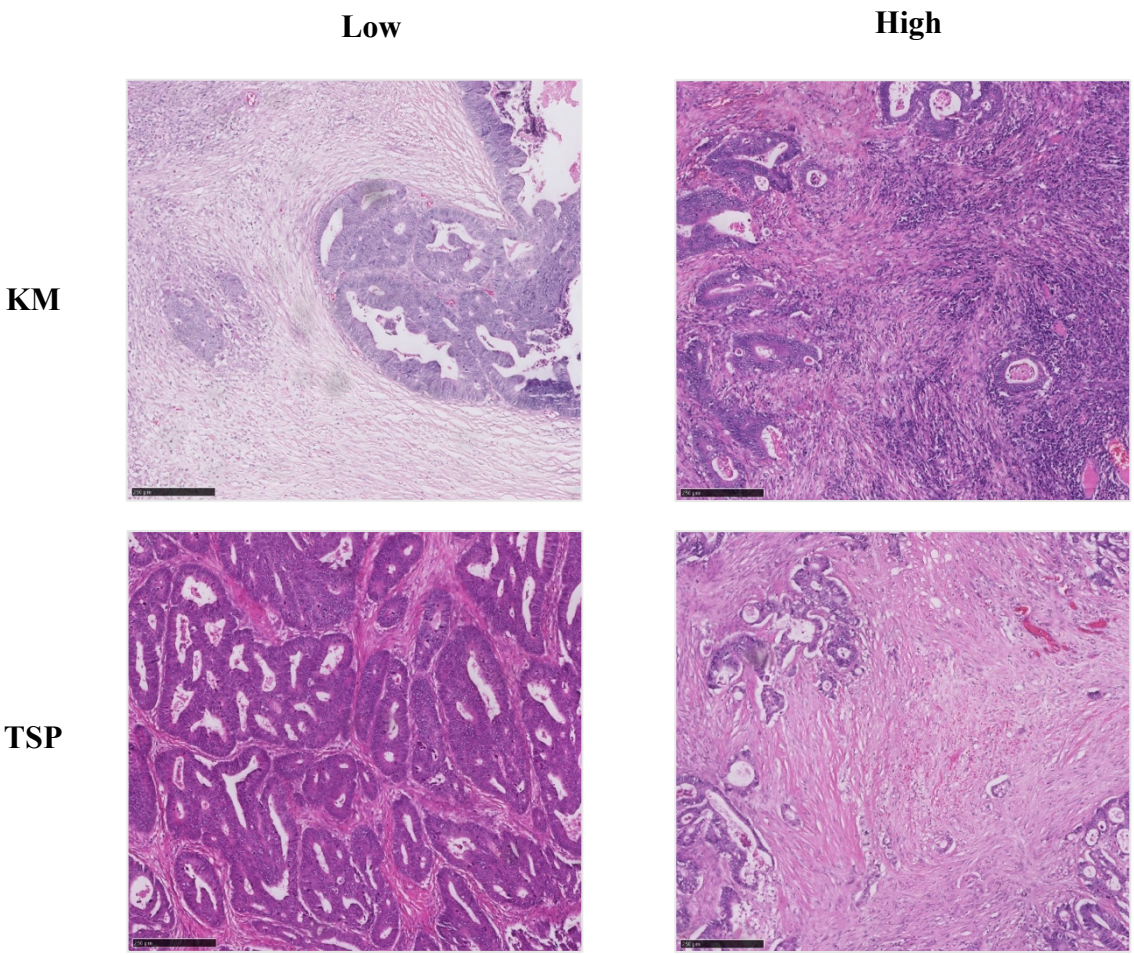

Figure 1.6 *Example of KM; low and high immune infiltration (top row) and TSP; ≤ 50% stroma for low and >50% stroma for high (bottom row) grades in colorectal cancer pathology slides.*

1.6.2. Immune microenvironment

Immune cells play a crucial role in inflammation and reported as either 'killing' or 'promoting' tumour cells (91). The study of immune cell populations in CRC led to the discovery of immune characterisation which has been shown to predict outcomes in CRC patients (92). For example, a tumour microenvironment (TME) enriched with T cell subsets, including cytotoxic T and memory T cells, is associated with a good prognosis in CRC (93-96).

The prognostic value of cytotoxic T cell- populations in CRC led to the development of an 'immunoscore®'. Immunoscore® assay is the first standardised immune-based assay for the classification of cancer (97). The score was obtained by measuring T cell infiltration of CD3+ and CD8+ from immunohistochemistry (IHC) slides staining. The T cell density is quantified in 2 regions of interest (ROIs); tumour core and invasive tumour edge, to determine

the prognosis survival in CRC patients (97). The use of immunoscore® has consistently been reported as a useful tool in the prediction of the efficacy of immunotherapy in CRC patients (98-100). However, studies have shown the association between immune infiltrating and CRC development (101). Other infiltrated immune cells such as macrophages, fibroblasts, neutrophils, naïve B cells, etc, should be considered for future immune-based prognostic scores (102, 103).

In addition to T cells, tumour-associated macrophages (TAMs) were reported to be the most common myeloid cells in the TME (104). The macrophage population has been classified into two subgroups: anti-tumour activity macrophages and pro-tumourigenic activity macrophages (105, 106). A high number of pro-inflammatory macrophages have been shown to mediate tumoricidal activity leading to substantial progression in CRC (107, 108). However, the prognostic role of macrophages in CRC progression remains controversial with different functions being observed across the tumour. (109, 110).

Neutrophils are also one of the major components of TME. Similar to M1-like and M2-like macrophages, tumour-suppressive (N1) and tumour-promoting (N2) neutrophils have been reported (111). N1 neutrophils were highly expressed in early CRC development and then later transformed to the N2- subtype (112). Additionally, studies have suggested a difference in the prognostic value of neutrophils across tumour subsites (113). Studies have consistently reported that neutrophil-to-lymphocyte ratio (NLR) can be used to determine prognosis and identify risk groups in CRC (114-116).

Overall, there is a promising correlation between tumour and its immune system. Studies suggested an impact of immune cells to progression and treatment in CRC (117). Understanding the immune cell types and its associated pathway activation has led to the development of immune-based therapeutics (118). The crosstalk between tumour cells and immune microenvironment could be one of the key factors for the future CRC treatment.

1.7. Metastasis in CRC

Incidence rates of CRC have been decreasing in high-income countries partly due to the development of screening programs (2). However, 30% of CRC patients developed synchronous or metachronous metastasis (119). Of these, fewer than 20% with metastasis CRC survive for 5 years after diagnosis (120). It is, therefore, one of the main challenges in cancer research to develop targeted treatment and increase the survival rate of those with metastatic CRC (121).

1.8. Tumour Budding (TB)

1.8.1. TB and its prognostic value in CRC

Tumour budding (TB) is a single cell or small cluster of up to 4 cells found at the invasive front of a tumour (Figure 1.7). It has been reported to be a prognostic factor related to tumour recurrence and metastasis (122, 123). TB has been reported as an independent prognostic marker associated with adverse clinicopathological factors such as lymphatic invasion, venous invasion, and disease recurrence (124-126). Studies have suggested a prognostic role for TB in several types of cancer, such as head and neck (12, 127, 128), pancreatic (9), lung adenocarcinoma (13), hepatocellular carcinoma (129, 130) as well as colorectal (131) and breast (10, 11, 132).

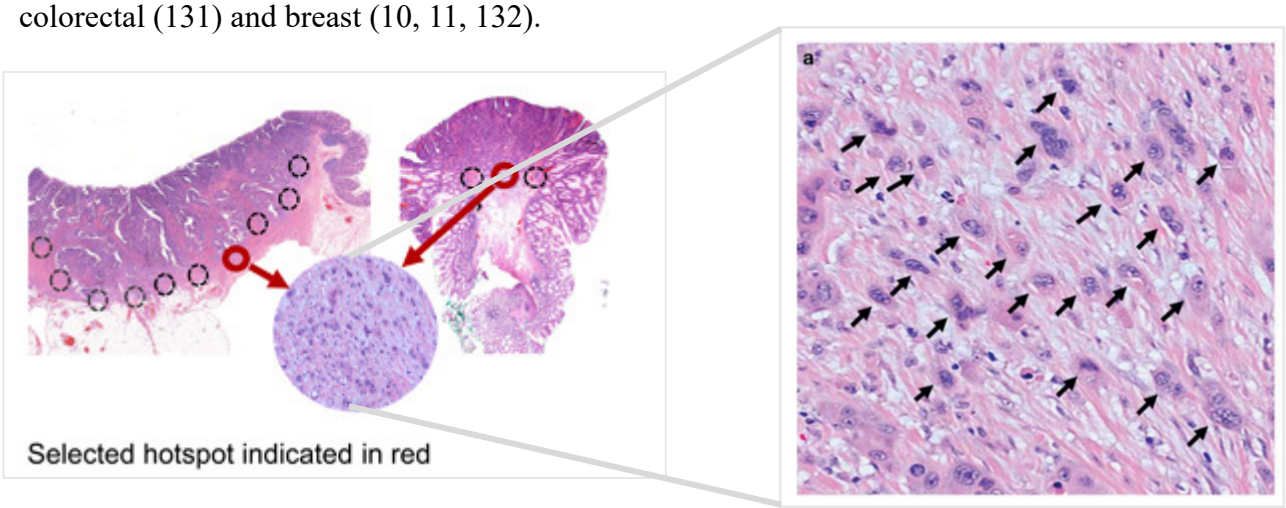

Figure 1.7 *Example of tumour budding defined as single tumour cells or cluster of up to four cells (dark arrows) at the tumour invasive edge (8).*

In CRC, tumours with high TB are significantly associated with worst survival and adverse features such as serosal involvement and venous invasion (19, 122). Despite the use of TNM staging, many studies have proposed a potential prognostic value for TB in CRC. According to the international tumour budding consensus conference (ITBCC) 2016, the presence of TB should be included in clinical reporting of CRC, and a grading score based on tumour budding number was suggested and classified into BD1 (0-4 buds/hotspot 0.785mm2), BD2 (5-9 buds/hotspot 0.785mm2) and BD3 (≥10 buds/hotspot 0.785 mm2) (8).

The study from Zlobec et al. suggested that TB and tumour grade (G) correlate. G3 showed 18% in BD1 cases while high tumour grade and TB were associated with higher pT stages, lymph node metastasis, and distant metastasis (133). However, unlike tumour grade, high TB correlated with worse overall and disease-free survival and was reported as an independent prognostic factor in CRC (133-137). In addition, Zlobec and colleagues found that TB provides more biologically relevant information in CRC prognosis and that tumour grade and TB are not equivalent as stated by ITBCC 2016 (133). Consistent with other peer reviewed studies (138, 139) , Zlobec and colleagues suggested that TB and tumour grade should be reported separately, and it is worth considering that TB alone has a predictive prognostic value in cancer treatment.

Several studies have indicated that TB can be used as a prognostic marker and may be used to stratify specific groups (123, 140). Garfinkle et al. reported that TB independently associated with an increased recurrence in pT2N0 patients after resection (141). Similarly, a meta-analysis of over 10,000 CRC patients demonstrated a strong correlation between TB and nodal metastasis in pT1, albeit a different method was used to count the buds (142). In addition, high-grade budding was associated with worse overall survival, and it was suggested that it could be used to predict recurrence in stage II CRC patients (143-147). Recently, using the

ITBCC criteria for TB assessment, the prognostic and predictive values of TB have been reported in stage II CRC from both SACURA (148) and QUASAR (7) trials.

According to Nozawa et al., there was a similar risk of recurrence in stage II and III CRC indicating the importance of the CRC subgroup to identify whether patients should be given additional therapy (149). Interestingly, studies reported a similar survival outcome for stage II, when tumours exhibited high TB, compared to stage III CRC (150, 151). Moreover, there are a few studies which have reported the prognostic value of TB in stage IV CRC (152, 153), although it is not clear whether TB in stage IV could be used as an independent predictor of CRC survival.

1.8.2. The correlation between TB and mutational status in CRC

Recently, we published the systematic review regarding the possible correlation between budding phenotype and common mutations in CRC (154). According to the meta-analysis, a total of over 6000 CRC patients were included, high TB phenotypes significantly correlated with mutated *KRAS* as well as tumours with MSS/pMMR. We proposed that TB phenotype could perhaps formed by the complex interplay between genetic, mRNA and protein level that needed further studies to confirm this hypothesis.

1.8.3. Molecular mechanism of TB in CRC

Studies have suggested that TB could undergo EMT leading to their association with disease metastasis (14, 155). However, there is still an argument that TB could perhaps undergo partial EMT, and that other tumour-related signalling could be involved in their formation in CRC (16). Our published review article has been reported the possible signalling related to TB phenotype recently in CRC (21). Many tumour-related signalling was reported related to TB, though there are no consistent reports. TGF-β signalling shown to be the promising pathway correlated with TB. Study from Li et al, recently proposed that TB may be induced by the synergistic activation of TGF-β and TNF-α pathway (156). This is warranting further studies

to prove the underlying mechanism of TB in CRC. Moreover, stem cells signature has also constantly been reported. The ability to drive the metastasis and adjusted to the hard conditions has been suggested to correlate with stem cell properties (157). Having said that, most of the study investigate the correlation between TB phenotype and other factors in CRC. There is a limit knowledge of the gene signature within the budding cells.

Recent study from Haddad et al. reported a similar budding-like structure called pseudobudding (PsB) which could not be identified by standard H&E or PanCK staining (158). Using spatial transcriptomics, Haddad and colleagues were able to identify the differences between true TB and PsB based on the proliferation status (Ki67 immunohistochemistry staining).

1.8.4. TB and its correlation with immune microenvironment in CRC

There is an inverse correlation between inflammation and TB phenotype in CRC (159). Few studies showed the possible correlation between budding phenotype and immune cells that could lead to the understanding of its crosstalk leading to disease metastasis and development (18, 160). Moreover, we recently published the prognostic value of combined TB and local inflammatory score (GMS; combined KM and TSP) in CRC patients suggests the possible interaction between tumour microenvironment and TB development in CRC (161).

1.9. Research aims and hypotheses.

The majority of studies have reported a potential prognostic value for TB in CRC, however, there is little understanding of the underlying mechanism of TB formation in CRC (6, 162, 163). In addition, TB has been reported to have a potential role in immunosuppression leading to the invasion of tumour cells (19, 21). This suggests a possible correlation between TB and TME. Therefore, in this thesis, an investigation into TB phenotype in CRC was conducted with the main objectives as follows.

1. To identify TB status and its prognostic value in Glasgow CRC patient cohort.

2. To investigate the underlying mechanism of TB, it is necessary to identify a specific biomarker(s) of TB, which in turn would help elucidate the biology of budding cells, how budding relates to disease metastasis, and also help identify novel therapeutic targets in CRC.
3. To investigate the relationship between TB and the TME as well as the spatial relationship between budding and immune cells within the tumour invasive area in CRC.
4. The TB formation will be reinvestigated *in vitro* to further understand the formation of TB. The genes identified from aim2 will be used to establish if TB formation can be studied within an *in vitro* setup.

Chapter 2. Materials and Methods

2.1. Tissue studies

2.1.1. Cohorts

2.1.1.1. Glasgow royal infirmary (GRI) cohort

A cohort of 787 patients with stage I-III CRC who had undergone surgical resection at Glasgow Royal Infirmary (Glasgow, UK) between 1997 and 2013 were included. Patients who died within 30 days of surgery, had emergency surgery, or received neoadjuvant therapy were excluded. Tumour staging was carried out using the 5th Edition of the AJCC/UICC-TNM staging system by the time tissues were collected. Clinicopathological data were collected with a minimum of 5 years follow-up post-resection. Clinical follow up was last updated in 2020 from NHS GGC Safe Haven data. At this time, 231 patients (36%) had died of primary colorectal cancer, 241 (37%) had died of other causes and 170 (26%) were still alive. Survival data was missing for 1 patient. Cancer-specific survival (CSS), date of surgery until last follow up, was used as a clinical endpoint throughout this study. Mean follow-up time was 94 months. The study was approved by the West of Scotland Research Ethics Committee (REC 4: 22/ws/0207) and data is stored in Greater Glasgow and Clyde Safehaven (SH21ON012).

2.1.1.1. Thai cohort

A cohort of 290 patients were included with stage I-III CRC who had undergone surgical resection at Siriraj Hospital, Mahidol University between 2009 and 2015 were included. Patients who died within 30 days of surgery, or received neoadjuvant therapy were excluded. Tumour staging was carried out using a previous TNM staging system (164). Clinicopathological data were collected with a minimum of 5 years follow-up post-resection. Clinical follow up was last updated in 2017 and approved by Siriraj Institution Review Board (Si.628/2021). At this time, 190 patients (74%) had died of primary colorectal cancer, 13 (5%) had died of other causes and 50 (20%) were still alive. Survival data were missing for 4 patients.

Overall survival was used as a clinical endpoint throughout this study. Mean follow-up time was 74 months.

2.2. Tumour phenotyping

2.2.1. Haematoxylin and Eosin (H&E) staining protocol

Tumour sections, with 5um thickness, were deparaffinized in Histoclear (Agar Scientific, Essex, UK) (3 x 3 minutes) and then rehydrated through a series of graded alcohols; 2 x 3 minutes 100% ethanol, 1 x 3 minutes 95% ethanol, 1 x 3 minutes 90% ethanol, 1 x 3 minutes 80% ethanol, 1 x 3 minutes 70% ethanol, 1 x 3 minutes 50% ethanol, 1 x 30% ethanol. Sections were then washed in deionised water for 5 minutes and placed in Harris Haematoxylin for 3 minutes. After rinsing in water for 5 minutes slides were dipped in acid alcohol (3% HCl in 70%) for 3 seconds and rinsed for 2 minutes in water. Sections were then added to Eosin for 30 seconds and passed through a series of graded alcohols to dehydrate; 1 x 2 minutes 30% ethanol, 1 x 2 minutes 50% ethanol, 1 x 2 minutes 70% ethanol, 1 x 2 minutes 80% ethanol, 1 x 2 minutes 90% ethanol, 1 x 2 minutes 95%, 2 x 2 minutes 100% ethanol. Slides were then placed in Histoclear for 3 x 3 minutes. Sections were mounted using dystrene plasticiser and xylene (DPX) and left to dry overnight. Sections were scanned onto NDP Viewer (Hamamatsu, Hertfordshire, UK) at x20 magnification using a Hamamatsu NanoZoomer (Hertfordshire, UK) by Glasgow Tissue Research Facility (GTRF). Staining was performed by Dr Jennifer Hay (JH).

2.2.2. Tumour budding scoring protocol

Following the guideline from the International Tumor Budding Consensus Conference (ITBCC) 2016 (8), budding scores were assessed in the GRI cohort. The 20x objective magnification was utilised and validated the number of TB at the invasive area (0.785 mm^2). Ten specific areas were marked to quantify the number of TB for further evaluation. The densest area of buds was representative of the budding profile of each CRC case. Budding

status was determined in the GRI cohort by HW and PH. Originally, the criteria were divided into 3 groups: BD1 (0-4buds), BD2 (5-9 buds) and BD3 (>10buds) (Figure 2.1) (Table 2.1). However, in this project BD1 and BD2 were combined and defined as low budding while BD3 represent a high budding phenotype.

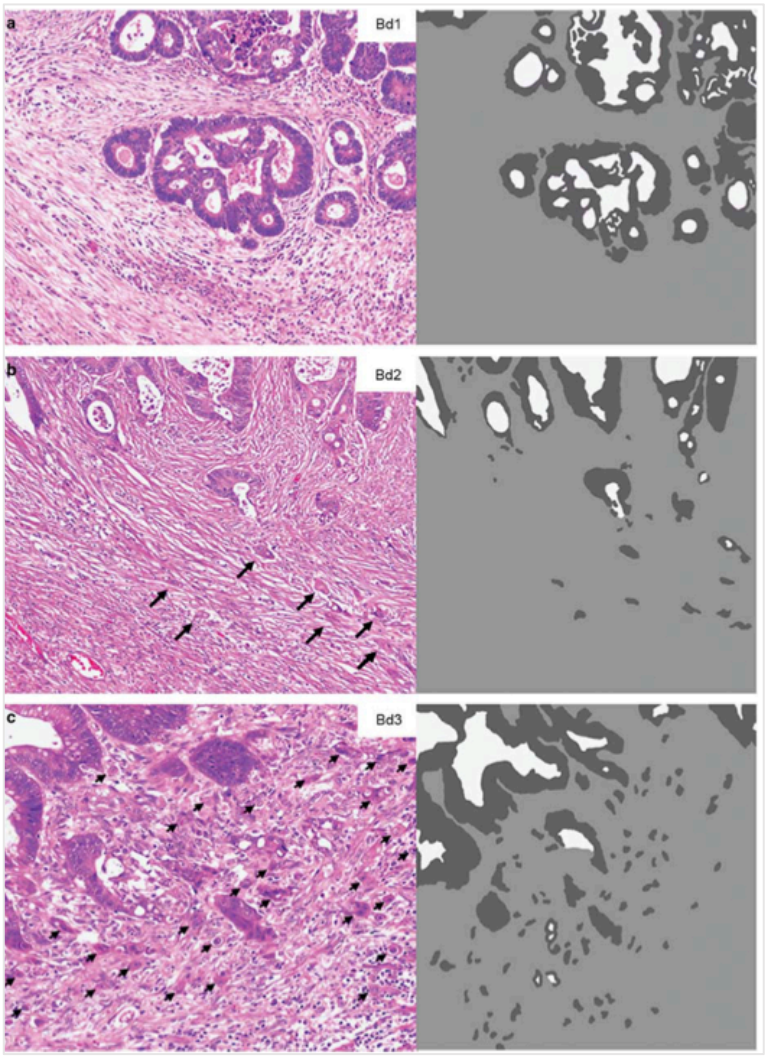

Figure 2.1 *Representative images in different of tumour budding grades (20x objective) at the invasive front of colorectal cancer based on the ITBCC 2016. (a): Bd 1 (low), (b): Bd 2 (intermediate) and (c): Bd 3 (high). Black arrows point at the budding cells (8).*

Table 2.1 *Tumour budding criteria according to ITBCC*

BD1 (low)	0-4 buds*
BD2 (intermediate)	5-9 buds*
BD3 (high)	≥ 10 buds*

*Per 0.785 mm^2

2.3. Transcriptomics data analysis

Single tissue sections from CRC cohort (n=787) who had undergone resection for CRC were used for Templated Oligo-Sequencing (TempO-Seq) analysis using a Whole Transcriptome panel. Briefly, formalin-fixed paraffin-embedded (FFPE) tissue was deparaffinised prior to tissue digestion. The tissue lysate was combined with detector oligos which were annealed in immediate juxtaposition to each other on the targeted RNA template and ligated (165). Amplification of ligated oligos was performed using a unique primer set for each sample, introducing a sample-specific barcode and Illumina adaptors. Barcoded samples were pooled into a single library and run on an Illumina HiSeq 2500 High Output v4 flowcell. Sequencing reads were demultiplexed using BCL2FASTQ software (Illumina, USA). FASTQ files were aligned to the Human Whole Transcriptome v2.0 panel, which consists of 22,537 probes, using STAR (166). Up to two mismatches were allowed in the 50-nucleotide sequencing read.

Statistical analyses were performed in R Studio (RStudio, Boston, MA, USA). Raw counts were normalised using DESeq2 and analysed for high and low budding groups. Analysis was performed using the full 22,000 gene probes by Bioclavis (Bioclavis, Glasgow, UK). DESeq2 was used to construct tables of differential gene expression. Heatmaps of differential expression of genes were constructed by PH using R packages. PCA plots were constructed to determine any clustering of gene expression between histological groups. Volcano plots were plotted to visualise differentially expressed genes between high and low budding groups.

In addition, the normalised counts of CRC patients (n=633) from DESeq2 were utilised and analysed through the GSEA program (167) (https://www.gsea-msigdb.org/gsea/msigdb/index.jsp). The molecular signature database (MSigDB) was used based on the comparison between tumours with low and high budding phenotype (168). The enrichment pathways were determined based on the nominal P-value and normalized

enrichment score (NES). For the purposes of this study significance was set to p-value, padj or nominal p ≤0.05 with a false discovery rate (FDR) <0.25 was considered statistically significant.

In addition to GSEA, STRING database was used to predict the protein interaction of differential genes with others possible related protein signalling. It quantifies the integration of the data within the target organism to determine if there is any significant association where applicable (169).

2.4. Multiplex immunofluorescence (mIF) staining

Multiplex staining was employed to stain multiple antibodies to be able to identify multiple marker detections within the same tissue sample. The process includes staining, stripping, and re-staining for antibodies in the loop until finish (Figure 2.2).

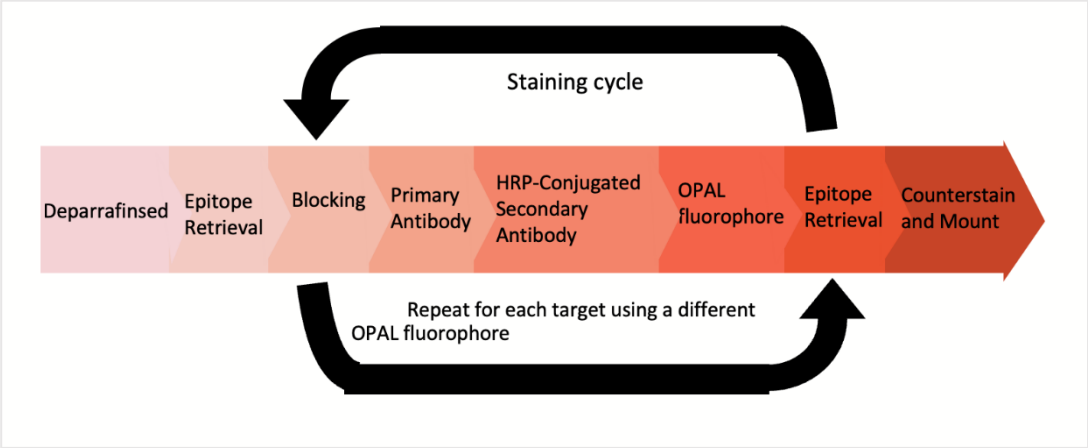

Figure 2.2 *mIF staining cycle. The primary and secondary antibodies corresponding to the first target of interest are deposited. The antibodies are removed from the tissue using epitope retrieval and the process is repeated until all the targets have been labeled.*

2.4.1. mIF protocol

TMA (n=787) and full CRC sections (n=18) were requested from NHS GGC Biorepository and provided by Glasgow Tissue Research Facility (GTRF). Slides were stored at 4^{O}C before use. Immediately before staining, TMA sections were baked at 60^{O}C for 30 minutes to minimise the loss of cores.

2.4.1.1. Deparaffinised and Epitope retrieval

Deparaffinisation and antigen retrieval was performed using PT module in Epredia™ Dewax and Heat Induced Epitope Retrieval (HIER) buffer pH 9 (Fisher scientific, TA999DHBH) at 98 ^{O}C for 30 minutes.

2.4.1.2. Blocking

The program was set to stain the following protocol in autostainer (Thermofisher). The commercial reagent from Ultravision quanto detection system HRP (Epredia™ TL125QHL, fisher scientific) was utilized. First, UVQ H2O2 was applied onto the slides to block endogenous peroxidase for 10 minutes then slides were rinsed with 1X TBS-tween (100ml 10X TBS (Tris 7.33g EDTA 87.6g) with 50ml 20% Tween in 900ml distill water). After that, non-specific protein binding was blocked using UVQ protein block for 10 minutes.

2.4.1.3. Primary antibodies

The solution was removed then primary antibodies were added. Antibodies concentration was optimised prior to the experiment (PH) (Supplementary table 2.1). After that, optimised conditions were used as described in Table 2.2 and slides were incubated for 30minutes. After incubation, slides were washed in TBST and then incubated in UVQ amplifier for 10 minutes to amplify the signals.

Table 2.2 *Listed of antibody panel used in multiplex staining matched with opal colours.*

Lymphocyte panel

Antibodies order	**Company**	**Antigen retrieval (pH)**	**Dilution**	**OPAL order**	**Dilution**
FOXP3	Abcam (ab20034)	9	1:1000	O480	1:100
CD3	Novocastra/Leica (NCL-CD3-565)	9	1:1000	O520	1:200
CD8	Dako (M7103)	9	1:1300 then 1:4	O570	1:200
Ki67	Dako (M7240)	9	1:2500	O650	1:200
PanCK	Thermofisher (MS-343-P)	9	1:200	Dig TSA / O780	1:200 / 1:50

				DAPI	30ul / 500ul TBST

Myeloid panel

Antibodies order	**Company**	**Antigen retrieval (pH)**	**Dilution**	**OPAL order**	**Dilution**
CD68	Dako (M0876)	9	1:2500	O650	1:100
CD163	Abcam (ab182422)	9	1:45000	O520	1:400
CD66b	Novus Biological (NB100-77808)	9	1:8000	O570	1:100
PanCK	Thermofisher (MS-343-P)	9	1:200	Dig TSA / O780	1:200 / 1:50
				DAPI	30ul / 500ul TBST

2.4.1.4. HRP-Conjugated secondary antibody

Slides were rinsed again with TBST then applied UVQ HRP for 10 minutes.

2.4.1.5. OPAL fluorophore

TBST was used to wash the slides then, distilled water, then finally OPAL solution was applied for 10 minutes. The optimized concentration was used (Table 2.2).

2.4.1.6. Epitope retrieval

To finish one cycle and strip off antibodies, slides were put into PT module with Epitope Retrieval (HIER) BufferpH 9 and heat to boil for 30 minutes at 98 ^{O}C. The cycle is repeated until all targets have been labeled.

2.4.1.7. Counterstain and mounting

Slides were brought to boil in Epitope Retrieval (HIER) Buffer pH 6 in a microwave with full power (800W) for 5 minutes then boiled for 25 minutes at 40% power then left to cool down for 15-30 minutes. The last step before imaging is to counterstain with DAPI (1 drop in 500ul of TBST) for 5 minutes followed by washing the slides with water twice then allowed to

air dry. Slides were mounted using Vectashield hardset antifade mounting medium (11250, vector) before applying coverslips.

2.4.2. mIF panels on CRC TMAs

2.4.2.1. Panel of CD3 CD8 FOXP3 CD68 aSMA and PanCK

A fully automated mIF assay was developed and done by the Le Quesne group. The Ventana Discovery Ultra autostainer platform (Roche Tissue Diagnostics, software version RUO Discovery Universal V21.00.0019) was utilised. Staining was performed on 4µm thick sections of previously constructed TMAs (n=787) with the optimised antibodies (Table 2.3) (Leah officer Jones). A negative control slide was used on each staining run to rule out non-specific staining. Whole slide images were captured at 10x magnification using the PhenoImager HT multispectral slide scanner (Akoya Biosciences V1.0.13), TMA maps were applied using Phenochart software (Akoya Biosciences V1.1.0), and core images were captured at 20x magnification. Core images were spectrally unmixed using Inform software (Akoya Biosciences, software version 2.5.1).

Table 2.3 *Listed of reagents used in multiplex staining.*

Reagent	**Supplier**	**Catalogue number**	**Dilution**	**Dispenser**
Discovery Inhibitor	Roche Tissue Diagnostics	07017944001	RTU	Disc Inhibitor
Goat Ig block	Roche Tissue Diagnostics	07988214001	RTU	Gt Ig Block
CD68	Cell Signaling Technology	76437	1:200	Antibody 4
Omnimap anti-rabbit HRP	Roche Tissue Diagnostics	05269679001	RTU	OMap antiRb HRP
OPAL 620	Akoya	FP1495001KT	1:100	Detection 1
FOXP3	Abcam	20034	1:20	Antibody 2
OPAL 690	Akoya	FP1497001KT	1:300	Detection 7
Smooth muscle actin	Roche Tissue Diagnostics	05268303001	RTU	SM Actin

Omnimap anti-mouse HRP	Roche Tissue Diagnostics	05269652001	RTU	OMap anti-Ms HRP
OPAL 540	Akoya	FP1494001KT	1:300	Detection 3
CD3	Roche Tissue Diagnostics	05278422001	RTU	Antibody 20
OPAL 570	Akoya	FP1488001KT	1:200	Detection 4
CD8a	Cell Signaling Technology	70306	1:100	Antibody 3
OPAL 520	Akoya	FP1487001KT	1:200	Detection 5
Cytokeratin AE1/AE3	Leica Biosystems	AE1/AE3-601-L-CE	1:250	Antibody 1
OPAL 650	Akoya	FP1496001KT	1:600	Detection 6
QD DAPI	Roche Tissue Diagnostics	05268826001	RTU	QD DAPI
Liquid coverslip	Roche Tissue Diagnostics	05264839001	RTU	NA
Reaction buffer	Roche Tissue Diagnostics	05353955001	RTU	NA
Discovery wash	Roche Tissue Diagnostics	07311079001	RTU	NA
Discovery CC1	Roche Tissue Diagnostics	06414575001	RTU	NA
CC2	Roche Tissue Diagnostics	05279798001	RTU	NA
Diluent	Dako	K8006	RTU	NA
TSA	Akoya	FP1498	RTU	NA
Diamond prolong	Thermo Fisher	P36970	RTU	NA
Negative control rabbit Ig	Roche Tissue Diagnostics	05266238001	RTU	NEG CTL Rbt Ig
Negative control monoclonal (MOPC21)	Roche Tissue Diagnostics	05266670001	RTU	NEG CTL Mab

2.4.2.2. Panel of CD163 CD66b and PanCK and CD3 CD8 FOXP3 Ki67 and PanCK

mIF was performed on 2.5 μm thick sections of previously constructed GRI TMAs (n=787) using the autostainer (Thermofisher) with optimised antibodies (Table 2.2). The assay was developed and stained by PH. The slides were scanned by NanoZoomer S60 digital slide scanner (Hamamatsu, USA) with 20x magnification. TMA maps were applied for further analysis in Visiopharm (version 2021.02.5.10297), digital precision pathology software.

2.4.3. mIF panel on CRC full sections

2.4.3.1. Panel of Lymphocytes and Myeloids markers

mIF was performed on 4um full CRC sections (n=18) using the optimized panel of lymphocyte (CD3 CD8 FOXP3 Ki67 and PanCK) and myeloid markers (CD68 CD163 CD66b and PanCK) (Table 2.2). The assay was developed and stained by PH. The slides were stained using the autostainer (Thermofisher) and scanned by NanoZoomer S60 digital slide scanner (Hamamatsu, USA) with 20x magnification. Visiopharm (version 2021.02.5.10297), digital precision pathology software, was used to perform the analysis.

2.4.4. Scoring mIF images

All multiplex images were analysed in Visiopharm®, a digital pathology program, to identify target phenotypes in CRC tissue. The APPs were developed to detect tumour and immune cellcompartments by PH. The process to analyse multiplex was divided into three steps: tumour, nuclear and phenotypic detection. Tumour detection APPs is the process which the program has been given to define tumour and stroma using specific staining of either PanCK (epithelial cells) or aSMA (fibroblast cells) (Figure 2.3A). After that, nuclear detection APPs were used to identify single cells using DAPI staining (Figure 2.3B). Lastly, target expression was classified using the phenotypic detection APP. The staining was detected by the intensity of each protein expression via opal fluorescence channel (Figure 2.3C). After

running the analysis, the percentage of positive cells were determined in either the tumour or stromal compartment. The total cell count in each area was used to normalised target cells (Supplementary figure 2.1). Therefore, cells density was reported for further analysis.

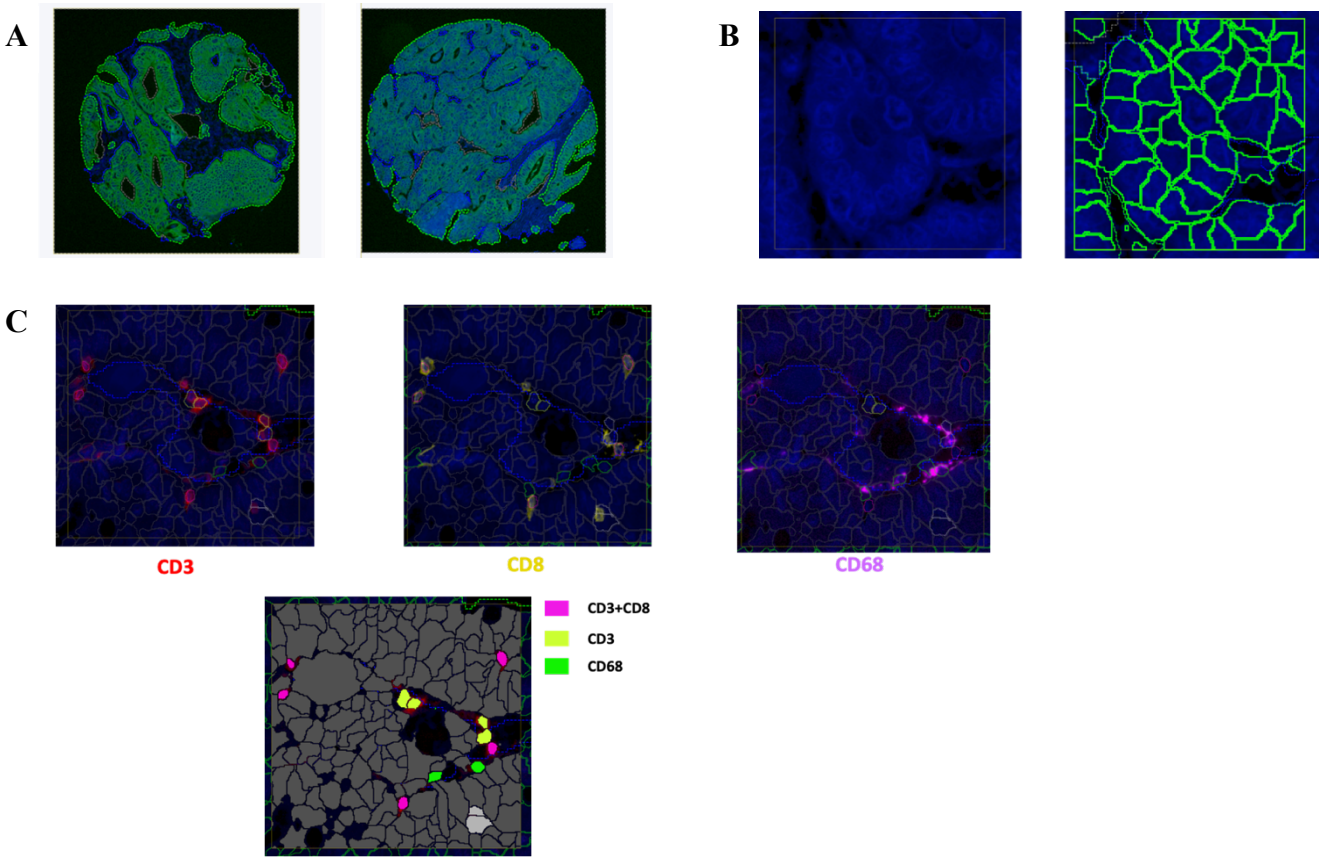

Figure 2.3 *Representative images for multiplex staining analysis using digital pathology program (A) Tumour detection (B) Nuclear detection and (C) Phenotypic detection.*

2.4.5. Advance image analysis

Cluster analysis was applied to identify the groups of budding clusters in the tumour invasive area (n=18) of CRC full sections using R packages. The classification of cluster analysis was based on the xy coordinates obtained from the multiplex staining images. As budding clusters have been identified from the image analysis using Visiopharm, the data then performed a cluster to classify the group of buds for further analysis (Figure 2.4).

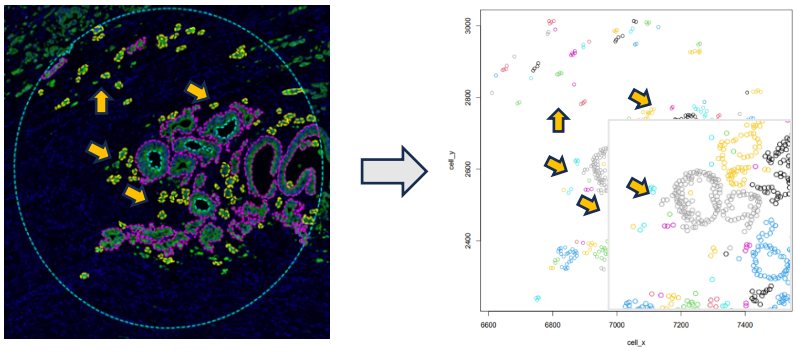

Figure 2.4 *Cluster analysis identified cluster of TB (yellow arrow).*

Once the budding cluster was identified, nearest neighbour analysis was performed to determine the distance from budding cluster to phenotypes using phenoptr R package (version 0.3.2). This package analyses the spatial relationship between cells in a single field. It finds the nearest neighbour cell in each of the provided phenotypes and reports the cell ID and distance to the nearest neighbour cells (Figure 2.5).

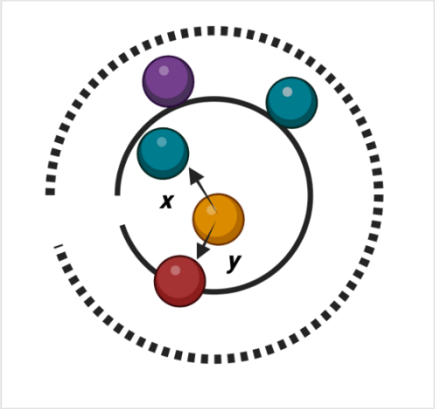

Figure 2.5 *Images illustrated distance from tumour cells (yellow) to phenotypes performed by nearest neighbour analysis. x and y represent the nearest distance measured from tumour cells to closest phenotype.*

The distance from budding cluster to specific phenotype then plots into xy correlation graph to investigate the close distance from budding cells to phenotypes (Figure 2.6). The area was divided into 4 quadrants as detail below.

- First quadrant represents the distance from budding cluster far from both phenotypes.
- Second quadrant represent the distance from budding cluster far from phenotype "X" but close to phenotype "Y'.

- Third quadrant represent the distance from budding cluster close to both phenotypes.
- Forth quadrants represent the distance from budding cluster close to phenotype “X” but far from phenotype “Y”

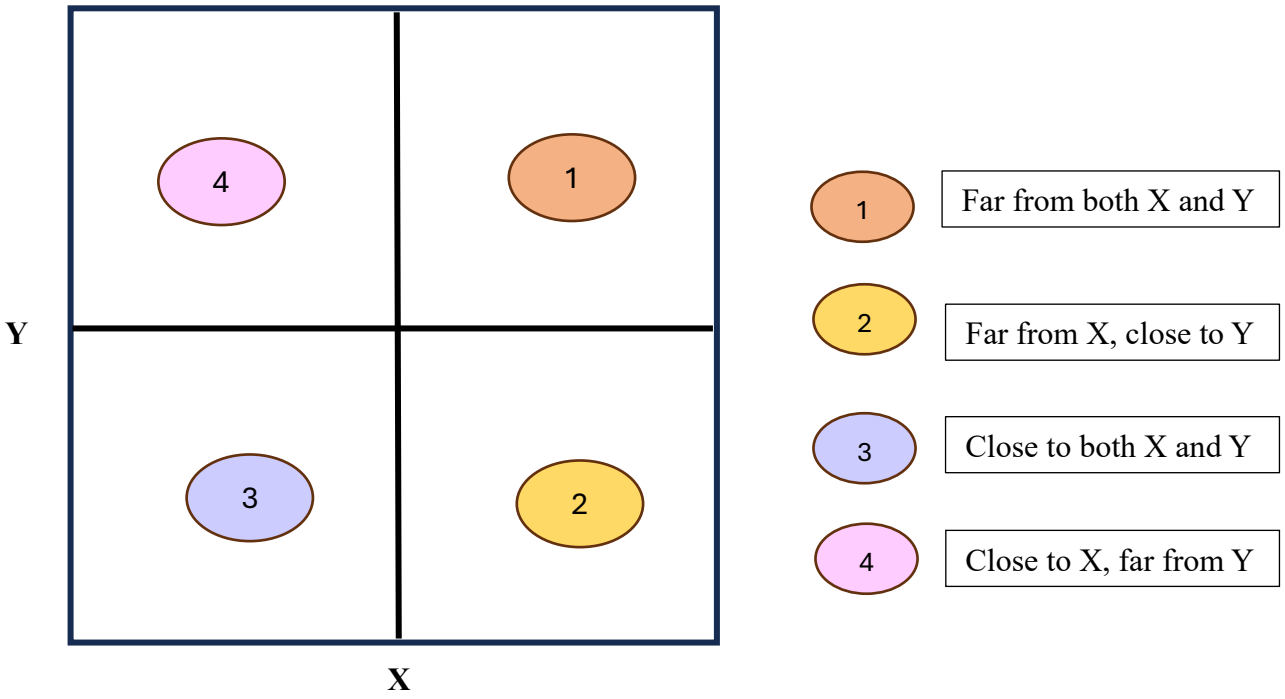

Figure 2.6 *The scatter plots diving into 4 quadrants representing the distance from tumours to two phenotypes (x and y).*

2.5. GeoMx Digital Spatial Profiler (DSP)

DSP provides the availability to access multiple areas on the same biological tissue to be able to investigate the heterogenous across the sample. The GeoMx platforms were illustrated in Figure 2.7. Staining will be performed with 1-4 specific antibody stained for tissue detection. After that, ROI will be imaged and selected using GeoMx suite. After the ROI selection, the machine will collect the sample by UV-cleavage of the specific oligo tag. The sample will be collected, and further analysis will be carried out using the readout platforms.

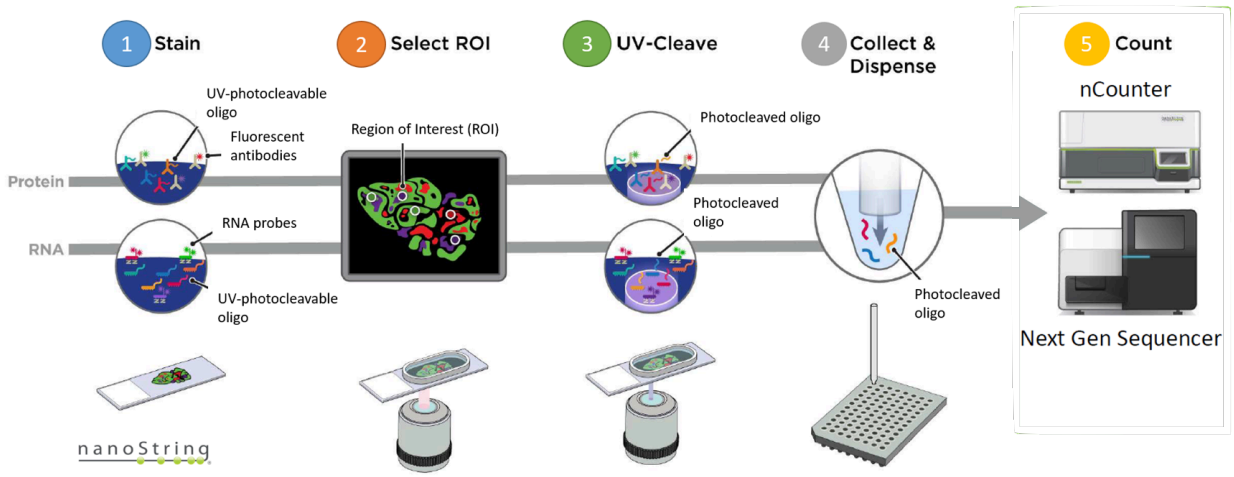

Figure 2.7 *GeoMx workflow provided by Nanostring. The sequence steps grouped into five phases: slide preparation (1), GeoMx instrument run (2-4) and readout (5).*

2.5.1. Preparation of slides

Twelve CRC full sections were cut at 5µm and baked for 30 minutes at 60 °C. The Leica BOND autostainer was employed to perform epitope retrieval (ER2, pH 9, 100°C) for 10 minutes and protein digestion using proteinase K (0.1µg/ml) for 15 minutes. The slides were then stored until required in 1X PBS. In-situ hybridisation of RNA-directed DNA oligo probes (Immune Pathways Panel, Nanostring) was performed according to the manufacturer's protocol. HybriSlip™ covers were applied prior to overnight incubation at 37°C for at least 16 hours (Thermofisher). After that slides were then washed twice with a 1:1 ratio of 100% deionized formamide (Ambion) and 4X SSC (Sigma Aldrich) at 37°C for 25 minutes. Immunofluorescence staining was performed using primary conjugated antibodies (pan-cytokeratin (PanCK), and CD45) and nucleic acid dye (SYTO 13). Slides were then stored at 4°C in SSC before being loaded on the GeoMx DSP instrument for collection. Multiplexed readout of RNAs using oligonucleotide tags was visualised by the cleaved tags that were attached to RNA probes. Region of interests was selected covering 1 to 5000 cells for the spatial profiling (170).

2.5.2. Region of interest selection (ROI)

Three ROIs were selected; invasive, stromal and tumour core area based on immunofluorescence staining of PanCK (Figure 2.8). The invasive front is defined as the area with a width of 500 µm from the main tumour. Positive PanCK was used to select tumour-rich regions, and negative PanCK was used to identify non-tumour region (i.e. stroma-rich regions). After ROIs were selected, the GeoMx platform used to automatically illuminate each ROI and specifically cleave barcodes. A microcapillary then collected the liberated barcodes from each region and plated them into an individual well on a microtiter plate. This process was repeated for each ROI before processing using Nanostring MAX/FLEX nCounter system.

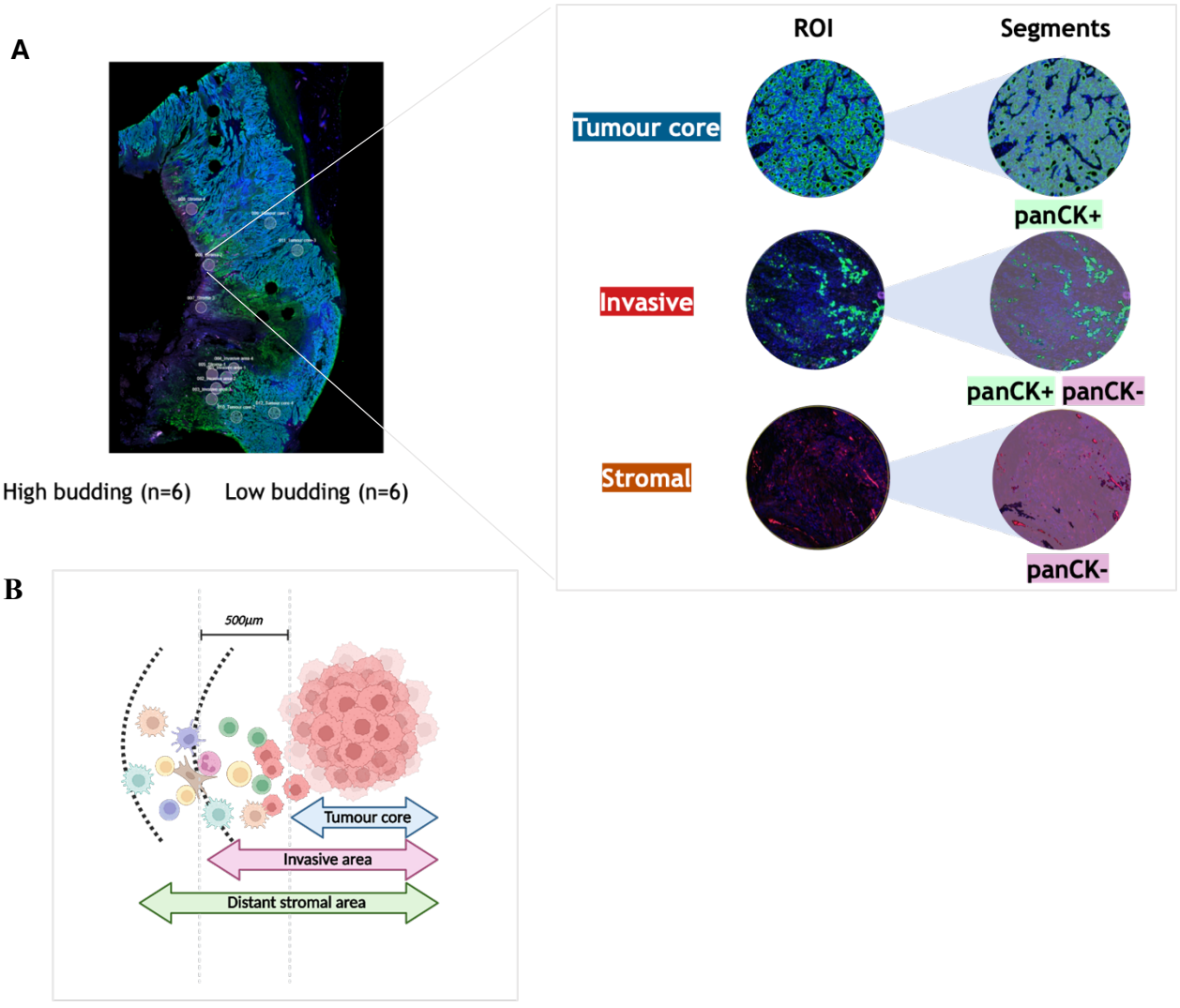

Figure 2.8 *(A)The fluorescent staining (PanCK+ and PanCK-) of CRC specimens and the ROI selected for each of the interested area. (B) Diagram shows defined area between tumour core, invasive and distant stromal areas.*

2.5.3. nCounter Hybridization Assay for Photocleaved Oligo Counting

nCounter readout of GeoMx DSP-collected probes was performed according to manufacturer's protocol (Nanostring, MAN-10089-08). Samples were resuspended in dH_20 prior to overnight incubation (16 – 24 hours) with hybridisation codes (Hyb Codes) at 65°C and heated lid (70°C), then pooled by column into 12-well strip tubes before processing on Nanostring's MAX/FLEX system. Data acquisition was performed in Nanostring's Digital Analyser (FOV, 555). Output files (.dcc) were then uploaded back on to the GeoMx system for preliminary analysis and data quality control (QC) checks using the GeoMx built-in analysis suite.

2.5.4. Data analysis

2.5.4.1. Quality control (QC)

GeoMx DSP analysis suite was used to perform preliminary analysis and QC checks on transcriptomic data follow quantification by Nanostring's nCounter system. Using the GeoMx data analysis suite, the sequenced data underwent technical QC to exclude regions with suboptimal binding density (<0.1, >2.25) and/or high positive control normalisation (>3). Signal-to-background ratio per target was visualised to determine the expression of genes within the panel (Figure 2.9). Target genes with less than 0 log signal-to-background would be considered a background signal.

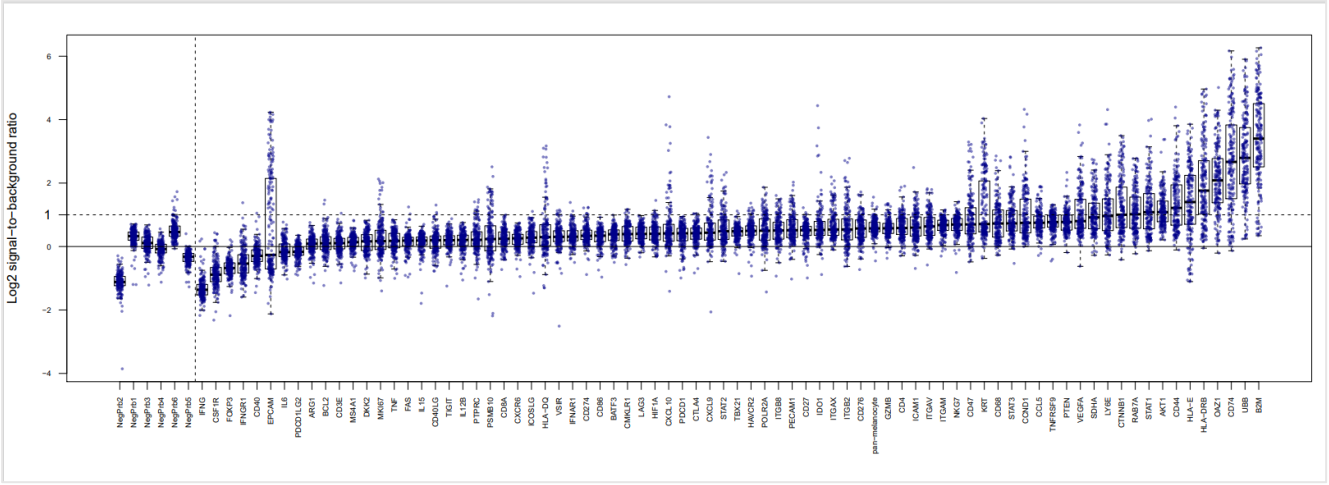

Figure 2.9 *Log2 signal to background ratio of genes in the panel for further quality control.*

2.5.4.2. Normalisation

The correlation between housekeeping genes was determined (*SDHA, POLR2A, UBB, OAZ1 and RAB7A*) (Figure 2.10) suggesting a consistency between individual genes. Next, the correlation between housekeeping genes and area / nuclei was determined. The weak correlation indicates the independence between variables suggesting that the housekeeping genes are suitable for data normalisation (Figure 2.11).

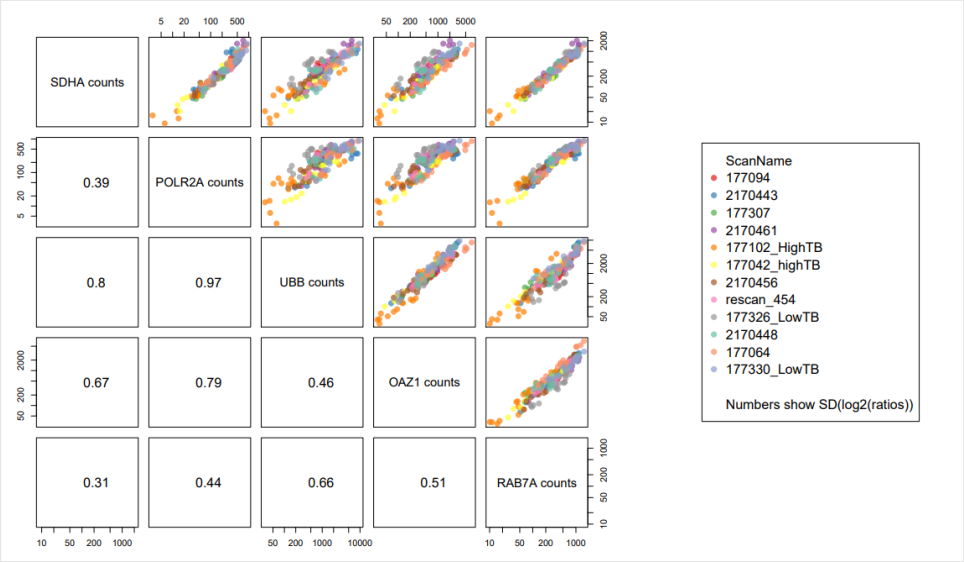

Figure 2.10 *The correlation between housekeeping genes across all CRC samples (n=12).*

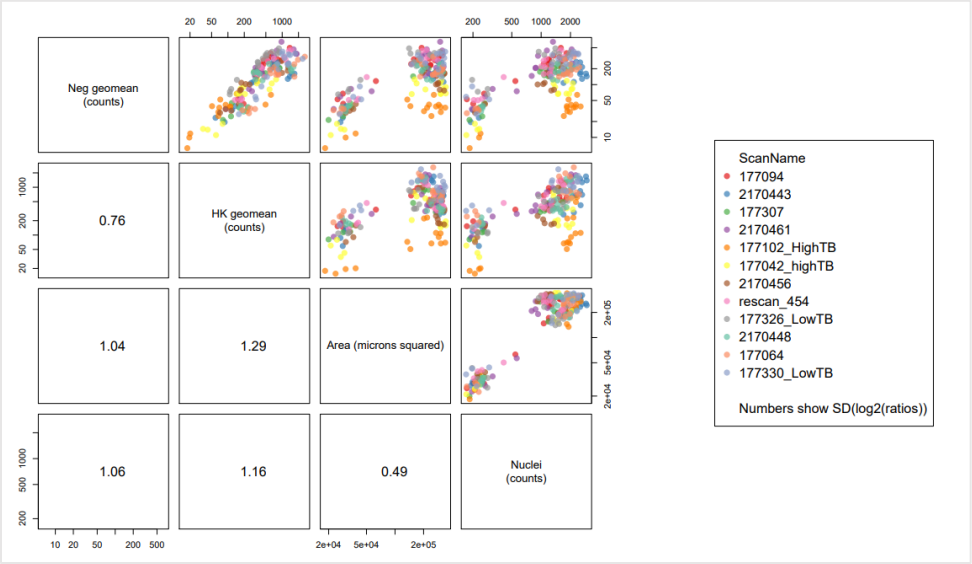

Figure 2.11 *The correlation between variables across all CRC samples (n=12).*

2.5.4.3. Statistical analysis

After normalisation, differential genes expression was determined between the groups of interested. Since the ROIs have been collected within the same sample, the linear mix model (LMM) statistical analysis was performed. The differentially expressed genes (DEGs) were screened out with the criteria of log2 fold change (FC) >± 1 and P-value <0.05. Volcano plots and heatmaps were selected for visualisation of the significant genes using GeoMx suite and R studio program to generate the plots.

2.6. Immunohistochemistry (IHC) staining to validate genes related to TB phenotype in CRC.

2.6.1. Antibody Validation

To ensure antibodies utilised were specific for the target protein, specificity testing was performed.

2.6.1.1. Protein measurement with Bradford assay

To make cell lysates, tumour cell lines HCT116, SW620, SW480, HT29 and MDAMB-231 were seeded in 75 cm^2 flasks and left until 80% confluent. After that, cells were then treated with 0.25% trypsin and washed with PBS. Cells were centrifuge at 2500rpm for 5 minutes and supernatant was carefully removed. Cell pellets were then moved to new Eppendorf tubes and wash three times with PBS to remove left over media then centrifuged at 8000rpm for 3 minutes. Consequently, PBS was discarded, and cell pellets were store in -20℃ until used.

To lyse protein for Bradford assay, 100ul of RIPA buffer (100ul RIPA, 1ul NH_3 1ul inhibitor and 1ul PMSF) (sc-24948A, Santa Cruz) was used to lysed cells. Cell pellets were mixed together with RIPA buffer and 0.5ml ultra-fine II Insulin Syring (328821, BD) was used to break the cells. The tubes were then incubated on ice for 1 hour to allow cells to lyse then centrifuged at 14000rpm for 10minutes to collect supernatant for further use. The protein concentration of each sample was determined using Bradford assay. The ratio of 1:20 was used

to fit the concentration in the standard curve. The standard curve (5000207, Bio-Rad) ranging from 0, 0.125, 0.25, 0.5, 0.75 and 1 was measured at 595nm then plotted to calculate the total protein concentration to run the gel. Each of the samples was measured three times per run to generate an average value.

2.6.1.2. Western blotting for antibody specificity

Gels were prepared in house (Table 2.4). Running buffer was prepared by diluting 100mL 10X running buffer (Tris 30g, Glycine 144g and SDS 5g) in 900mL distilled water. The gel tank was assembled, added to the Bio-Rad tank, and tested for leakage when the reservoir was filled with running buffer.

Table 2.4 *Table shows the reagents used to prepare per one gel for western blot.*

	Separating gel (ul)	**Stacking gel (ul)**
Deionised water	3180	1360
0.5M Tris HCL	2000	
1M Tris HCL		250
30% acrylamide	2660	340
10% ammonium persulfate (APS)	80	20
10% sodium dodecyl sulfate (SDS)	80	20
TEMED (catalyst)	4	4

Ladder (3µl) was loaded into lane 1 and 25-30 µl samples were added to remaining wells for each of the samples. Gels were run for 90 minutes or until the samples reached the edge of the gel at a constant 120 Volts. To prepare 1X running buffer, 100ml 10X Sodium dodecyl sulfate polyacrylamide gel electrophoresis (SDS-PAGE) with 900ml distilled water. To make 10X SDS-PAGE running buffer, 30g (0.12M) Tris, 144g (1M) Glycine, SDS 10g (0.02M) were dissolved 1L distilled water. Polyvinylidene fluoride (PVDF) membranes were soaked in methanol for 5-10 minutes. Sponges and filter paper were soaked in transfer buffer. The sandwich was prepared as outlined in Figure 2.12. A semi-dry transfer was used to transfer protein (cyclinD1) and Towbin buffer by diluting 100 ml of 10X Towbin (30.28g Tris, 144g

Glycine in 1L of distilled water) with 200ml Methanol, 5 ml 20% SDS in1L of distilled water was used as a transfer buffer. Both sandwiches will be rolled to remove any air bubbles. The assembled cassette was added to the tank and run at constant 300mA with 37amps per blot for 90 minutes to transfer protein from gels to the membranes.

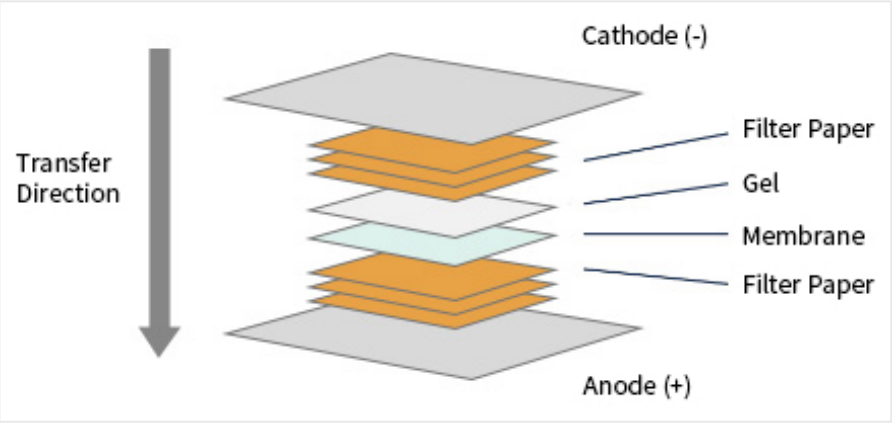

Figure 2.12 *Diagram showing the makeup of gel membrane sandwich utilised in western blot transfer step. Cited from* https://www.sinobiological.com/category/wb-semi-dry-transfer

Next, the sandwich was removed from the tank and membranes were blocked either in 5% skim milk or 3% BSA for 1 hour at room temperature. Membranes were incubated in appropriate primary antibody (diluted in 0.3% BSA) overnight at 4^{o}C and then washed in tris-buffered saline (TBST) 3 x 10 minutes. Membranes were incubated for 60 minutes in secondary antibodies (1:2000 for both anti-rabbit and anti-mouse antibodies diluted in 3% skim milk) at room temperature and then washed 3 x 10 mins in TBST. After washing, membranes were incubated in horse radish peroxidase (HRP) substrate enhanced chemiluminescence reagent (Pierce ECL) (Thermo Fisher Scientific, Waltham, MA, USA) for 5 minutes at room temperature. Consequently, membranes were blotted on blue roll and then imaged using Syngene Gene Sys (Syngene International Ltd, India).

2.6.1.3. Quantitative analysis of protein expression

The bands of protein expression from Western blot were quantified using imageJ program (version2.0.0-rc-43/1.52n). Briefly, the intensity of the bands was measured, and

housekeeping proteins were used to normalise the target protein expression, and the results were illustrated in box plot.

2.6.1.4. Cell pellets IHC staining

Cell pellets were used to validate the specificity of the antibpdies. Tumour cell lines (SW620, SW480, HT29, HCT119 and MDA-MB231) were passage into T75 flasks and incubated overnight. Cells were trypsinised and collected into a 15mL falcon tube with medium up to 10mL. Tubes were centrifuged for 5 minutes at 2500rpm. Supernatant was removed using an aspirator and the pellet resuspended in PBS then transferred to Eppendorf tubes. Cells were spun for 5 minutes at 2500rpm. Supernatant was removed and cells were resuspended in 1ml of 10% paraformaldehyde (PFA). The embedding process was carried out by the Department of Pathology, Faculty of Medicine, Siriraj Hospital. Slides were cut and store at 4 ℃ until used. Cell pellets were stained using the same IHC protocol outlined in Chapter2 section 2.6.2.

2.6.2. Immunohistochemistry (IHC) staining

TMAs were constructed to be representative either tumour core or invasive edge (n=439; low TB and n=180; high TB) from the GRI cohort were used to perform IHC for CD44, cyclinD1 by PH (tumour core) and JQ (invasive edge), STAT1 (BH) or IL6 receptor (AK).

For CD44, CRC full sections (n=290) of Thai cohort was also stained (PH).

2.6.2.1. Slide preparation

For the GRI cohort, TMA sections were requested from NHS GGC Biorepository and provided by Glasgow Tissue Research Facility. Slides were stored at 4^{o}C before use. Immediately before staining TMA sections were baked at 60^{o}C for 30 minutes to minimise the loss of cores.

For the Thai cohort, CRC full sections were requested from Department of Pathology, Faculty of Medicine, Siriraj Hospital. Slides were baked at 60^{O}C for 30 minutes prior to the staining.

2.6.2.2. Dewaxing and rehydration

For the GRI cohort, sections were parrafinised and retrieved antigen using PT module in Epredia™ Dewax and Heat Induced Epitope Retrieval (HIER) buffers pH 9 and 6 (fisher scientific, TA999DHBH) then heat up to 98C for 30 minutes.

For the Thai cohort, sections were dewaxed in Xylene (2 x 5 minutes) and rehydrated through a series of graded alcohols; (2 x 2 minutes in absolute ethanol, 1 x 2 minutes in 90% ethanol, 1 x 80% ethanol for 2 minutes) following with rinsing in running water.

2.6.2.3. Antigen retrieval

For the Thai cohort, formalin fixation antigen retrieval was performed using Tris EDTA buffer ph9 (Tris 1.12g, EDTA 0.37g in 1L distilled water). Appropriate buffer and pH were determined during antibody optimisation. After heating sections were left to cool for 30 minutes in buffer at room temperature and then rinsed in running water.

2.6.2.4. Blocking endogenous peroxidase activity

Slides were placed in 3% H2O2 (40ml H2O2 with 360ml distilled water for GRI cohort and 50ml 30% H2O2 with 450ml methanol for Thai cohort) for 10 minutes or 20 minutes (STAT1), to block endogenous peroxidases and reduce background staining then rinsed in running water.

2.6.2.5. Blocking non-specific binding

To prevent off-target non-specific binding, sections were incubated in a blocking solution. Tumour tissue on each slide was circled using a Dako pen (S2002, Dako, Agilent technologies, Stockport, UK) to prevent the solution running off the slides. 5% Horse serum (diluted with Blocking solution (5% horse serum) was added and slides were incubated for 1

hour at room temperature. Blocking solutions were diluted in antibody diluent (S0809, Dako, Agilent Technologies, Stockport, UK).

Table 2.5 *IHC conditions for each protein of interested.*

Protein	Buffer	Antibody dilution	Secondary
CyclinD1 (ab16663, abcam)	pH9	1:750	ImmPRESS® HRP Universal (Horse Anti-Mouse/Rabbit IgG) Dako Envision+ System HRP anti-rabbit (K4001) *
CD44 (156-3C11, Cell signalling)	pH9	1:400	ImmPRESS® HRP Universal (Horse Anti-Mouse/Rabbit IgG) Dako Envision+ System HRP anti-mouse (K4001)*
STAT1 (NB100-56314SS, Novusbio)	pH9	1:350	ImmPRESS® HRP Universal (Horse Anti-Mouse/Rabbit IgG)

**Stained in full sections in Thai cohort*

2.6.2.6. Primary antibody incubation

Antibodies were diluted to respective concentrations (Table 2.5) in antibody diluent for Glasgow (S0809, Dako, Agilent Technologies, UK) and 1X TBS (100ml 10X TBS (2.24g Tris and 0.74g NaCl in 2L distilled water) with 900 ml distilled water) for Thai cohort. Blocking solution was tapped off, diluted antibodies were added, and sections were incubated at 4^{o}C overnight.

2.6.2.7. Secondary antibody incubation

After incubation sections were washed twice in TBS for 5 minutes and then incubated in ImmPRESS® reagent (Vector Laboratories Inc, California, USA) for the Glasgow cohort or (K5007, Dako, Agilent Technologies, Stockport, UK) for Thai cohort for 30 minutes at room temperature. Slides were then washed twice in TBS for 5 minutes.

2.6.2.8. Visualisation with DAB substrate

Sections were incubated in DAB chromogen substrate from Vector Laboratories Inc, California, USA and Agilent Dako (K3468) for Glasgow and Thai cohort respectively. The

substrate was developed for 10 minutes at room temperature and subsequently rinsed in running water for 10 minutes.

2.6.2.9. Counterstaining, dehydration and mounting

Slides were counterstained in Harris Haematoxylin for 1 minute (for Glasgow cohort) or 10 minutes (for Thai cohort), then 5 minutes in lithium carbonate (for Thai cohort) or dipped in 1% acid alcohol (HCl in ethanol) for 3 seconds and blued in Scott's Tap Water Substitute (80mM Magnesium sulphate, 40mM sodium hydrocarbonate in distilled water) for 2 minutes in Glasgow cohort. Sections were dehydrated through a series of graded alcohols; 2 minutes in 70% or 80% ethanol (Glasgow and Thai cohort respectively), 2 minutes in 90% ethanol, 2 x 2 minute in absolute ethanol and then 2 x 1 minutes in Histoclear or Xylene (Glasgow and Thai cohort respectively). Coverslips were mounted onto slides using histological mounting medium Omnimount (HS-110, SLS, Nottingham, UK) or Agilent Dako (CS703) for Glasgow and Thai cohort respectively.

2.6.2.10. Slide scanning and visualisation

After staining slides were scanned onto NDP Viewer (Hamamatsu, Hertfordshire, UK) at x20 magnification using a Hamamatsu NanoZoomer (Hertfordshire, UK).

2.6.2.11. Scoring of IHC staining

For the GRI cohort, scoring was performed by a single observer (PH) blinded to clinical outcome data. Weighted histoscore assessment was performed at X20 magnification using: 0 x (% of cells not stained/negative) +1 x (% cells weakly stained) +2 x (% cells moderately stained) + 3 x (% cells strongly stained), giving a range of scores from 0-300. Manual histoscoring was employed to assess expression, 10% of cores were double scored by an independent observer with the correlation coefficient >0.7 achieved.

2.6.2.12. Statistical Analysis of IHC tissue-based studies

To set threshold values for high and low expression of each protein, log rank statistics were performed in R Studio (RStudio, Boston, MA, USA) using survminer, survival, tidyverse and maxstat packages. All further statistical analyses were completed using IBM SPSS version 28 (IBM, New York, USA). Kaplan Meier log rank curves were used to identify associations between protein expression and cancer-specific survival (CSS) within the GRI and Thai cohorts, Univariate and multivariate Cox hazard regression was performed to estimate the hazard ratio (HR) for CSS and identify the significant prognostic factors in CRC patients. Pearson's $\chi 2$ test was utilised to determine association between protein of interest and TB and the otherclinicopathological factors. Statistical significance was set to $p<0.05$.

2.7. RNAscope®

To detect soluble chemokines that may be involved in TB phenotype, a novel RNA in situ hybridisation RNAscope (ACD Bio, California, USA) was performed by Colin Nixon at the CRUK Beatson Institute on the Glasgow combined cohort TMAs (n=787). This technique enabled quantitative detection of CXCL9 and CXCL10, which were unable to be detected by IHC to a sufficient quality. At the same time of CXCL9 and CXCL10 probing, staining of housekeeping gene, UBC, was also performed in the GRI cohort. CXCL9 and CXCL10 counts was quantified using Halo digital pathology software (Indica Labs, Albuquerque, NM, USA). A classifier to distinguish between tumour and stromal rich areas was built to measure CXCL9 and CXCL10. Thresholds were set to measure the intensity of brown staining indicative of the level of CXCL9 and CXCL10 mRNA copies. Raw scores for CXCL9 and CXCL10 within the tumour and stroma were normalised to UBC scores. Cut offs for high and low phenotype were determined as for IHC protein expression and data were entered into IBM SPSS version 28 software (IBM, New York, USA). Statistical analyses were performed as for IHC protein expression (Chapter2 section 2.6.2.12)

2.8. In vitro studies

2.8.1. Colon cancer cell line culture

Colon cancer cell lines were cultured in ATCC recommended growth medium and FBS, as outlined in table 2.6. Cells were grown in T75 flasks at 37^{O}C 5% CO_2 and medium was changed every 2-3 days. Upon reaching 70% confluence cells were passaged using 0.05% Trypsin (Thermo Fisher Scientific, Waltham, MA, USA). Mycoplasma testing was performed once every 3 months. Brightfield images of HT29, HCT116, SW480 and SW620 were taken at X40 magnification pre-treatment to visualise distinct morphological differences between each cell line (Figure 2.13).

Table 2.6 *Table outlining colorectal cell lines used to study budding formation.*

Cell line	CMS	MSI	Mutation	Medium
HCT116	Mesenchymal	MSI-H	KRAS, PI3K	RPMI 1640 Media (Gibco), 10% FBS
HT29	Metabolic	MSS	BRAF, PI3K, TP53	Dulbeccos Modified Eagle Medium (DMEM) (Gibco), 10% FBS
SW480	Mesenchymal	MSS	KRAS, TP53	Dulbeccos Modified Eagle Medium (DMEM) (Gibco), 10% FBS
SW620	Mesenchymal	MSS	KRAS, TP53	Dulbeccos Modified Eagle Medium (DMEM) (Gibco), 10% FBS

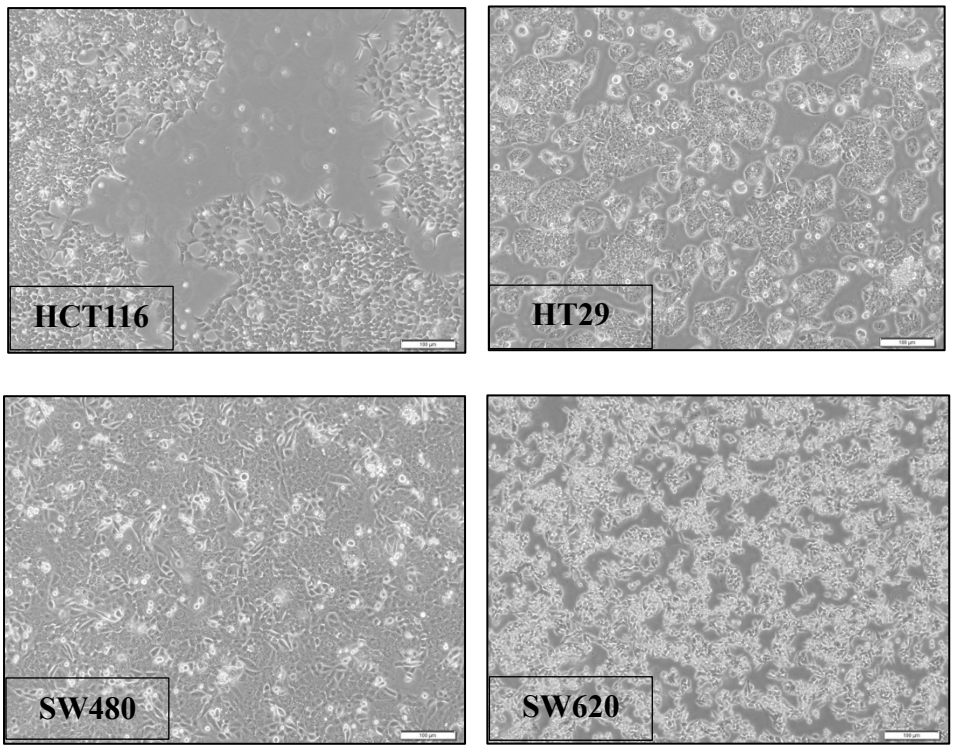

Figure 2.13 *Light microscopy images taken at X20 magnification of HCT116, HT29, SW480 and SW620 colorectal cell lines showing distinct morphologies.*

2.8.2. 2D experiment

CRC cell lines were used to investigate which signalling pathway might drive tumour progression and perhaps budding formation. CRC cell lines were seeded at $1x10^5$ cells per well of a 6 well plate. Cells were left to attach to the surface at 37 ^{O}C overnight. Then incubated with serum free media for 24 hours to reduce possible interfering factors for cell growth. Next, medium was changed, and cells were treated with either complete medium (DMEM or RPMI with 10%FBS), 0.01%HCL and TNF-α (20ng/ml). After 24 hours, the medium was change again with either complete medium (DMEM or RPMI with 10%FBS), 0.01%HCL and pretreated with TNF-α (20ng/ml) 24 hours then with TGF-β (10ng/ml) for another 24 hours at 37 ^{O}C. After that medium was removed and washed with PBS. 0.25% Trypsin was used to trypsinise cells and cell pellets were processed to run on western blots as describe in Chapter2 section 2.6.1.2.

2.8.3. Spheroid tumour cell lines

2.8.3.1. Treatment of TNF-α and TGF-β inducing budding formation

CRC cell lines (HT29) were seeded at $5x10^5$ cells with 100% BME onto coverslips in 6 well plates (20µL BME 'dot' per well; total6 dots). The media was added every 3 days. After they form an appropriate size, spheroids were treated with complete media (DMEM with 10%FBS), 0.01%HCL and TNF-α (20ng/ml), after 24 hours of incubation media was changed and cells were treated again with complete media (DMEM with 10%FBS), 0.01%HCL and TNF-α (20ng/ml)/TGF- β (10ng/ml) for 24 hours at 37 °C. Spheroids were collected and IF were used to visualise target protein.

2.8.3.2. Immunofluorescences (IF)

For each protein of interest 100-200 spheroids were required (2-3 wells) and during each IF experiment. Medium was removed using a P1000 Gilson pipette. Wells were washed with 500ul of PBSB (1X PBS with 0.1% BSA) then with 500ul cold PBS and left on ice for 10 minutes. Next, PBS was carefully removed, and cells were then washed again in cold PBS on ice for 30 minutes. Spheroids were fixed in 4% paraformaldehyde on ice for 30 minutes and then washed in PBS on ice for 10 minutes. PBSDT (PBS 1X 0.5% TritonX 1% DMSO 1% BSA 1% FBS) was used to block spheroids for 1-3 hours at room temperature with gentle agitation. Following the blocking, spheroids were incubated in primary antibody, diluted in PBS with 0.1% bovine serum albumin, as shown Table 2.7, for 24-48 hours at 4°C with gentle agitation. A negative control (no primary antibody) was included. Cells were then washed in PBSB and left to settle for 10 minutes at room temperature. Spheroids were resuspended in appropriate secondary antibody (Table 2.7), together with hoechst dyes (1:1000 in PBSB) for Nuclei detection, for 2-3 hours at room temperature in the dark. Spheroids were then washed in PBSB for 10 minutes at room temperature three times. Coverslips with spheroids were then placed onto slides with 50% glycerol in PBS placed onto the centre of a glass slide. Slides were

kept in the dark at 4^{O}C overnight. Visualisation was performed using a Zeiss LSM 780 confocal microscope (Carl Zeiss AG, Oberkochen, Germany). The 10x objective lens was used to locate organoids on the slide and images were taken with the x20 objective lens. Zeiss Zen 2 software (Carl Zeiss AG, Oberkochen, Germany) was used to adjust the gain and save images.

Table 2.7 *IF staining condition for CRC spheroids*

Primary antibodies	**Company**	**Dilution**	**Secondary antibodies**	**Dilution**
CyclinD1	Abcam (ab16663)	1:200	Anti-rabbit (IC1051G)	1:2000

2.8.4. Mouse-derived organoids

Mouse-derived organoids were kindly given by Samson group. These organoids were derived from primary tumours of induced *villin*Cre^{ER}*Apc*$^{fl/fl}$ *Kras*$^{G12D/+}$ *Trp53*$^{fl/fl}$ *Trgfbrl*$^{fl/fl}$ (AKPT) mice. Organoids were cultured in Advanced DMEM/F12 supplemented with penicillin/streptomycin (100 U/ml/100 µg/ml) (15140122), 2 mM L-Glutamine (25030081), 10 mM HEPES (15630080), N2-supplement (17502001) and B27-supplement (17504044) (all from Gibco, Life Technologies or ThermoFisher-Scientific). Other supplements were added before the media was used, 50 ng/ml Recombinant Human EGF (Peprotech, AF-100-15) and 100 ng/ml Recombinant Murine Noggin (Peprotech, 250-38). Organoids were cultured in 6 wells plate with 100% BME (20ul BME 'dot') at 37 ^{O}C. Media was changed every three days.

2.8.4.1. Incucyte assay

AKPT organoids were grown to 70-80-% confluence then cultured in 96 well plates to perform live cell imaging with 50% BME each well at 37 ^{O}C. Organoids were plated in 96 well plates for 24 hours before being placed into the Incucyte for imaging. After 24 hours, the plate was taken out and the organoids were treated with media supplemented with TNFα for 24

hours. Following by media supplemented with both TNF-α and TGF-β, then left for 72 hours. The live imaging monitored budding formation over time.

2.8.5. Data quantification and analysis

2.8.5.1. IF Quantification

The images were quantified using ImageJ analysis program (version 1.8.0_345 (64-bit)). The intensity was measured to determine the differences in fluorescence signal between comparison groups.

2.8.5.2. Organoid's roundness

The roundness of organoids was determined to identify the differences between control and treated groups. ImageJ (version 1.8.0_345 (64-bit)) was used and the plugin was applied regarding the measurement.

2.8.5.3. Statistical analysis

For IF spheroid staining, unpair welch's t test was used for statistical differences (significant value, $p<0.05$). In additions, the statistical differences between the roundness of organoids in treated and control groups was determined using 2way ANOVA statistical test for different time periods.

Chapter 3. Assessment of tumour budding and its association with clinical data in colorectal cancer clinical specimens

3.1. Introduction

Colorectal cancer (CRC) is the third most diagnosed cancer and the second most lethal malignancy worldwide. In 2018, nearly 2 million cases of CRC were registered (1), and the global trend is likely to increase in the coming decades (171). Metastasis is the major cause of CRC-related death with increasing evidence of multiple factors and pathways modulating the metastatic route in patients with colorectal carcinoma (70). Currently, there is no pathological feature available to identify which patients are at risk of disease recurrence, making the treatment of CRC patients very challenging. Therefore, novel prognostic markers are required to guide the prognostic accuracy and effective targeted therapeutic strategies in CRC patients. Tumour budding (TB) is a prognostic marker now included in standard pathological reporting for CRC and is known to be associated with tumour progression and metastasis (6). Tumours with high TB have been shown to have the worst outcome in many types of cancer including CRC (138). Moreover, an international budding consensus conference (ITBCC) has recommended the inclusion of TB in clinical reports (8). With regards to the correlation between poor survival in CRC, the relationship between TB and adverse clinical factors has been reported (172-177), demonstrating it is a strong prognostic marker in CRC.

Along with inflammation, there is strong evidence that supports the role of the tumour microenvironment (TME) in tumour development, making it a crucial target for therapeutic treatment (71, 72). Moreover, the interaction between the tumour and its TME has been shown to play an important role in tumour progression and metastatic progression in various types of cancer including CRC (96, 178). With regards to budding phenotype, the relationship between TB and the TME has recently been the focus of intense investigation. High numbers of TB at the invasive margin of the tumour inversely correlate with cytotoxic T cells (18, 179) indicating the suppression of cytotoxic anti-tumour activity when a tumour is enriched with a high number of budding cells. One study from Dawson *et. al* proposed a combination score using number

of TB and the density of CD8+/CD3+ T cells demonstrating a strong prognostic marker of the combined scores compared to those with only TB or T cells phenotype (180). Thus, the TME may play a crucial role in influencing TB to provide suitable conditions for CRC progression and metastasis. Recently, multiplex immunofluorescence (mIF) technologies have been widely used as they have the advantage of detecting multiple biomarkers in a single tissue section (181). A few studies have reported the correlation between TB and its TMEs using mIF, giving a spatial TME profile within the budding area in the same CRC tissue (18, 179, 182).

This research aims to investigate the underlying mechanism of TB and its association with surrounding TMEs. The verification of the prognostic role of TB in CRC patients will be investigated. The interaction between budding cells and the correlation with TMEs will also be investigated.

3.1. Clinicopathological parameters of colorectal cancer patient cohort

644 patients were included in this study after the exclusion criteria were applied. Full CRC H&E sections were used to identify the budding phenotype (HW and PH), mGPS and GMS (PA) scores. DNA sequencing of CRC tissue was performed to determine the mutational status of either *KRAS* or *BRAF* (CW). IHC staining was used to identify MMR status within the cohort (JH). In addition, a previously constructed TMA (n=787) from tumour core was utilised for mIF staining in this study. Three cores were selected to represent the biology of CRC patients in the primary tumour area. Cancer-specific survival (CSS) was employed as a primary endpoint for patients' survival in months from the date of surgery until recurrence or cancer-cause mortality. 205 (32%) patients were under 65, 208 (32%) were between 65-74 and 231 (36%) were over 75 years of age, with 353 males and 291 females. Clinical characteristics were collected to further investigate the association with patients' survival or other biological markers in CRC (Table 3.1).

Table 3.1 *Patients characteristic in GRI cohort (N=644)*

Characteristic		
Sex		
	Female	291 (45%)
	Male	353 (55%)
Age		
	<65	205 (32%)
	65-74	208 (32%)
	>75	231 (36%)
Tumour site		
	Right	260 (40%)
	Left	384 (60%)
Recurrence status		
	No	441 (68%)
	Local	38 (6%)
	Distant	110 (17%)
	Both local/distant	17 (3%)
	Missing data	38 (6%)
Adjuvant therapy		
	No	486 (76%)
	Yes	157 (24%)
	Missing data	1 (0%)
TNM stage		
	I	87 (14%)
	II	308 (48%)
	III	249 (39%)
T stage		
	1	30 (5%)
	2	74 (12%)
	3	375 (58%)
	4	165 (25%)
N stage		
	0	395 (61%)
	1	182 (28%)
	2	67 (10%)
Margin involvement		
	No	608 (94%)
	Yes	36 (6%)
Peritoneal involvement		
	No	498 (77%)
	Yes	146 (23%)
Perineural invasion		
	No	249 (39%)
	Yes	65 (10%)
	Missing data	330 (51%)
Tumour perforation		
	No	631 (98%)
	Yes	13 (2%)

Lymph nodes	>12 nodes <12 nodes	485 (75%) 159 (25%)
Venous invasion	No Yes	320 (50%) 324 (50%)
TB	Low High Missing data	441 (69%) 180 (28%) 23 (3%)
KRAS mutational status	Wildtype Mutant Missing data	420 (65%) 211 (33%) 13 (2%)
BRAF mutational status	Wildtype Mutant Missing data	588 (91%) 43 (7%) 13 (2%)
MMR status	dMMR pMMR loss 2 sets (MLH1/PMS2 or MHS2/6) Missing data	111 (17%) 418 (65%) 100 (16%) 15 (2%)
TSP	Low High Missing data	490 (76%) 133 (21%) 21 (3%)
KM	Low High Missing data	519 (81%) 103 (16%) 22 (3%)
GMS	0 1 2 Missing data	103 (16%) 399 (62%) 120 (19%) 22 (3%)
mGPS	0 1 2	409 (64%) 137 (21%) 98 (15%)

TB =Tumour budding, dMMR = deficient mismatch repair, pMMR = proficient mismatch repair, TSP = Tumour stroma percentage, KM = Klintrup-Mäkinen, GMS = Glasgow Microenvironment Score, mGPS = modified Glasgow prognostic score

3.2. The assessment of tumour budding in CRC specimens

According to ITBCC guidelines, the assessment of TB was made using tissue sections stained with H&E. The guideline stated that 20x objective magnification should be applied and the number of TB was counted at the invasive tumour area. Ten specific areas at the invasive front (0.785 mm^2) were marked to quantify the number of TB for further evaluation. The densest area of buds represents the budding phenotype of each CRC case. The criteria were divided into 3 groups: BD1 (0-4buds), BD2 (5-9 buds) and BD3 (>10buds) (8). However, for the purpose of this project, BD1 and BD2 are combined and defined as low budding while BD3 represents a high budding phenotype to produce the most distinct phenotype between high and low budding in CRC patients (Figure 3.1). Of the 644 patients, budding cells could not be identified, due to the heavy fat area, highly inflamed tissue and not enough tumour (less than 10% of the whole slide) showed, in 23 cases therefore 621 patients were included to further validate the prognostic role of TB in the CRC cohort.

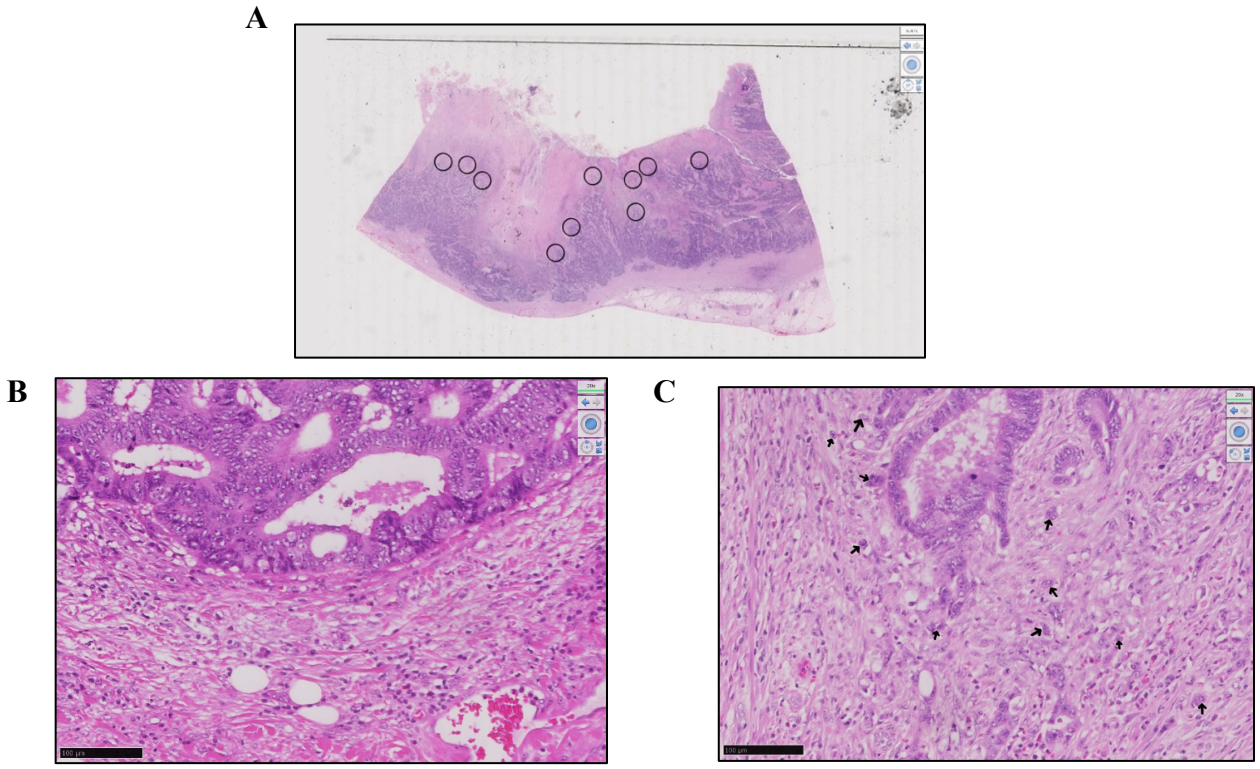

Figure 3.1 *(A) H&E stained with the 10 hotspots area at the invasive front (B) Representative image for (B) low and (C) high budding phenotype in CRC sections.*

3.3. The prognostic role of tumour budding in CRC patients.

The survival of patients with high TB (n=180) was significantly lower than those with low TB when Kaplan-Meier survival analysis was performed (n=439) (HR=1.934, 95%CI; 1.408-2.658, log-rank p<0.001) (Figure 3.2). Life tables demonstrated that 60% of patients with high budding versus 75% of patients with low budding were alive 10 years after initial diagnosis.

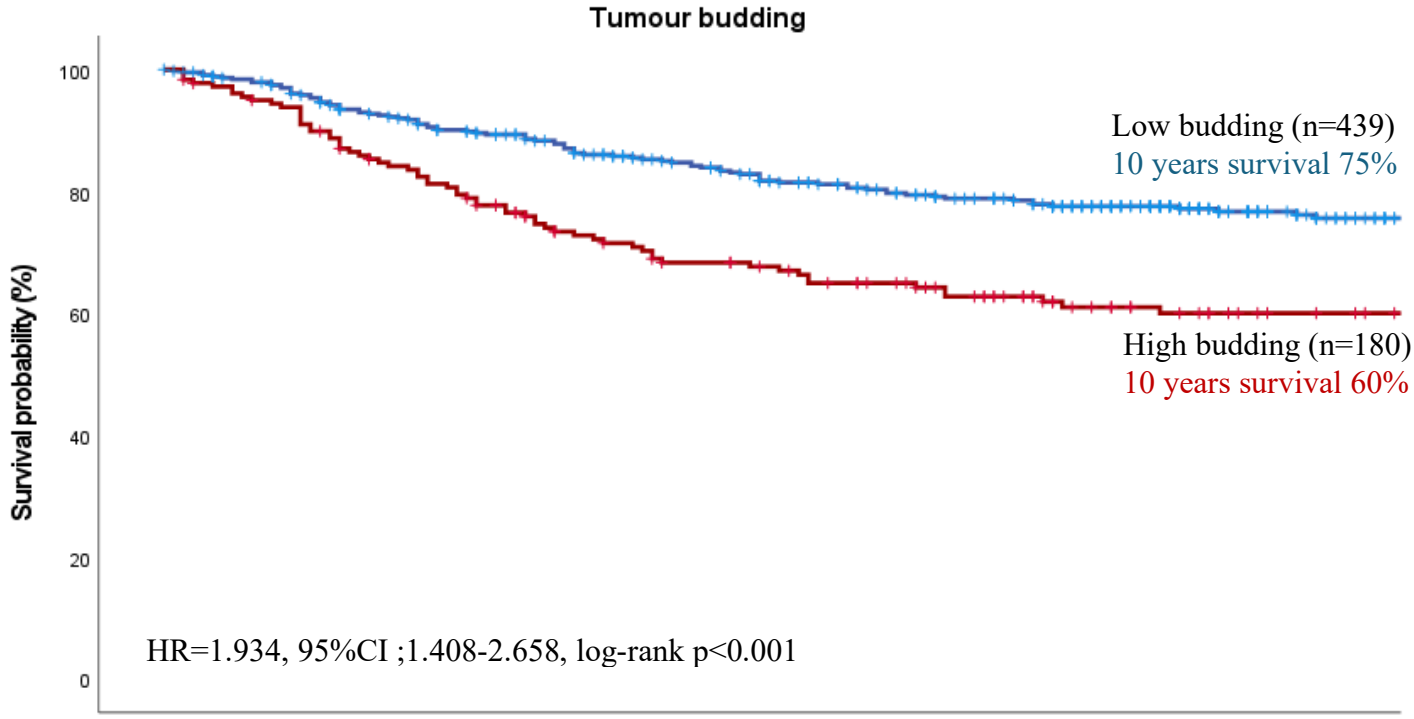

months	0	12	24	36	48	60	72	84	96	108	120
Low budding	439(0)	416(12)	383(23)	357(37)	327(53)	303(66)	277(84)	258(97)	222(129)	165(185)	132(215)
High budding	180(0)	167(3)	144(8)	127(12)	112(19)	103(23)	93(28)	83(35)	66(50)	57(58)	52(63)

Figure 3.2 *Kaplan-Meier survival analysis based on tumour budding phenotype for cancer specific survival (CSS) in CRC patients. Hazard ratio (HR) was reported with 95% confidence intervals. P Values were calculated using the log-rank test comparing low (n=439) and high (n=180) budding phenotype.*

Additionally, there is a significant positive correlation between high tumour budding and clinical characteristics of CRC patients such as TNM (TNMIII, P=0.003), T stage (T4, P=0.004), N stage (N2, P=0.002), adjuvant therapy (Yes, P<0.001), Recurrence (local, P=0.002), tumour perforation (positive, P=0.046), venous invasion (positive, P=0.006), peritoneal involvement (positive, P=0.002), perineural invasion (positive, P=0.012), Klintrup

Mäkinen score (KM) (High, P=0.015) and a negative association with Glasgow microenvironment score (GMS) (GMS0, P=0.046). (Figure 3.3) (Table 3.2). When the clinical characteristics and TB phenotype was entered into Cox regression analysis, multivariate analysis revealed that age, MMR status, recurrence status, n stage, margin involvement and TB were shown to be independent prognostic factors for CRC CSS survival (p=0.006, p=0.032, p<0.001, p<0.001, p<0.001 and p=0.040 respectively) (Table 3.3).

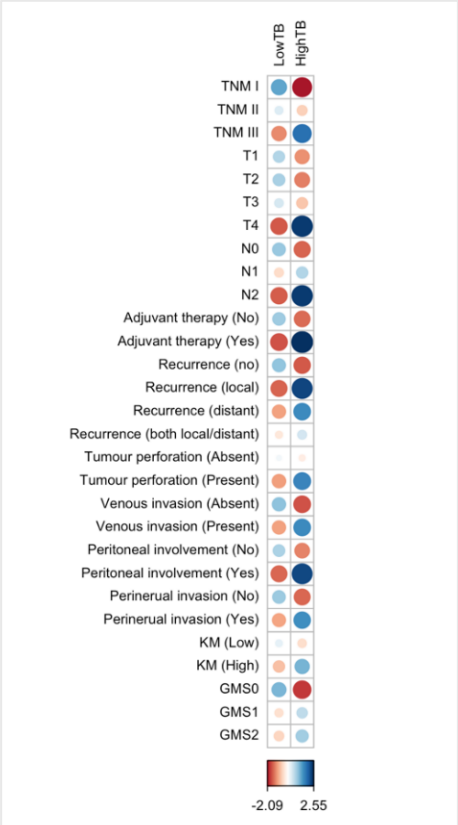

Figure 3.3 *The correlation plot for the Pearson's chi-square test residual for TB phenotype with other clinical factors (p value <0.05); positive associations are in blue and no association in orange, the bigger size of the circle the more significant association was found).*

Table 3.2 *The relationship between budding status and clinicopathological characteristic using the Pearson's chi-square analysis in CRC patients (n=621)*

	Low budding n=441	**High budding n=180**	**P-value**
Host characteristics			
Age <65 65-74	 141 (32) 138 (31)	 57 (32) 62 (34)	0.710

>75	162 (37)	61 (34)	
Sex			0.719
Female	203 (46)	80 (44)	
Male	238 (54)	100 (56)	
Tumour characteristics			
Tumour site			0.566
Right	171 (39)	78 (43)	
Left	148 (33)	57 (32)	
Rectum	122 (28)	45 (25)	
TNM stage			**0.003**
I	70 (16)	14 (8)	
II	215 (49)	80 (44)	
III	156 (35)	86 (48)	
T stage			**0.004**
1	24 (5)	5 (3)	
2	57 (13)	15 (8)	
3	263 (60)	97 (54)	
4	97 (22)	63 (35)	
N stage			**0.002**
0	285 (65)	94 (52)	
1	121 (27)	57 (32)	
2	35 (8)	29 (16)	
Adjuvant therapy			**<0.001**
No	347 (79)	118 (66)	
Yes	93 (21)	62 (34)	
Recurrence			**0.002**
No	320 (77)	106 (62)	
Local	18 (4)	18 (11)	
Distant	67 (16)	40 (24)	
Both local/distant	11 (3)	6 (3)	
Tumour perforation			**0.046**
Absent	435 (99)	173 (96)	
Present	6 (1)	7 (4)	
Margin involvement			0.107
No	421 (95)	166 (92)	
Yes	20 (5)	14 (8)	
Lymph nodes			0.615
<12 Nodes	112 (25)	139 (77)	
>12 Nodes	334 (75)	42 (23)	
Venous invasion			**0.006**
Absent	232 (52)	73 (40)	
Present	209 (48)	107 (60)	

Peritoneal involvement			**0.002**
No	355 (81)	124 (69)	
Yes	86 (19)	56 (31)	
Perineural invasion			**0.012**
No	185 (82)	58 (70)	
Yes	38 (17)	25 (30)	

Table 3.3 *Univariate and Multivariate analysed for cancer specific survival (CSS).*

Clinicopathological characteristics	Univariable analysis		Multivariate analysis	
	Hazard ratio (95% CI)	***P***	**Hazard ratio (95% CI)**	***P***
Sex	1.286 (0.94-1.76)	0.117		
Age	1.29 (1.07-1.56)	0.008	1.49 (1.12-1.99)	0.006
MMR status	0.65 (0.49-0.85)	0.002	0.58 (0.36-0.95)	0.032
Recurrence status	4.29 (3.64-5.07)	<0.001	4.72 (3.59-6.19)	<0.001
TNM stage	2.64 (2.02-3.46)	<0.001		
T stage	1.89 (1.49-2.39)	<0.001		
N stage	2.19 (1.80-2.67)	<0.001	1.87 (1.33-2.63)	<0.001
Margin involvement	4.22 (2.69-6.63)	<0.001	6.67 (3.16-14.07)	<0.001
Perineural invasion	3.63 (2.35-5.60)	<0.001		
Peritoneal involvement	2.10 (1.52-2.89)	<0.001		
Tumour perforation	2.79 (1.23-6.31)	0.014		
Venous invasion	1.60 (1.17-2.19)	0.003		
TB	1.93 (1.40-2.65)	<0.001	1.64 (1.02-2.62)	0.040

MMR = Mismatch repair, TB = Tumour budding

3.4. The association between tumour budding and sex differences in colorectal cancer patients.

The chi-square test revealed no association between TB and sex difference (Table 3.4) as well as the differences in budding cells between males and females (Figure 3.4). The survival analysis showed no significant difference in patient survival; however, male patients tend to have a poorer outcome when compared to female patients in both low (HR=1.345, 95% CI;0.885-2.045 log-rank p=0.165) and high (HR=1.169, 95% CI;0.712-1.922 log-rank p=0.537) budding groups (Figure 3.5). The life table showed that, in the low budding group, the percentage of female (80%) survivors is higher than males (72%). A similar trend was reported

in the high budding group, females (65%) survive longer than male (56%) after 10 years of diagnosed.

Table 3.4 *The relationship between budding status and sex difference using the Pearson's chi-square analysis in CRC patients (n=621)*

	Low budding n=441	**High budding n=180**	**P-value**
Sex			0.719
Female	203 (46)	80 (44)	
Male	238 (54)	100 (56)	

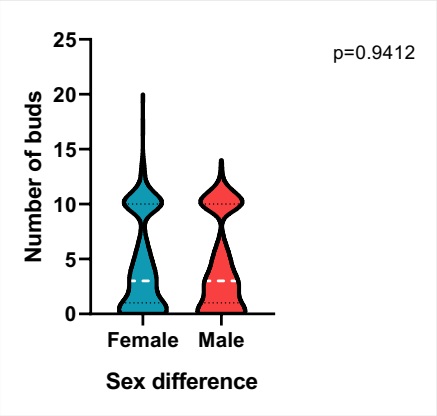

Figure 3.4 *Violin plots show the continuous number of buds compared between female and male.*

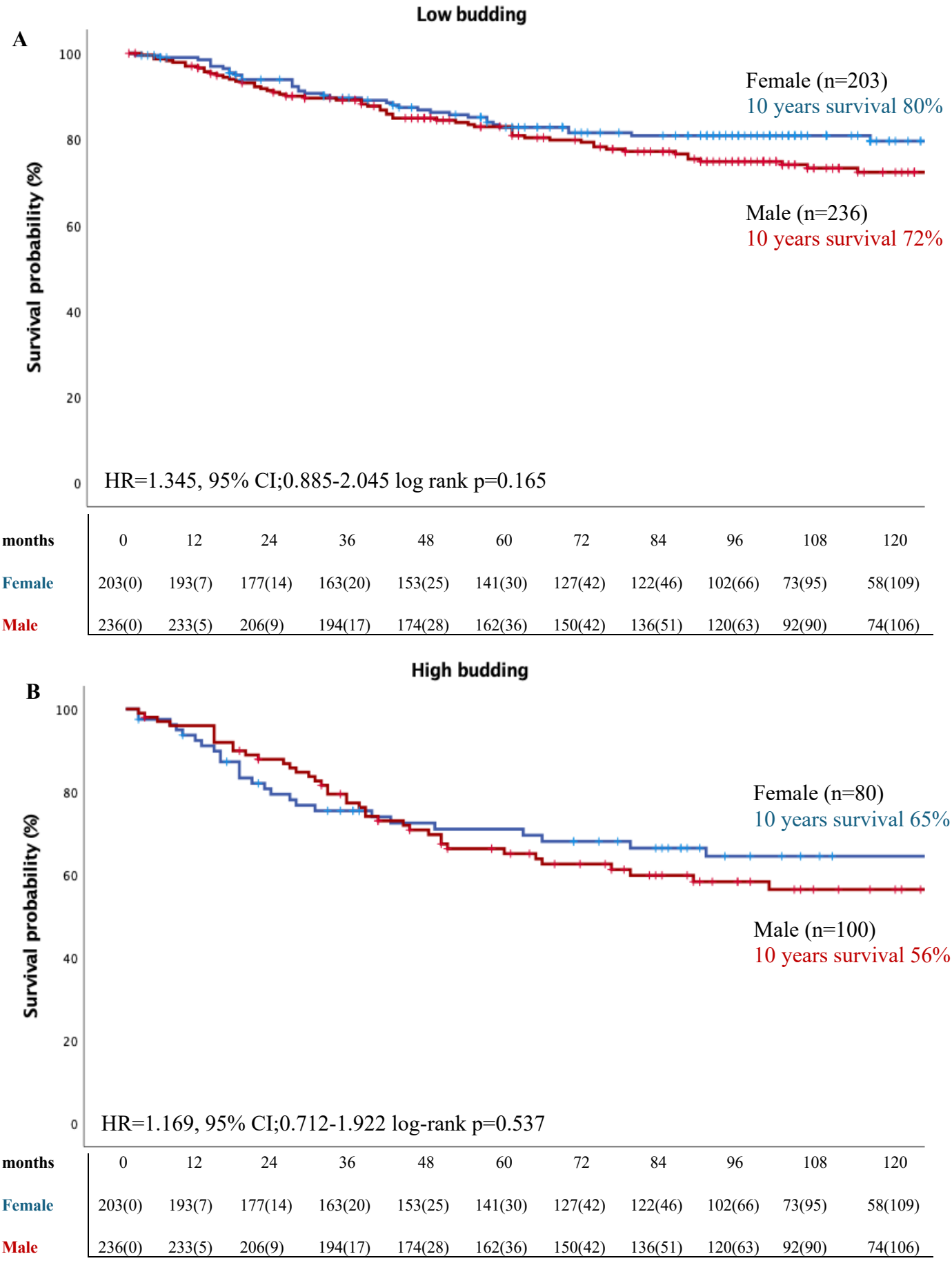

Figure 3.5 *Kaplan-Meier survival analysis based on sex difference status stratified by (A) low and (B) high budding phenotype for cancer specific survival (CSS) in CRC patients. Hazard ratio (HR) was reported with 95% confidence intervals. P Values were calculated using the log-rank test comparing each budding group with sex differences.*

3.5. The association between tumour budding and mutational status in colorectal cancer patients.

The correlation between TB and mutational genes was investigated in the GRI CRC cohort to determine if the mutational landscape could be involved in CRC budding phenotype. According to the Chi-square statistical test, there is no significant association between TB and CRC mutational status (Table 3.5). However, it was hypothesised that tumours with/without mutation may have different outcomes regarding budding phenotypes. Therefore, further analysis was conducted to investigate if TB phenotype could have an impact on patients' survival when exhibiting certain types of mutations.

Table 3.5 *The relationship between budding status and mutational status using the Pearson's chi-square analysis in CRC patients (n=621)*

	Low budding n=441	**High budding n=180**	**P-value**
KRAS Wild type Mutant	 290 (67) 141 (33)	 116 (65) 63 (35)	0.554
BRAF Wild type Mutant	 398 (92) 33 (8)	 170 (95) 9 (5)	0.243
MMR status dMMR pMMR lost 2 set of MLH1/PMS2 or MHS2/6	 75 (17) 288 (67) 69 (16)	 32 (18) 118 (68) 25 (14)	0.861

3.5.1. KRAS/BRAF mutations

When stratified with budding phenotype, the CSS of patients with or without KRAS and BRAF mutations did not differ significantly in either low (HR=0.683, 95% CI;0.426-1.097 log rank p=0.115 and HR=1.119, 95% CI;0.517-2.419 log-rank p=0.776 respectively) or high (HR=1.207, 95% CI;0.734-1.982 log-rank p=0.458 and HR=1.207, 95% CI;0.734-1.982 log rank p=0.458 respectively) budding CRC (Figure 3.7-3.8). However, patients with mutated *KRAS* experienced a shorter survival with a 10-year cumulative survival of 55% when

compared to 63% of those with wildtype *KRAS* in high budding group. Interestingly, a higher proportion of patients with mutated *BRAF* (65%) was found after 10 years when compared to wild type group (59%). In concordance with the above finding, though no significant differences, there is a higher number of average budding cells when tumours presented with *KRAS* mutations compared to wild type *KRAS* (p=0.3013) whereas a low number of buds was frequently found in mutated *BRAF* when compared to the wildtype group (p=0.034) (Figure 3.6). Although no statistical significance was found, high TB may have a role in an aggressive tumour characteristic in CRC.

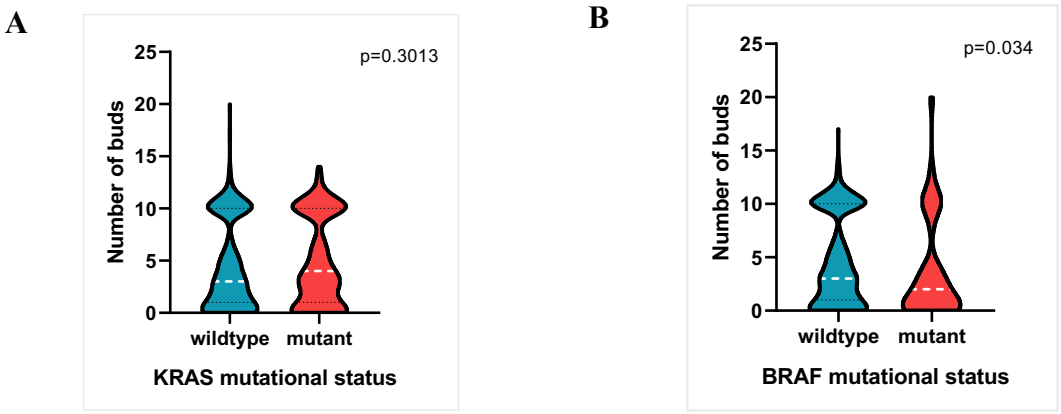

Figure 3.6 *Violin plots show the continuous number of buds compared between wildtype and mutant (A) KRAS, (B) BRAF.*

A

KRAS

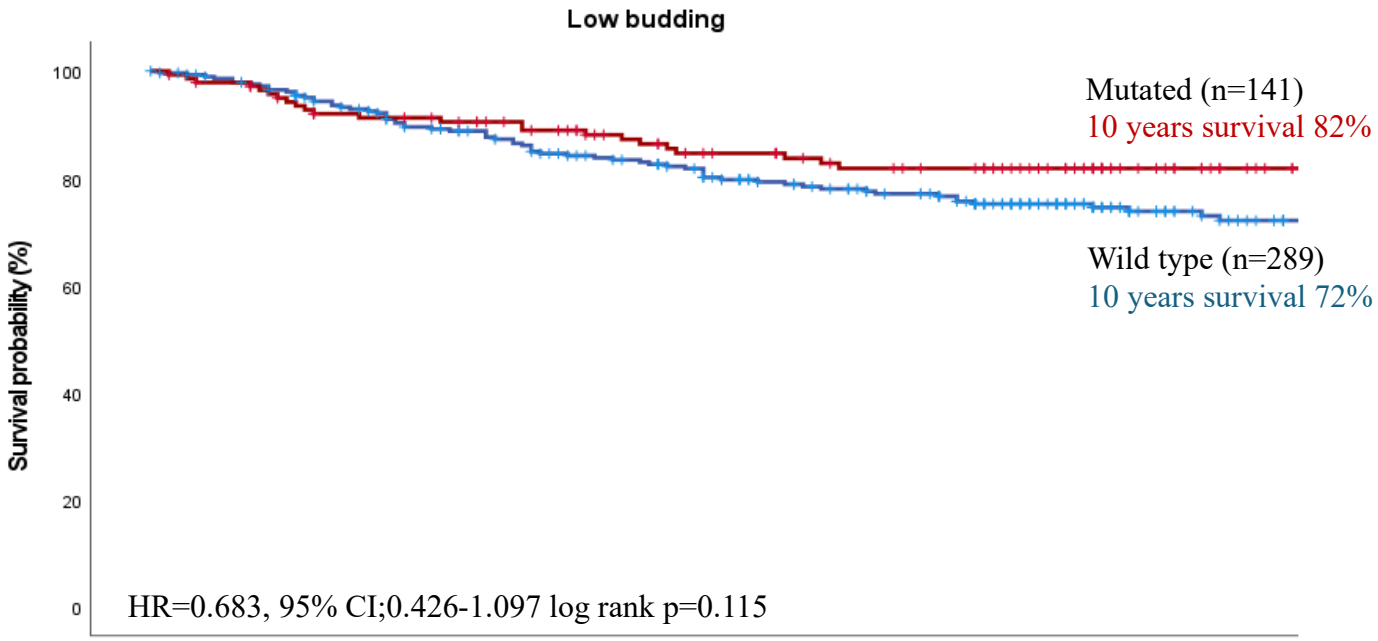

months	0	12	24	36	48	60	72	84	96	108	120
Wildtype	289(0)	275(7)	254(15)	232(26)	213(33)	200(40)	180(53)	168(61)	140(85)	103(121)	81(140)
Mutant	141(0)	133(4)	122(7)	118(10)	107(19)	96(25)	90(30)	84(34)	76(42)	56(62)	46(72)

B

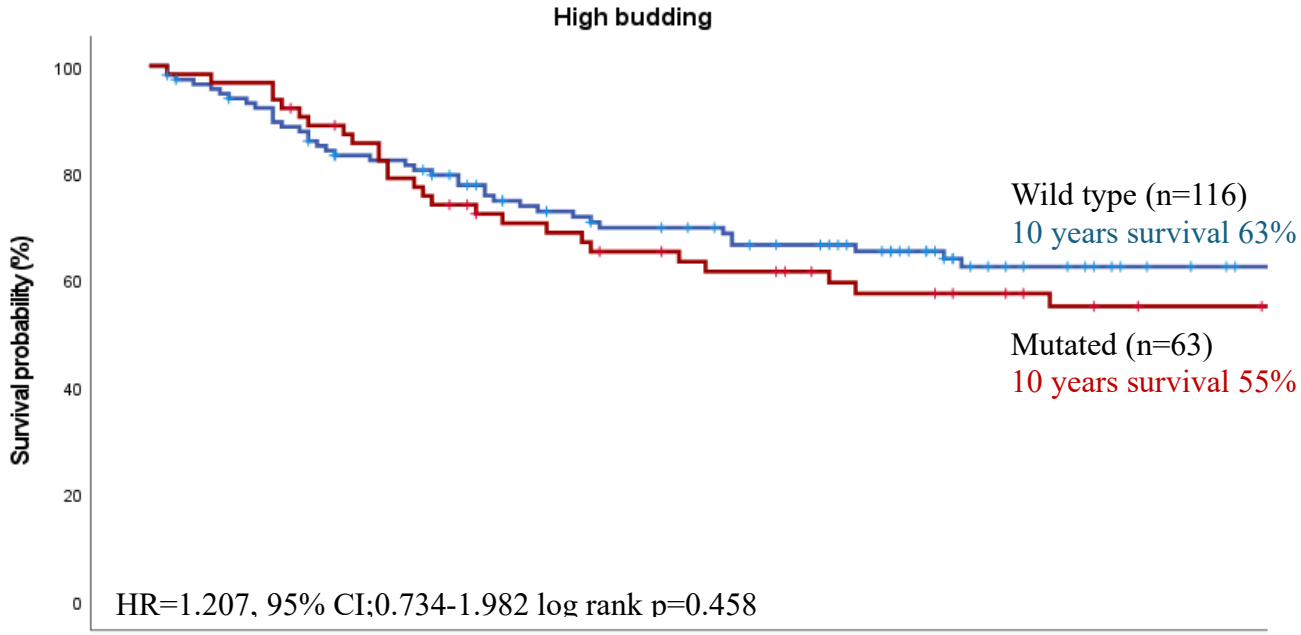

months	0	12	24	36	48	60	72	84	96	108	120
Wildtype	116(0)	105(3)	91(6)	82(9)	72(14)	67(16)	60(20)	54(25)	40(37)	35(42)	31(46)
Mutant	63(0)	61(0)	52(2)	44(3)	39(5)	35(7)	32(8)	28(10)	26(12)	22(15)	21(16)

Figure 3.7 *Kaplan-Meier survival analysis based on KRAS mutational status stratified by (A) low and (B) high budding phenotype for cancer specific survival (CSS) in CRC patients. Hazard ratio (HR) was reported with 95% confidence intervals. P Values were calculated using the log-rank test comparing each budding group with KRAS mutational status.*

BRAF

A

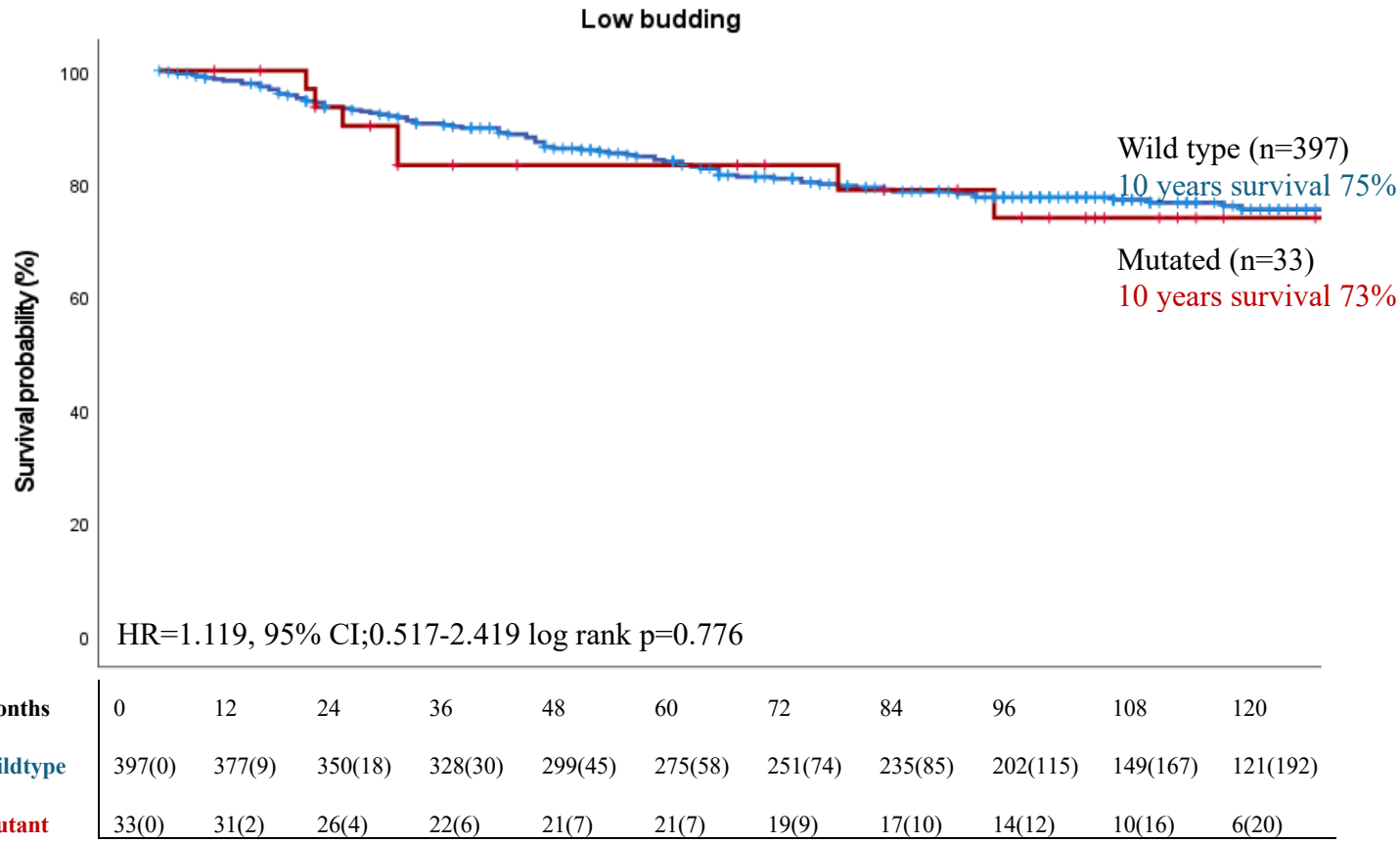

Months	0	12	24	36	48	60	72	84	96	108	120
Wildtype	397(0)	377(9)	350(18)	328(30)	299(45)	275(58)	251(74)	235(85)	202(115)	149(167)	121(192)
Mutant	33(0)	31(2)	26(4)	22(6)	21(7)	21(7)	19(9)	17(10)	14(12)	10(16)	6(20)

B

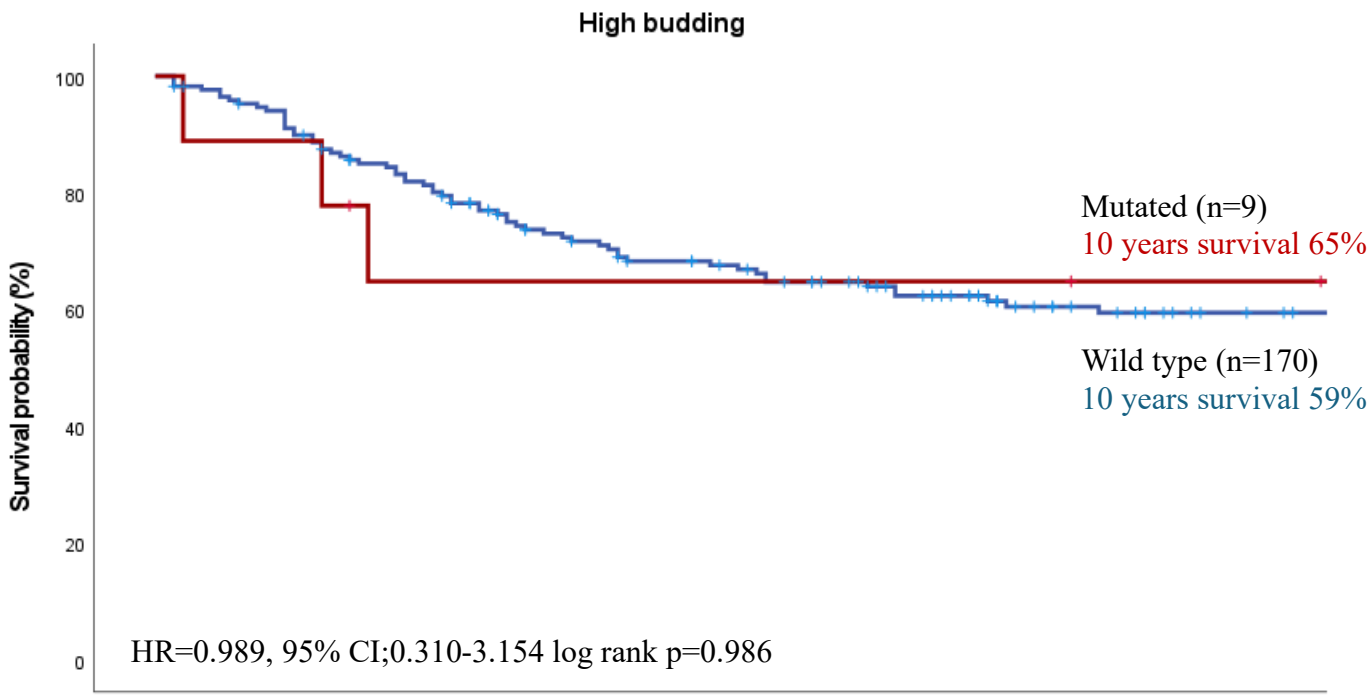

Months	0	12	24	36	48	60	72	84	96	108	120
Wildtype	170 (0)	158 (3)	138 (7)	121 (11)	106 (18)	97 (22)	87(27)	77(34)	61(48)	53(55)	48(60)
Mutant	9 (0)	8 (0)	5 (1)	5 (1)	5 (1)	5 (1)	5(1)	5(1)	5(1)	4(2)	4(2)

Figure 3.8 *Kaplan-Meier survival analysis based on BRAF mutational status stratified by (A) low and (B) high budding phenotype for cancer specific survival (CSS) in CRC patients. Hazard ratio (HR) was reported with 95% confidence intervals. P Values were calculated using the log-rank test comparing each budding group with BRAF mutational status.*

3.5.2. DNA mismatch repair (MMR)

No significant difference between budding phenotype and MMR status was identified in our CRC cohort (Table 3.5). The survival analysis also revealed a significant difference in patients' survival between the three MMR subgroups; pMMR, dMMR and loss of 2 sets of MLH1/PMS2 or MHS2/6 genes when stratified with low (HR=0.628, 95% CI;0.438-0.900 log-rank p=0.011) and high (HR=0.649, 95% CI;0.423-0.995 log-rank p=0.047) budding groups (Figure 3.10). According to the life table, patients with dMMR tumours had the worst outcome in both low (66%) and high (54%) budding groups 10 years after diagnosis, when compared to other MMR subgroups. Moreover, although not significant, there are a higher number of average budding cells in the dMMR tumours when compared to those with pMMR and group with loss of 2 sets of MLH1/PMS2 or MHS2/6 genes (Figure 3.9). This could suggest the association between a budding phenotype and a poor prognosis. However, mutational landscapes may not solely drive the budding phenotype, further study is needed to unravel the underlying mechanism of TB in CRC.

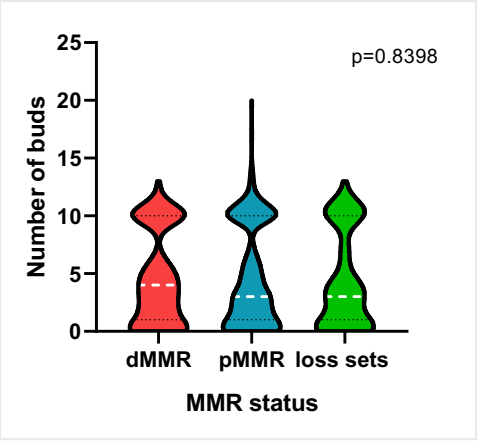

Figure 3.9 *Violin plots show the continuous number of buds compared between mismatch repairs groups.*

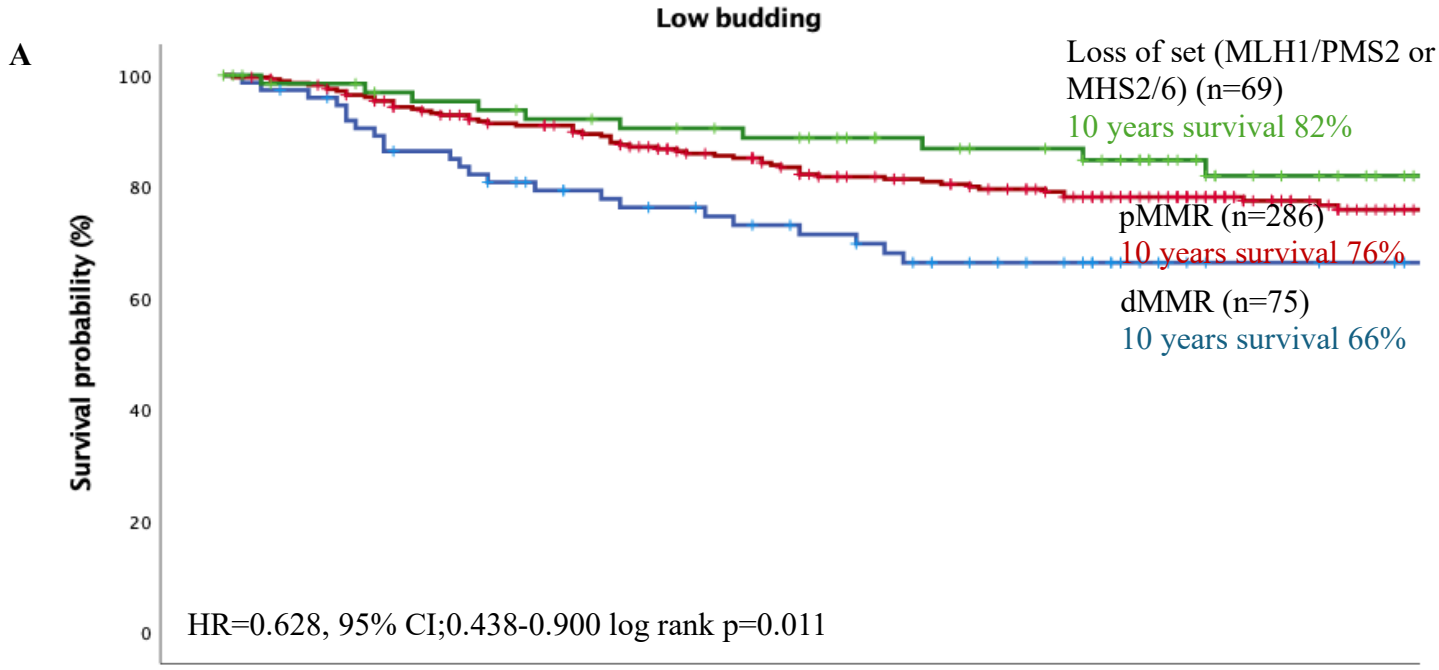

Months	0	12	24	36	48	60	72	84	96	108	120
dMMR	75(0)	70(2)	62(3)	54(6)	49(9)	45(11)	40(13)	34(18)	25(27)	20(32)	19(33)
pMMR	286(0)	274(5)	253(13)	239(22)	216(34)	199(43)	184(53)	174(59)	152(78)	115(115)	90(137)
Loss of set (MLH1/PMS2 or MHS2/6)	69(0)	64(4)	60(6)	57(7)	55(8)	52(10)	46(16)	43(18)	38(22)	26(33)	22(37)

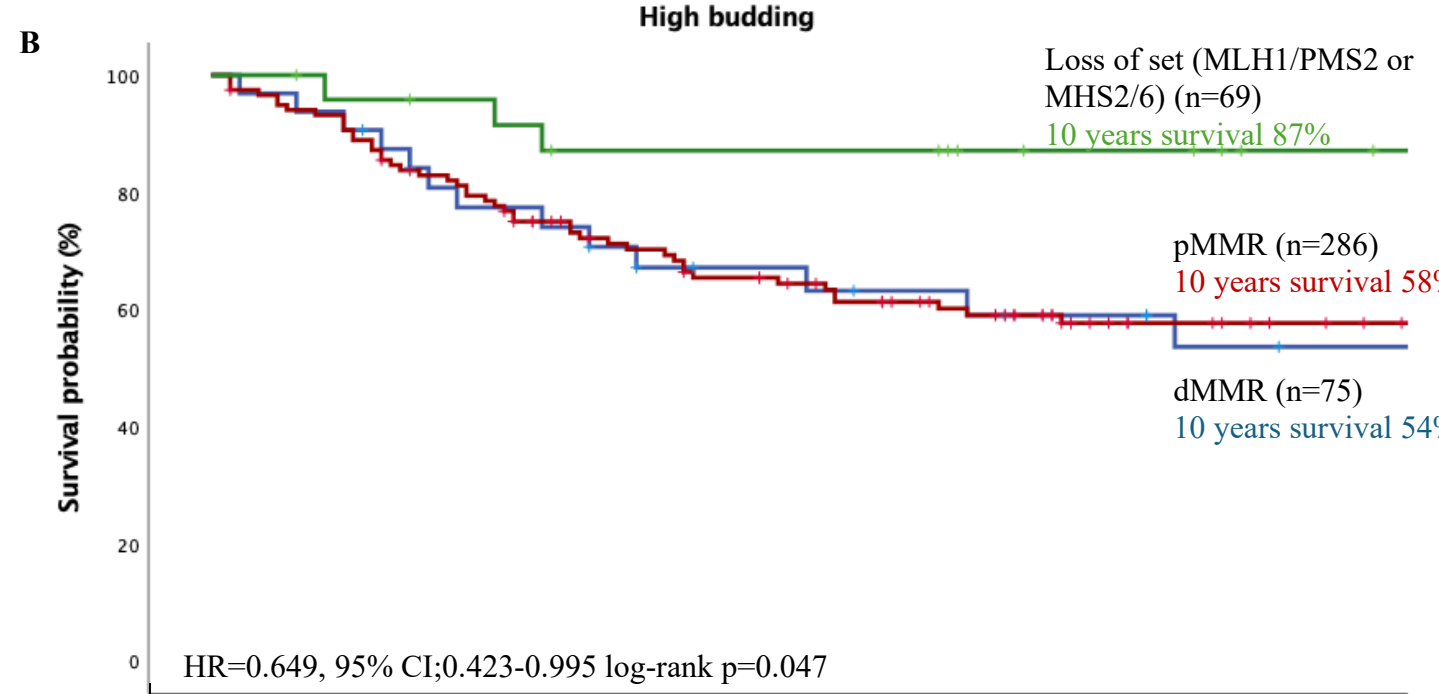

Months	0	12	24	36	48	60	72	84	96	108	120
dMMR	32(0)	30(2)	24(2)	22(2)	18(4)	17(5)	15(6)	14(6)	13(7)	10(9)	9(10)
pMMR	118(0)	109(1)	95(3)	82(7)	73(11)	65(14)	57(18)	51(22)	37(35)	33(39)	30(42)
Loss of set (MLH1/PMS2 or MHS2/6)	25(0)	24(1)	22(2)	20(2)	19(3)	19(3)	19(3)	16(9)	15(10)	13(12)	12(13)

Figure 3.10 *Kaplan-Meier survival analysis based on mismatch repairs group stratified by (A) low and (B) high budding phenotype for cancer specific survival (CSS) in CRC patients. Hazard ratio (HR) was reported with 95% confidence intervals. P Values were calculated using the log-rank test comparing each budding group with MMR status.*

3.6. The association between budding status and modified Glasgow prognostic score (mGPS)

mGPS was utilised to identify the correlation between high budding tumours and systemic inflammation. According to chi-square analysis, there is no significant association between TB phenotype and mGPS scores (Table 3.6). Additionally, when comparing the number of budding cells, there is no significant difference between mGPS groups, although tumours with mGPS1 tend to have the highest number of buds (Figure 3.11). Survival analysis revealed that when stratified with budding phenotype, patients with mGPS2 showed a worse survival when the tumour exhibited high budding (HR=1.505, 95% CI;1.113-2.035 log-rank p=0.008) (Figure 3.12). The life table demonstrated 43% of patients with mGPS2 and 67% of mGPS0 patients were alive at 10 years after initial diagnosis. A similar trend was observed in the groups of low budding tumours (HR=1.313, 95% CI;1.015-1.698 log-rank p=0.038), however, there are no obvious differences between the percentage survival of mGPS subgroups after 10 years.

Table 3.6 *The relationship between budding status and mGPS scores using the Pearson's chi-square analysis in CRC patient (n=621)*

	Low budding n=441	**High budding n=180**	**P-value**
mGPS 0 1 2	 283 (64) 90 (20) 68 (15)	 111 (62) 43 (24) 26 (14)	0.628

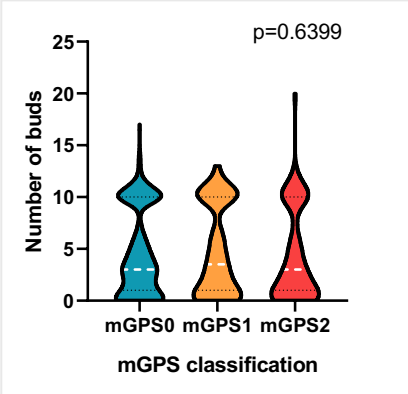

Figure 3.11 *Violin plots show the continuous number of buds compared between mGPS groups.*

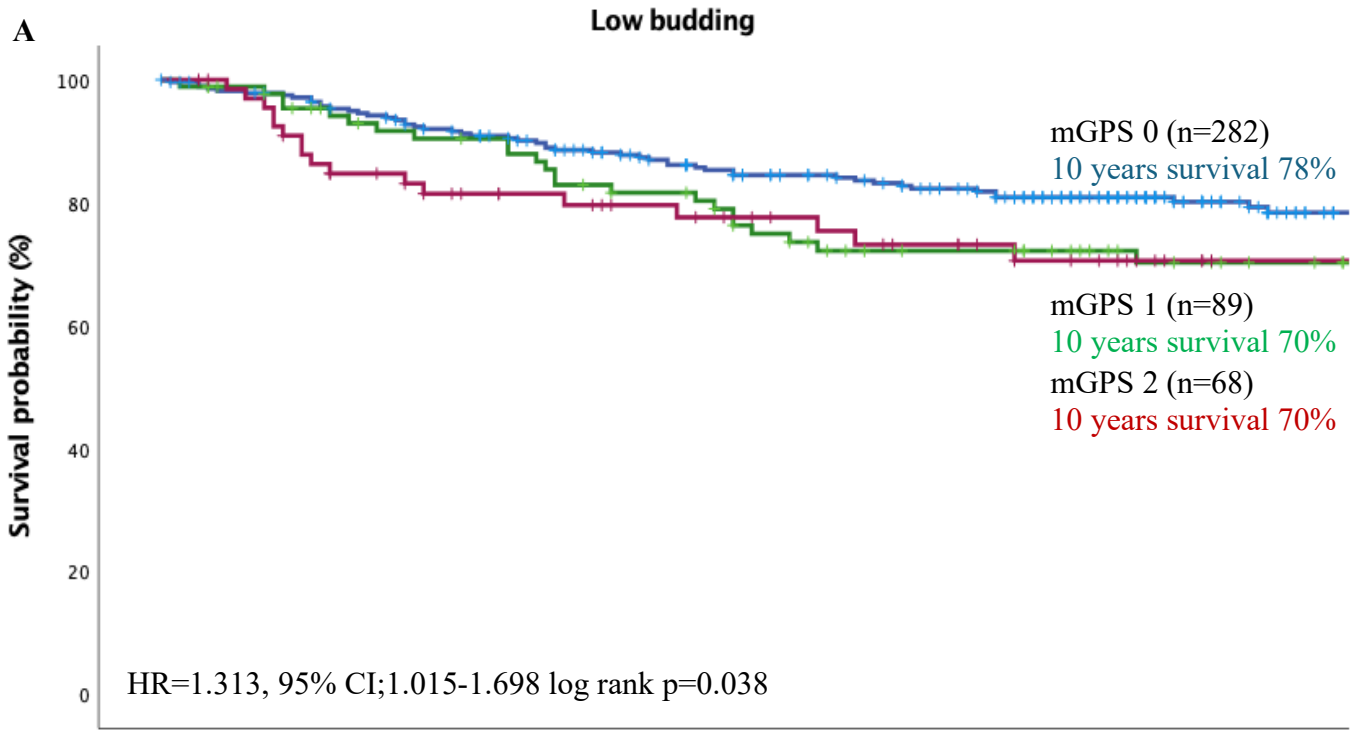

months	0	12	24	36	48	60	72	84	96	108	120
mGPS0	282(0)	270(7)	257(9)	239(18)	221(29)	206(37)	193(48)	180(56)	153(80)	109(124)	83(147)
mGPS1	89(0)	83(4)	74(8)	72(9)	65(10)	59(13)	50(17)	47(20)	43(24)	37(29)	33(33)
mGPS2	68(0)	63(2)	52(6)	46(10)	41(14)	38(16)	34(19)	31(21)	26(25)	19(32)	16(35)

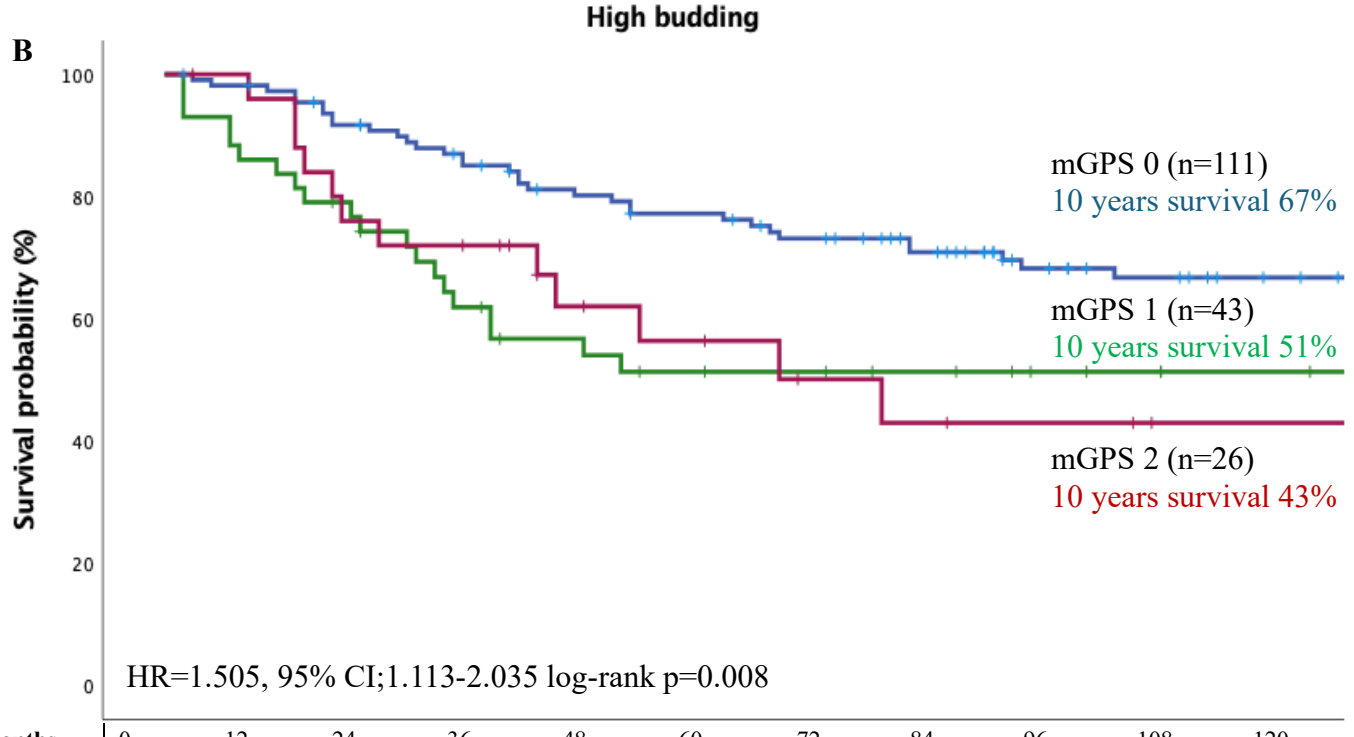

months	0	12	24	36	48	60	72	84	96	108	120
mGPS0	111(0)	106(2)	96(5)	88(7)	81(9)	77(10)	70(13)	62(19)	49(30)	45(33)	40(38)
mGPS1	43(0)	37(0)	30(2)	22(3)	20(4)	17(6)	16(7)	15(8)	12(11)	9(14)	9(14)
mGPS2	26(0)	24(1)	18(1)	17(2)	11(6)	9(7)	7(8)	6(8)	5(9)	3(11)	3(11)

Figure 3.12 *Kaplan-Meier survival analysis based mGPS groups stratified by (A) low and (B) high budding phenotype for cancer specific survival (CSS) in CRC patients. Hazard ratio (HR) was reported*

with 95% confidence intervals. P Values were calculated using the log-rank test comparing each budding group with mGPS groups.

3.7. The association between budding status and Glasgow microenvironment score (GMS)

Glasgow microenvironment score (GMS) is a combination of tumour stromal percentage (TSP) and Klintrup–Mäkinen (KM) scores. These scores were used to investigate the relationship between the tumour and its microenvironment in the CRC cohort. There is a significant inverse association between TB and KM (p=0.015) indicating a relationship between inflammation and the budding phenotype in CRC (Figure 3.13) (Table 3.7).

GMS scores were generated by combining KM and TSP. These were classified into 3 subgroups: GMS0 for strong KM regardless of TSP, GMS1 for weak KM and low TSP and GMS2 with weak KM and high TSP. Chi-square analysis revealed a significant association between TB and GMS scores (p=0.046) (Figure 3.13) (Table 3.7). Interestingly, the number of budding cells was reported to be significantly higher in tumours with GMS2 when compared to GMS0 (p=0.0384) (Figure 3.14). Moreover, survival analysis revealed the worst outcomes in GMS2 (n=77 and 39) tumours while GMS0 (n=83 and 20) showed better survival when stratified in both low and high budding groups respectively. Although a similar trend was reported in both tumours with low (HR=1.460, 95% CI;1.051-2.027 log-rank p=0.024) and high (HR=2.129, 95% CI;1.392-3.256 log-rank p<0.001) budding groups, a strong association with CSS was found in tumours with high buds (Figure 3.15). The life table showed 46% of GMS2 patients compared to 100% GMS0 while 72% was reported in GMS2 and 86% in GMS0 after 10 years of initial diagnosed in groups with high budding and low budding respectively.

Table 3.7 *The relationship between budding status and tumour microenvironment scores using the Pearson's chi-square analysis in CRC patient (n=621)*

	Low budding n=441	**High budding n=180**	**P-value**
TSP			0.194

Low High	342 (80) 86 (20)	133 (75) 44 (25)	
KM Low High	344 (81) 83 (19)	157 (89) 20 (11)	**0.015**
GMS 0 1 2	83 (19) 266 (62) 78 (18)	20 (11) 118 (67) 39 (22)	**0.046**

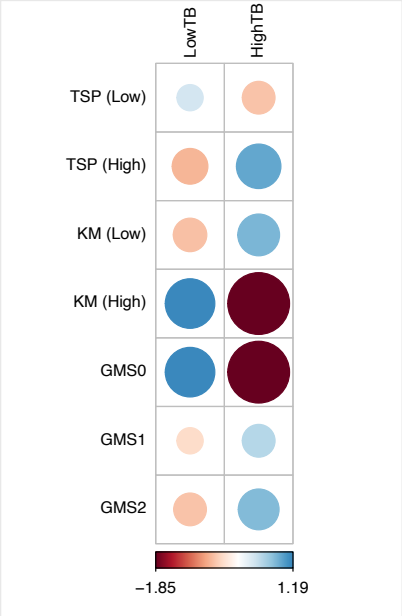

Figure 3.13 *The correlation plot showed the standardised residual of data; positive associations are in blue and no association in orange, the bigger size of the circle the more significant association was found.*

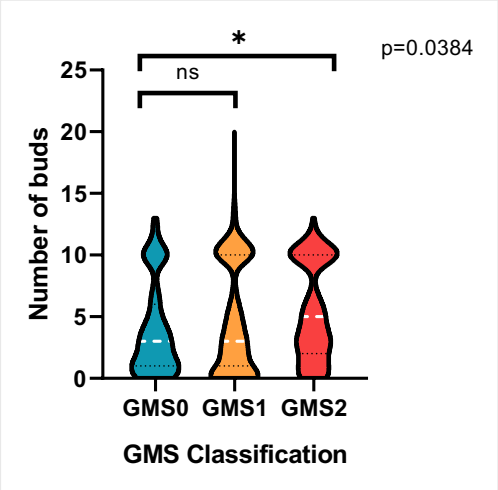

Figure 3.14 *Violin plots show the continuous number of buds compared between GMS groups.*

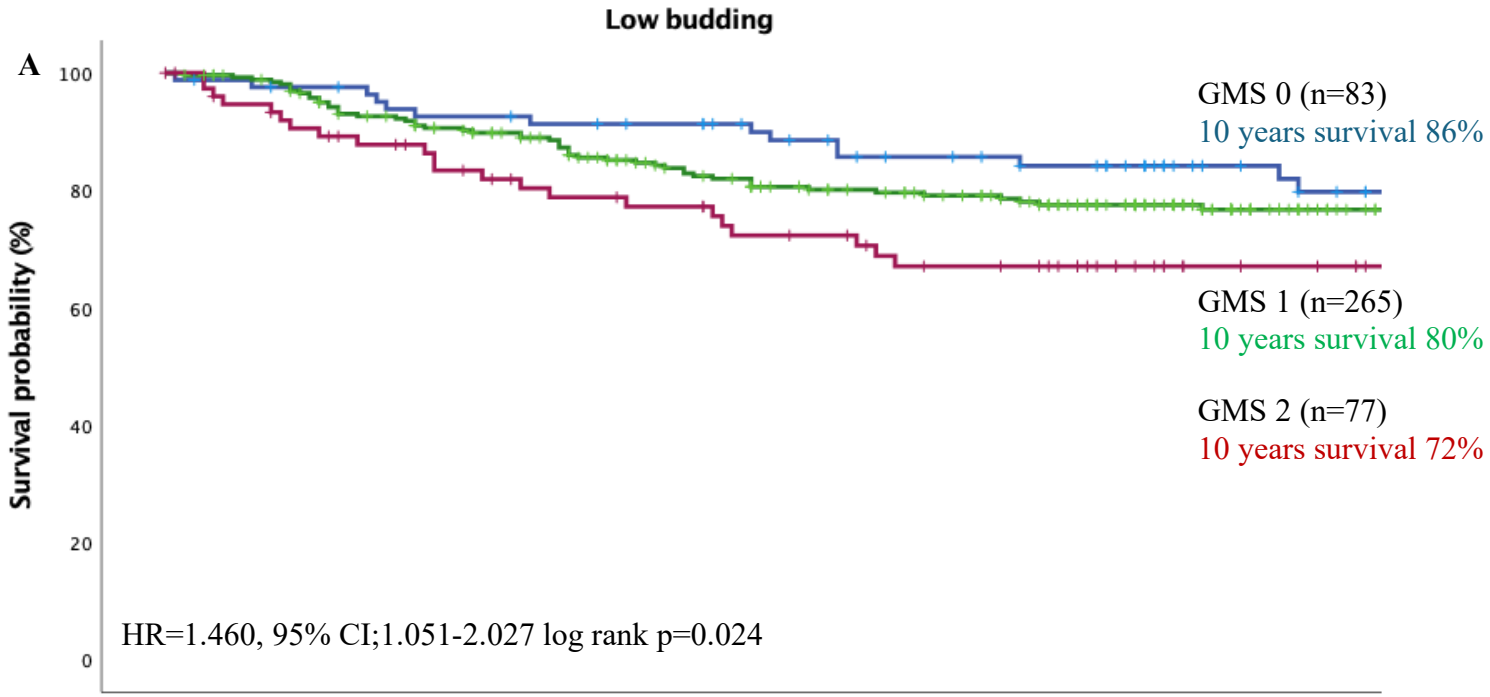

months	0	12	24	36	48	60	72	84	96	108	120
GMS0	83(0)	79(2)	75(3)	74(3)	71(5)	67(9)	60(12)	57(15)	54(17)	40(32)	35(35)
GMS1	265(0)	255(6)	232(14)	215(24)	192(36)	178(44)	162(56)	153(63)	129(84)	98(115)	72(140)
GMS2	77(0)	68(4)	62(6)	54(10)	50(12)	44(14)	42(16)	37(18)	30(25)	20(35)	18(37)

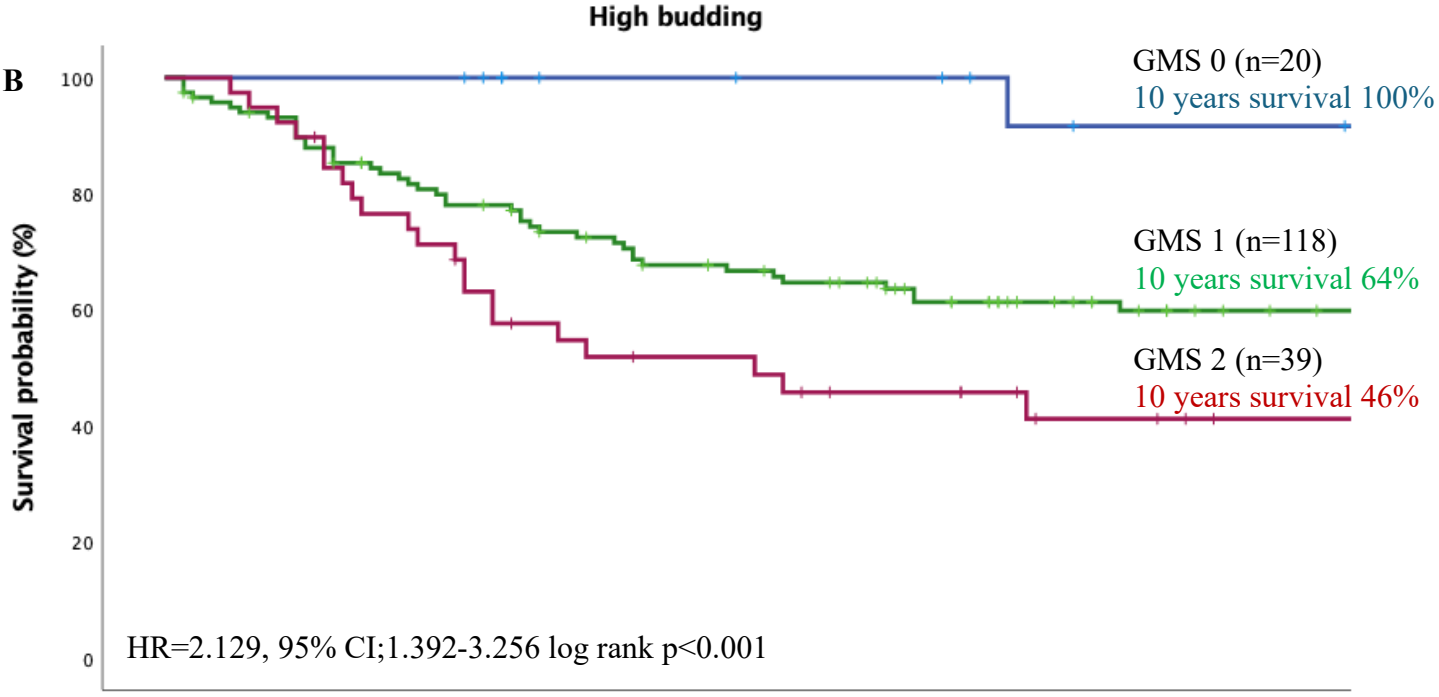

months	0	12	24	36	48	60	72	84	96	108	120
GMS0	20(0)	20(0)	20(0)	18(2)	15(5)	15(5)	14(6)	13(7)	11(8)	10(9)	10(9)
GMS1	118(0)	107(3)	92(7)	85(8)	76(11)	68(14)	63(16)	54(22)	44(32)	37(38)	34(41)
GMS2	39(0)	37(0)	29(1)	21(2)	18(3)	17(4)	13(6)	13(6)	8(10)	7(11)	5(13)

Figure 3.15 *Kaplan-Meier survival analysis based on GMS groups stratified by (A) low and (B) high budding phenotype for cancer specific survival (CSS) in CRC patients. Hazard ratio (HR) was reported with 95% confidence intervals. P Values were calculated using the log-rank test comparing each budding group with GMS group.*

3.8. The association between tumour budding and infiltrated immune cells.

In addition to the inflammatory scores, mIF staining was performed, as described in Chapter2 section 2.4, in a previously constructed tumour core TMAs (n=787). A marker of specific immune phenotypes was selected; lymphocyte (CD3 CD8 FOXP3) and myeloid (CD68 CD163 CD66b), to investigate the role of these immune cells in tumours with low/high budding phenotype (Figure 3.16). The immune profile was measured and quantified in Visiopharm, image analysis software. Tumour and stromal areas were defined, and single-cell detection was used to quantify the number of cells and for statistical purposes.

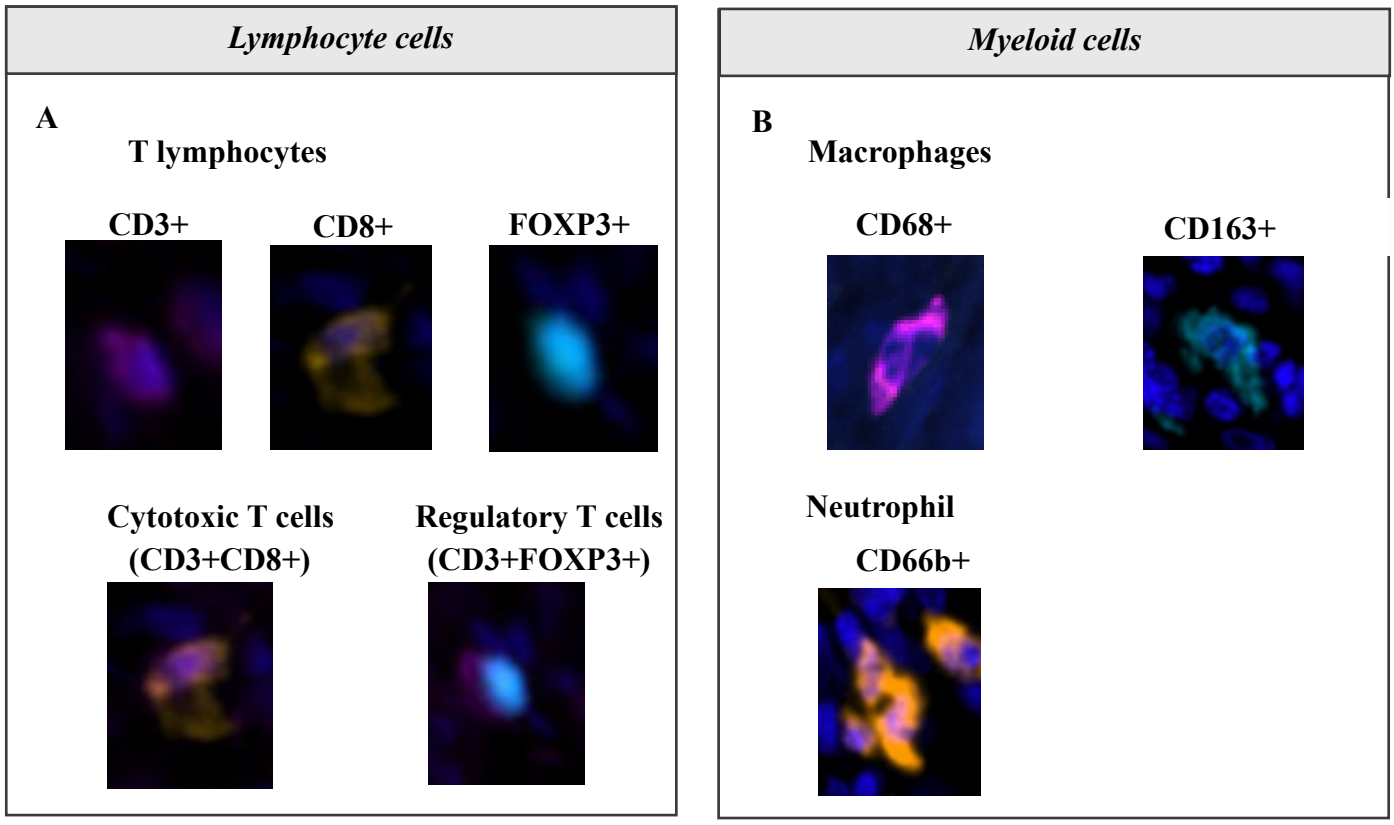

Figure 3.16 *Multiplex immunofluorescence panel showing different cell phenotype co-localisation in in tumour and immune cells from CRC sample. (A) Marker expression of CD3+ on immune T cells, expression of CD8+ cells, expression of FOXP3+ cells, co-localisation with CD3+CD8+ for cytotoxic T-cells and co-localisation with CD3+FOXP3+ for regulatory T-cells. (B) Marker expression of CD68+ anti-inflammatory pan-macrophages, CD163+ pro-inflammatory macrophages and CD66b+ neutrophil cells.*

3.8.1. Relationship between TB and T lymphocytes

3.8.1.1. CD3+ cells

CD3+ T cells were quantified and normalised with the total number of cells in the stromal region. There is no significant association between budding status and the percentage CD3+ cells in the CRC cohort (Table 3.8). Although there is a high number of CD3+ cells in the high budding group, no significant difference was found between low and high budding groups (Figure 3.17). Moreover, when patients were stratified by budding status, survival analysis revealed that tumours with a strong infiltrate of CD3+ cells (n=186) had a significantly longer survival time than those patients with low CD3+ infiltrate (n=202) in tumours with a low budding phenotype (HR=0.590, 95% CI;0.382-0.910 log rank p=0.017) (Figure 3.18A). Although there is a similar pattern of CD3+ cells in high budding tumours, there is no difference in patient survival (HR=0.662, 95% CI;0.402-1.089 log rank p=0.104) (Figure 3.18B). Additionally, the life table shows a difference between high CD3+ (78%) and low CD3+ (67%) in low budding tumours while 63% and 55% of high and low CD3+ cells were reported in high budding tumours 10 years from diagnosed.

Table 3.8 *The relationship between budding status and percent CD3+ cells using the Pearson's chi-square analysis in CRC patient (n=621)*

	Low budding n=395	**High budding n=175**	**P-value**
CD3+ Low High	 186 (48) 202 (52)	 78 (45) 95 (55)	 0.513

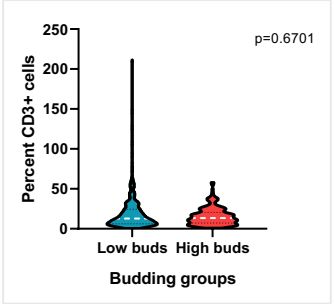

Figure 3.17 *Violin plots show the percent CD3+ cells compared between budding groups; low (blue) and high (red) TB.*

A

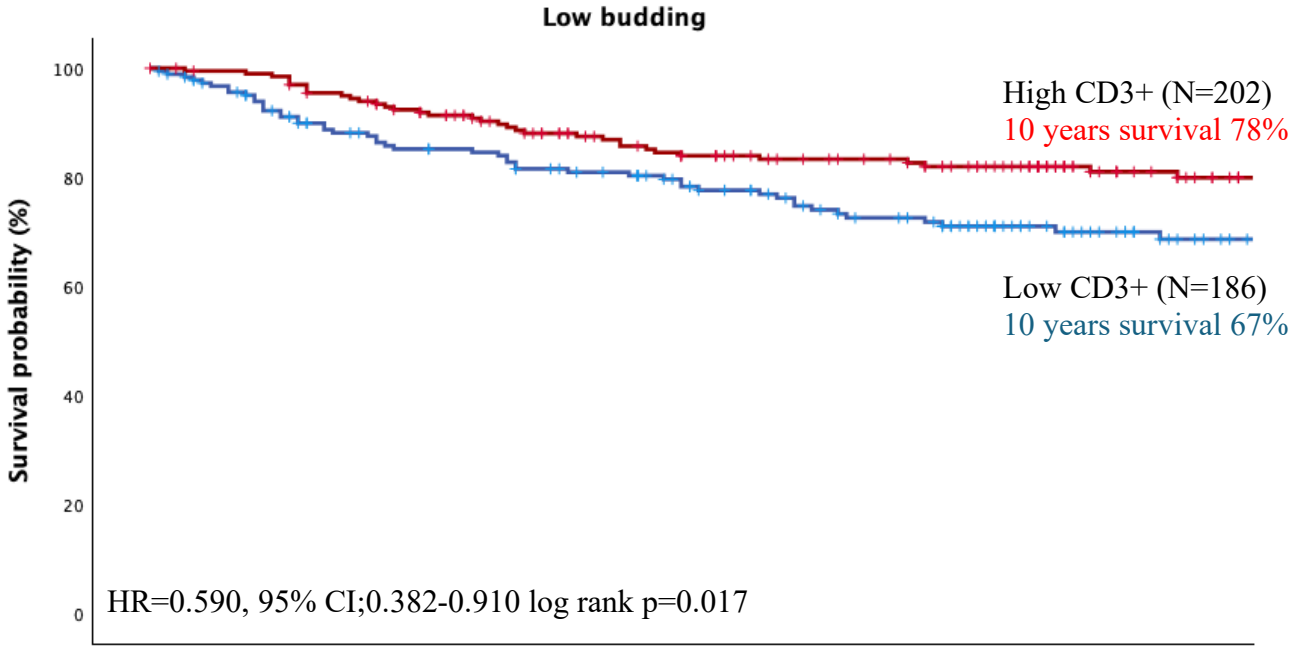

months	0	12	24	36	48	60	72	84	96	108	120
LowCD3+	186(0)	168(9)	149(16)	141(19)	131(23)	120(31)	108(39)	97(44)	80(59)	62(73)	49(85)
HighCD3+	202(0)	197(3)	186(5)	171(14)	154(25)	143(30)	131(40)	126(45)	113(56)	85(84)	71(96)

B

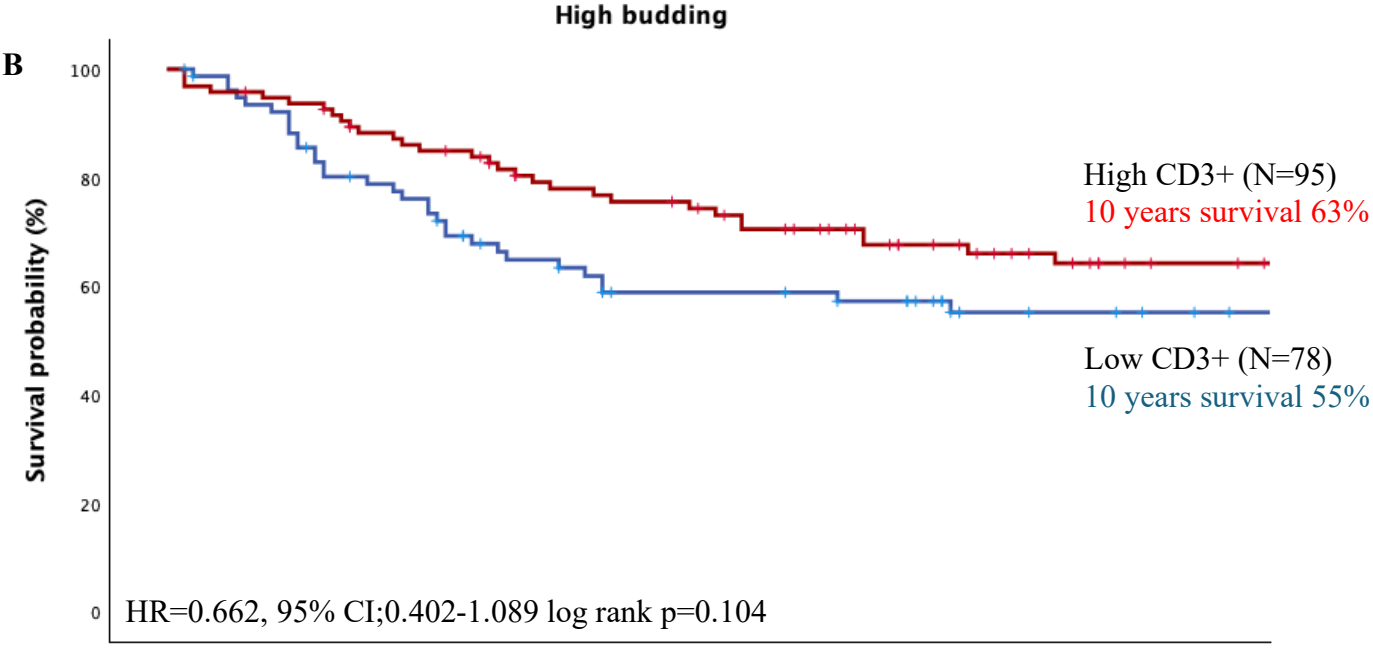

months	0	12	24	36	48	60	72	84	96	108	120
LowCD3+	78(0)	71(2)	58(4)	47(7)	42(9)	37(11)	36(12)	34(13)	24(22)	23(23)	20(26)
HighCD3+	95(0)	89(1)	80(4)	75(5)	65(10)	61(12)	54(15)	46(21)	39(27)	32(33)	30(35)

Figure 3.18 *Kaplan-Meier survival analysis based on percentage of CD3+ cells stratified by (A) low and (B) high budding phenotype for cancer specific survival (CSS) in CRC patients. Hazard ratio (HR) was reported with 95% confidence intervals. P Values were calculated using the log-rank test comparing each budding group with patients with low and high CD3+ phenotypes.*

3.8.1.2. Cytotoxic T cells (CD3+ CD8+)

Cytotoxic T cells (CD3+CD8+) were counted and normalised within the CD3+ population. Chi-square analysis demonstrated no significant association between TB and the percentage of cytotoxic T cells (Table 3.9). However, the percentage of CD3+CD8+ cells is significantly decreased in the high budding group (p=0.0062), indicating immune suppression activity when the tumour has high budding phenotype (Figure 3.19). The survival analysis, when stratified with budding phenotype, showed that patients with high cytotoxic T cell infiltration (n=299) experienced a better survival compared to those with low CD3+CD8+ cells (n=36) in the tumour with low budding group (HR=0.478, 95% CI;0.268-0.854 log rank p=0.013) (Figure 3.20A). There is no significant difference in patients' survival regarding cytotoxic T cell (CD3+CD8+) infiltration in tumours with high budding (HR=0.795, 95% CI;0.358-1.765 log rank p=0.573) (Figure 3.20B). The life table shows that, 76% of patients with high cytotoxic infiltration were alive after 10 years as compared to 56% of those with low infiltration.

Table 3.9 *The relationship between budding status and percent CD3+CD8+ cells using the Pearson's chi-square analysis in CRC patient (n=621)*

	Low budding n=395	**High budding n=175**	**P-value**
CD3+CD8+ Low High	 35 (10) 314 (90)	 21 (13) 138 (87)	 0.333

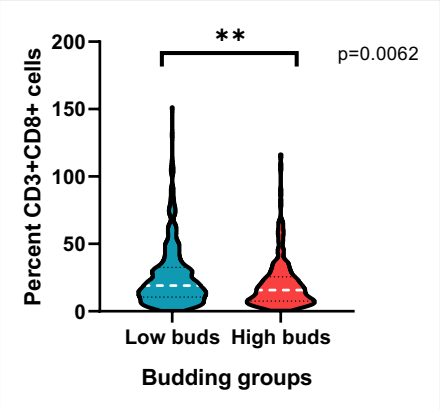

Figure 3.19 *Violin plots show the percent CD3+CD8+ cells compared between budding groups*; *low (blue) and high (red) TB.*

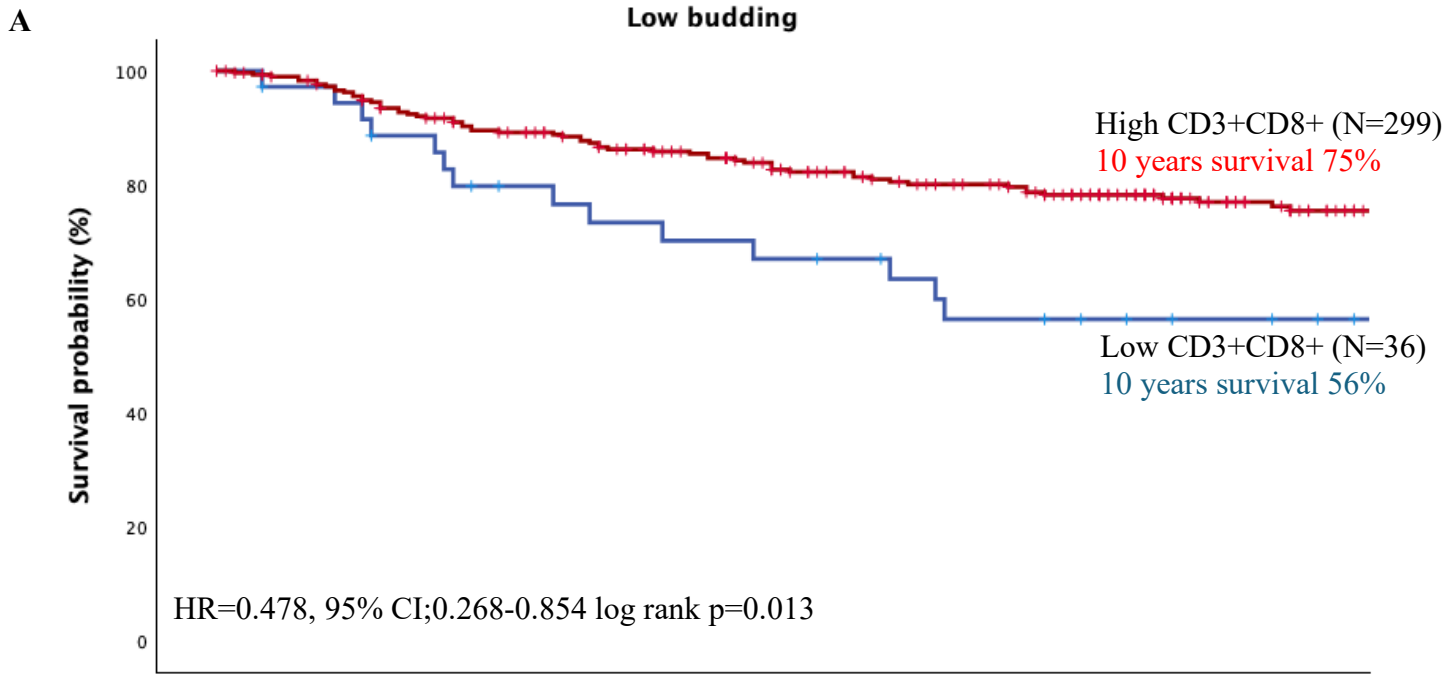

months	0	12	24	36	48	60	72	84	96	108	120
LowCD3+CD8+	36(0)	34(1)	30(2)	25(4)	23(4)	21(4)	20(5)	16(6)	14(8)	12(10)	11(11)
HighCD3+CD8+	299(0)	283(9)	260(15)	244(24)	226(34)	208(46)	188(60)	177(68)	156(85)	117(123)	95(142)

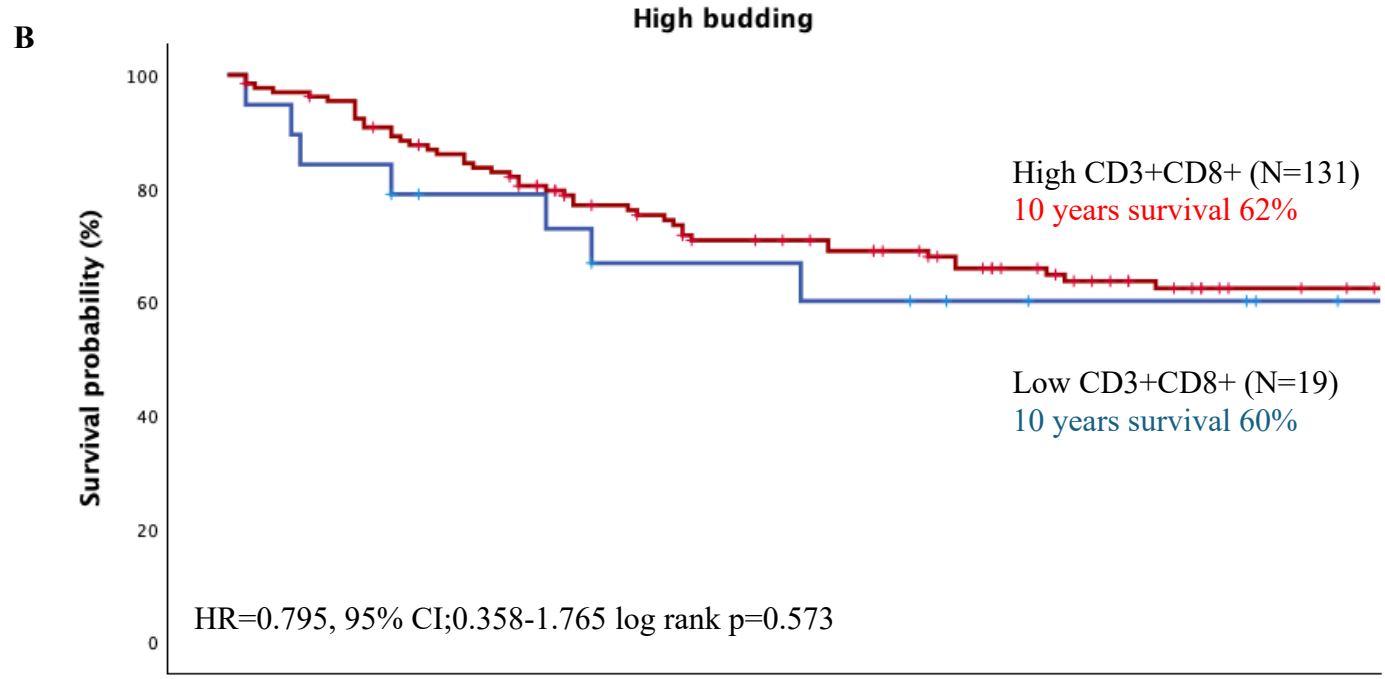

months	0	12	24	36	48	60	72	84	96	108	120
LowCD3+CD8+	19(0)	16(0)	13(2)	12(0)	10(3)	10(3)	9(3)	7(5)	6(6)	6(6)	4(8)
HighCD3+CD8+	131(0)	123(2)	108(5)	96(9)	85(15)	77(18)	71(22)	63(27)	54(34)	46(41)	43(44)

Figure 3.20 *Kaplan-Meier survival analysis based on percentage of CD3+CD8+ cells stratified by low (A) and high (B) budding phenotype for cancer specific survival (CSS) in CRC patients. Hazard ratio (HR) was reported with 95% confidence intervals. P Values were calculated using the log-rank test comparing each budding group with patients with low and high CD3+CD8+ phenotypes.*

3.8.1.3. T regulatory cells (CD3+ FOXP3+)

Image analysis was performed to quantify T regulatory (CD3FOXP3) cells. The counts were then normalised within the CD3+ population. Although a high number of regulatory cells was frequently observed in tumours with high buds (Figure 3.21), the chi-square test showed no significant association between TB status and percentage of CD3+FOXP3+ cells (Table 3.10). Survival analysis revealed that, when stratified with budding status, patients with high infiltrated CD3+FOXP3+ (n=202 and 94) showed poorer survival than those with low CD3+FOXP3+ T cells (n=136 and 58) in tumours with both low and high budding (HR=1.813, 95% CI;1.110-2.963 log rank p=0.017) (Figure 3.22A). There is no difference in patient survival within the high budding group (HR=0.999, 95% CI;0.535-1.868 log rank p=0.998) (Figure 3.22B). The life table, in those with low buds, showed 59% of patients with high CD3+FOXP3+ versus 76% of those with low CD3+FOXP3+ survived after 10 years from diagnosed.

Table 3.10 *The relationship between budding status and percent CD3+FOXP3+ cells using the Pearson's chi-square analysis in CRC patient (n=621)*

	Low budding n=395	**High budding n=175**	**P-value**
CD3+FOXP3+ Low High	 136 (40) 202 (60)	 58 (38) 94 (62)	 0.637

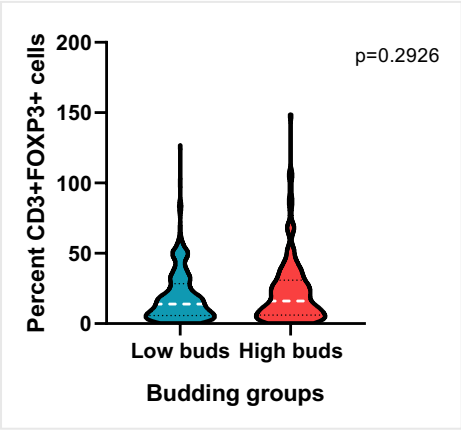

Figure 3.21 *Violin plots show the percent CD3+FOXP3+ cells compared between budding groups; low (blue) and high (red) TB.*

A

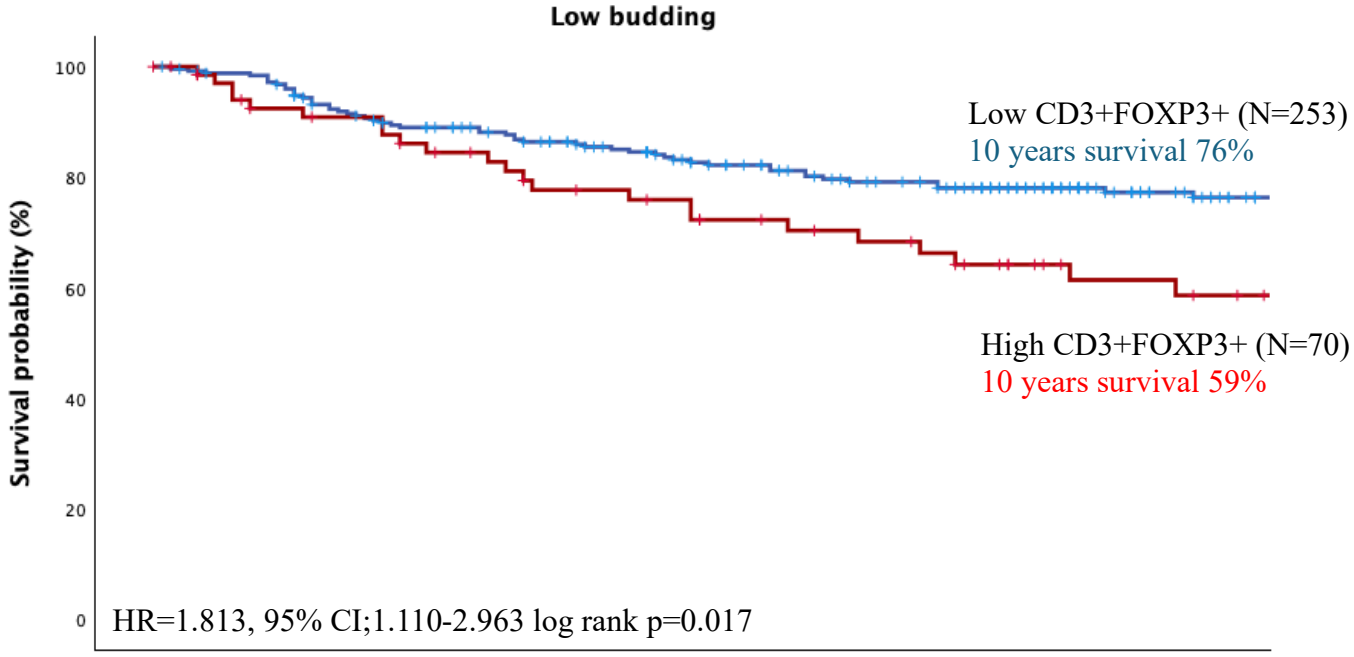

months	0	12	24	36	48	60	72	84	96	108	120
LowCD3+FOXP3+	253(0)	245(4)	220(11)	206(20)	192(28)	175(38)	160(49)	149(56)	130(73)	98(105)	81(130)
HighCD3+FOXP3+	70(0)	59(6)	57(7)	51(9)	45(11)	42(13)	37(16)	34(17)	29(20)	22(26)	20(27)

B

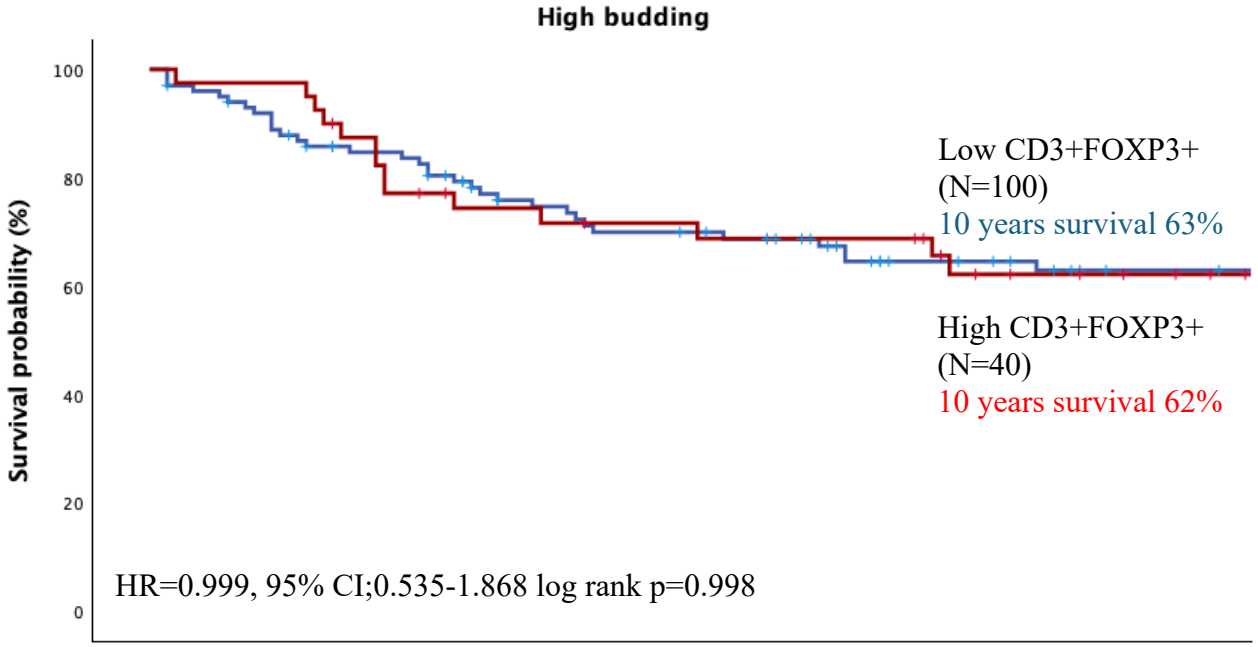

months	0	12	24	36	48	60	72	84	96	108	120
LowCD3+FOXP3+	100(0)	91(2)	79(6)	72(8)	63(13)	59(13)	54(17)	45(23)	41(27)	35(32)	34(33)
HighCD3+FOXP3+	40(0)	39(0)	34(1)	27(3)	26(3)	25(4)	24(4)	24(4)	17(9)	15(11)	13(13)

Figure 3.22 *Kaplan-Meier survival analysis based on percentage of CD3+FOXP3+ cells stratified by low (A) and high (B) budding phenotype for cancer specific survival (CSS) in CRC patients. Hazard ratio (HR) was reported with 95% confidence intervals. P Values were calculated using the log-rank test comparing each budding group with patients with low and high CD3+FOXP3+ phenotypes.*

3.8.2. Relationship between TB and macrophages

In this study, anti-inflammatory pan-macrophage (CD68) and pro-inflammatory macrophage (CD163) markers were included in a multiplex panel to represent two subtypes of macrophages. According to the findings, there is no association between TB status and the percentage of CD68+ cells (Table 3.11). Interestingly, albeit with no significant difference, the distribution of CD68+ cells were higher in high budding when compared to low budding groups (p=0.1028) (Figure 3.23). Moreover, patients with a high percentage of CD68+ cells (n=10) showed a significant decrease in survival when compared to those with low CD68+ cells (n=152) (HR=2.78, 95% CI;1.655-4.669 log-rank p<0.001) in patients with high budding phenotype (Figure 3.24B). There is no significant difference in patient survival in low (n=380) and high (n=20) infiltrating macrophages in tumours with low budding phenotype (HR=1.791, 95% CI;0.827-3.881 log-rank p=0.139) (Figure 3.24A). Additionally, the life table showed a percentage of 68% and 7% of low and high infiltrated CD68+ cells after 10 years post-diagnosis in patients with high budding.

Table 3.11 *The relationship between budding status and percent CD68+ cells using the Pearson's chi-square analysis in CRC patient (n=621)*

	Low budding n=400	**High budding n=162**	**P-value**
CD68+ Low High	 380 (10) 20 (90)	 152 (13) 10 (87)	 0.566

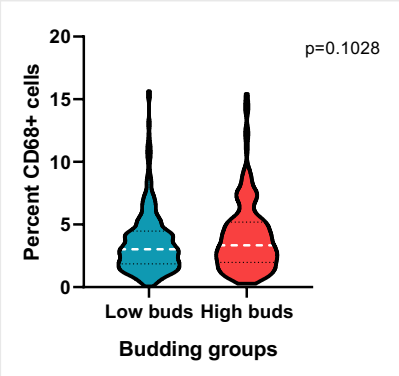

Figure 3.23 *Violin plots show the percent CD68 + cells compared between budding* groups*; low (blue) and high (red) TB.*

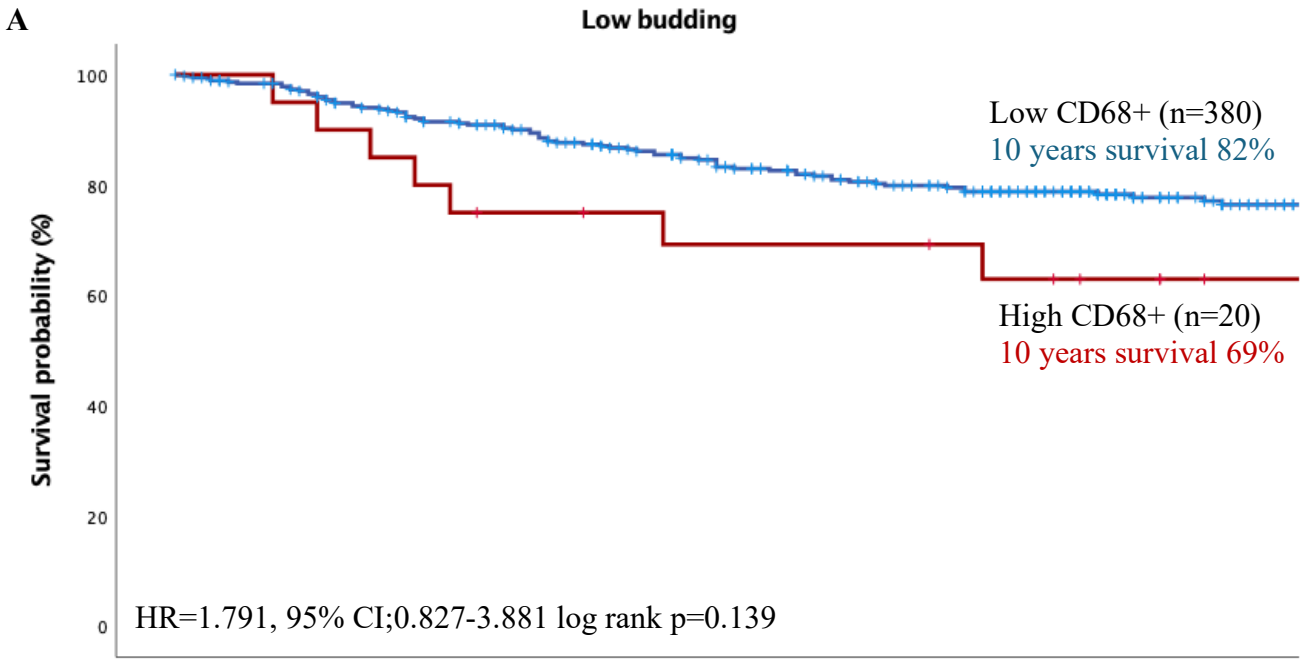

months	0	12	24	36	48	60	72	84	96	108	120
LowCD68+	380(0)	362(12)	335(22)	313(34)	287(48)	265(61)	243(75)	224(88)	191(118)	138(170)	111(194)
HighCD68+	20(0)	19(0)	17(0)	14(1)	13(2)	12(2)	12(2)	12(2)	10(3)	8(5)	5(8)

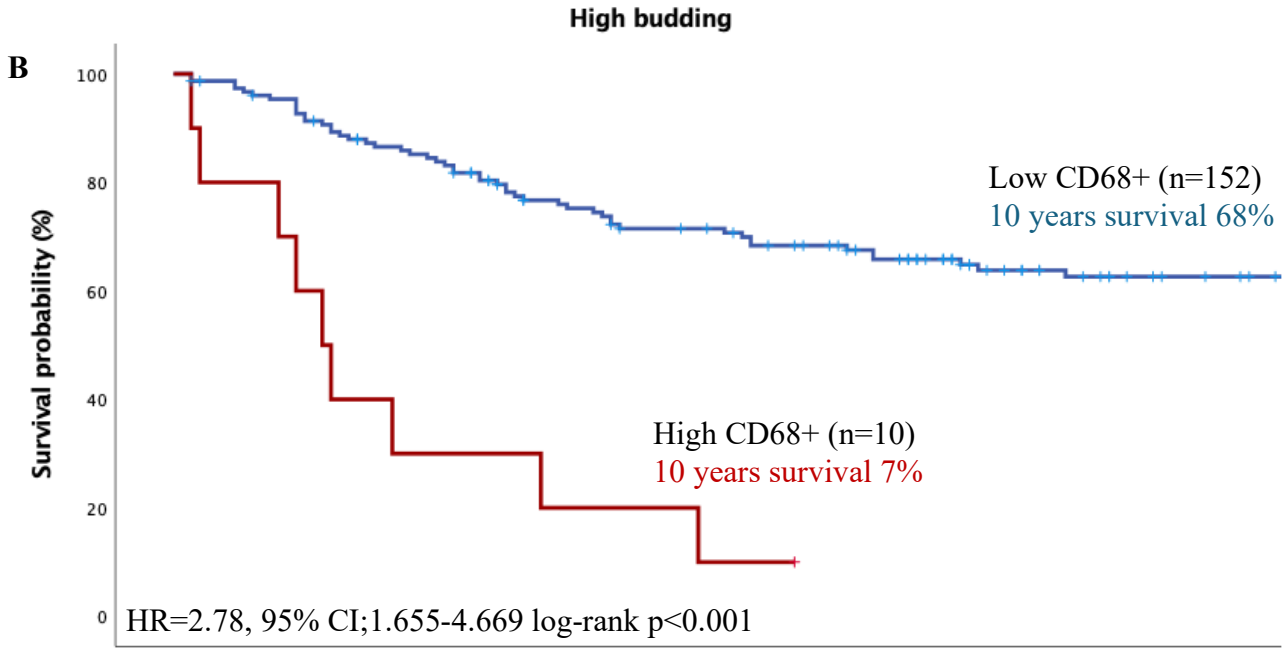

months	0	12	24	36	48	60	72	84	96	108	120
LowCD68+	152(0)	142(3)	126(6)	114(9)	101(15)	93(18)	85(22)	76(28)	59(43)	50(51)	46(55)
HighCD68+	10(0)	8(0)	4(0)	3(0)	2(0)	2(0)	-	-	-	-	-

Figure 3.24 *Kaplan-Meier survival analysis based on percentage of CD68+ cells stratified by low (A) and high (B) budding phenotype for cancer specific survival (CSS) in CRC patients. Hazard ratio (HR) was reported with 95% confidence intervals. P Values were calculated using the log-rank test comparing each budding group with patients with low and high CD68+ phenotypes.*

In addition to the anti-inflammatory macrophage, staining of CD163+, pro-inflammatory macrophage, was performed in another set of previously constructed TMAs (n=787). Statistical testing showed no association between TB phenotype and infiltrating CD163+ cells (Table 3.12). Also, there is no obvious difference in the number of CD163+ cells across low and high budding groups (Figure 3.25). According to the survival analysis, when stratified with budding phenotype, patients with a higher percentage of CD163+ (n=333) showed a significantly better outcome when compared to those groups with low CD163+ (n=220) (HR=0.605, 95% CI;0.386-0.949 log-rank p=0.029) in patients who present with low budding status (Figure 3.26A). In contrast, there is no difference in patient survival regarding the percentage of CD163+ cells in tumours with high budding (HR=0.978, 95% CI;0.584-1.637 log-rank p=0.932) (Figure 3.26B). The life table demonstrated 86% and 76% of tumours with high and low infiltrated CD163+ cells in the low budding group while 67% and 65% were reported in high and low CD163+ cells in the high budding group 10 years after diagnosis.

Table 3.12 *The relationship between budding status and percent CD163+ cells using the Pearson's chi-square analysis in CRC patient (n=621)*

	Low budding n=385	**High budding n=155**	**P-value**
CD163+ Low High	 209 (54) 176 (46)	 80 (52) 75 (48)	 0.556

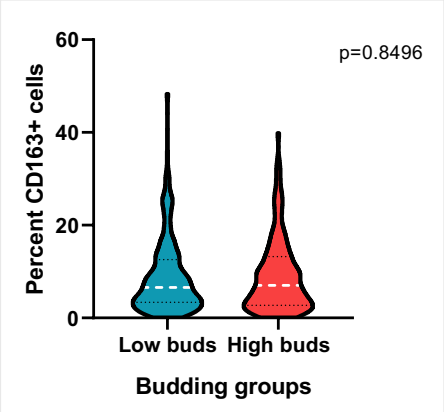

Figure 3.25 *Violin plots show the percent CD163+ cells compared between budding groups; low (blue) and high (red) TB.*

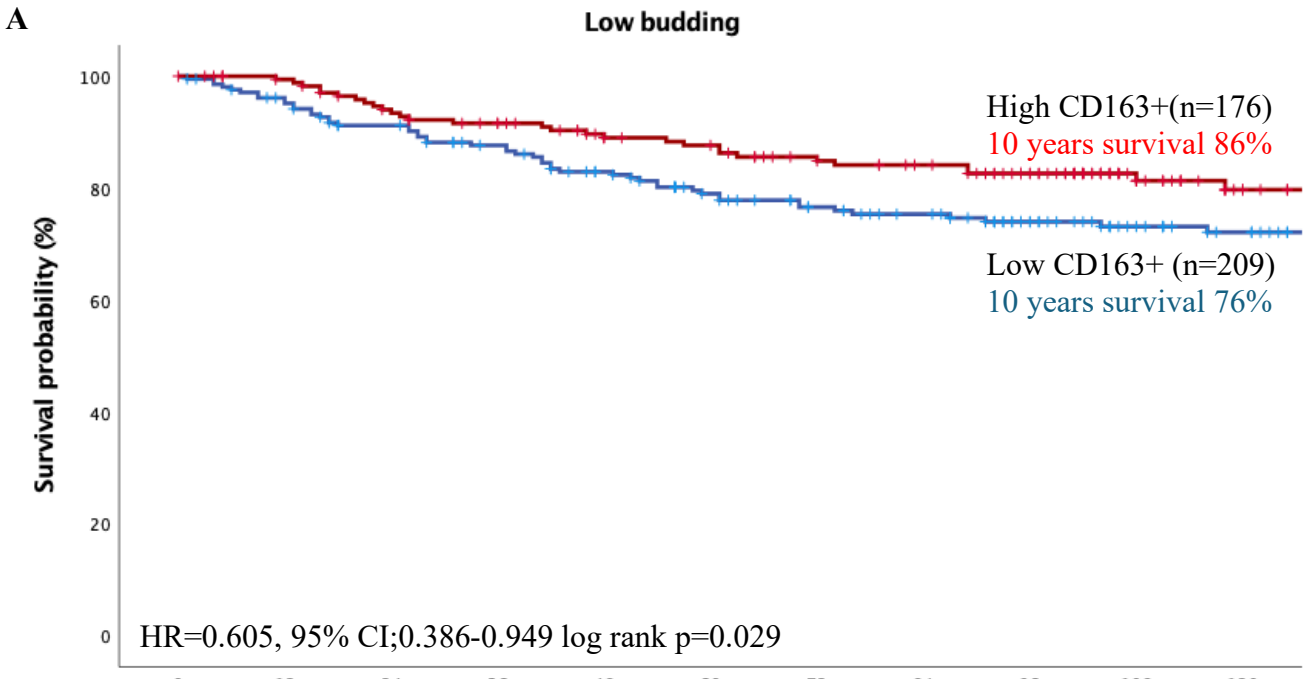

months	0	12	24	36	48	60	72	84	96	108	120
LowCD163+	209(0)	196(5)	181(10)	168(16)	152(24)	135(34)	123(42)	115(48)	95(66)	79(81)	69(90)
HighCD163+	176(0)	168(7)	155(11)	147(15)	135(24)	129(27)	119(34)	112(39)	98(51)	63(86)	46(101)

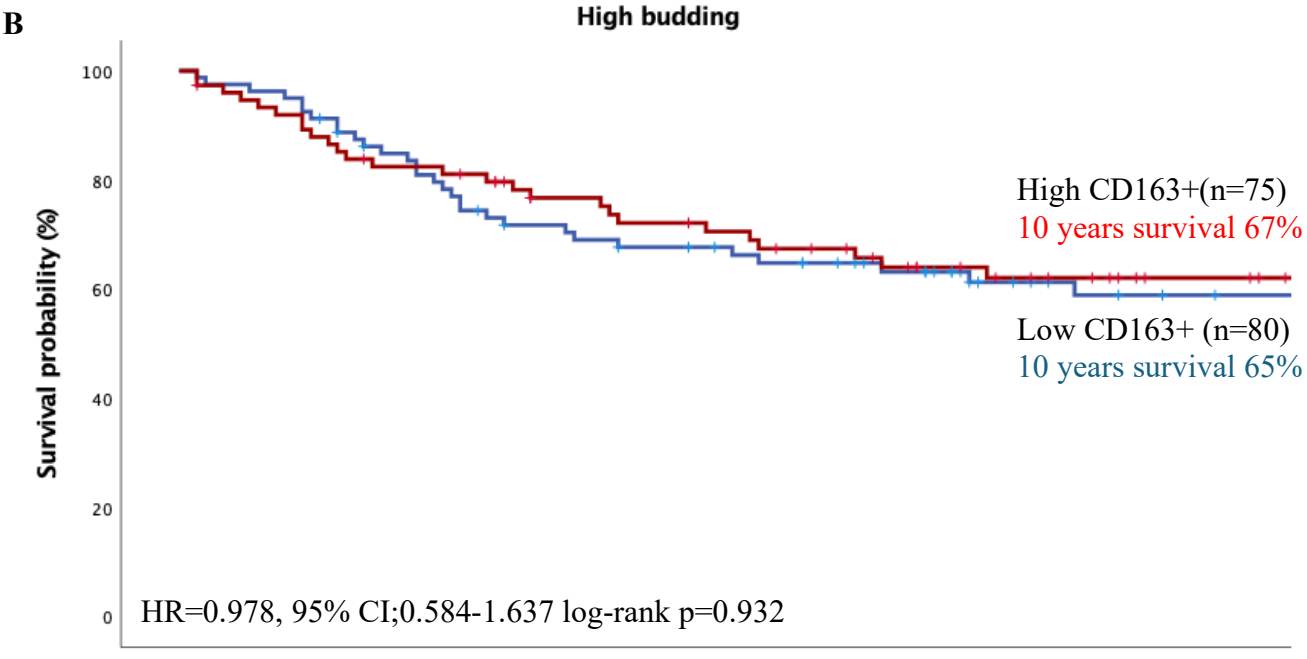

months	0	12	24	36	48	60	72	84	96	108	120
LowCD163+	80(0)	77(0)	65(3)	55(4)	51(5)	48(7)	43(10)	39(13)	28(23)	24(26)	22(28)
HighCD163+	75(0)	68(1)	60(2)	57(3)	50(8)	46(9)	42(10)	36(14)	31(18)	26(23)	24(25)

Figure 3.26 *Kaplan-Meier survival analysis based on percentage of CD163+ cells stratified by low (A) and high (B) budding phenotype for cancer specific survival (CSS) in CRC patients. Hazard ratio (HR) was reported with 95% confidence intervals. P Values were calculated using the log-rank test comparing each budding group with patients with low and high CD163+ phenotypes.*

3.8.3. Relationship between TB and neutrophils

According to the results, there is no statistical difference between budding status and percentage of CD66b+ cells (Table 3.13) or the number of infiltrating CD66b+ cells between high and low budding groups (Figure 3.27). Survival analysis revealed no significant difference in patient survival, when stratified between low HR=0.765, 95% CI;0.462-1.266 log-rank p=0.297 and high (HR=0.583, 95% CI;0.337-1.009 log-rank p=0.054) budding groups, between low and high infiltrating CD66b+ cells. Nevertheless, the survival analysis showed that patients with high CD66b+ (n=315) had a better survival when compared to those with low CD66b+ (n=232) in high budding tumours (Figure 3.28). The life table showed a higher percentage of cumulative survival of patients with high CD66b+ infiltration (77% and 64%) than those with low CD66b+ (69% and 50%) 10 years after diagnosis in low and high budding group respectively.

Table 3.13 *The relationship between budding status and percent CD66b+ cells using the Pearson's chi-square analysis in CRC patient (n=621)*

	Low budding n=376	**High budding n=159**	**P-value**
CD66b+ Low High	 81 (10) 295 (90)	 43 (13) 116 (87)	 0.186

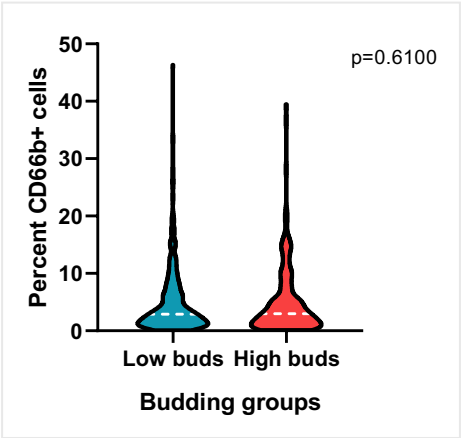

Figure 3.27 *Violin plots show the percent CD66b+ cells compared between budding groups; low (blue) and high (red) TB.*

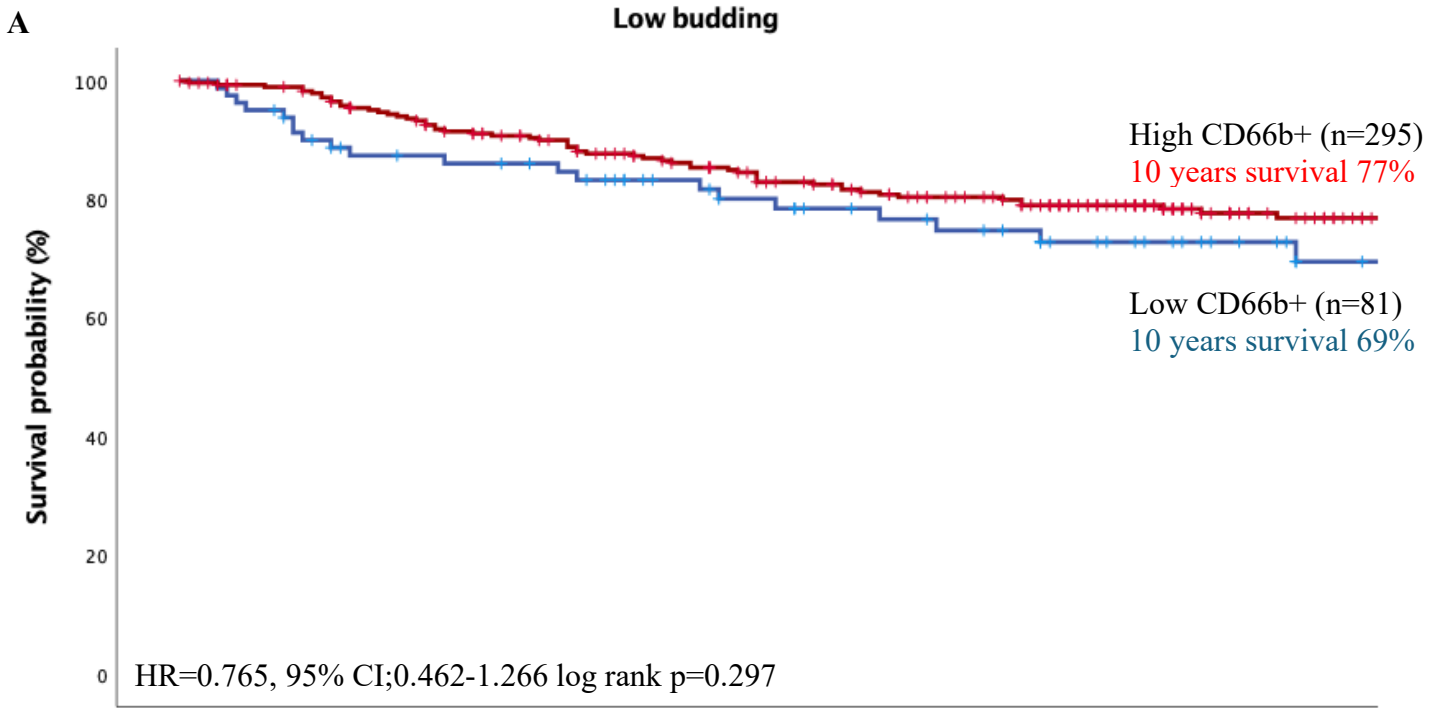

months	0	12	24	36	48	60	72	84	96	108	120
LowCD66b+	81(0)	74(2)	65(6)	63(7)	55(13)	49(17)	43(22)	40(23)	33(29)	27(35)	19(42)
HighCD66b+	295(0)	282(10)	262(16)	244(25)	226(35)	209(44)	192(54)	179(64)	153(87)	110(129)	91(146)

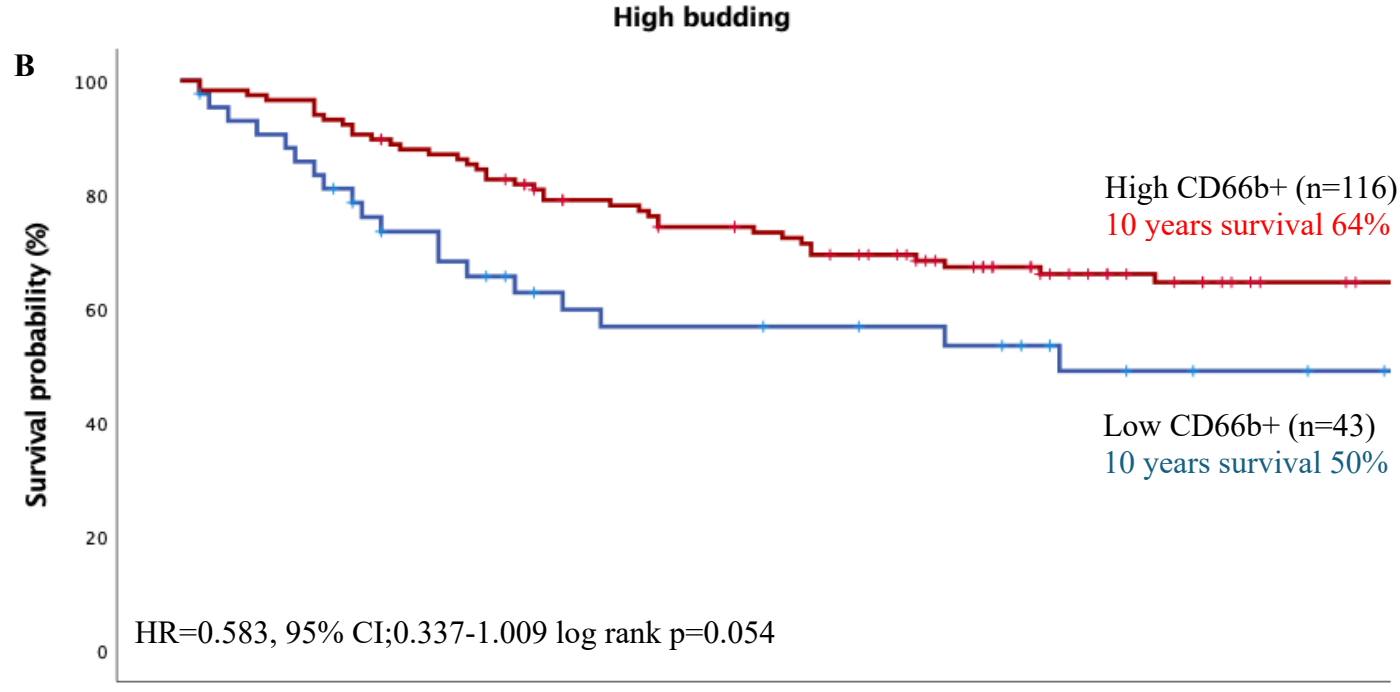

months	0	12	24	36	48	60	72	84	96	108	120
LowCD66b+	43(0)	37(1)	28(4)	22(6)	19(7)	19(7)	17(9)	16(9)	11(13)	9(15)	8(16)
HighCD66b+	116(0)	112(0)	100(2)	92(3)	83(8)	76(11)	69(13)	60(20)	49(30)	42(36)	38(40)

Figure 3.28 *(A) Kaplan-Meier survival analysis based on percentage of CD66b+ cells stratified by low (A) and high (B) budding phenotype for cancer specific survival (CSS) in CRC patients. Hazard ratio (HR) was reported with 95% confidence intervals. P Values were calculated using the log-rank test comparing each budding group with patients with low and high CD66b+ phenotypes.*

3.9. Discussion

Tumour-Nodes-Metastasis (TNM) staging is a useful tool for staging CRC patients and selecting them for a specific treatment, however, many patients experience various outcomes within the same TNM stage (183). There are a number of studies that have reported TB as a poor prognostic marker in CRC patients, however, there were no standard criteria for budding counts. However, tumours with high buds have been used to demonstrate a strong prognostic role in predicting poor outcome in CRC patients (138). In 2018, ITBCC proposed the criteria for TB counts and evaluation in CRC patients. It was agreed to divide TB phenotype into 3 groups: BD1 (0-4), BD2 (5-9) and BD3 (>10) and suggested that the number of TB should be counted in H&E stained CRC tissue sections and also be included in the clinical report (8).

In this chapter, the aim is to identify the prognostic role of TB as well as the correlation with adverse clinical factors in the CRC cohort. To evaluate TB, the ITBCC guideline were followed and defined CRC patients into low (<10 buds) and high (>10 buds) budding groups. Survival analysis showed that patients with high TB (n=180) had significantly poorer survival than patients with low TB (n=439). These results are in agreement with many other peer studies demonstrating that a high budding phenotype reflects a worse outcome in CRC (138). The finding also validates that TB is an independent biological marker against other adverse clinical factors including CRC stages, disease recurrence, venous invasion, and peritoneal involvement. The multivariate analysis revealed that budding exerted an independent impact on patient survival in the cohort which re-enforces the strong prognostic role of TB in CRC development (7).

Recent studies reported the association between TB and adverse clinical factors in CRC (172, 173, 175, 177). These explain the crucial role of TB as a prognostic marker in the progression and metastasis of CRC. Thus, unfavourable factors from the CRC database were selected to identify associations with TB in the CRC cohort. The prognostic role of sex was

consistently reported in a variety of cancers including CRC (184). The incidence showed that patients over 65 years with CRC is higher in women compared to men (22). The molecular profile based on sex differences also showed that women tend to have a higher number of mutated BRAF and MSI tumours compared to men (185). Moreover, recent studies emerging on CRC transcriptomes which could unravel the prognostic biomarker as to whether it is sex-specific (186). However, the finding showed no association between sex and TB, although males tend to have a poorer outcome in both low and high-budding groups.

In addition, the alteration of gene mutation was showed to be one of the factors that could drive tumour metastasis in CRC (41, 187-189). As TB is known to be associated with disease recurrence, a few studies tried to understand if there is any correlation between TB and mutational status in CRC (46, 154). Therefore, mutational landscape; *KRAS/BRAF* and MMR genes, were studied to clarify if it could be related to tumours that exhibited high budding phenotype. A study from Trinh et. al demonstrated that mutated *KRAS/BRAF* is associated with high TB tumours (n=1320) (46), suggesting the involvement of gene mutation in CRC budding formation. However, no significant association between TB and mutated genes was found in the current study. This may be due to the number of patients involved. However, a higher number of buds in patients with *KRAS* mutation was observed although no statistical significance was found. Additionally, a meta-analysis study reported a significant association between pMMR/MSS tumour and TB in CRC patients (154). Results from the current study demonstrated the highest number of TB in dMMR tumours and that dMMR tumours showed the worst outcome in cancer-specific survival of tumours with both low and high TB phenotypes. Although there is no significant association between MMR tumours and TB, poorer survival of dMMR tumours in patients with both low and high TB confirms the strong prognostic value when tumours exhibit dMMR in this CRC cohort regardless of budding phenotype. Generally, our findings showed no significant correlation between TB and known

mutational phenotypes in CRC. This suggests that perhaps there are other factors drive TB formation as it is not clear what drives TB in terms of genetic background in this CRC cohort.

Aside from mutated genes, the prognostic score of high CRP and low albumin level were studied as there is evidence to suggest this leads to poorer survival in cancer patients (190). In 2003, Forrest et. al, proposed a combination of these two scores which indicate the systemic inflammatory response in CRC; this combined score is called the mGPS. The mGPS was suggested as a prognostic factor that could classify patients who could potentially benefit from additional treatment in CRC (81, 191). Regarding the correlation with TB, our findings showed no significant association between TB and mGPS. However, in high TB tumours, mGPS2 patients significantly experienced the worst outcome while no significance was found between the mGPSs group in low TB tumours. This suggested the positive relationship between activation of acute inflammation and the present of high TB in CRC which, thereby, leading to a micro-invasion of budding cells and its prognostic value in CRC.

Apart from mGPS, the combination of KM and TSP has been suggested as a predictive biomarker in CRC (90, 192). However, few studies have investigated if this marker correlates with the TB phenotype (159). Interestingly, we recently published the prognostic value of combined TB and GMS scores (161). The combination between budding tumour and inflammation score could also lead to the new treatment combination in CRC patients. GMS2 represent a weak inflammation (KM) and high TSP. Patients with GMS2 are consistently reported to have the worst outcome in cancer patients (90, 193, 194). Interestingly, in our CRC cohort, there is a significant difference in the number of budding cells between GMS0 and GMS2. Although there is no significant correlation between TB phenotype and inflammatory scores, tumours with high TB may have distinct characteristics that could alter the microenvironment around the budding cells to be suitable for cancer growth and metastasis. In addition to confirming this hypothesis, further studies were carried out to identify the

correlation between TB and the TMEs to investigate the possible correlation between immune cells and high TB tumour.

The prognostic value of TMEs have gradually been uncovered and shown to have an impact in CRC progression and metastasis (195). Applying immunotherapy to standard treatment improves patient survival in certain types of cancer such as the use of immune-checkpoint inhibitors for non-small cell lung cancer patients (196). However, not all types of cancer respond, and drug resistance remains an issue (73, 74). High cytotoxic T cell activity has been reported to favour good clinical outcome (197, 198) while high infiltration of T regulatory cells was reported as a poor prognostic marker in CRC (199-201). Moreover, T-cell infiltration has been shown to have a promising role in CRC survival including its correlation with TB (18, 131). To confirm this correlation, mIF technology was performed. Image analysis was used to determine the specific immune profile differently expressed in groups of low and high budding.

According to the findings, patients with high infiltrating T cells (CD3+) and cytotoxic (CD3+CD8+) T cells experienced significantly higher survival than those with low infiltration T cells in low TB tumours. Interestingly, the percentage cytotoxic T cells count showed that there is a significantly higher number of infiltrating T cells in tumours with low compared to high TB. In contrast, for tumours infiltrated with high regulatory T cells (CD3+FOXP3+), the survival analysis showed a poorer outcome than those with low CD3+FOXP3+ in tumours with high budding phenotype, although there was no significant difference. This finding suggested that a tumour which produces fewer buds, had higher infiltrating cytotoxic T cells and this was shown to associate with better outcomes. The poor outcomes of tumours with high budding, high infiltration of regulatory cells indicates recruitment of suppressive T cells from tumours to initiate metastasis. This observation corresponds to the previous studies that reported a

reduction of immune cells in tumours which exhibit a high number of budding cells at the invasive front compared to low budding tumours (18, 160, 202).

In contrast to the anti/pro-tumorigenic role of T cells, macrophages have been reported to play a crucial role in CRC development and metastasis (106, 203). Different polarization between pro-inflammatory and anti-inflammatory are consistently reported demonstrating a counteractive function between the two groups (204, 205). There is less evidence regarding the correlation between TB and macrophages, although one study reported that pro-inflammatory macrophages could induce TB when co-culture with patients-derived colonospheres (206). In this study, there is no correlation between budding status and the percentage of anti-inflammatory pan-macrophages CD68+ as well as pro-inflammatory macrophages CD163+. Having said that, when tumour exhibited high budding, there is a significant association regarding CRC survival compared between tumours with low and high infiltrated CD68+ cells. Tumours with a high number of CD68+ cells were shown to have a poorer survival compared to low CD68+ cells. In contrast, tumours with a high number of CD163+ infiltrating cells were shown to have prolonged survival compared to those with low CD163+ cells. These results suggest the opposite role of macrophages which have been reported in the literature, however, the role these anti-and pro-inflammatory macrophages in relation to budding phenotype is still unclear.

Neutrophils have been studied in relation to their role in CRC microenvironment (111). The anti-tumour function of neutrophils and their prognostic value in CRC was reported in a several studies along with their relationship with TB (131, 207). It has been revealed that some populations of neutrophils; tumour-associated neutrophils (TANs), play an important role in tumour-supportive function in CRC (208). However, inthis study, no significance was found regarding the percentage of infiltrating CD66b+ cells and TB status. In addition, there is no

significant association between CD66b+ cells and patient survival in the cohort when stratified with budding status.

In summary, mutated genes (*KRAS/BRAF*) showed a promising correlation to TB although this lacked statistical power. It could be indicated that mutational level may not solely drive budding phenotype. Recently, consensus molecular subtype (CMSs) was proposed as the most robust classification system for CRC (61). There is evidence showing the correlation between TB phenotype and the CMS4 subgroup which is reported as mesenchymal-related, characterised by high transforming growth factor- β (TGF-β) expression, stromal invasion and angiogenesis (46). Moreover, the transcriptomic studies showed alterations may not be detected at the genomic level (209). High throughput technologies were utilised for RNA sequencing and the RNA transcripts were measured, and gene expression was analysed to reveal the potential biological marker in cancer research (210). For this reason, investigating the translational expression of pathway signalling would perhaps unravel the mechanism underlying TB in CRC. In this study, the correlation between budding and CMSs subgroup together with the analysis of the transcriptomic data were next investigated to help identify the novel marker that could predict budding phenotype in CRC.

This study revealed, albeit no significant correlation, the possible link between prognostic scores for inflammatory response and TB. Tumours with high TB were shown to have a positive correlation with the weak inflammatory response suggesting its association with disease metastasis and poor outcome in CRC. Also, the findings reveal a promising correlation between T cells and tumours with high TB. As T cells are major components of the adaptive immune system (211), this could suggest that T cells, but not myeloid cells, were targeted and suppressed by budding cells, to create pro-tumour conditions which favoured metastasis. However, there is still no evidence of how the individual population of buds could affect the surrounding microenvironment. Also, there is emerging knowledge of how intratumoral and

peritumoral inflammation may have a distinct immune profile which could lead to the association with patient survival (212). A limitation of this study was that it was conducted in tumour core TMAs, therefore, not at the invasive area of the tumour where buds are usually found. Taking this into account, quantification of immune cells at the invasive edge may be a more appropriate method to observe a spatial correlation between budding cell and its surrounding microenvironment.

Chapter 4. The relationship between tumour budding and molecular CMSs subtype and the bulk RNA transcriptomic analysis.

4.1. Introduction

According to the previous chapter, data shows no significant correlation between mutated *KRAS/BRAF* and TB phenotype. This could suggest that the mutational status of key driving CRC genes may not drive budding phenotype and that downstream transcription/translation signalling may play a vital part. Recently, the use of high-throughput sequencing emerged and led to numerous discoveries in biology, especially in cancer research (210, 213). Examination of differential mRNA expression can be used to identify potential biomarkers in cancer treatment as well as the stratification of the disease subtypes (214, 215).

In CRC, the consensus molecular subtypes (CMS) were introduced based on their related signalling pathways and genes expression profiles (216). Four distinct features were reported: CMS1, a group of hypermutated and microsatellite unstable (MSI) with a strong immune activation. CMS2, a high level of chromosomal instability (CIN) subgroup with WNT and MYC signalling activation. The frequent KRAS mutation was observed in CMS3 subgroups together with an increase in metabolic pathways. Lastly, the CMS4 group contains a high stromal density and presents with activation of genes associated with epithelial-mesenchymal transition (EMT) induced by transforming growth factors-β (TGF-β), stromal invasion and angiogenesis (61). The impact of CMS subtypes on patients with metastatic CRC was consistently reported regarding the different responses to the treatment and patients' survival (217-219).

According to research studies, it has been demonstrated that tumours with high TB are likely to be characterised as CMS4, consistent with the shift from epithelial to mesenchymal subtype from tumour mass to TB regions. Moreover, the EMT-related genes were shown to be highly expressed in budding cells when compared to the tumour mass in CRC (14, 46). The relationship between TB and EMT has been increasingly reported, however, there is no solid evidence demonstrating that TB is driven by the EMT process (14-16, 220, 221). Nevertheless,

some studies suggested that budding cells may only undergo partial EMT, and that other tumour-related signalling could play a part in this scenario (12, 16, 17, 21).

For this reason, the association between TB and CMSs subtype was investigated together with the study of the whole transcriptome bulk RNA sequencing in 787 patients from the Glasgow Royal Infirmary (GRI) cohort. This chapter aims to determine if there is a correlation between TB and molecular subtype in CRC as well as profile the transcriptomic state for the TB phenotype It was hypothesised that TB may be correlated with the stromal CMS4 subtype which has been shown to have the worst outcome among CRC patients. Moreover, the aim was to identify if there is a difference in an underlying transcriptome of patients between low and high budding, and that high TB may be involved in signalling which led to the worst outcomes in CRC.

4.2. The association between TB and CMS subtypes

According to the statistical chi-square test, there is no significant difference between TB and CMS groups (p=0.080) (Table 4.1). However, there is a significant difference in the number of buds across CMS groups (p=0.0186) (Figure 4.1). Interestingly, CMS4, an EMT-associated subgroup, was shown to have the highest number of buds compared to other subgroups (CMS1-3) (Figure 4.1). Additionally, the survival analysis revealed no significance in CMS groups regarding the patient's specific cancer survival when stratified with the budding phenotype (Low TB; HR=1.097, 95% CI;0.845-1.425 log rank p=0.487, and High TB; HR=1.287, 95% CI;1.000-1.656 log rank p=0.050) (Figure 4.2). However, in high TB tumours, CMS4 have the worst outcomes (Figure 4.2B). The life table revealed no differences in survival time of patients with CMS subgroups in low TB tumours (78% CMS1, 71% CMS2, 63% CMS3 and 69% CMS4). However, in tumours with high TB, 82%, 69%, 61% and 44% of patients with CMS1, 2, 3 and 4 respectively survived 10 years after diagnosis.

Table 4.1 *The relationship between budding status and CMS groups using the Pearson's chi-square analysis in CRC patients (n=621)*

	Low budding n=441	High budding n=180	P-value
CMS			0.080
1	58 (20)	29 (22)	
2	161 (57)	67 (50)	
3	22 (8)	6 (4)	
4	43 (15)	33 (24)	

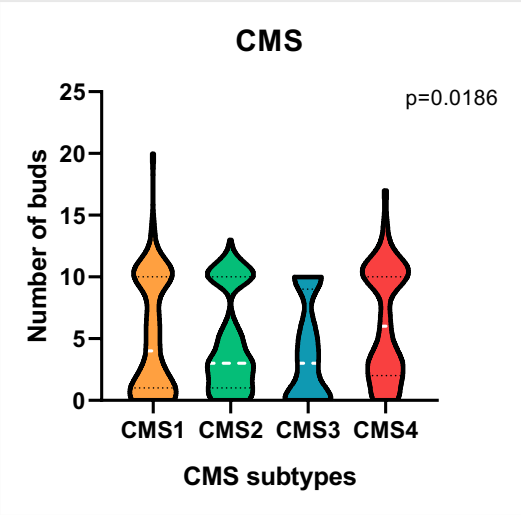

Figure 4.1 *Violin plots show the number of buds compared between CMS groups.*

A

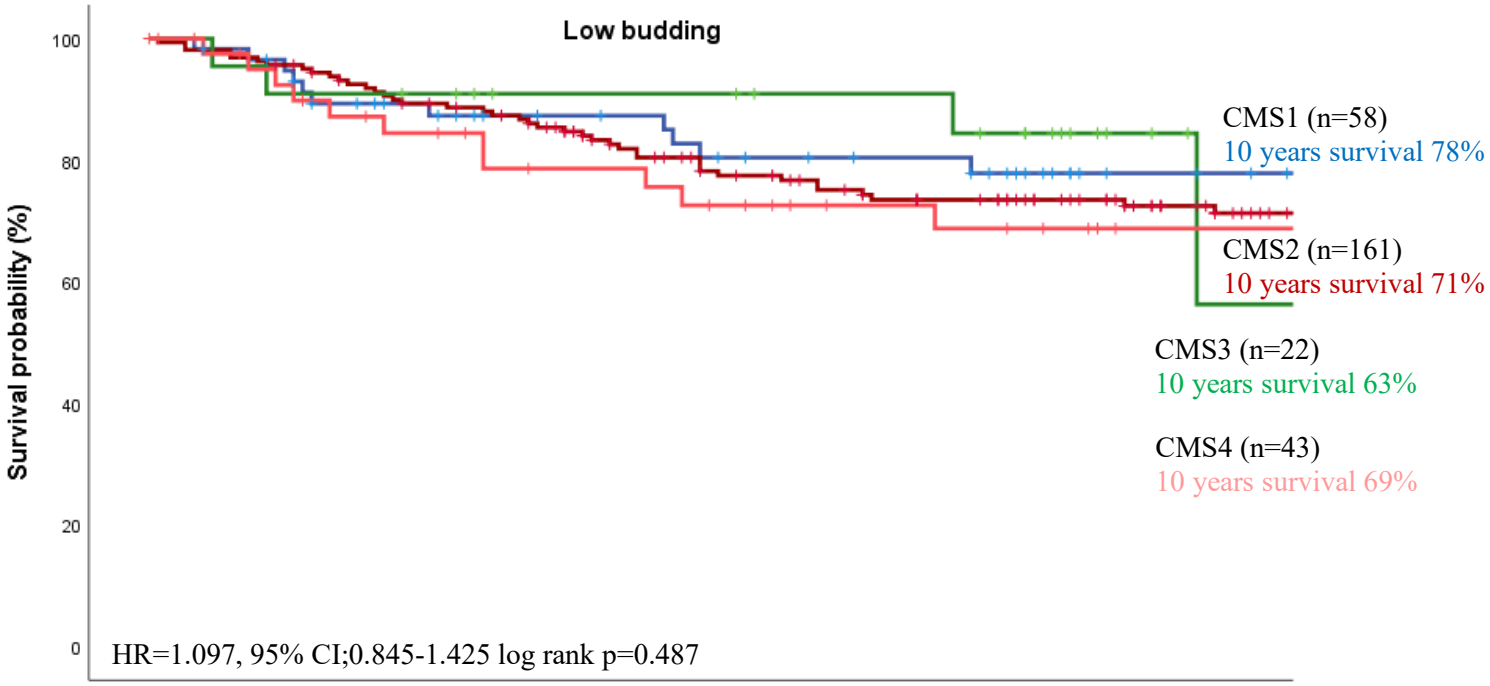

months	0	12	24	36	48	60	72	84	96	108	120
CMS1	58(0)	58(0)	56(2)	54(4)	52(6)	52(6)	51(7)	51(7)	51(7)	51(7)	50(8)
CMS2	161(0)	160(1)	157(4)	155(6)	152(9)	151(10)	151(10)	149(12)	149(12)	148(13)	146(15)
CMS3	22(0)	21(1)	21(1)	21(1)	19(3)	17(5)	16(6)	16(6)	15(7)	14(8)	14(7)
CMS4	43(0)	43(0)	42(1)	42(1)	42(1)	41(2)	41(2)	41(2)	41(2)	41(2)	41(2)

B

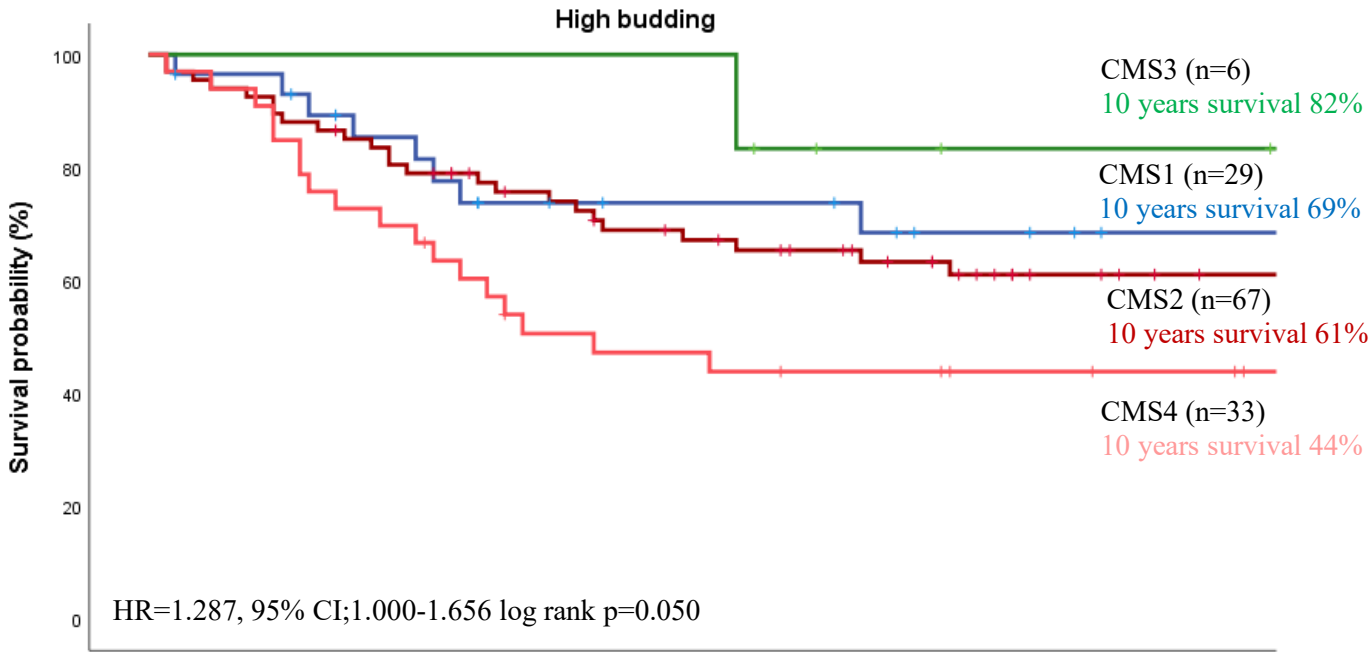

months	0	12	24	36	48	60	72	84	96	108	120
CMS1	29(0)	29(0)	29(0)	29(0)	29(0)	29(0)	27(2)	27(2)	27(2)	27(2)	27(2)
CMS2	67(0)	64(2)	62(3)	59(4)	58(5)	58(5)	58(5)	57(6)	56(6)	55(6)	54(6)
CMS3	6(0)	6(0)	6(0)	6(0)	6(0)	6(0)	6(0)	6(0)	6(0)	6(0)	6(0)
CMS4	33(0)	33(0)	33(0)	33(0)	33(0)	33(0)	32(0)	32(0)	31(1)	31(1)	31(1)

Figure 4.2 *Kaplan-Meier survival analysis based on CMS groups stratified by (A) low and (B) high budding phenotype for cancer specific survival (CSS) in CRC patients. Hazard ratio (HR) was reported with 95% confidence intervals. P Values were calculated using the log-rank test comparing each budding group with patients with CMS groups.*

4.3. Identification of a gene signature associated with TB in CRC

4.3.1. Gene-level differential analysis

The underlying mechanism of TB in CRC was investigated using the transcriptomic data for the GRI cohort (n=612). Before applying the analysis, a batch effect was observed (Figure 4.3A) and therefore have been corrected (Figure 4.3B) to improve clustering performance for the interpretation of the results.

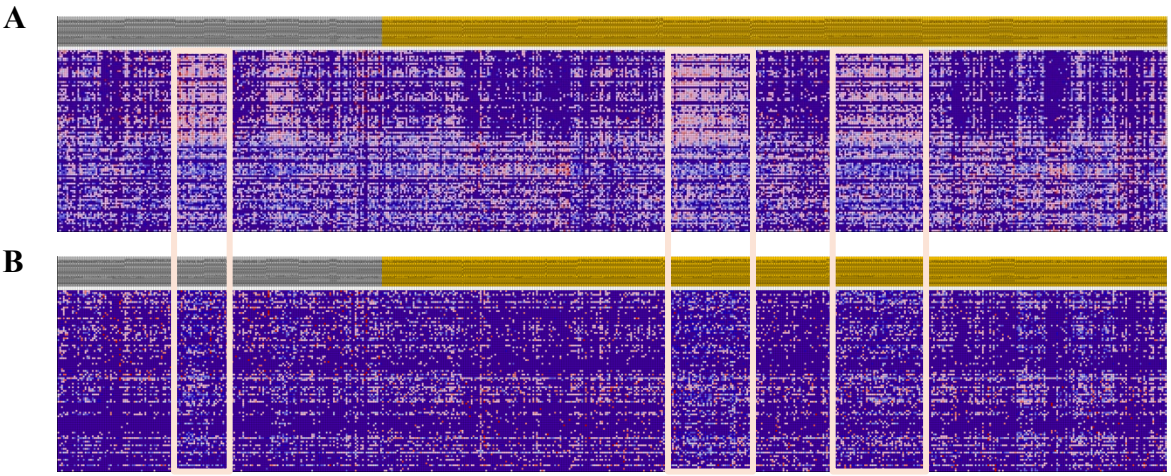

Figure 4.3 *The hierarchical clustering (A) before and (B) after batch correction.*

After the corrected batch effect, differential gene expressions have been evaluated based on two groups of low (n=433) and high buds (n=179). The principal component analysis (PCA) was performed to visualise the groups of tumours based on the expression level of genes. According to the results, there is no obvious cluster between the two groups (Figure 4.4).

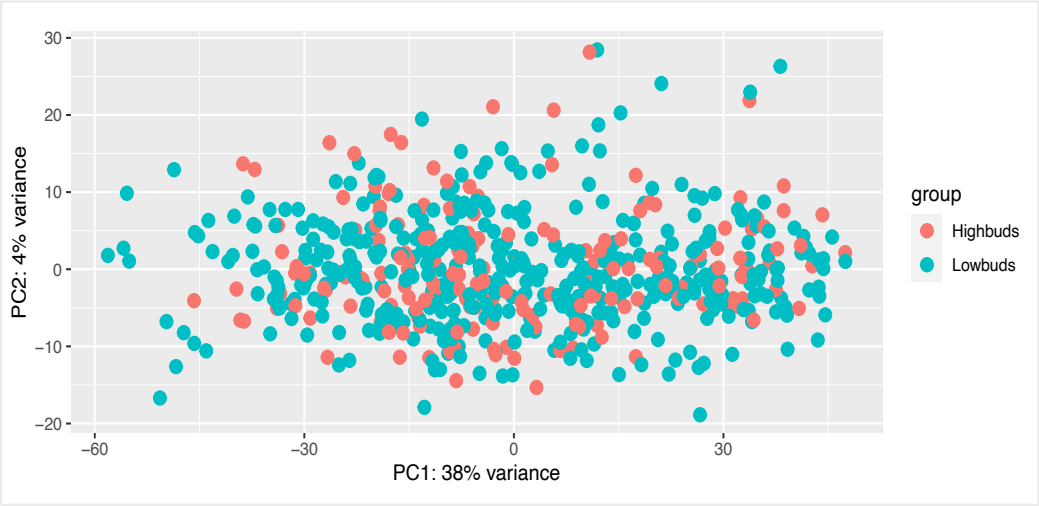

Figure 4.4 *Principal component analysis (PCA) showed the clustering pattern of high (red) and low (green) budding group and.*

Moreover, differential expression was then performed to identify the genes upregulated in tumours with either low or high budding using DESeq2 R package. According to the results, the top 10 genes significantly expressed in both low and high budding groups were reported (Figure 4.5) (Table 4.2). Interestingly, genes upregulated in high budding tumours such as *MRAS, SEMA6D, PON2* and *WDR86* are known to have a possible prognostic role in CRC.

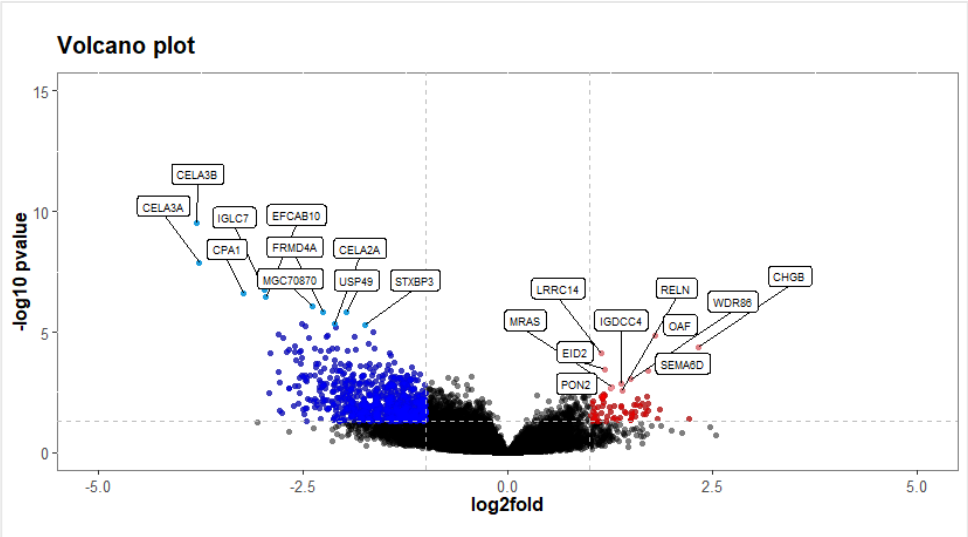

Figure 4.5 *Volcano plot shows significant genes regulated in high budding groups; red is up regulated, and blue is down regulated.*

Table 4.2 *The top 10 genes significantly expressed in tumours with either low or high budding CRC.*

Gene	Gene title	*p*-value	FC
Low budding group			
CELA3B	Chymotrypsin Like Elastase 3B	2.860187e-10	-3.794851
CELA3A	Chymotrypsin Like Elastase 3A	1.333563e-08	-3.768068
IGLC7	Immunoglobulin Lambda Constant 7	1.707667e-07	-2.975840
CPA1	Carboxypeptidase A1	2.420796e-07	-3.226840
EFCAB10	EF-Hand Calcium Binding Domain 10	3.578534e-07	-2.955565
MGC70870	C-terminal binding protein 2 pseudogene	8.396996e-07	-2.383310
USP49	Ubiquitin Specific Peptidase 49	1.507430e-06	-1.967944
FRMD4A	FERM Domain Containing 4A	1.445580e-06	-2.252808
STXBP3	Syntaxin Binding Protein 3	4.914932e-06	-1.744023
CELA2A	Chymotrypsin Like Elastase 2A	4.727264e-06	-2.115581
High budding group			
OAF	Out At First Homolog	1.398285e-05	1.805113
CHGB	Chromogranin B	4.068497e-05	2.331881
LRRC14	Leucine Rich Repeat Containing 14	7.363763e-05	1.141377
EID2	(EP300 Interacting Inhibitor of Differentiation 2	3.484568e-04	1.183384
SEMA6D	Semaphorin 6D	4.063599e-04	1.709184
WDR86	WD Repeat Domain 86	9.050859e-04	1.501940
IGDCC4	Immunoglobulin Superfamily DCC Subclass Member 4	1.393668e-03	1.381396
MRAS	Muscle RAS Oncogene Homolog	1.962166e-03	1.269912
PON2	Paraoxonase 2	2.051291e-03	1.248192
RELN	Reelin	2.762477e-03	1.395796

**Abbreviation; FC, foldchange. Negative (-) value indicates down-regulation.*

In addition, using the string analysis, most of the genes upregulated in high budding groups seem to have a correlation with EGFR signalling (Figure 4.6). Nevertheless, there is no obvious signalling that may drive budding formation in CRC.

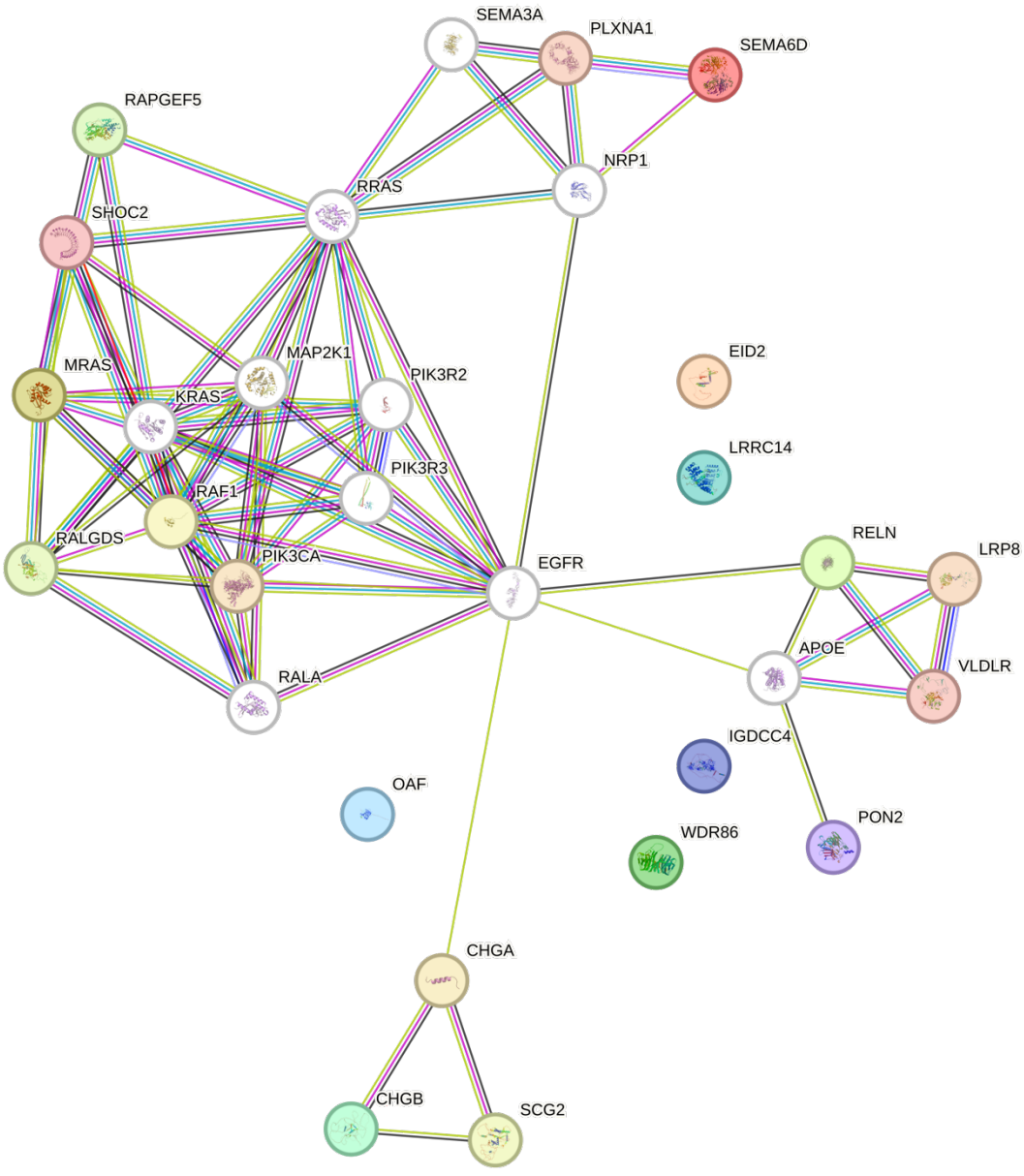

Figure 4.6 *STRING analysis of proteins increased in tumour with high budding group. Proteins are shown as nodes and the query proteins are highlighted in color.*

4.3.2. Pathway analysis

A computational method called gene set enrichment analysis (GSEA) and single sample GSEA (ssGSEA) were performed to evaluate the enrichment scores of samples with either low or high TB in CRC. This method was used to identify the gene sets from transcriptomic data that were highly expressed/represented in the dataset that may associate with different phenotypes.

Therefore, the transcriptomic data from the GRI CRC cohort was utilised (n=612) to compare the enrichment scores between two groups of tumours with high (n=179) and low budding (n=433). According to the heatmap analysis, there is no obvious distinction regarding the genes signature between tumours with low and high budding (Figure 4.7).

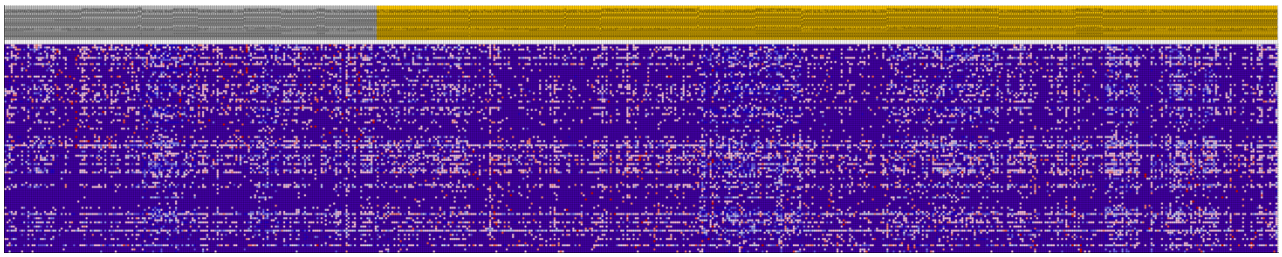

Figure 4.7 *The hierarchical clustering of the top 50 most differentially expressed genes between tumour with low (Amber) and high (Grey) budding phenotype.*

Moreover, the differential expression of genes related to the hallmark of cancer from the GSEA database was also examined. According to the analysis, there are four gene sets; angiogenesis (p=0.572, FDR=1.000), epithelial mesenchymal transition (EMT) (p=0.566, FDR=0.971), reactive oxygen species (ROS) pathway (p=0.851, FDR=1.000) and interferon alpha (IFNA) response (p=0.946, FDR=0.964), that were comparatively highly expressed in tumours with high TB compared to low TB group, although this was not statistical significant (Figure 4.8) (Table 4.3). Additionally, the comparison between tumours with low and high TB regarding the hallmark pathway was visualised in the heatmap based on ssGSEA analysis (Figure 4.9). The results showed no clear pattern in the differences between the two groups.

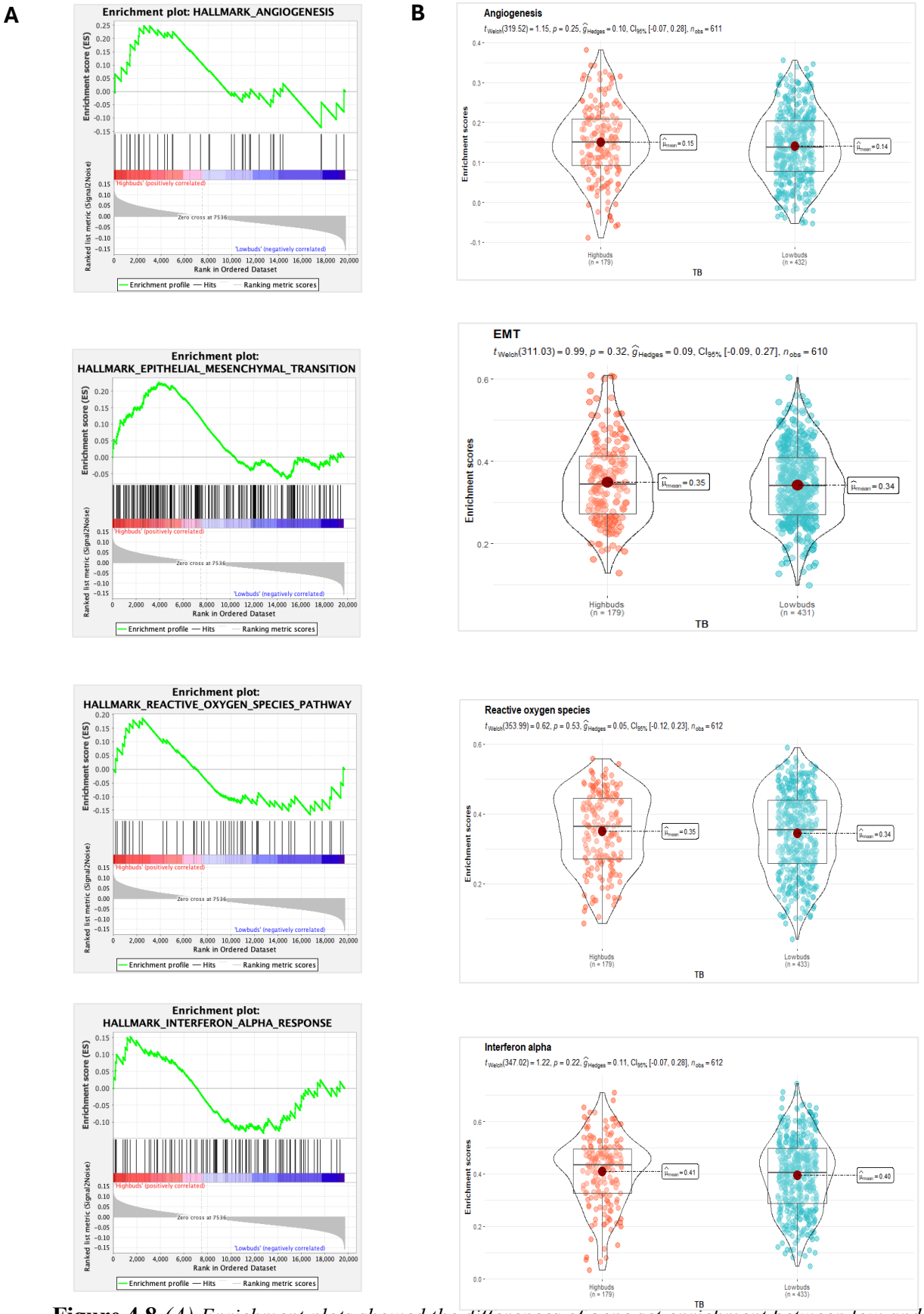

Figure 4.8 *(A) Enrichment plots showed the differences of gene set enrichment between low and high budding group using GSEA and (B) the box plots showed the single sample by ssGSEA for each of the pathway (h.all.v2023.2.Hs.symbols.gmt database).*

Table 4.3 *Enrichment analysis by tumour with low and high TB in CRC from GSEA*

Gene set name	Nominal p	FDR
Angiogenesis	0.498	1.000
Epithelial Mesenchymal transition	0.556	0.854
Reactive oxygen species	0.867	1.000
Interferon alpha response	0.930	0.968

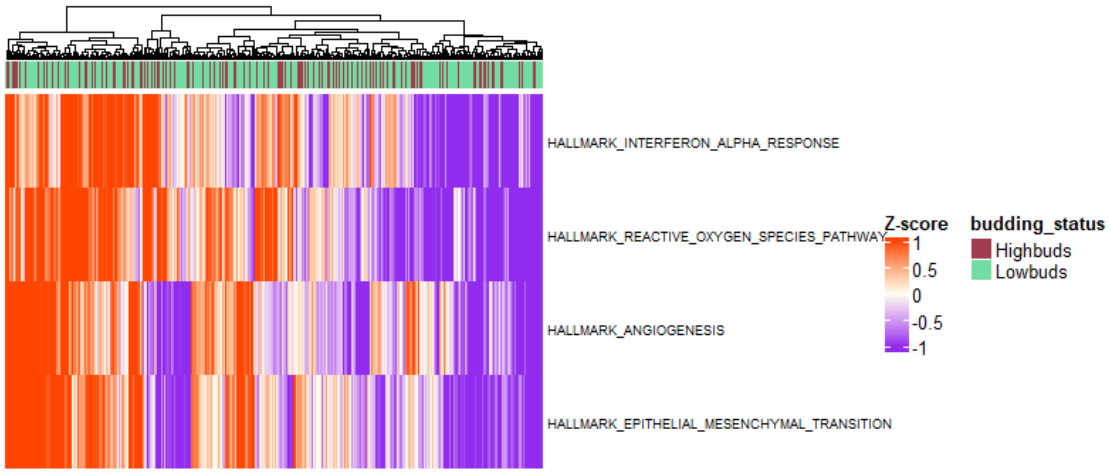

Figure 4.9 *Hierarchical clustering of the four hallmark gene sets between tumours with low (green) and high (brown) budding phenotype.*

Additionally, when analysed using the oncogenic signature database there were 27 genes involved in tumour development signalling including KRAS mutation (p=0.767, FDR=1.000), MEK (p=0.694, FDR=1.000), P53 (p=0.838, FDR=1.000) and YAP1 (p=0.734, FDR=1.000), upregulated in tumours from the high budding groups. However, there was no significant difference between the two groups (Figure 4.10) (Table 4.4). The comparison between tumours with low and high TB regarding the oncogenic pathway was visualised in the heatmap based on ssGSEA analysis (Figure 4.11). No clear pattern was found between the two groups.

A **B**

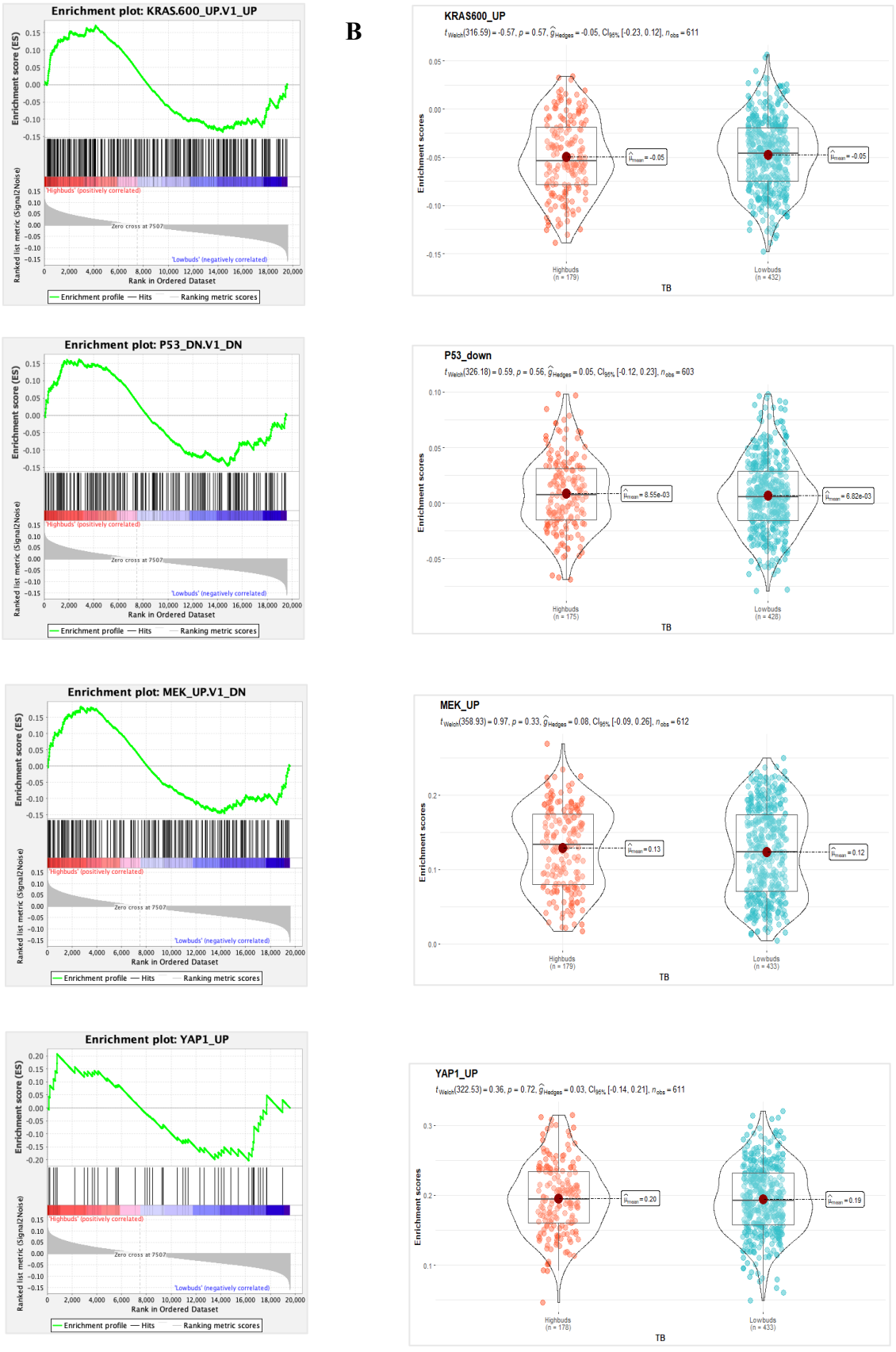

Figure 4.10 *(A) Enrichment plots showed the differences of gene set enrichment between low and high budding group using GSEA (c5.all.v2023.2.Hs.symbols.gmt database) and (B) the box plots showed the single sample by ssGSEA for each of the pathway.*

Table 4.4 *Enrichment analysis by tumour with low and high TB in CRC from GSEA*

Gene set name	Nominal p	FDR
KRAS600	0.767	1.000
P53	0.838	1.000
MEK	0.694	1.000
YAP1	0.734	1.000

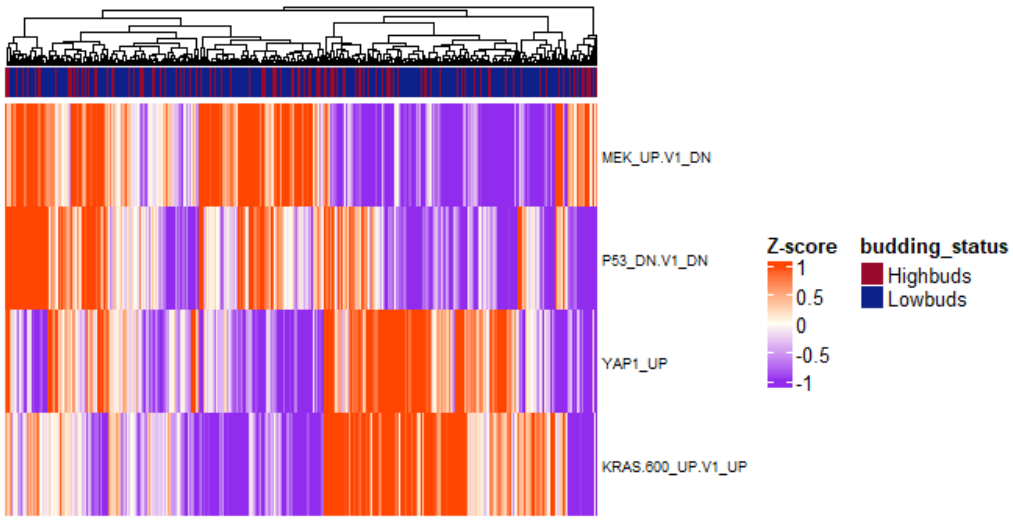

Figure 4.11 *Hierarchical clustering of the four hallmark gene sets between tumour with low (green) and high (brown) budding phenotype.*

4.4. Discussion

TB is well-established as a strong prognostic marker in CRC. However, there is a lack of studies reporting the underlying mechanism of TB formation (21). Molecular classification of CRC patients using CMS subtypes has been shown to predict response (64, 222). The finding shows that the number of tumour buds was significantly different between CSM4 and CMS subtypes 1-3, with tumours classed as CMS4 exhibiting the highest number of budding cells. The survival analysis also revealed that, when tumours exhibited high TB, those with CMS4 subtypes tended to have the worst outcomes. This was supported by the studies that tumours with high TB may correlated with CMS4 mesenchymal subtype (14, 223). CMS4 subtype is known as a mesenchymal subtype that is characterised by high expression of EMT signatures and also is the worst prognostic subgroup regarding its correlation with disease progression and metastasis in CRC (224). According to the findings, it could be suggested that tumours with high TB are more likely to be CMS4 subtypes, which could provide important clues to unravelling the mechanism underlying TB in CRC. However, few studies have shown any correlation between the TB phenotype and CMS subtype, and therefore future work would need to test hypothesis.

Aside from the possible correlation between TB and CMS4, the underlying mechanism of TB remains unclear. Therefore, further investigation on the transcriptomic level was conducted. Transcriptome analysis has been proven to identify the key mechanism in disease development and metastasis leading to the development of a novel treatment in cancer research (225). The transcriptomic data from RNA sequencing of CRC tissue provided by Bioclavis (TempOSeq) was analysed. This technique is highly specific and allows for RNA sequencing of formalin-fixed paraffin-embedded tissue samples enabling easy profiling of patient cohorts (166). According to the results, genes associated with poor outcomes in CRC are significantly upregulated in tumours with high buds. For example, a muscle RAS oncogene homolog,

MRAS, part of the RAS family, has been shown to be associated with the development of tumours (226-228). Paraoxonase 2 (PON2), the membrane-associated lactonase, is shown to be upregulated in tumours when compared to normal tissue (229). There is no report regarding its association with patient outcome however, evidence showed its association with tumour progression and chemoresistance in CRC (230). Although the function of CHGB (chromogranin-B, CgB) is limited, it has been suggested that CHGB could be used as a prognostic marker and may correlated with CRC patient's survival (231).

In addition, string analysis showed that those genes upregulated in high TB tumours may be involved in EGFR signalling. Epidermal growth factor receptor (EGFR) is one of the most important pathways inducing proliferation, migration, differentiation and cell apoptosis which have been reported to have an impact on cancer patients' survival including CRC (232). Many downstream signalling that has been known to stimulate metastasis are also derived or activated by EGFR including EMT (233). Regarding its relationship with TB, it is rarely reported whether TB could be induced by EGFR signalling. Therefore, the enrichment pathway analysis was performed to identify if there is any tumour-related signalling pathway involved in high TB tumours. The results revealed four gene sets enriched in tumours with high TB: EMT, angiogenesis, interferon alpha and reactive oxygen using the hallmark of the cancer database. EMT was well-established regarding its association with tumour development and metastasis (234). The transition from epithelial to mesenchymal cells modulates many factors causing the disease recurrence (235-237). In agreement with this finding, Jensen et al. reported that GSEA analysis reviewed the two most enriched gene sets in tumour budding which were from EMT and TGF-β signature (155). This could imply that the process of EMT could be one of the key inducers for budding cell formation. However, a few studies suggested that, due to the heterogeneity among budding cells, EMT could play a role but not solely induce budding formation (12, 16, 220).

In addition to EMT, angiogenesis was also identified as being associated with budding, which is the process of developing new blood vessels and organs during the embryonic process (238). When dysfunctional, it could also benefit tumour growth, invasion and metastasis (239). During the process of tumour development, many growth factors and cytokines are released therefore stimulating angiogenesis for the supply of nutrients and oxygen (240). It has been shown that inhibiting the development of new blood vessels could help prevent tumour growth and improve outcomes in cancer patients (241). In agreement to the finding above, one study showed that TB could recruit CCL5 leading to the activation of angiogenesis by enhancing VEGFA expression and collagen synthesis in CRC (242). Moreover, TB has been reported to correlate with hypoxia-induced hypo-vascularisation in CRC. Righi et al. demonstrated that budding could escape self-destruction by expressed hypoxia-induced factor 1a (HIF-1a) leading to its poor prognosis in CRC (243). The association between TB and the ROS pathway is rarely reported, however, it could be one of the factors that help budding cells to survive and modulate the microenvironment at the invasive tumour to be able to induce metastasis (243, 244). Though not significant, GSEA showed that tumours with high TB also have genes enriched in interferon alpha signalling pathways which is known to play an important role in the human immune response (245). This signalling comprises the complex regulatory system of both innate and adaptive immune responses. Besides, IFNs can also be involved in the regulation of cancer cell proliferation and metastasis (246). Many studies suggested that, when tumours produced high TB, it could alter their microenvironments and allow tumour cells to escape from immunosurveillance leading to disease metastasis which explains its prognostic value in CRC (13, 159, 223).

Moreover, analysis from the oncogenic signature database showed that genes regulated in KRAS, P53, MEK and YAP signalling were likely to be enriched in tumours with high TB when compared to low TB tumours. In the previous chapter, it has been shown that tumours

with high TB may be associated with tumours that exhibited KRAS mutation (154). Interestingly, studies reported that YAP activation could be involved in the upregulation of the hypoxic condition and its downstream signalling could be used as a potential indicator of TB (247-249). Nevertheless, there is no correlation found between P53 and MEK signalling and TB. However, these two signalling pathways are known to be associated with tumour development and metastasis (250, 251).

In conclusion, CMS4 subtypes seem to have a possible correlation with high TB phenotype in CRC patients, however, an understanding of the underlying mechanism of budding formation is needed. The finding, from bulk RNA sequencing, revealed a potential genes and signatures involved in TB phenotype as describe above. However, there is not enough evidence and no statistically significant difference in GSEA analysis to support this hypothesis. The non-significant results could suggest that the gene expression from whole tissue may not fully describe the underlying mechanism of budding cells. New technologies are emerging that unravel the expression profile of individual cells as well as the spatial mapping of cell types in complex tissue (252, 253). One study proposed a possible way to capture the area of high budding cells and reveal the potential mechanism of an EMT signatures and there is a switch from epithelial subtype in tumour bulk to a mesenchymal subtype in TB cells (14). This could resolve the limitation of bulk RNA in which to identify the key regulatory mechanism of gene expression in tumour budding cells at the invasive tumour front. The next chapter describes the use of the Nanostring GeoMx digital spatial profiler (DSP) to determine the gene expression profile within regions rich for budding cells, which may provide additional insight into the TB mechanism in CRC.

Chapter 5. The assessment of the spatial transcriptomic profile related to budding phenotype in CRC.

5.1. Introduction

Emerging multi-omics technologies have resulted in the generation of a vast amount of data allowing insightful knowledge into tumour biology (254-256). Integrating data from translational RNA and protein is required to improve our understanding of cancer cells with a view to developing new therapies. Previously, bulk expression profiling was used to characterise the expression of genes specific to certain types of tumours (257-259). However, bulk methodologies do not account for tumour heterogeneity and patient survival may be influenced by different transcriptomic or protein expression profiles for different cell types or regions within or proximal to the tumour (14, 260).

Spatial imaging technology was introduced to address the unmet need from whole tumour bulk expression by focusing on its spatial expression in specific areas of the tumour tissue (261). Digital spatial profiling (DSP) is a method for highly multiplex spatial profiling of RNAs or proteins to discover and elucidate biomarkers that predict patients' response to therapy (262). Understanding the spatial transcriptomic/proteomic level has led to an identification and quantification RNA/protein expression in tissue sections and has been shown to identify biomarkers therefore contributing to potential improvement of treatment (263-265).

As discussed in chapter 4, bulk transcriptomic revealed a possible pathway related to TB phenotype. However, bulk RNA can only provide information on the tumour as a whole and does not represent genes expressed within the budding cells. Therefore, the use of spatial technology to identify the characteristics of TB in CRC was employed. DSP has been introduced to capture the differential expression of genes within the rich-budding area (158, 182). It has been shown that budding cells seem to express genes related to EMT signature and have a distinct TME that could lead to novel treatment in CRC. However, few studies have investigated the tumour-related pathways associated with TB and further studies are needed.

In this chapter, an investigation of the spatial transcriptomic underlying TB cells was carried out. The onco-immune panel of 96 target genes was utilised and the region of interests: tumour core, invasive and stromal area, were selected to compare the differential expression of genes related to TB phenotype in the whole CRC sections. It was hypothesized that DSP results could reveal the genes expressed in buds and describe the tumour microenvironment (TME) surrounded by the budding rich regions which would allow a better understanding of the mechanism of TB as well as the surrounding TME in CRC.

5.2. ROI selections and data analysis

DSP was performed in twelve CRC specimens; cases were chosen with regards to budding profile; high budding (n=6) and low budding (n=6). To investigate the underlying mechanism of TB in CRC, the mRNA panel of 96 curated immuno-oncology targets (84 targets plus controls) was utilised. Pan-Cytokeratin (PanCK), CD45 and SYTO13 were used for tissue visualization to represent epithelial tumour cells, immune cells and the nucleus respectively. ROIs were selected and collected as described in chapter2 sections 2.5.2 Data was then analysed using the GeoMx suite where the number of nuclei less than 150 cells was excluded. The normalisation was performed using five different housekeeping genes (*OAZ1, POLR2A, RAB7A, SDHA and UBB*). After the normalisation, the data was grouped and analysed with PanCK staining used to identify tumour (PanCK+) and stromal (PanCK-) compartments (Figure 5.1). The differential expression was compared between tumours with low and high budding phenotype ROIs (Table 5.1)

Table 5.1 *The groups comparison between tumours with high and low budding across different regions of interest (ROIs).*

Tumours with high/low budding
Tumour core (PanCK+)
Invasive area (PanCK+)
Invasive area (PanCK-)
Distant stromal area (PanCK-)

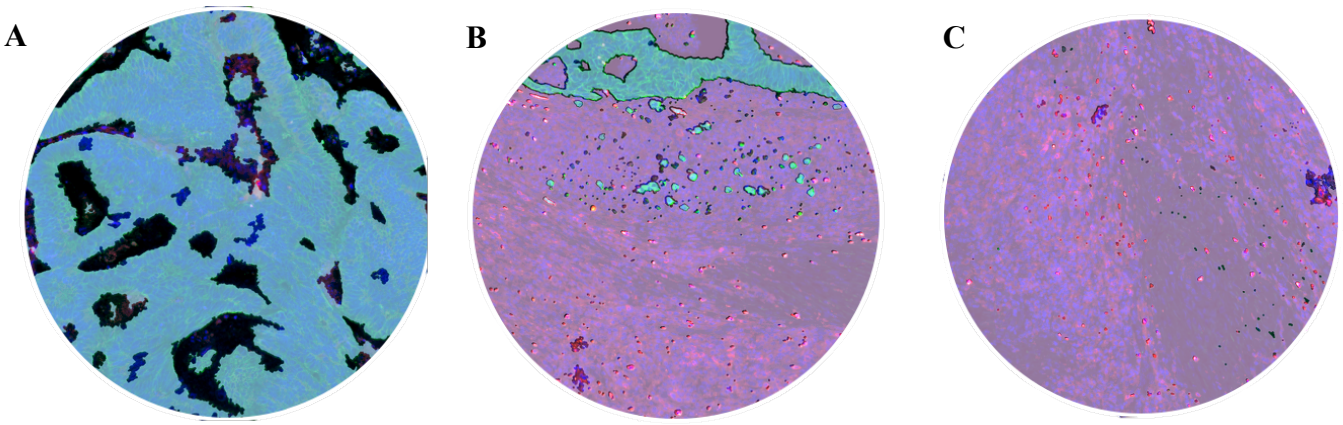

Figure 5.1 *Representative ROIs selected in different tumour sites (A) Tumour core, (B) Invasive area and (C) Distant stromal area. PanCK+ (green mask) is applied for epithelial cells selection and PanCK- (pink mask) is applied for non-epithelial cells selection.*

5.3. Differential genes expression in the tumour core area

The differential expression of genes in the tumour core area was compared between tumours with low and high budding phenotype. According to the results, PSMB*10* (Proteasome Subunit beta type-10) genes were reported to be significantly expressed in tumour core area of low TB tumours (p=0.049) compared to those with high buds (Figure 5.2A). In tumours with high budding, though only two cases, *CD44* was observed to be highly expressed (p=0.089) (Figure 5.2B).

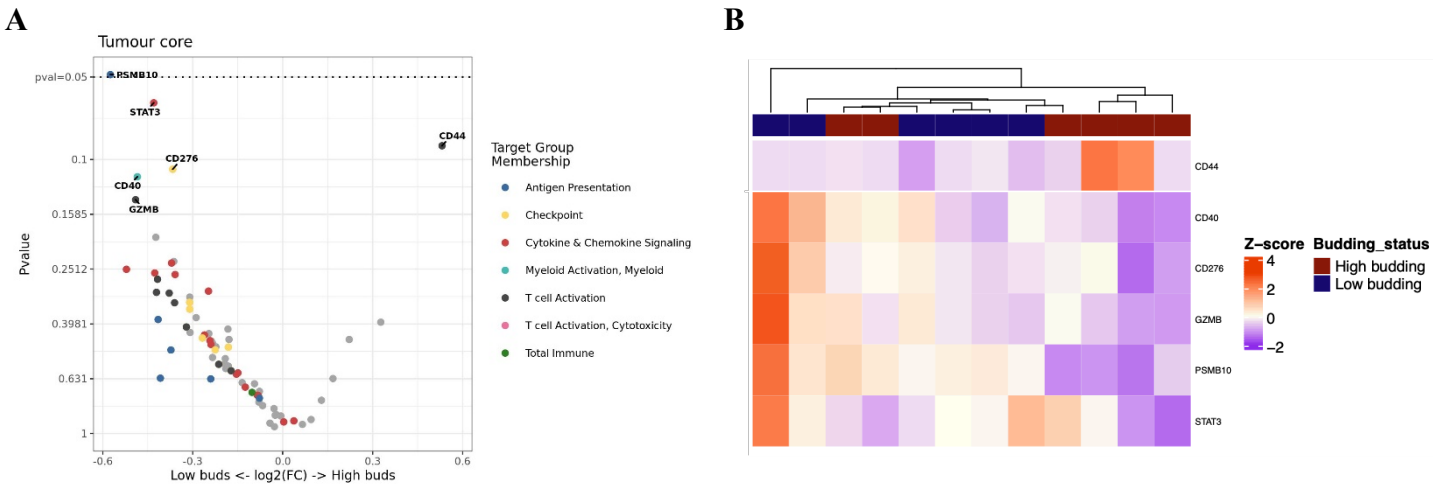

Figure 5.2 *(A) Volcano plot of the gene expression in the main tumour core between tumour with low (n=6) and high (n=6) budding phenotype. (B) Heatmap illustrated the expression of the genes in two different groups.*

5.4. Differential genes expression in the invasive area (PanCK+)

The epithelial compartment (PanCK+) was selected at the invasive tumour front to investigate differential expression of genes between tumours with low and high budding. There is no significant difference in gene expression between the two groups (Figure 5.3A). However, heatmap analysis showed that the expression of *CCND1*, a gene that encodes for the cyclinD1 protein, which controls cell cycle activity, was shown to be higher in high budding as compared to low budding groups (Figure 5.3B).

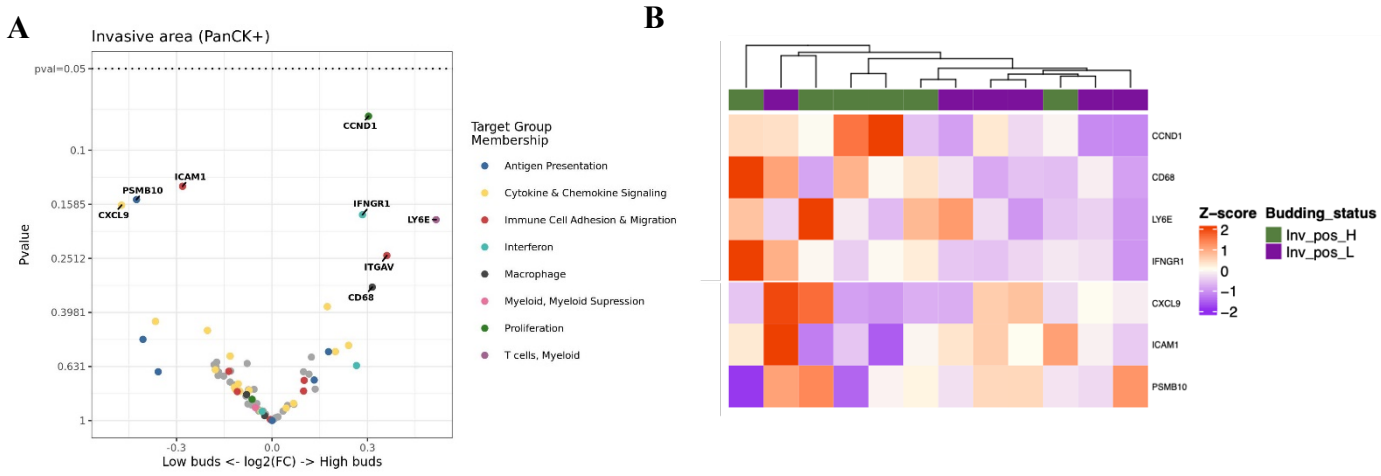

Figure 5.3 *(A) Volcano plot of gene expression in the invasive tumour area between tumours with low (n=6) and high (n=6) budding profile. (B) Heatmap illustrating the expression of the genes in the two different groups.*

5.5. Differential genes expression in the invasive area (PanCK-)

The non epithelial compartment (PanCK-) in the invasive area was studied to compare differential gene expression in the invasive stromal area between tumours with low and high budding phenotype. The results revealed that four genes were significantly expressed in the stromal area at the invasive front for tumours with a low number of buds (i.e. *CXCL9 (p=0.019), CXCL10 (p=0.023), PTPRC (p=0.036), CD44 (p=0.043))* (Figure 5.4A). There is a clear pattern, when heatmap analysis was applied, of the differential gene expression between tumours with low and high budding (Figure 5.4B).

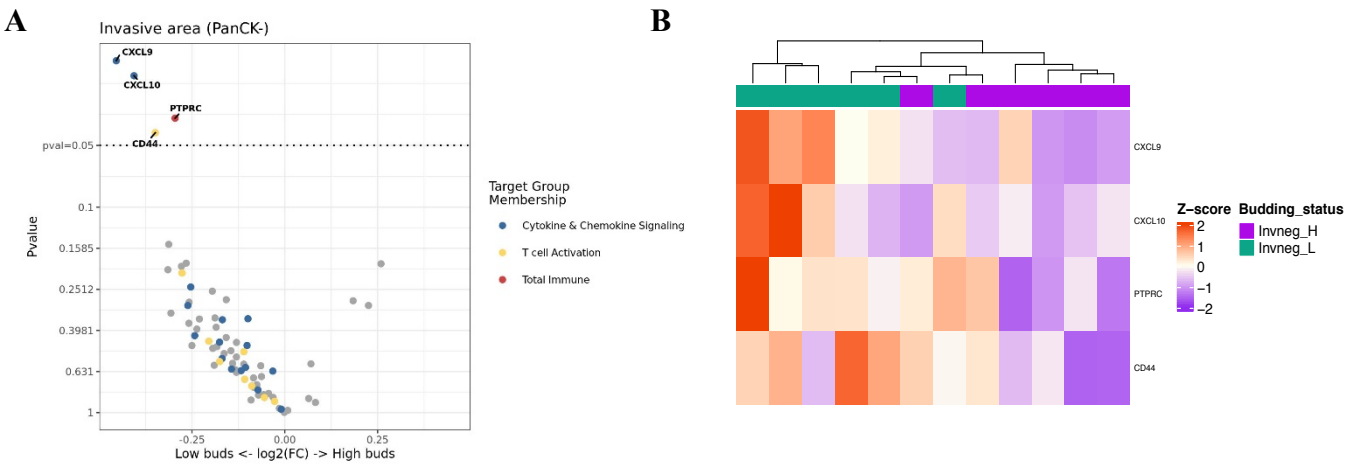

Figure 5.4 *(A) Volcano plot of the gene expression in the invasive stromal area between tumours with low (n=6) and high (n=6) budding profile. (B) Heatmap illustrated the expression of the genes in two different groups.*

5.6. Differential genes expression in the distant stromal area

The results showed no significant genes when distant stromal area was compared between tumours with low and high buds. However, CD68 and IL6 were shown to be highly expressed in the distant stromal area of tumours with high budding. In contrast, STATs signalling was highly expressed in tumours with low budding compared to high budding groups (Figure 5.5).

A

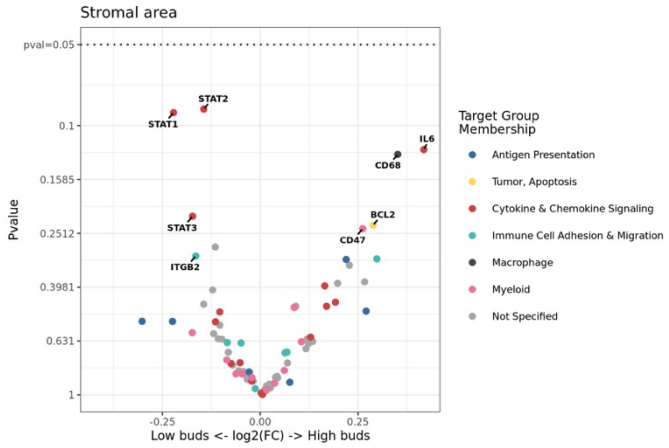

B

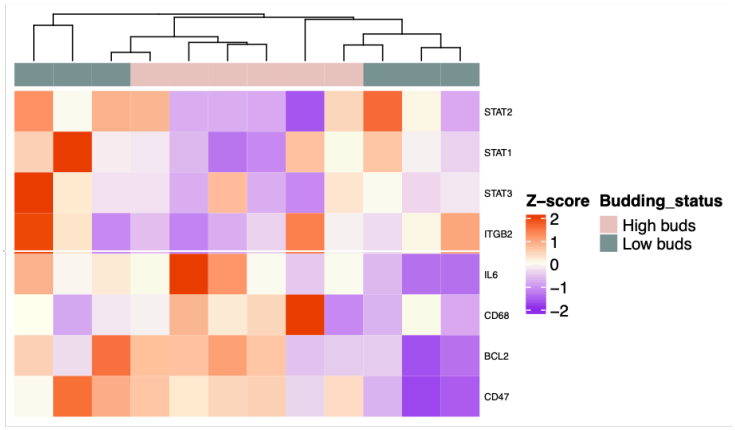

Figure 5.5 *(A) Volcano plot of the gene expression in the distant stromal area between tumours with low (n=6) and high (n=6) budding profile. (B) Heatmap illustrated the expression of the genes in two different groups.*

5.7. Validation of mRNA expression using IHC protein staining

The results from DSP revealed some genes which may play a role in the budding phenotype in CRC. However, the experiment was performed on a small number of samples (n=12; 6 cases for both low and high budding tumours). Therefore, it was decided that these DSP RNA results should be validated at the protein expression levels. To address this, immunohistochemistry (IHC) staining was performed in the previously constructed tissue microarrays (TMAs) for the CRC cohort (n=787). The assessment of each specific protein was investigated regarding its prognostic role and the association with TB within the different areas of CRC tissue.

5.7.1. Tumour core

From the previous results (section 5.3), CD44 was identified as a promising gene that could be expressed in the core of tumours that exhibit high budding phenotype.

To validate this finding, the antibody was selected based on its specificity, using a meta-analysis of peer studies that reported the use of the relevant antibody (Supplementary figure 5.1). DepMap database was then used to identify cancer cell lines known to express the target protein. Cell pellet IHC staining and western blot analysis, therefore, was performed to confirm its specificity based on the online DepMap analysis (Supplementary figure 5.2).

After specificity test, IHC staining of CD44 was performed in previously constructed tumour core TMAs (n=787) in Glasgow cohort (Figure 5.6A). Membrane staining of CD44 was quantified using weighted histoscore and the cut point obtained from R packages was applied to categories patients into groups with low and high CD44 expression (Supplementary figure 5.3).

Kaplan Meier (KM) survival analysis was performed in SPSS statistical program to determine the prognostic value of CD44 and its association with TB status in the Glasgow cohort. The survival analysis showed that patients with high CD44 (n=103) expression had better survival compared to those with low CD44 (n=479) (HR=0.507, 95% CI;0.302-0.852 log-rank p=0.010) with 10 years survival of 81% and 58% respectively (Figure 5.6B). There is no significant association, according to chi-square analysis, between CD44 protein expression and budding phenotype in the CRC cohorts. (Table 5.2). This was also shown when comparing the uncategorised CD44 protein expression data between tumours with low and high budding (Figure 5.7).

A

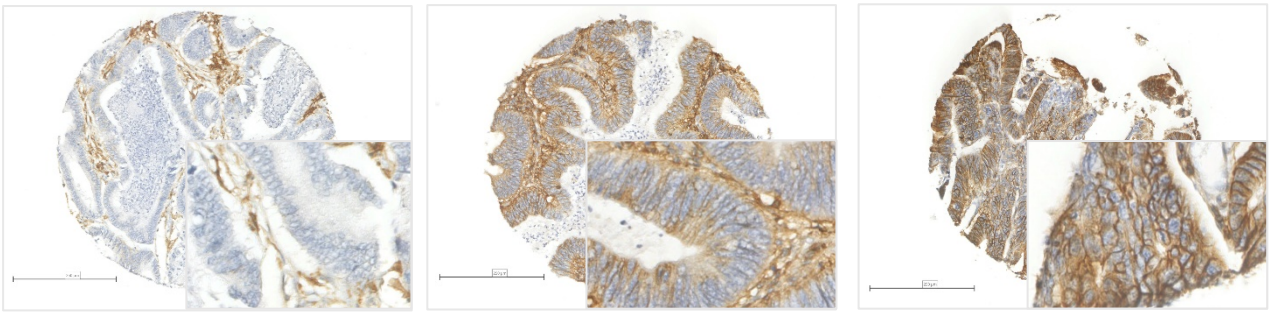

B

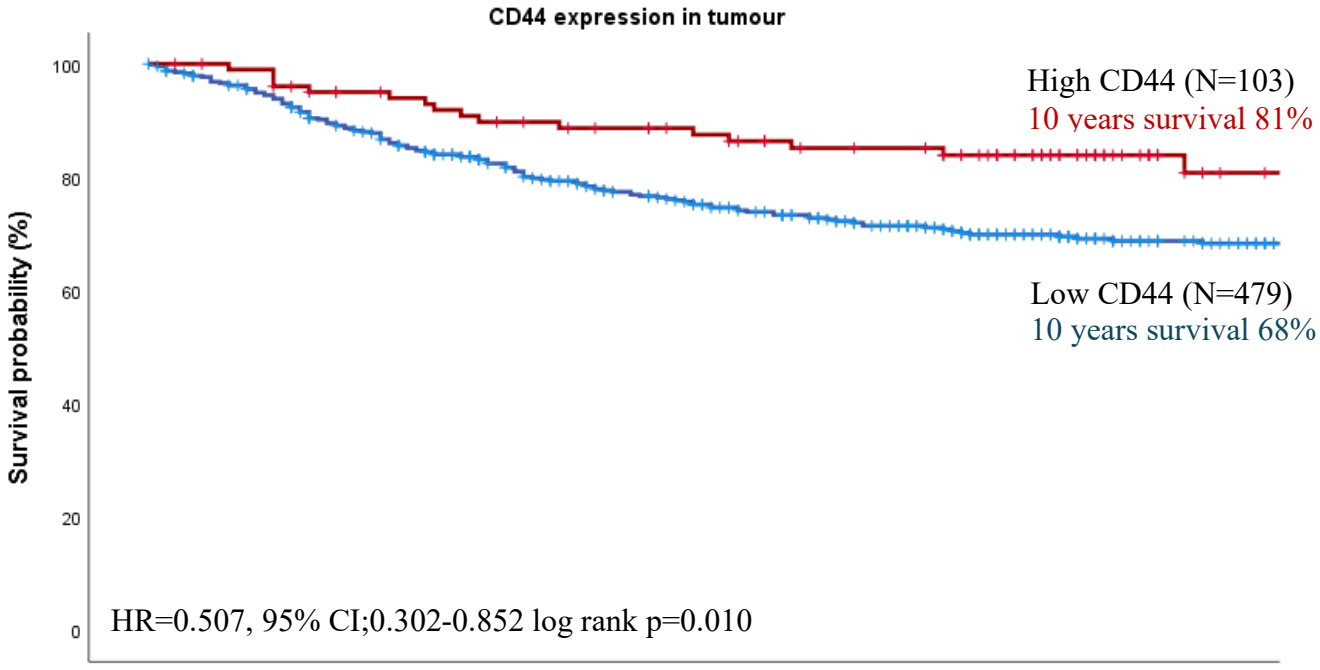

months	0	12	24	36	48	60	72	84	96	108	120
LowCD44	479(0)	446(12)	403(21)	365(38)	329(56)	302(68)	274(86)	248(105)	208(140)	172(174)	152(192)
HighCD44	103(0)	100(2)	91(7)	86(8)	81(11)	77(15)	71(19)	68(21)	57(31)	35(53)	24(63)

Figure 5.6 *(A) IHC staining of CD44 membrane protein expression in the tumour core with low medium and high expression using 20x magnification. and (B) Kaplan-Meier survival analysis based on CD44 for cancer specific survival (CSS) in the tumour core in Glasgow cohort. Hazard ratio (HR) was reported with 95% confidence intervals. P Values were calculated using the log-rank test comparing patients with low (n=103) and high (n=479) CD44 expression.*

Table 5.2 *The association of CD44 expression to clinical pathological features using the Pearson's chi-square analysis in CRC Glasgow cohort (n=621).*

	Low budding (n=390)	High budding (n=244)	P-value
CD44			0.494
Low	320 (82)	147 (84)	
High	72 (18)	28 (16)	

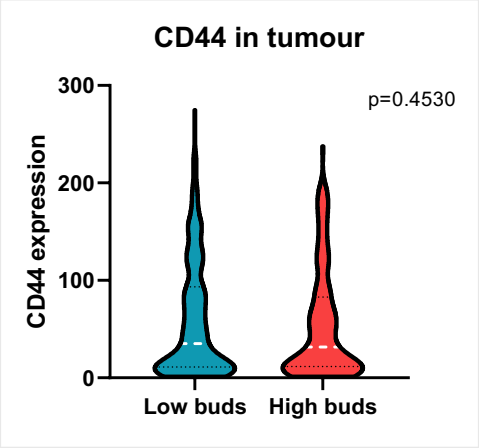

Figure 5.7 *Violin plots show continuous variable of CD44 expressed in the tumour core area compared between budding groups in Glasgow cohort.*

To corroborate these results, IHC staining was also repeated in whole CRC sections from an independent Thai cohort (n=290). The same antibody was used, and the membrane staining was scored manually (Figure 5.8A). Three different tumour core areas were selected to represent the biology of each patient.

Survival analysis revealed similar results. Patients with high CD44 (n=155) tend to have a better prognostic when compared to those with low CD44 (n=85) expression (HR=0.619, 95% CI;0.327-1.174 log rank p=0.130) (Figure 5.8B). The percentage survival 10 years after diagnosis showed that patients with high CD44 (81%) have higher survival compared to those with low CD44 (76%). In addition, there is no significant association between CD44 and TB status, although the expression of CD44 is higher in tumours with low TB compared to high TB (Table 5.3) (Figure 5.9).

A

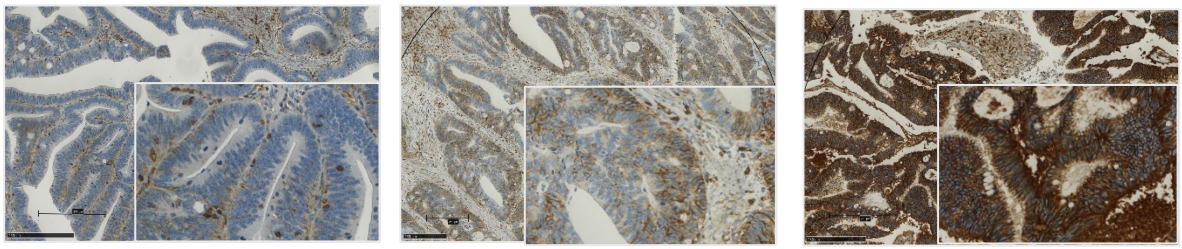

B

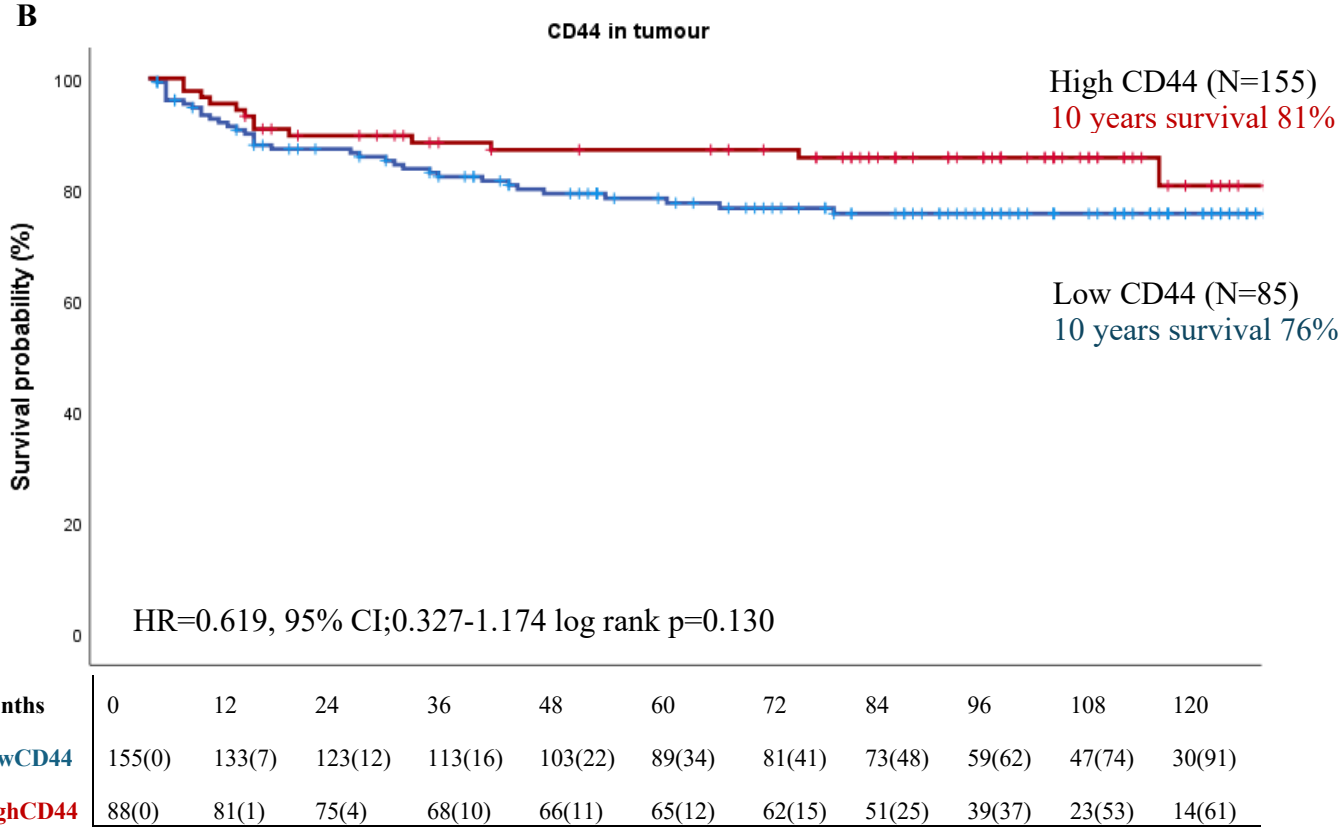

months	0	12	24	36	48	60	72	84	96	108	120
LowCD44	155(0)	133(7)	123(12)	113(16)	103(22)	89(34)	81(41)	73(48)	59(62)	47(74)	30(91)
HighCD44	88(0)	81(1)	75(4)	68(10)	66(11)	65(12)	62(15)	51(25)	39(37)	23(53)	14(61)

Figure 5.8 *(A) IHC staining of CD44 membrane protein expression in the tumour core with low medium and high expression using 20x magnification. and (B) Kaplan-Meier survival analysis based on CD44 for cancer specific survival (CSS) in the tumour core in Thai cohort. Hazard ratio (HR) was reported with 95% confidence intervals. P Values were calculated using the log-rank test comparing patients with low (n=155) and high (n=85) CD44 expression.*

Table 5.3 *The association of CD44 expression to clinical pathological features using the Pearson's chi-square analysis in CRC Thai cohort (n=251).*

	Low budding (n=95)	High budding (n=156)	P-value
CD44			0.741
Low	58 (63)	99 (65)	
High	34 (37)	53 (35)	

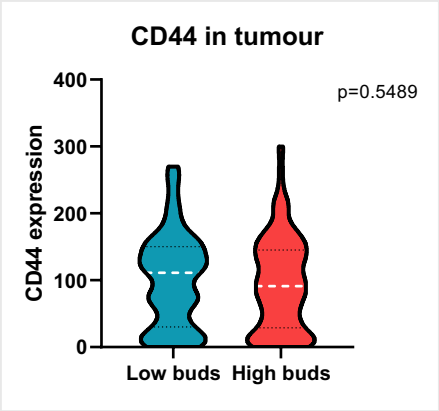

Figure 5.9 *Violin plots show continuous variable of CD44 expressed in the tumour core area compared between budding groups in Thai cohort.*

In addition to the prognostic value of CD44, the previous DSP finding also revealed that STAT3 mRNA was highly expressed in tumours with low budding compared to high budding groups at the tumour core, although there were no significant differences which could cause by the low number of cases included (section 5.3). To further validate this, the previously made CRC TMA (n=787) was used to investigate the role of STAT3 in CRC patients. Protein expression of phospho-STAT3 (pSTAT3) was investigated the phosphorylation of STAT3 activities. Antibody specificity testing was previously carried out within the group. The assessment of pSTAT3 protein expression in the tumour core was performed by a project student (Umar Hashmi) (Figure 5.10A). The IHC staining was carried out in the previously constructed tumour core TMA (n=787). Weighted histoscore was manually counted and the cut point obtained from R packages was applied to identify groups with low and high pSTAT3 expression.

Patients with high pSTAT3 (n=263) had a poorer survival when compared to low pSTAT3 groups (n=359) (HR=1.358, 95% CI;0.995-1.854 log rank p=0.053) (Figure 5.9B). 10 years survival were reported to be 74% and 67% in patients with low and high pSTAT3 respectively. According to the chi-square test, there is no significant association between pSTAT3 expression and TB status (Table 5.4) as well as its continuous expression when compared between low and high budding in CRC (Figure 5.11)

A

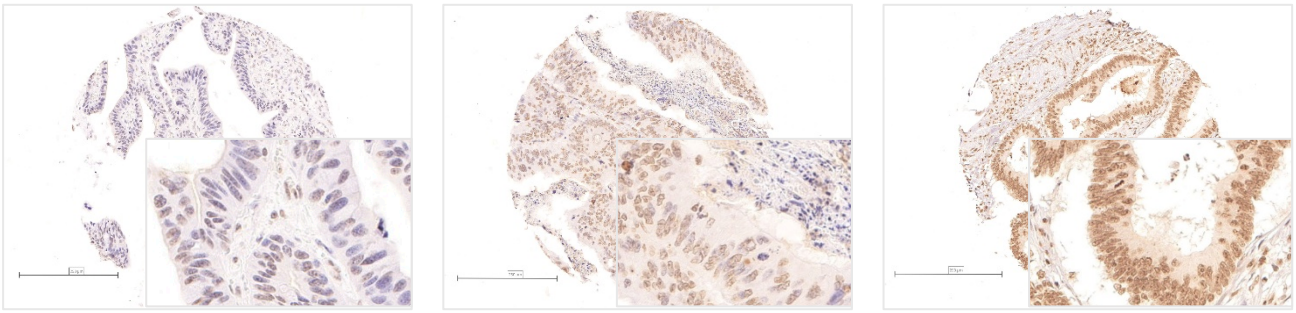

B

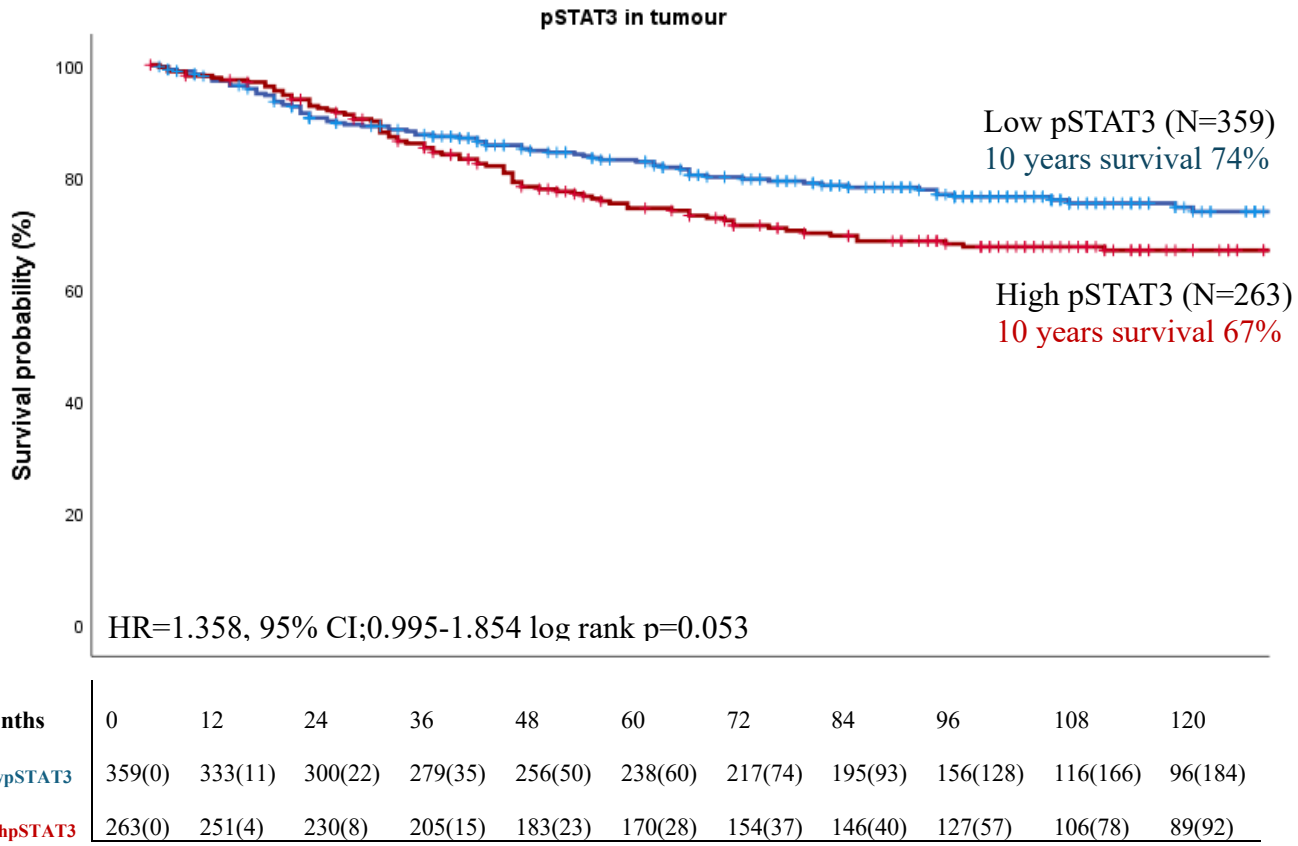

months	0	12	24	36	48	60	72	84	96	108	120
LowpSTAT3	359(0)	333(11)	300(22)	279(35)	256(50)	238(60)	217(74)	195(93)	156(128)	116(166)	96(184)
HighpSTAT3	263(0)	251(4)	230(8)	205(15)	183(23)	170(28)	154(37)	146(40)	127(57)	106(78)	89(92)

Figure 5.10 *The differential expression of genes from transcriptomic data demonstrates in (A) IHC staining of nuclear pSTAT3 protein expression in the tumour core with low medium and high expression using 20x magnification and (B) Kaplan-Meier survival analysis based on pSTAT3 for cancer specific survival (CSS) in CRC patients. Hazard ratio (HR) was reported with 95% confidence intervals. P Values were calculated using the log-rank test comparing patients with low (n=359) and high (n=263) phospho-STAT3 expression.*

Table 5.4 *The association of pSTAT3 expression to clinical pathological features using the Pearson's chi-square analysis in CRC patients (n=621).*

	Low budding (n=390)	**High budding (n=244)**	**P-value**
pSTAT3			0.785
Low	251 (59)	101 (58)	
High	175 (41)	74 (42)	

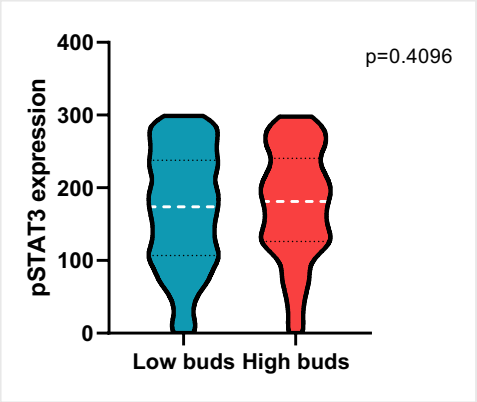

Figure 5.11 *Violin plots show continuous variable of pSTAT3 expression in the tumour core compared between budding groups.*

5.7.2. Invasive area (PanCK+)

According to the previous results, *CCND1*, which codes for cyclinD1 protein, was observed to be higher in the invasive area of high budding tumours (section 5.4).

To validate the results at the protein level, CRC cell lines were selected based on the range of target protein expressions (i.e. low medium and high), shown in DepMap, to verify the specificity of the antibody. Western blot analysis demonstrated the same results compared to the online DepMap database (Supplementary figure 5.5B). IHC staining of cell pellets was also conducted (Supplementary figure 5.5C).

Nuclear expression of cyclinD1 was accessed in a previously constructed invasive tumour TMA (n=787). The weight histoscore was used to classify groups into low and high cyclinD1 expression based on generated cut point (Figure 5.12A) (Supplementary figure 5.6). There was no difference in the survival between those patients with low (n=210) and high (n=328) cyclinD1 expression (HR=0.829, 95% CI;0.601-1.143 log rank p=0.253) (Figure 5.12B). The percentage of 10 years survival in high and low cyclinD1 at the invasive edge is 69% and 67% respectively. Moreover, there is no association between cyclinD1 expression and budding phenotype in CRC patients (Table 5.5) (Figure 5.13).

A

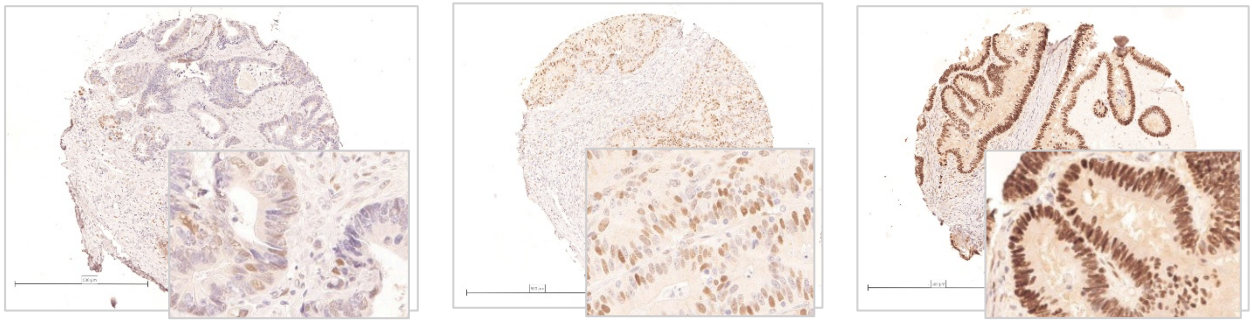

B

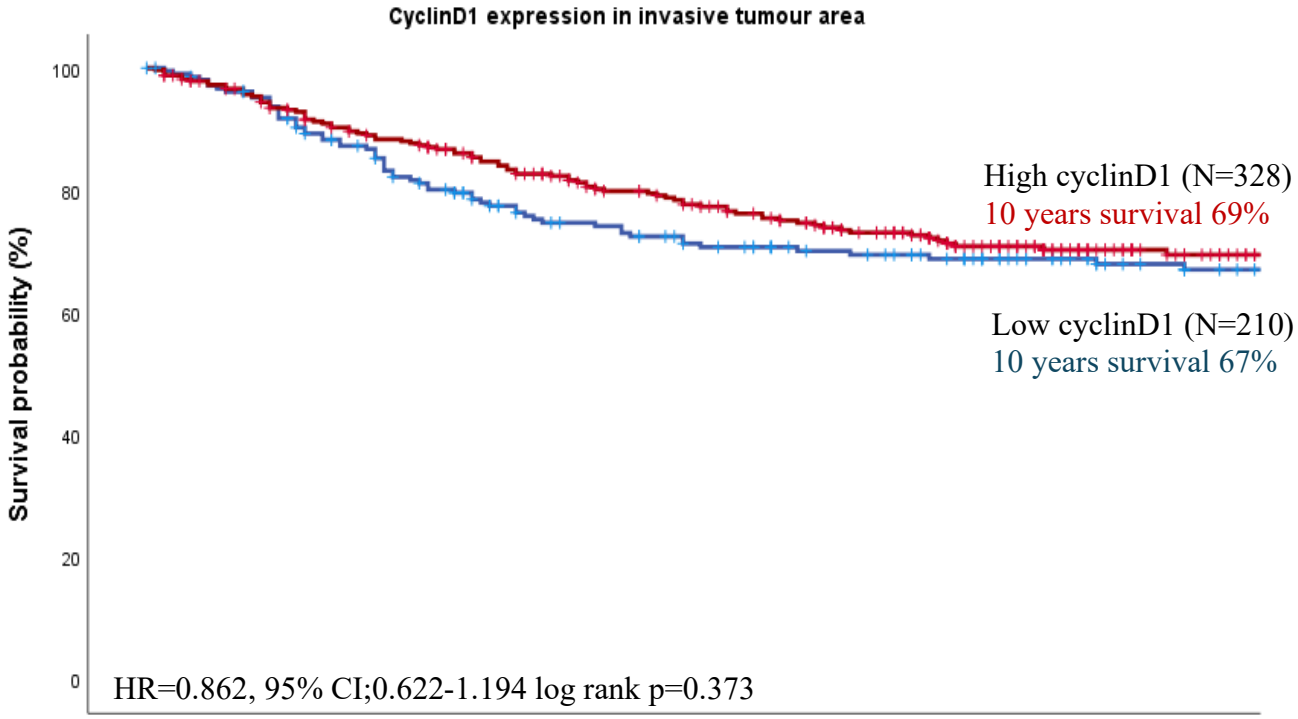

months	0	12	24	36	48	60	72	84	96	108	120
LowCyclinD1	210(0)	197(5)	173(11)	151(18)	133(27)	126(30)	114(39)	109(42)	94(56)	81(69)	71(77)
HighCyclinD1	328(0)	305(9)	278(17)	258(26)	236(37)	216(47)	198(56)	176(72)	142(101)	98(144)	81(160)

Figure 5.12*(A) IHC staining of cyclinD1nuclear protein expression in TMA of the invasive edge with low medium and high expression using 20x magnification and (B) Kaplan-Meier survival analysis based on cyclinD1 for cancer specific survival (CSS) at the invasive edge. Hazard ratio (HR) was reported with 95% confidence intervals. P Values were calculated using the log-rank test comparing patients with low (n=210) and high (n=328) cyclinD1 expression.*

Table 5.5 *The relationship between budding status and invasive edge cyclinD1 using the Pearson's chi-square analysis in CRC patient (n=621)*

	Low budding n=395	**High budding n=175**	**P-value**
CyclinD1 Low High	 137 (39) 217 (61)	 68 (40) 104 (60)	 0.854

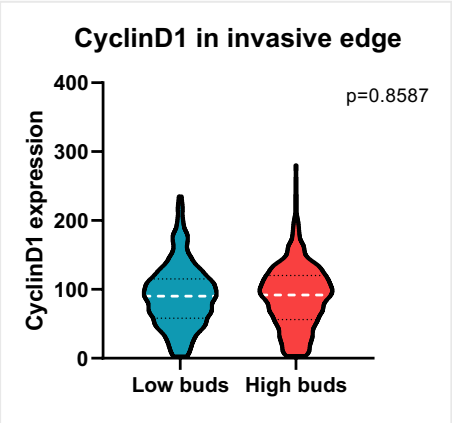

Figure 5.13 *Violin plots show continuous variable of cyclinD1 expressed in the invasive tumour edge compared between budding groups.*

However, when accessing cyclinD1 expression in bud cells, there is a difference in the expression of cyclinD1 in the budding population (Figure 5.14A). Patients who have high (n=61) cyclinD1 expression in buds showed a poorer survival when compared to those with low (n=88) cyclinD1 in buds (HR=1.516, 95% CI;0.893-2.573 log rank p=0.123) (Figure 5.13B). The survival rate 10 years after diagnosis is 51% and 65% for high and low cyclinD1 in buds respectively.

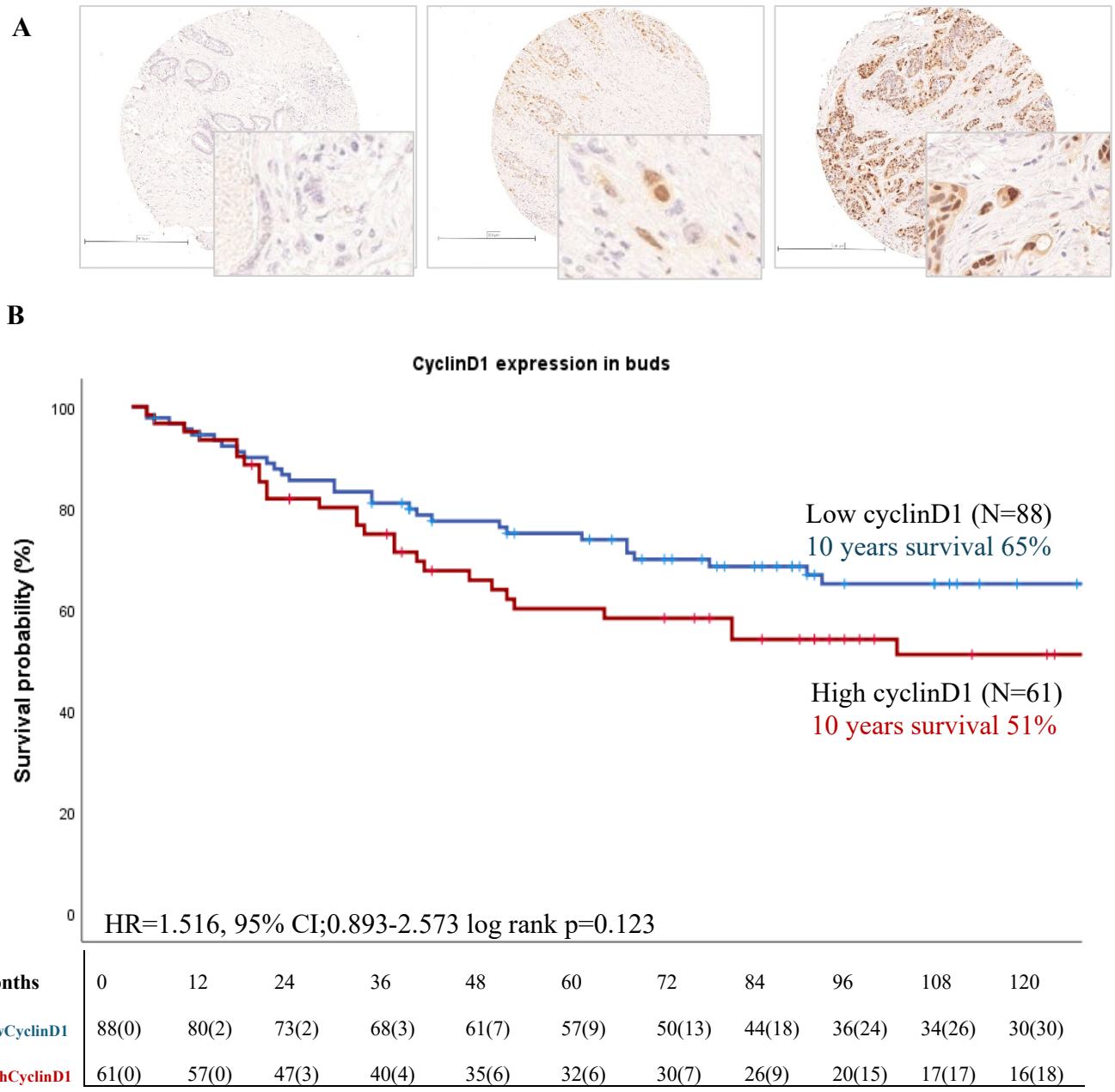

Figure 5.14 *(A) IHC staining of cyclinD1 nuclear protein expression in TMA of budding cells with low medium and high expression using 20x magnification and (B) Kaplan-Meier survival analysis based on cyclinD1 for cancer specific survival (CSS) in budding cells. Hazard ratio (HR) was reported with 95% confidence intervals. P Values were calculated using the log-rank test comparing patients with low (n=88) and high (n=61) cyclinD1 expression.*

5.7.3. Invasive area (PanCK-)

To validate the previous DSP results (section 5.5), RNA in situ hybridization was conducted for *CXCL9* and *CXCL10* in the previously constructed TMA from tumour core CRC (n=787) (Figure 5.15). The validation of the probes was undertaken by the Beatson Histology Service. Freshly cut TMA was used and the house keeping probe was used to verify if the tissue is suitable to perform the experiment. After the validation, the target probes (CXCL9, CXCL10) were stained and Halo, an image analysis platform, was used to quantify the stained probes. A housekeeping gene (*UBC*) was used to normalise positive cells per area. The raw counts were obtained, the percentage of positive cells was used and applied to survminer R package to classify groups into low and high *CXCL9/ CXCL10 (*Supplementary figure 5.7-5.8)

Patients with low CXCL9 (n=389) have the worst outcome when compared to those with high CXCL9 (n=243) (HR=0.535, 95% CI;0.377-0.758 log rank p<0.001) (Figure 5.16) The survival rate after 10 years of being diagnosed for low and high CXCL9 is 80% and 65% respectively. Despite the prognostic value, statistical tests showed no correlation between CXCL9 and budding status (Table 5.6) (Figure 5.17).

A similar trend was observed when CXCL10 was analysed. Patients with high CXCL10 (n=202) had improved survival when compared to low CXCL10 (n=427) group (HR=0.513, 95% CI;0.354-0.745 log rank p<0.001) with 82% and 65% 10 years survival after diagnosis respectively (Figure 5.18). There is no significant association between CXCL10 and tumour budding status (Table 5.7) (Figure 5.19).

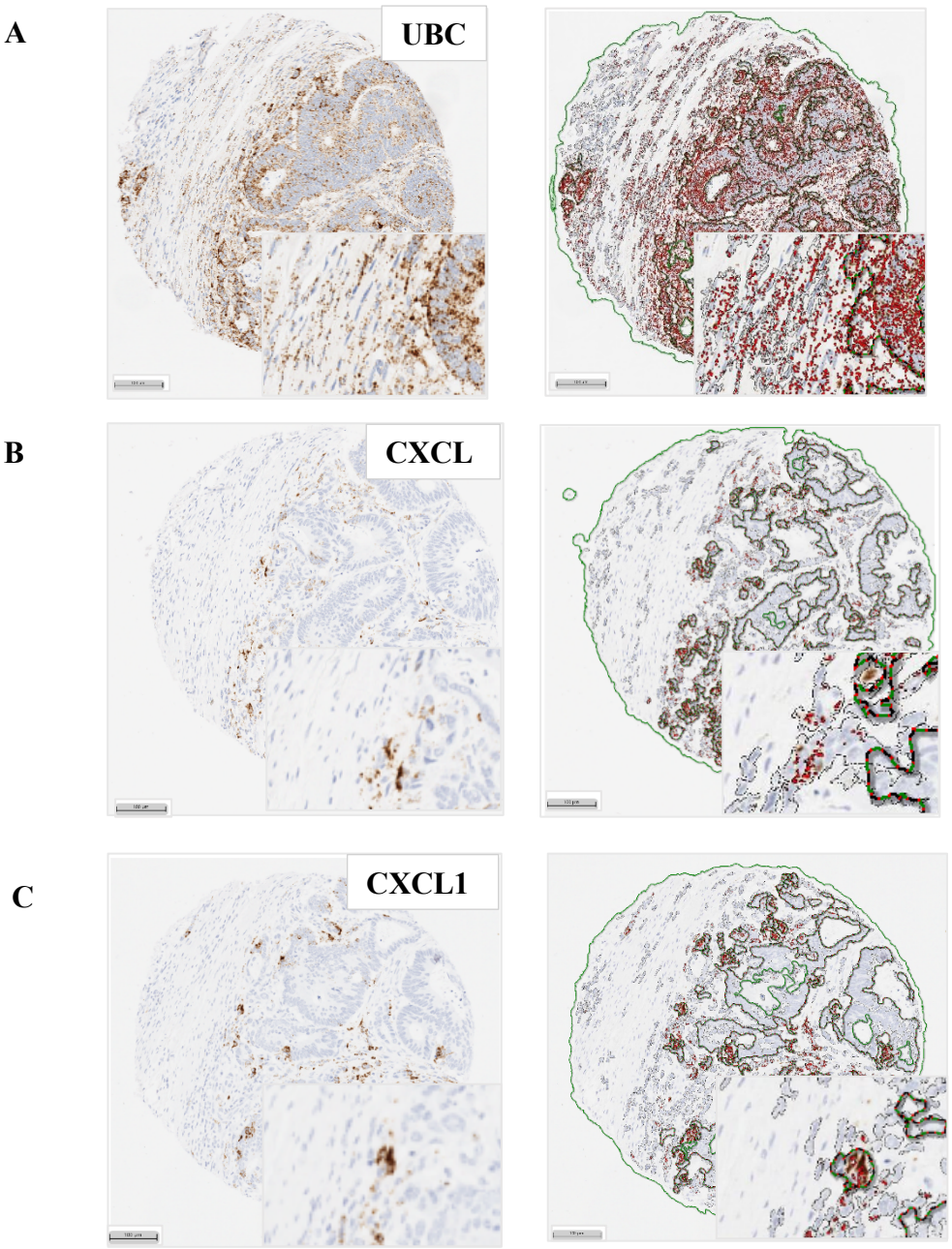

Figure 5.15 *Example images of RNAscope-stained for(A) UBC (positive control), (B) CXCL9 and (C) CXCL10 probes in TMA of the tumour core. The original image on the left and the analysed images, using HALO image analysis, are on the right.*

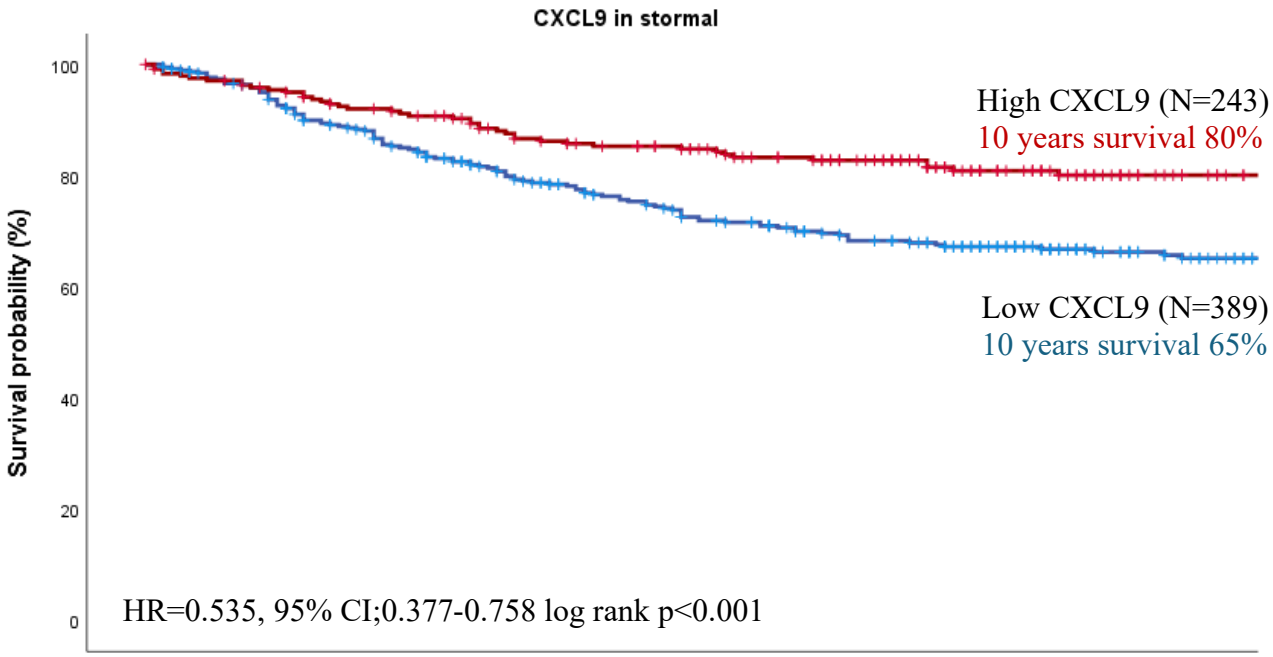

months	0	12	24	36	48	60	72	84	96	108	120
LowCXCL9	389(0)	364(11)	325(21)	290(34)	258(52)	238(58)	216(70)	199(79)	172(103)	131(143)	112(159)
HighCXCL9	243(0)	230(4)	214(10)	203(17)	188(23)	175(34)	160(45)	146(58)	115(86)	91(109)	73(127)

Figure 5.16 *Kaplan-Meier survival analysis based on CXCL9 for cancer specific survival (CSS). Hazard ratio (HR) was reported with 95% confidence intervals. P Values were calculated using the log-rank test comparing patients with low (n=389) and high (n=243) CXCL9 phenotype.*

Table 5.6 *The association of CXCL9 to clinical pathological features using the Pearson's chi-square analysis in CRC patients (n=621).*

	Low budding (n=390)	High budding (n=244)	P-value
CXCL9			0.564
Low	269 (62)	107 (60)	
High	163 (38)	72 (40)	

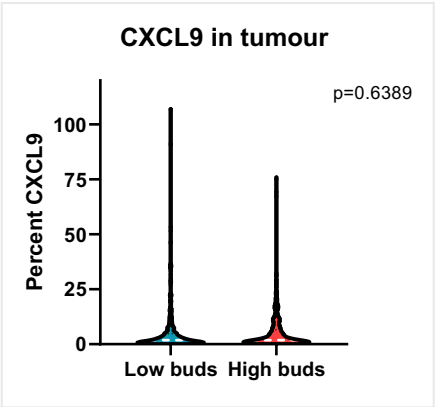

Figure 5.17 *Violin plots show continuous variable of the number of CXCL9 probe in the stromal tumour core compared between budding group.*

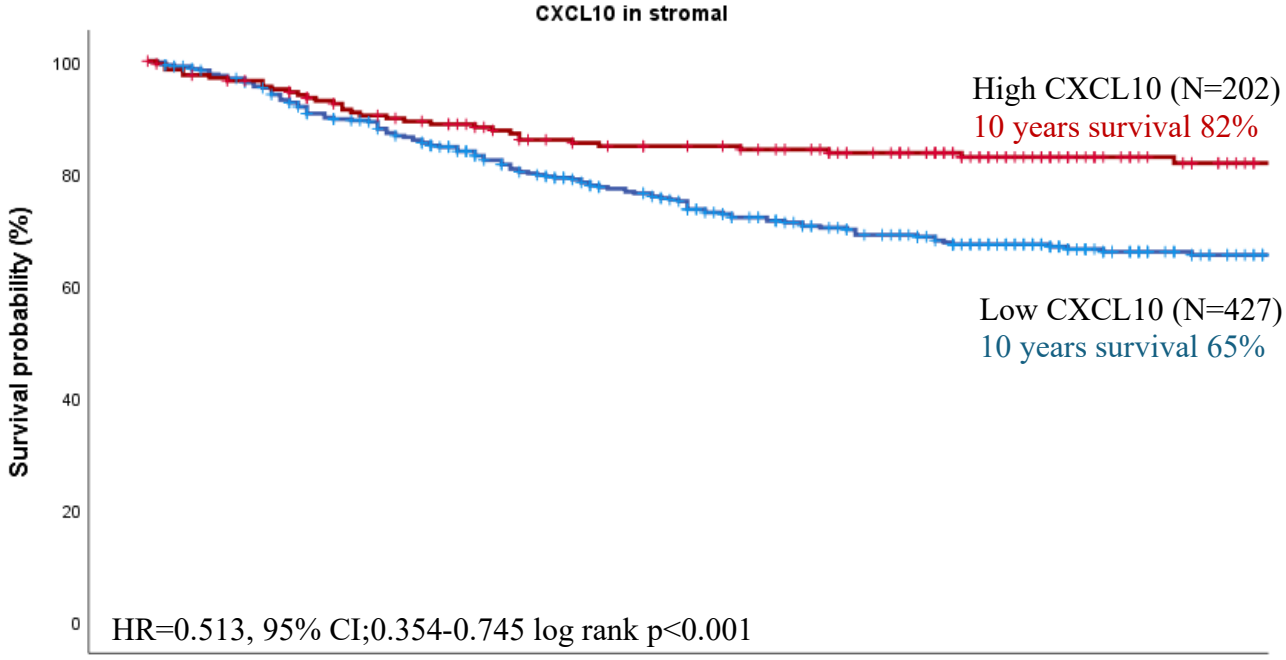

months	0	12	24	36	48	60	72	84	96	108	120
LowCXCL10	427(0)	401(10)	362(21)	326(35)	291(52)	265(64)	234(82)	213(95)	180(123)	139(162)	113(186)
HighCXCL10	202(0)	190(5)	174(10)	164(16)	152(23)	145(28)	139(33)	129(42)	104(66)	83(81)	72(91)

Figure 5.18 *Kaplan-Meier survival analysis based on CXCL10 for cancer specific survival (CSS). Hazard ratio (HR) was reported with 95% confidence intervals. P Values were calculated using the log-rank test comparing patients with low (n=427) and high (n=202) CXCL10 phenotype.*

Table 5.7 *The association of CXCL10 expression to clinical pathological features using the Pearson's chi-square in CRC patients (n=621).*

	Low budding (n=390)	High budding (n=244)	P-value
CXCL10			0.862
Low	293 (68)	120 (67)	
High	137 (32)	58 (33)	

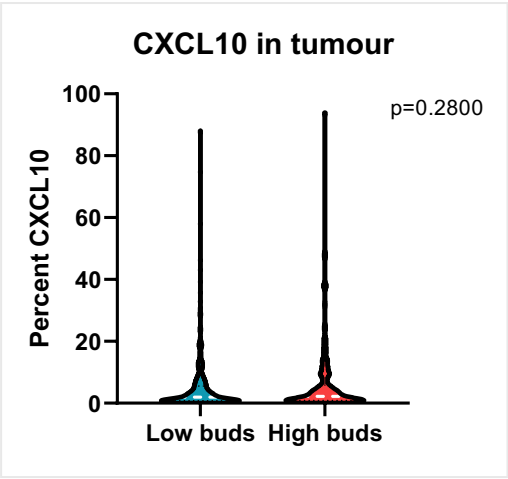

Figure 5.19 *Violin plots show continuous variable of the number of CXCL10 probe in the stromal tumour core compared between budding groups.*

5.7.4. Distant stromal area

The results from DSP revealed that, in the distant stromal area of the tumour, IL6 was higher in the high budding group when compared to the group with low buds. (section 5.6). Due to the unavailable staining for IL6, IHC protein staining of IL6 receptor (IL6R) was used to determine regulation of IL6 activities and its prognostic value in CRC within the tumour area. The IHC staining and subsequent analysis was carried out by Ahmad Kurniawan as part of his Masters project (Figure 5.20A). Cytoplasmic IL6R was quantified using Qupath image analysis and survminer R package used to classify patients into low and high IL6R expressers.

Patients with high IL6R (n=66) experienced a poorer outcome when compared to those with low IL6R (n=413) (HR=1.637, 95% CI;1.046-2.561 log rank p=0.031) (Figure 5.20B). The percentage at 10-year survival was 60% and 73% of patients with high and low IL6R respectively. Interestingly, there is a positive association between IL6R and budding phenotype (high, p=0.02) (Table 5.8) and that high expression of IL6R is significantly higher in tumours with high TB compared to low TB groups (p=0.0253) (Figure 5.21).

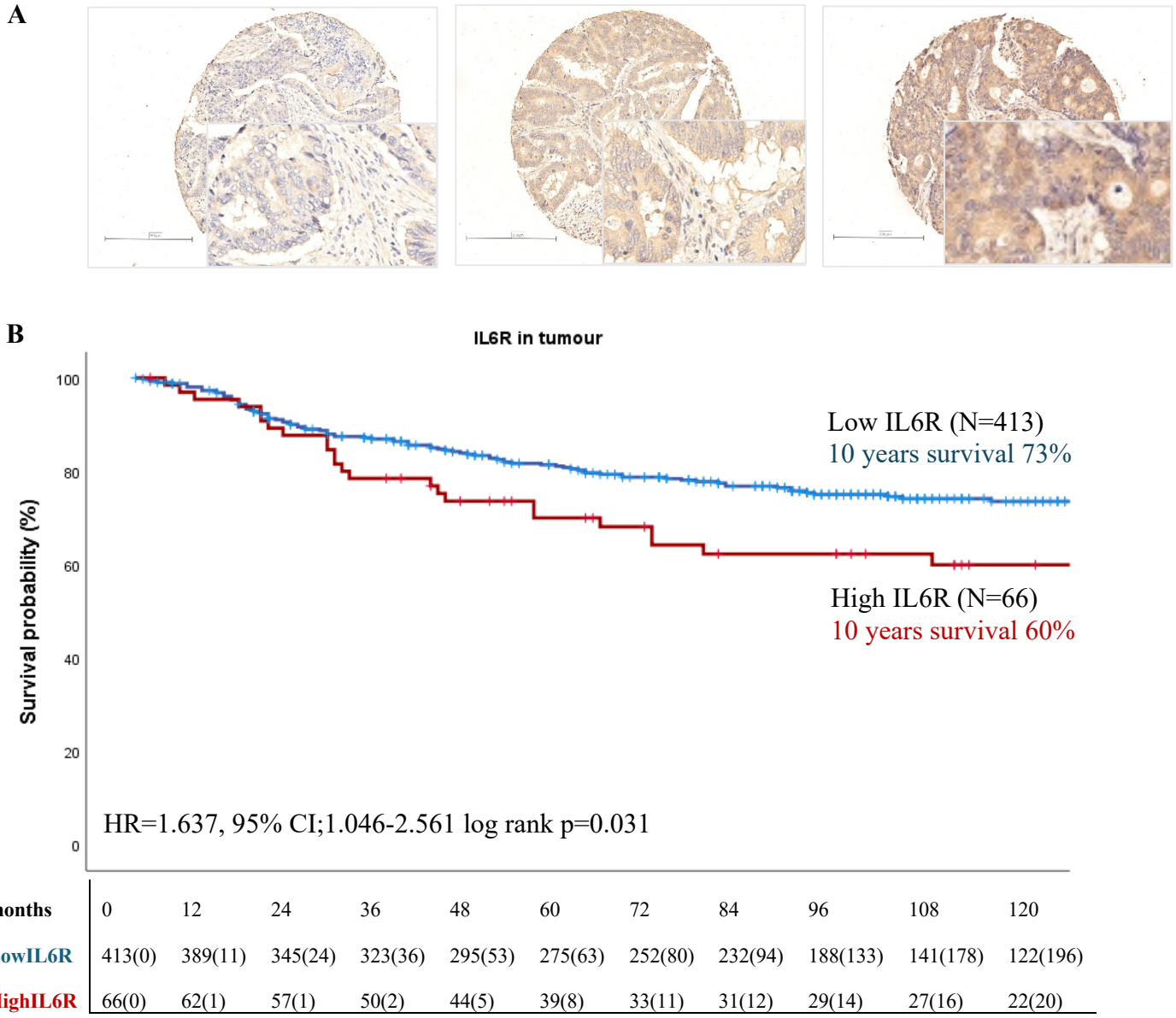

Figure 5.20 *(A) IHC staining of IL6R cytoplasmic protein expression in TMA of the tumour core with low medium and high expression using 20x magnification and (B) Kaplan-Meier survival analysis based on IL6R for cancer specific survival (CSS) in CRC patients. Hazard ratio (HR) was reported with 95% confidence intervals. P Values were calculated using the log-rank test comparing patients with low (n=413) and high (n=66) IL6R expression.*

Table 5.8 *The association of IL6R expression to clinical pathological features using the Pearson's chi-square in CRC.*

	Low budding (n=390)	**High budding (n=244)**	**P-value**
IL6R			0.020
Low	292 (89)	113 (81)	
High	37 (11)	27 (19)	

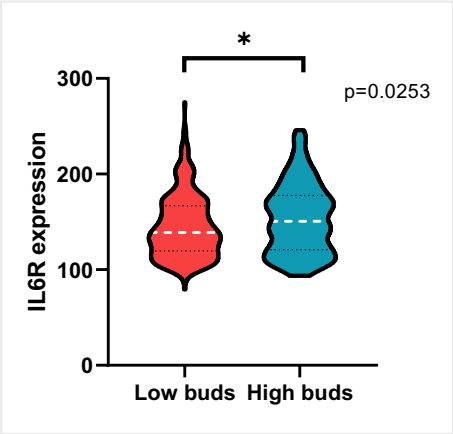

Figure 5.21 *Violin plots show continuous variable of IL6R expressed in tumour core compared between budding groups.*

STAT1 was shown to be highly expressed in the distant stroma of tumours with low budding (section5.6). The assessment of cytoplasmic total STAT1 protein expression was performed by MSc student, Bronte Kerrigan, (Figure 5.22A). Protein quantification was determined using Qupath image analysis (Figure 5.22B). Survminer R package was applied to classify patients into low and high STAT1 expression groups.

Patients with low STAT1 (n=192) experienced a significantly poor survival when compared to those with high STAT1 (n=268) (HR=0.640, 95% CI;0.445-0.919 log rank p=0.016 (Figure 5.21C). The 10-year survival was 74% and 65% of patients with low and high STAT1 respectively. In addition, there is no significant association between STAT1 and budding status in CRC patients (Table 5.9). However, the continuous variable of STAT1 expression showed that there is a higher expression of STAT1 in the stroma of tumours with high TB phenotype, although no statistical significance was found (Figure 5.23).

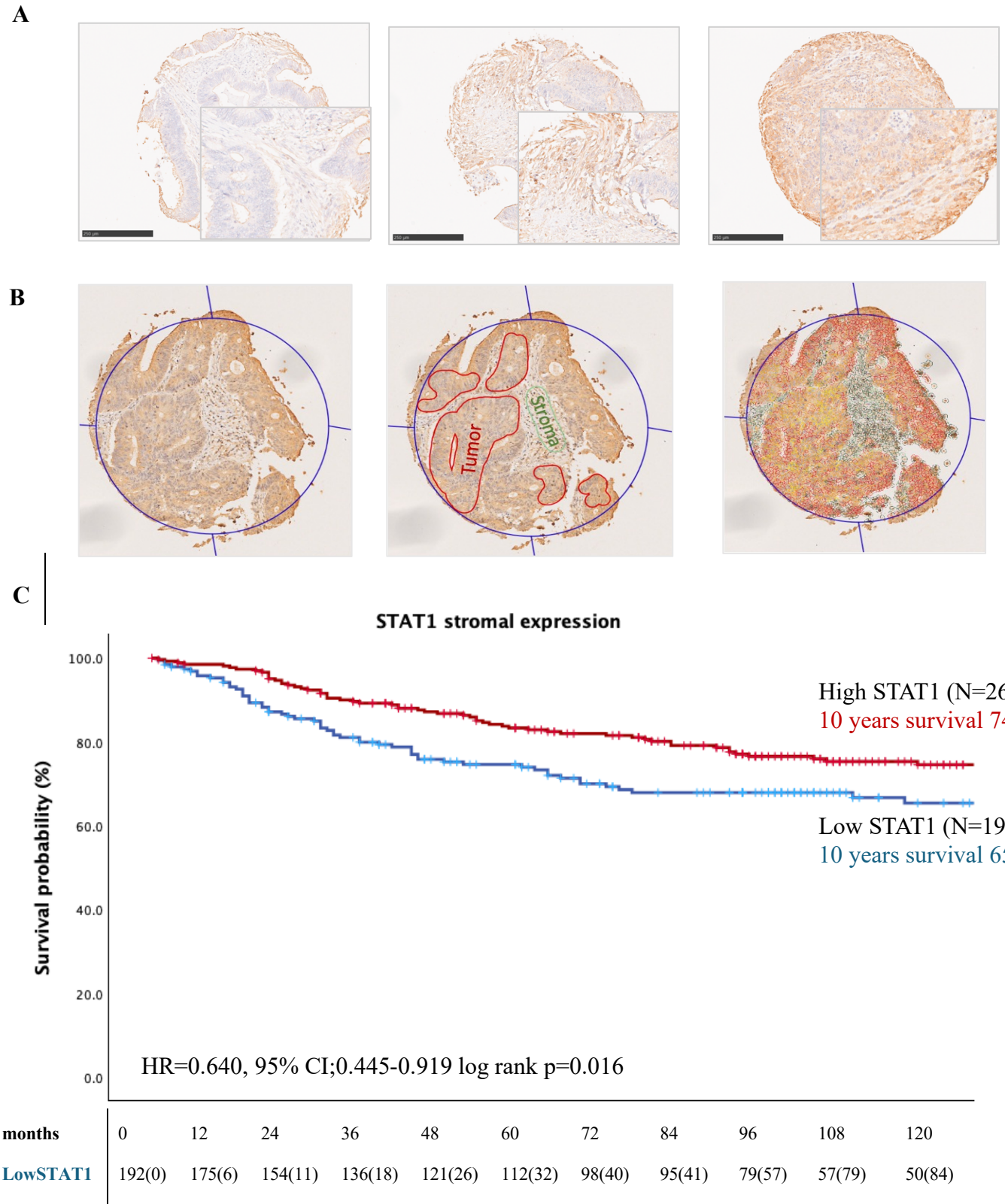

Figure 5.22 *(A) IHC staining of STAT1 cytoplasmic protein expression in the stromal area of the TMAs from tumour core with low medium and high expression using 20x magnification and (B) Representative images of QuPath analysis steps used to obtain H-score (dearraying, annotations, detection classification). (C) Kaplan-Meier survival analysis based on STAT1 for cancer specific survival (CSS) in CRC patients. Hazard ratio (HR) was reported with 95% confidence intervals. P Values were calculated using the log-rank test comparing patients with low (n=192) and high (n=268) STAT1 expression.*

Table 5.9 *The association of STAT1 expression in stromal to clinical pathological features using the Pearson's chi-square in CRC.*

	Low budding (n=390)	High budding (n=244)	P-value
STAT1			0.270
Low	131 (43)	52 (37)	
High	176 (57)	88 (63)	

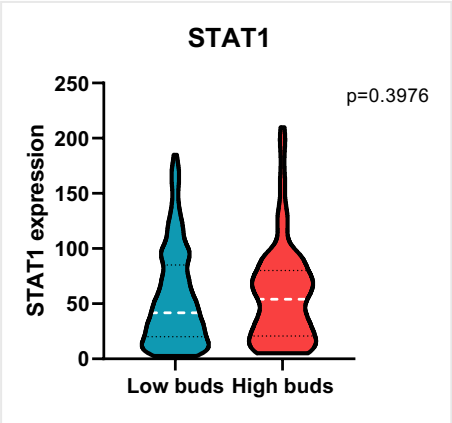

Figure 5.23 *Violin plots show continuous variable of STAT1 expressed in stromal area of the tumour core compared between budding groups.*

5.8. Discussion

The use of spatial imaging technology has potentially identified novel biomarkers that could lead to new cancer treatments in many types of cancers (266). To investigate the underlying mechanism of TB in CRC, GeoMX DSP was utilised. When comparing gene expression between different ROIs (tumour core, invasive edge and distant stromal area) for tumours with either low or high TB, differential gene expression patterns were observed (Table5.10).

Table 5.10 *List of genes differentially expressed between low and high budding tumours.*

	Tumour core	**Invasive tumour**	**Invasive stromal**	**Distant stromal**
Low buds	*PSMB10, STAT3*		*CXCL9, CXCL10, PTPRC, CD44*	*STAT1, STAT2*
High buds	*CD44*	*CCND1*		*IL6, CD68*

High expression of *PSMB10* was found in the core area of tumours with low budding (p=0.049). The function of PSMB10 is to regulate the generation of MHC class I receptor in cancer (267), which is known to regulate inflammation. This could suggest that, when tumours exhibit low TB cells, the activation of an anti-tumour activity is maintained. In contrast, expression of CD44, the stem cell marker, was reported to be enriched in high TB compared to low TB tumours. However, when reviewing the raw data, only 2 high TB cases with high CD44 were reported. Therefore, the validation of CD44 protein expression by IHC staining in two independent cohorts was performed. Patients with high CD44 tend to have a better survival than those with low CD44 expression in both cohorts. However, these did not reach statistical significance, and no association was found between budding status and the expression of CD44. CD44 is a well-known cancer stem cell marker that has been used to study tumour stem cell characteristics (268). Tumours with stem cell characteristics were reported to be aggressive resulting in lymphovascular invasion, peritumoral budding and grading in CRC (269).

However, studies have reported conflicting results regarding the role of cancer stem cells markers (270). There is no standard set of cancer stem cell markers that could be used to evaluate the role of stem cells in CRC. Therefore, investigating the expression of additional stem cell markers may be worth investigating to clarify the association between tumour stemness and budding formation in CRC.

Apart from the gene expression at the tumour core area, DSP revealed that *CCND1*, the gene codes for cyclinD1, was shown to be highly expressed in the invasive tumour area of high budding when compared to low budding tumours. Statistical significance was not achieved; however, this may be due to the small sample size (n=6). CyclinD1 has been shown to correlate with tumour progression in CRC (271). This could be related to the mechanism of budding formation; therefore, a further study was conducted to validate these results at a proteomic level in the full CRC cohort (n=787). There is no significant difference in patients' survival at the invasive tumour between low and high TB. However, when cyclinD1 expression was assessed in tumour buds, survival analysis showed that patients with high cyclinD1 in budding cells showed a poorer survival when compared to those buds with low cyclinD1. These findings suggested that the activation of cell cycle signalling might be involved in the regulation of TB. Cell cycle signalling is one of the key factors that helps tumour cells grow and maintain their viability with continuous division (272). As cyclinD1 controls G1 phase, it may be that, when produced, buds may undergo an early stage of the cell cycle to maintain their ability to survive waiting for the right time to invade other parts of the body. In concordance with this finding, nuclear protein marker (Ki67) associated with cell proliferation was reported to be highly expressed in the late phases of the cell cycle which may explain the recent findings from a few studies as buds were found to be less proliferative (158, 261, 273).

DSP results also showed that *CXCL9, CXCL10, CD44 and PTPRC* genes were found in the stromal compartment of the invasive tumour area in low budding group (n=6). CXCL9

and CXCL10 were constantly reported as favorable prognostic factors in CRC (274-277). This was aligned with the findings reported in this thesis as high CXCL9 and CXCL10 tend to be highly enriched in the invasive stromal area of tumours with low budding. Although no association was found between CXCL9, CXCL10 and TB phenotype, the significant correlation with better survival when tumours had increased levels of these two cytokines could suggest a possible role in the better prognosis in the low TB group. However, the quantification of CXCL9 and CXCL10 was accessed in tumour core TMAs and should be assessed in the invasive edge to confirm the DSP results, to understand how these proteins may relate to the budding phenotype in CRC. PTPRC (CD45) is known to be expressed on activated immune cells (278). Having high inflammation has been reported to associate with prolonged survival in CRC (279). The DSP results revealed a high expression of PTPRC in tumours with low buds, this could explain the prolonged survival and the correlation of anti-inflammatory cells when tumours exhibited a low number of buds in CRC (18).

Lastly, differential gene expression analysis was performed to compare the distant stromal area in tumours with low and high TB to determine if there were any differences in gene expression patterns between the two groups. Although no significant difference was found between the two groups, tumours with high buds were likely to have higher expression of CD68 and IL6 when compared to low budding group. These findings perhaps suggested that, when the stroma has an enriched population of macrophages, the macrophages may create a metastatic niche that could lead to tumour progression (280). Interestingly, one of the factors produced by macrophages is interleukin6 (IL6), which is an important mediator of the production of neutrophils and regulatory T cells. Studies have shown that IL6 may be regulate the activity of downstream signalling that plays an important role in tumourigenesis (281). CD68 and IL6 are both highly expressed in the distant stromal area of tumours with high buds, suggesting the possible role of macrophages to induce microinvasion. To validate mRNA

expression from DSP, protein expression of IL6 receptor (IL6R) was accessed using IHC staining. The results showed that high IL6R expression in the tumour core was significantly associated with poor survival. Interestingly, high IL6R is significantly associated with high budding tumours. In addition, as IL6R protein was studied in tumour core area, investigate the expression of IL6R within the invasive tumour area with budding cells should be conducted to understand its role in budding regulation in CRC. Interestingly, as IL6 is known to recruit pro-tumorigenic cytokines, the significant association between IL6R and TB phenotype could suggest a role in the aggressive characteristics of tumours with high buds and its poor prognosis in CRC.

Despite that, high STAT1 in stromal area of low TB was found when compared to high TB groups. The protein expression validated in the TMA previously made from tumour core showed that patients with high stromal STAT1 expression had a significantly better survival compared to those with low stromal STAT1 expression. This may confirm the favorable prognostic value of STAT1 that has been reported in CRC (282) . Although further studies are needed to identify its correlation with TB.

Together, these results identified possible genes related to high budding tumours. However, these results need further investigation, due to the small number of cases studies between low and high budding tumours. DSP was also used to compare the differential expression of genes across different areas of high budding tumours which will be discussed in the next chapter.

Chapter 6. Differential expression of genes between different area of tumours with high budding

6.1. Introduction

The heterogenous nature of cancer has been reported for many decades (283). Different types of cancer may express different gene signatures leading to the development of targeted treatments (284). Interestingly, recent studies also reported that, within the same cancer type, gene expression profiles allow a subtyping approach, highlighting the unique characteristics between different tumour-specific areas (285-287). This subtyping approach has now been reported to significantly associate with clinical outcome across multiple different cancer types (287, 288).

Spatial transcriptomics is a ground-breaking profiling methodology used to investigate the underlying molecular biology leading to the identification of gene signatures specific to different cell types (289). This has been reported to be a potential way of identifying new tissue-specific biomarkers which could lead to new targeted treatment options (290). GeoMx Digital Spatial Profiler (DSP) has been widely used to provide spatial transcriptomics data which may provide novel biological insight that bulk whole tissue approaches cannot (291).

IHC staining was used to determine the prognostic value of the genes associated with the budding phenotype and the possible significant correlation with adverse features in CRC patients. Conventional IHC is widely used to identify target protein expression in tissue sections (292), however, this has been limited to only one marker per tissue slide (181). This limitation was recently overcome with the development of multiplex techniques allowing simultaneous detection of multiple markers on a single tissue section (293). This high throughput multiplex staining technique has been used for highly reproducible, efficient, and cost-effective tissue studies (294). The use of this technique in translational research has provided a greater insight into underlying cancer mechanisms especially in relation to immunotherapy (72).

Following the GeoMx DSP results in the previous chapter, this chapter reports the differential gene expression comparing the regions of interest (ROIs); tumour core, invasive and distant stromal area, only in tumours with a high budding phenotype. The results were validated at the protein expression level by utilising immunohistochemistry (IHC) and multiplex immunofluorescence (mIF) including the spatial interaction using advanced single cells analysis.

6.2. Differential expression of PanCK+ cells between tumour core and the invasive edge.

This comparison allows the investigation of tumour cells from the main tumour bulk and tumour cells from the invasive budding area. The expression of *STAT1, IDO1, CXCL9, CXCL10, and IFNG* was significantly enriched at the invasive tumour edge (tumour budding region) compared to the tumour core area. Furthermore, the expression of two specific stem cell markers, *CD44 and EPCAM,* was significantly enriched in the tumour core area compared to invasive tumour edge (tumour budding region) (Figure 6.1A). The raw gene expression for each sample was plotted as a heatmap. Z-score illustrates the difference in gene expression with the colour from red representing high expression and purple low expression (Figure 6.1B).

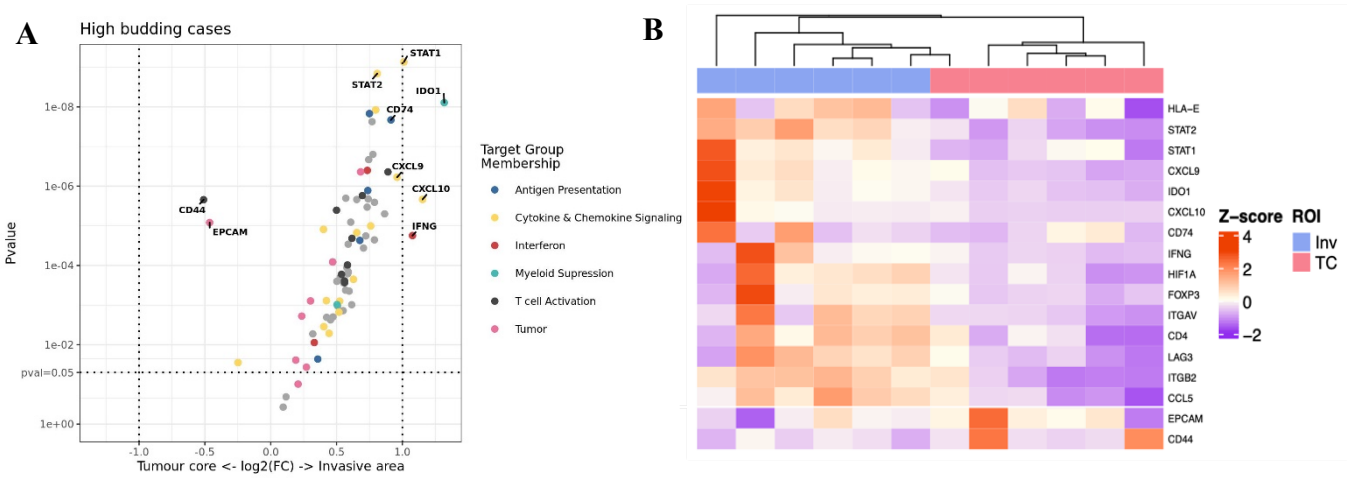

Figure 6.1 *(A)Volcano plot of the gene expression between the area in the main tumour and invasive stromal area of high budding tumours (n=6). (B) Heatmap illustrated the expression of the genes in two different areas.*

6.3. Differential expression of PanCK- non epithelial cells at the invasive and distant stromal area.

Immune-related genes, such as *NKG7, CMKLR1, IFNAR1, CD47, IL6, ITGB8, FAS, BCL2, TNF, CXCR6, CD3E, and VSIR,* were significantly expressed in the distant stromal area when compared to the invasive stromal surrounded by buds.

In contrast, fewer genes were detected in the invasive area: *HLA-E, B2M, STAT1, LY6E, and CD74* (Figure 6.2A). This may suggest that, when tumours exhibit a high budding phenotype, budding cells might suppress the activity of immune cells, leading to the poorer prognosis of high tumour budding in CRC patients. The raw gene expression data was illustrated in a heatmap demonstrating the differences in the distinct gene expression between the two regions (Figure 6.2B).

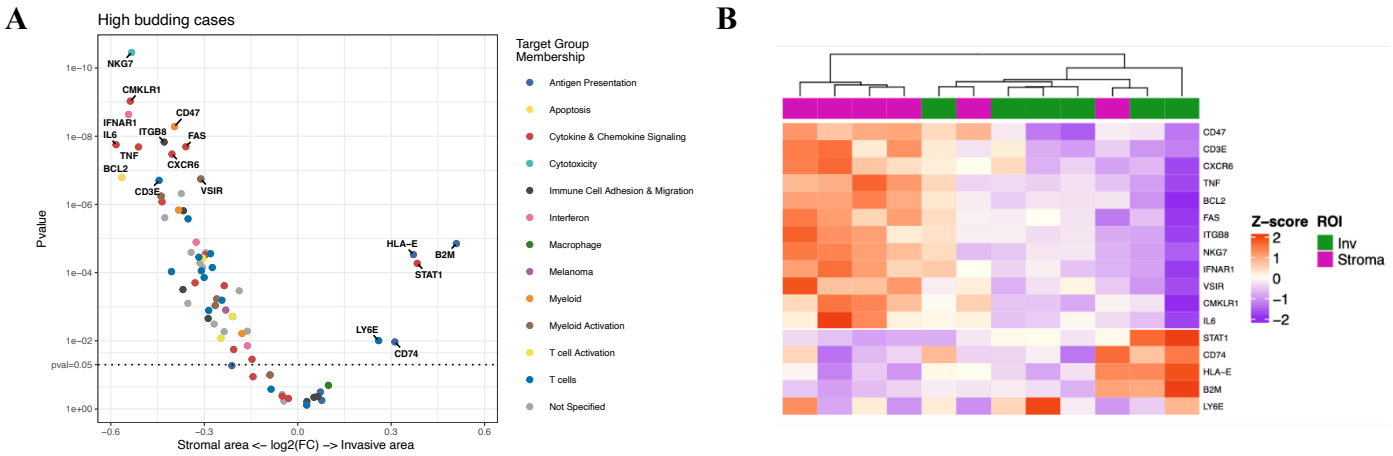

Figure 6.2 *(A) Volcano plot of the gene expression between distant and invasive stromal areas of high budding tumours (n=6). (B) Heatmap illustrated the expression of the genes in two different areas.*

6.4. Validation of mRNA expression using IHC

The transcriptomic data revealed *STAT1* expression at the invasive tumour edge was significantly higher when compared to the tumour core (Figure 6.1) in high TB tumours. However, the experiment was performed in a small sample size (n=6). To validate this, protein expression level was determined by IHC on previously constructed tissue microarrays (TMAs)

from high budding tumour invasive areas (n=180). The assessment of total STAT1 expression at the invasive edge was performed by MSc student, Bronte Kerrigan (BK) (Figure 6.3A).

CRC cases with high budding were selected to investigate the role of STAT1 protein expression. Patients with high STAT1 (n=61) at the tumour invasive area are shown to have poorer overall prognosis compared to those with low STAT1 (n=21) (HR=1.430, 95% CI;0.621-3.296 log-rank p=0.401). The 5 years survival rate was 60% for low STAT1 and 55% for high STAT1 patients. (Figure 6.3B)

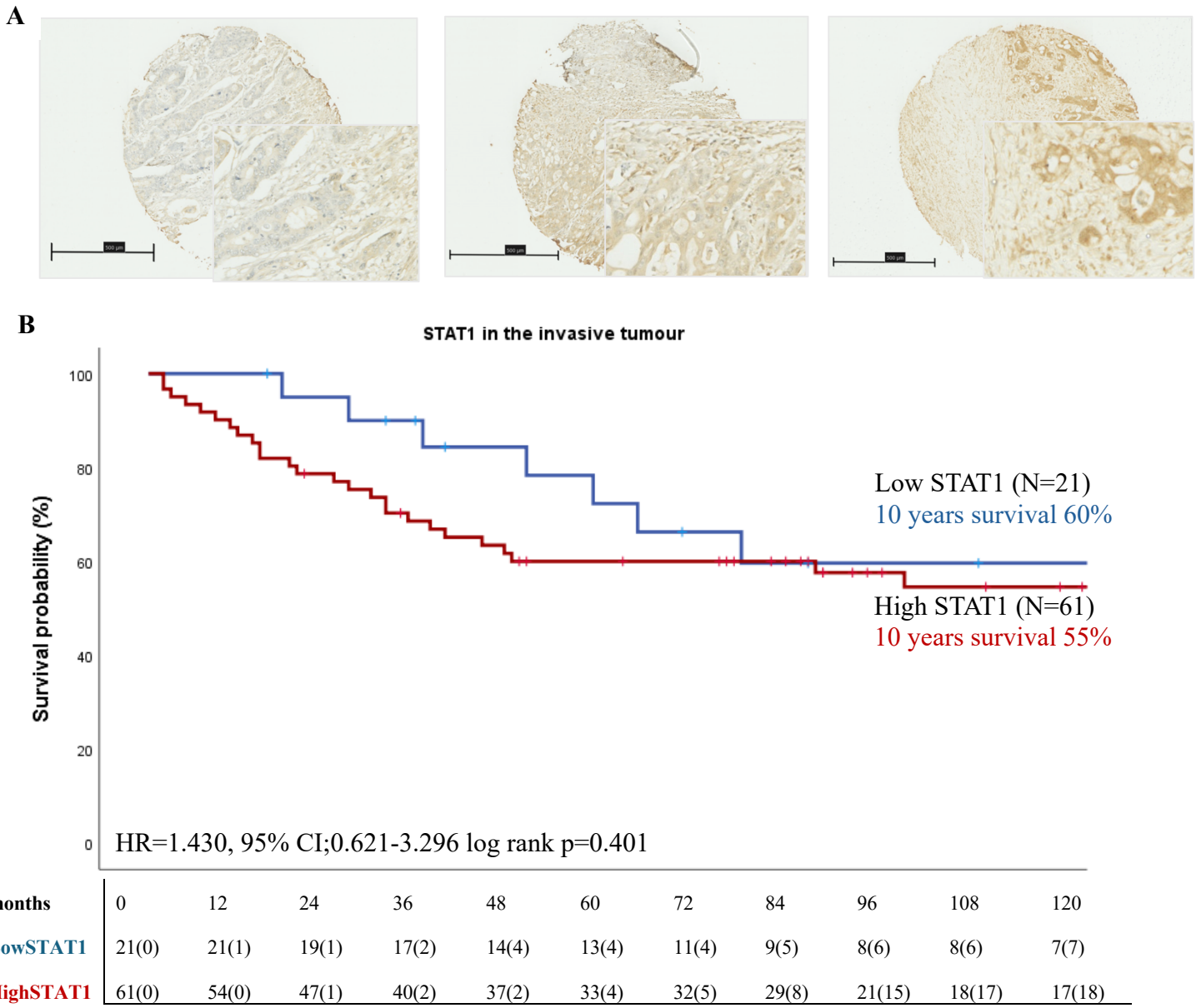

Figure 6.3 *(A) IHC staining of total STAT1 protein expression in TMA from the invasive edge tumours. (B) Kaplan-Meier survival analysis based on STAT1 for cancer specific survival (CSS) in CRC patients. Hazard ratio (HR) was reported with 95% confidence intervals. P Values were calculated using the log-rank test comparing patients with low (n=21) and high (n=61) STAT1 expression.*

6.5. Validation of mRNA expression using multiplex staining

According to the previous findings from GeoMx DSP (section 6.2.2), a reduction of activated inflammatory cells was found in the invasive area when compared to the distant stromal area in tumours with high TB.

To understand the budding microenvironment, further work has been undertaken to investigate the relationship between TB and the surrounding immune cells. Multiplex immunofluorescence (mIF) was performed, as described in section 2.4, in full CRC tissue sections (n=18). Panels for specific phenotypes (lymphocytes; CD3, CD8, FOXP3, Ki67, and PanCK and myeloid; CD68, CD163, CD66b, and PanCK) were selected to investigate the role of lymphocyte and myeloid cells in relation to TB in CRC patients (Figure 6.4).

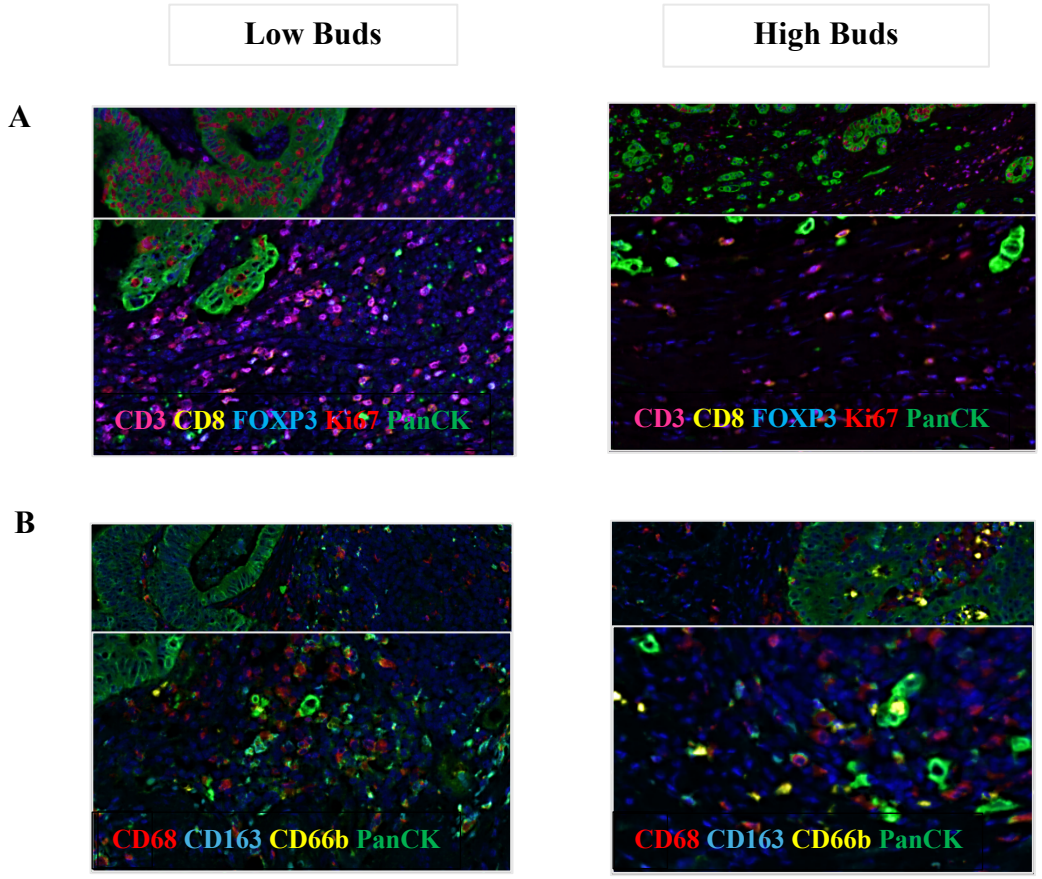

Figure 6.4 *Multiplex staining in CRC full sections between low (n=9) and high (n=9) budding tumours for two panels of the immune-related markers (A) Lymphocyte (CD3 CD8 FOXP3 KI67 and PanCK) and (B) Myeloid (CD68 CD163 CD66b and PanCK) panels.*

6.5.1. T cells

The total number of positive cells was quantified using the image analysis software, Visiopharm, and the percentage of regulatory (CD3+FOXP3+) and cytotoxic T (CD3+CD8+) cells was calculated within the total population of CD3+ cells. The cell density was determined at the invasive stromal area, in which budding cells were found, and distant stromal area.

In tumours with high TB, the percentage of regulatory cells (CD3+FOXP3+) is significantly higher in the invasive compared to distant stromal areas (p=0.012). There is no significant difference in the percentage of cytotoxic T cells (CD3+CD8+), although a smaller number of cytotoxic T cells was found at the invasive compared to distant stromal areas. (Figure 6.5B). There were no significant differences in the number of these cells between the two areas in tumours with low budding (Figure 6.5A). The results demonstrated no statistical difference of T cells comparing between tumours with low and high TB at the invasive stromal (Figure 6.6).

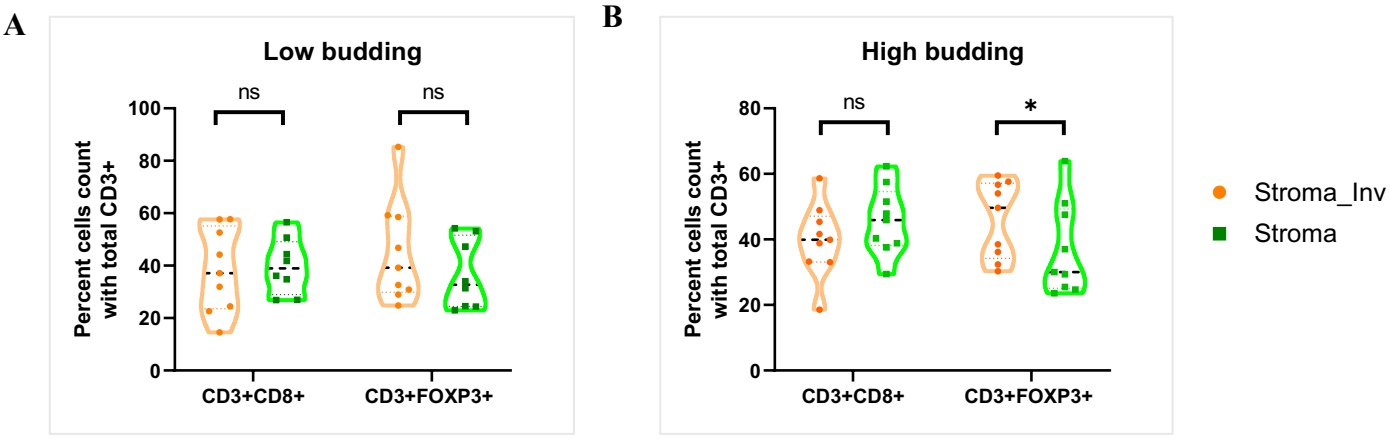

Figure 6.5 *CRC full sections multiplex staining shows a percent count of CD3+CD8+ and CD3+FOXP3+ cells compared between invasive (orange) and distant stromal (green) area in tumours with (A) low (n=9) and (B) high (n=9) TB phenotype.*

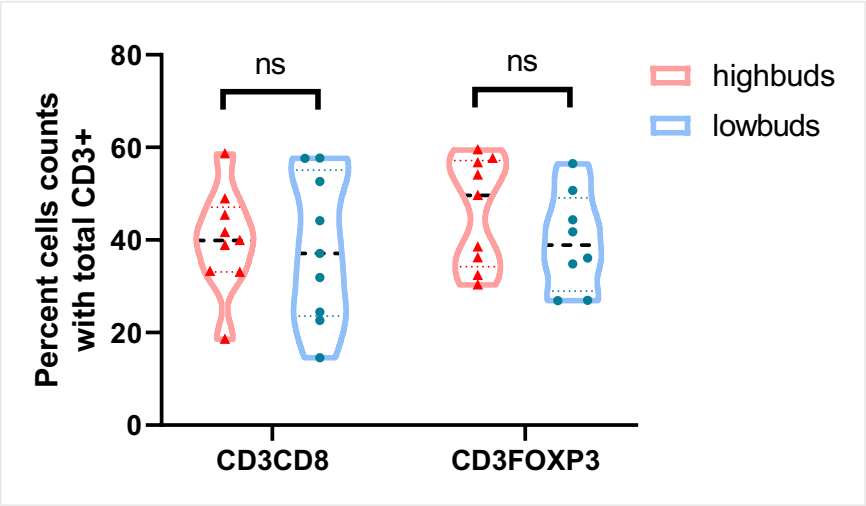

Figure 6.6 *The percentage of T cells infiltration at the invasive stromal area compared between tumours with low (n=9) (blue) and high (n=9) (red) budding phenotype.*

6.5.2. Macrophages

The percentage of CD68+ (pan-macrophages) and CD68+CD163+ (pro-tumourigenic macrophage) cells was investigated in both invasive and distant stromal areas. The density was calculated as the total number of macrophage populations.

The results demonstrate that the number of CD68+ cells is significantly higher in the invasive when compared to distant stromal areas in both tumours with high (n=9) (p=0.004) and low (n=9) (p=0.012) TB. Additionally, there is a significantly lower number of CD68+CD163+ cells in the invasive compared to the distant stromal area in both high (n=9) (p=0.004) and low (n=9) (p=0.020) budding groups (Figure 6.7).

However, the results demonstrated no significant difference when comparing the percentage of macrophages at the invasive stromal between tumours with high and low budding. However, the number of CD68+ is lower while CD68+CD163+ counts are slightly higher at the invasive front in tumours with high buds (n=9) (Figure 6.8).

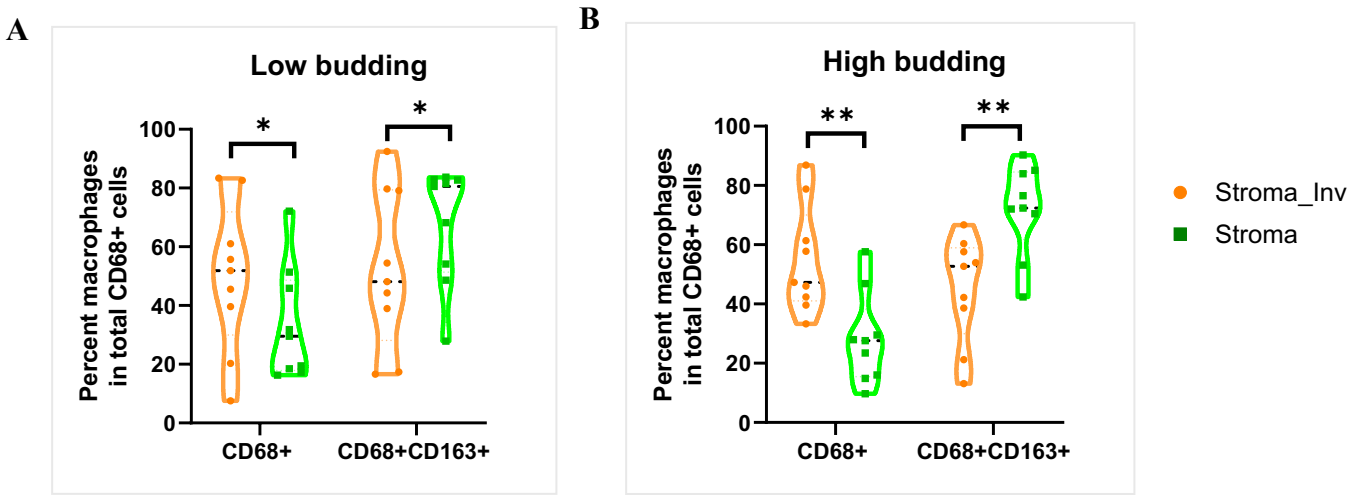

Figure 6.7 *Box plots show the percentage count of CD68+ and CD68+CD163+ cells compared between invasive (orange) and distant stromal (green) area in tumours with (A) low (n=9) and (B) high (n=9) TB phenotype. * p<0.05, **p<0.01*

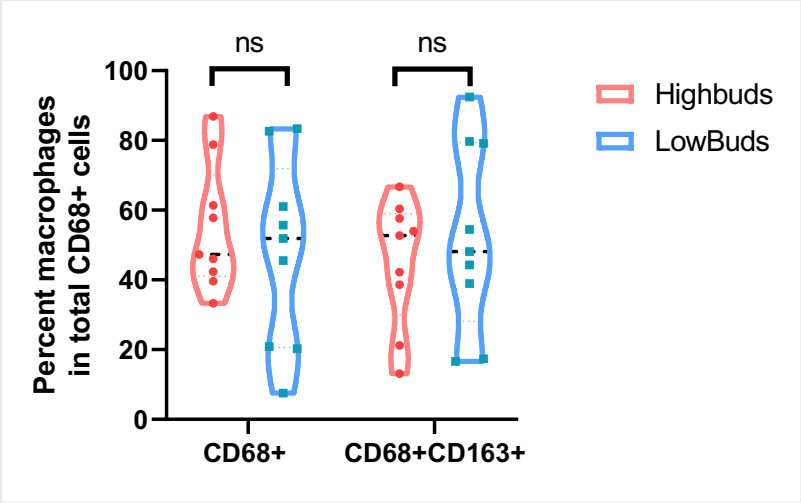

Figure 6.8 *The percentage of macrophage subtypes at the invasive stromal area compared between tumours with low (n=9) (blue) and high (n=9) (red) budding phenotype.*

6.5.3. Neutrophils

In addition to the macrophage population, the number of neutrophils was also investigated using CD66b as a marker. The percentage of neutrophils was calculated from the total number of stromal cells within the area of interest.

The results revealed that a higher number of neutrophils were found at the invasive front compared to the distant stromal area in both tumours with low (n=9) (p=0.02) and high (n=9) (p=0.09) budding (Figure 6.9). However, when comparing the percentage of CD66b+

cells between tumours with high and low buds at the invasive stromal area, a higher number of CD66b+ cells was observed in tumours in the low budding group (n=9) (Figure 6.10).

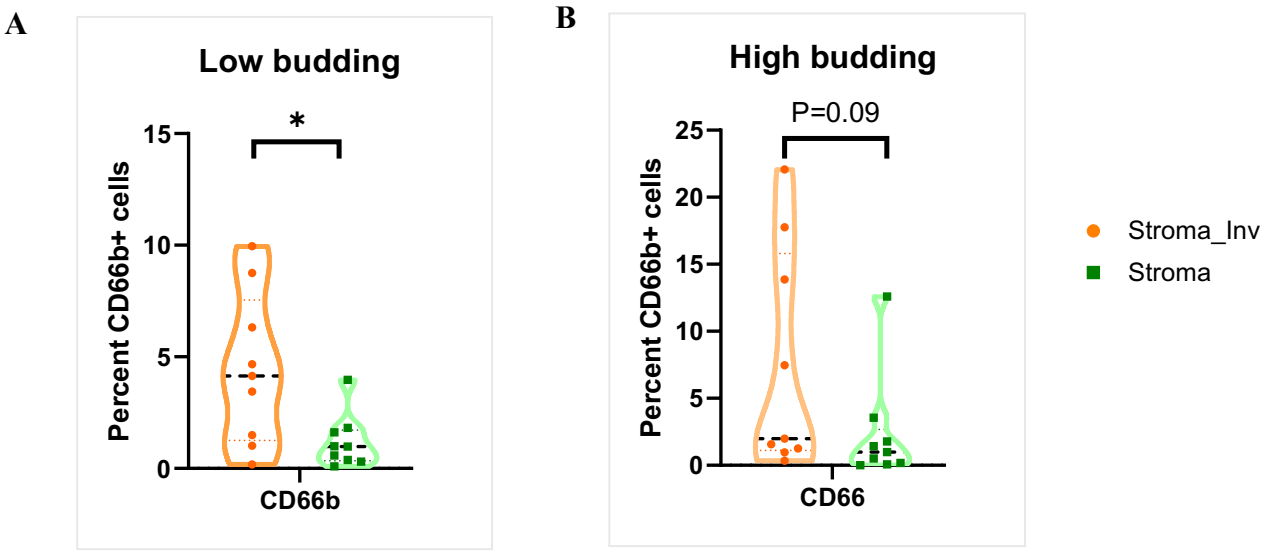

Figure 6.9 *Box plot shows the percent counts of CD66b+ cells compared between invasive (orange) and distant stromal (green) area in tumours with (A) low (n=9) and (B) high (n=9) TB phenotype. * p<0.05*

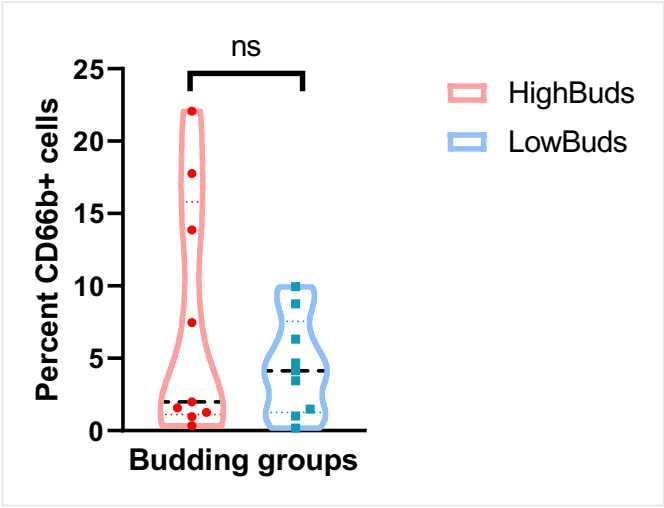

Figure 6.10 *The percentage of CD66b+ cells at the invasive stromal area compared between tumours with low (n=9) (blue) and high (n=9) (red) budding phenotype.*

6.6. Cell clustering and Nearest neighbour analysis.

The mIF results revealed that the percentage of immune cells in the invasive stromal area may have an immunosuppressive role in TBs. To investigate this further, cell clustering and nearest neighbour analysis were performed, from mIF studies above (n=18), to identify the interaction between individual budding clusters and immune cells.

To determine the spatial relationship between buds and immune phenotypes, cell clustering analysis was first performed to identify individual bud clusters using the R package (DBSCAN). A cluster of buds (single cells or group of up to 4 cells) was filtered and selected for further nearest neighbour analysis (Figure 6.11). Budding cluster was studied regardless of TB phenotype between samples.

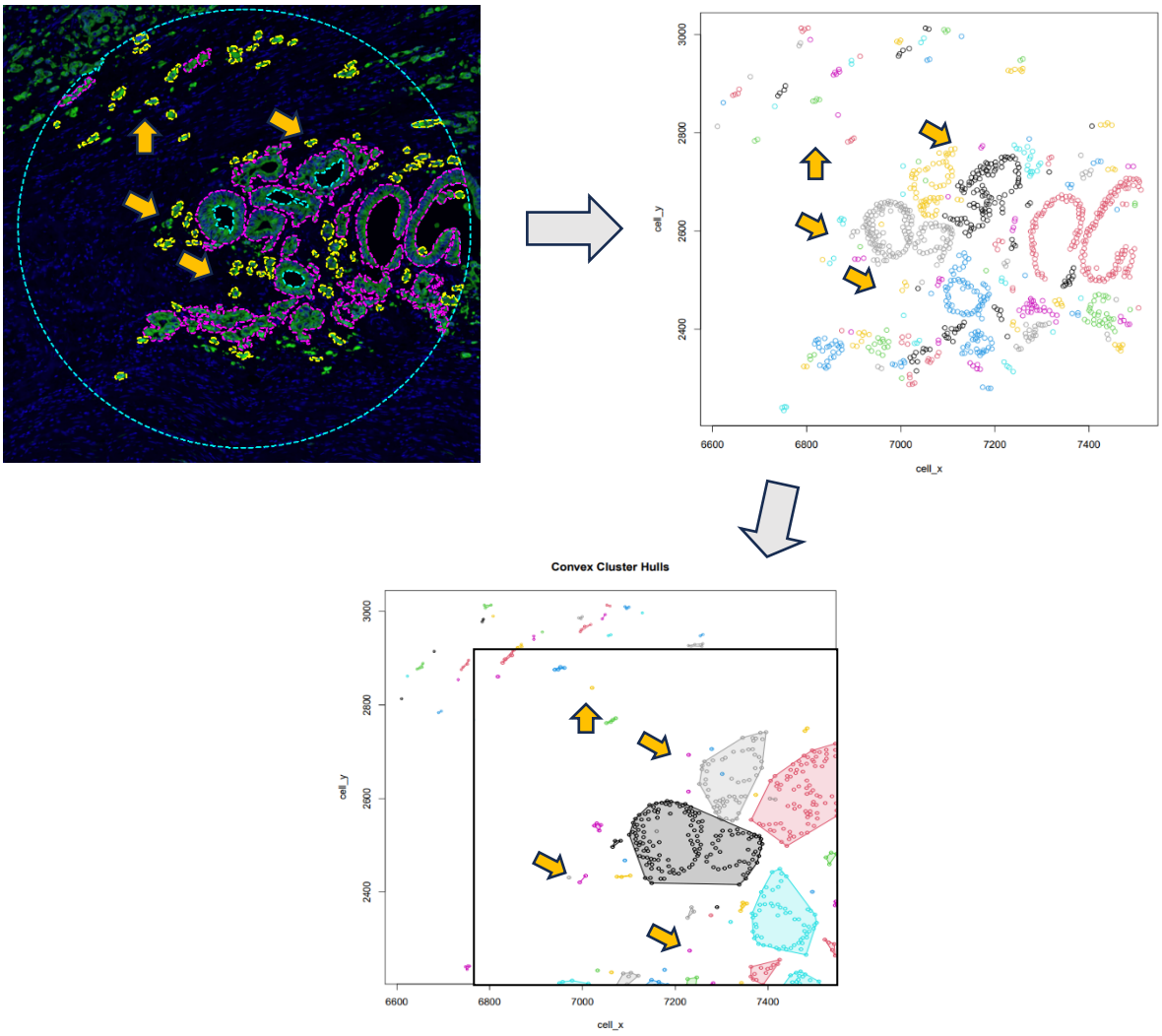

Figure 6.11 *Cluster analysis identified cluster of TB (yellow arrow); one or up to four tumour cells.*

After identifying individual budding clusters, nearest neighbour analysis was performed to determine the nearest distance from budding clusters to immune phenotypes using the R package (phenoptr). The smaller the number the closer the distance from budding cells to phenotypes. In addition, scatter plots were utilised to determine the distance of budding clusters to two immune phenotypes. The median distance from budding to each phenotype was used to generate the cut point for quadrant generation. Individual budding clusters were then grouped into four categories as illustrated in Figure 6.12.

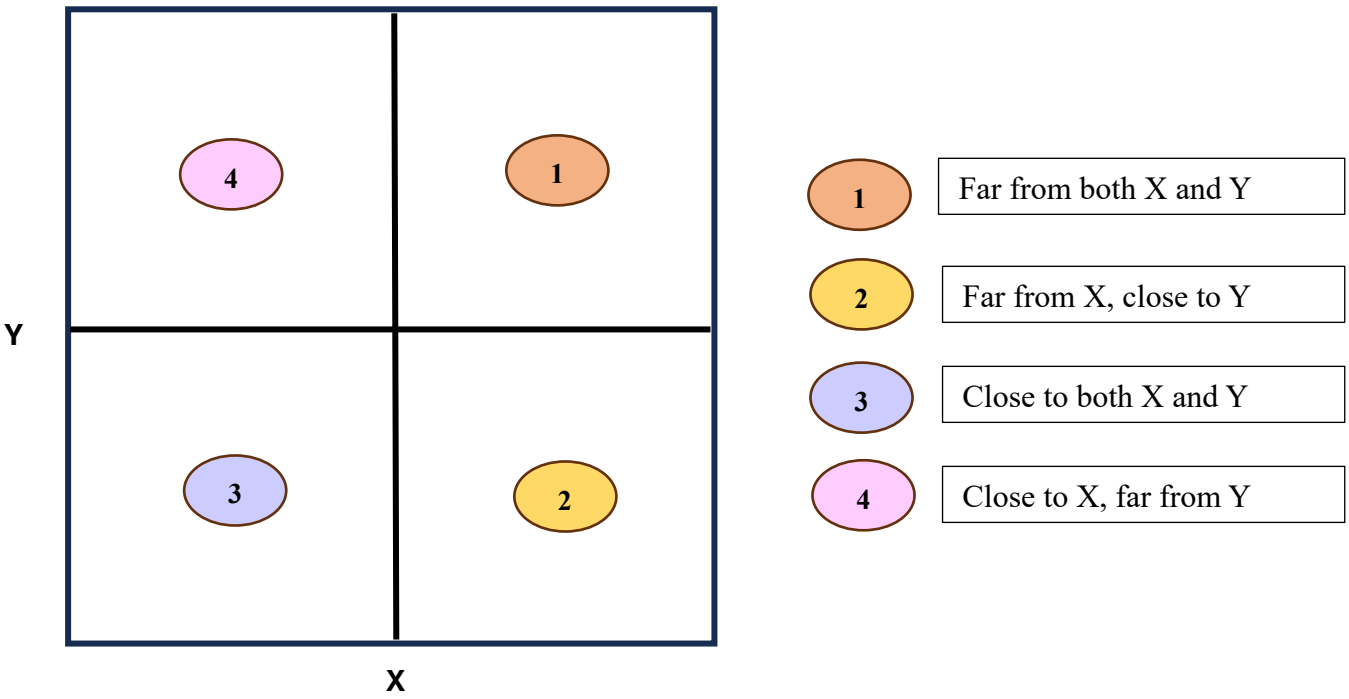

Figure 6.12 *The scatter plots diving into 4 quadrants representing the distance from tumours to two phenotypes (x and y).*

6.6.1. Lymphocyte cells

When the distance was compared between two phenotypes (cytotoxic; CD3+CD8+ and regulatory; CD3+FOXP3+ T cells), although no significant differences were observed, the budding clusters were observed to be closer to the regulatory cells with an average of 41.3 µm compared to cytotoxic T cells (48.3 µm) (Figure 6.13).

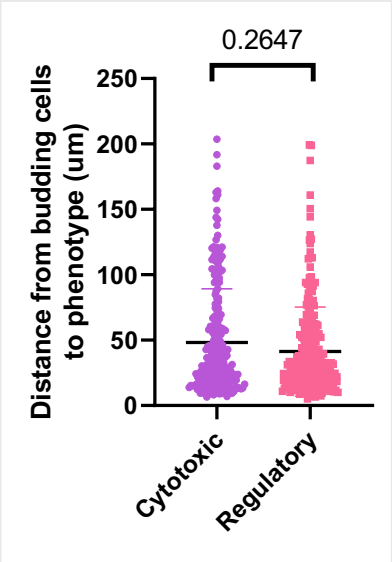

Figure 6.13 *The comparison between distances from budding clusters to cytotoxic (CD3+CD8+) and regulatory (CD3+FOXP3+) cells.*

A scatter plot was generated (x= CD3+CD8+, y= CD3+FOXP3+), and the quadrant groups were listed for each of the budding clusters identified in CRC cases (n=18). Therefore, the distance from budding cells to both T cell populations was determined (Figure 6.14).

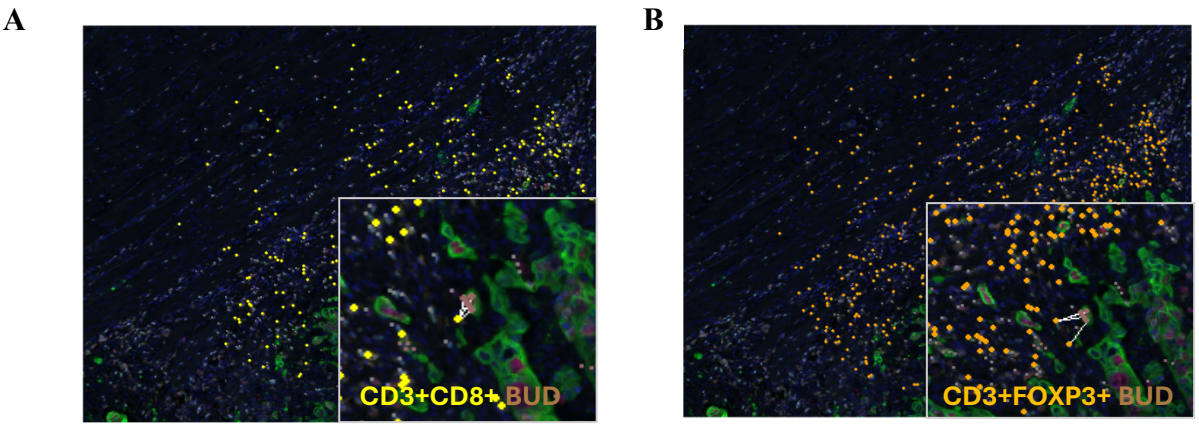

Figure 6.14 *Images showed the distance of bud cluster (brown) to (A) cytotoxic (CD3+CD8+) and (B) regulatory (CD3+FOXP3+) T cells performed by nearest neighbour analysis.*

The percentage distance was calculated from the total number of budding clusters to determine the differences in the distances from budding clusters to phenotypes. When classifying those clusters into four-quadrant subgroups, the results showed that the budding clusters tend to behave differently within the same CRC cases (Figure 6.15A) (Supplementary figure 6.1). Most of the budding clusters are, significantly, found in quadrant three indicating the close distance proximity from budding cells to both cytotoxic (CD3+CD8+) and regulatory (CD3+FOXP3+) cells (Figure 6.15B).

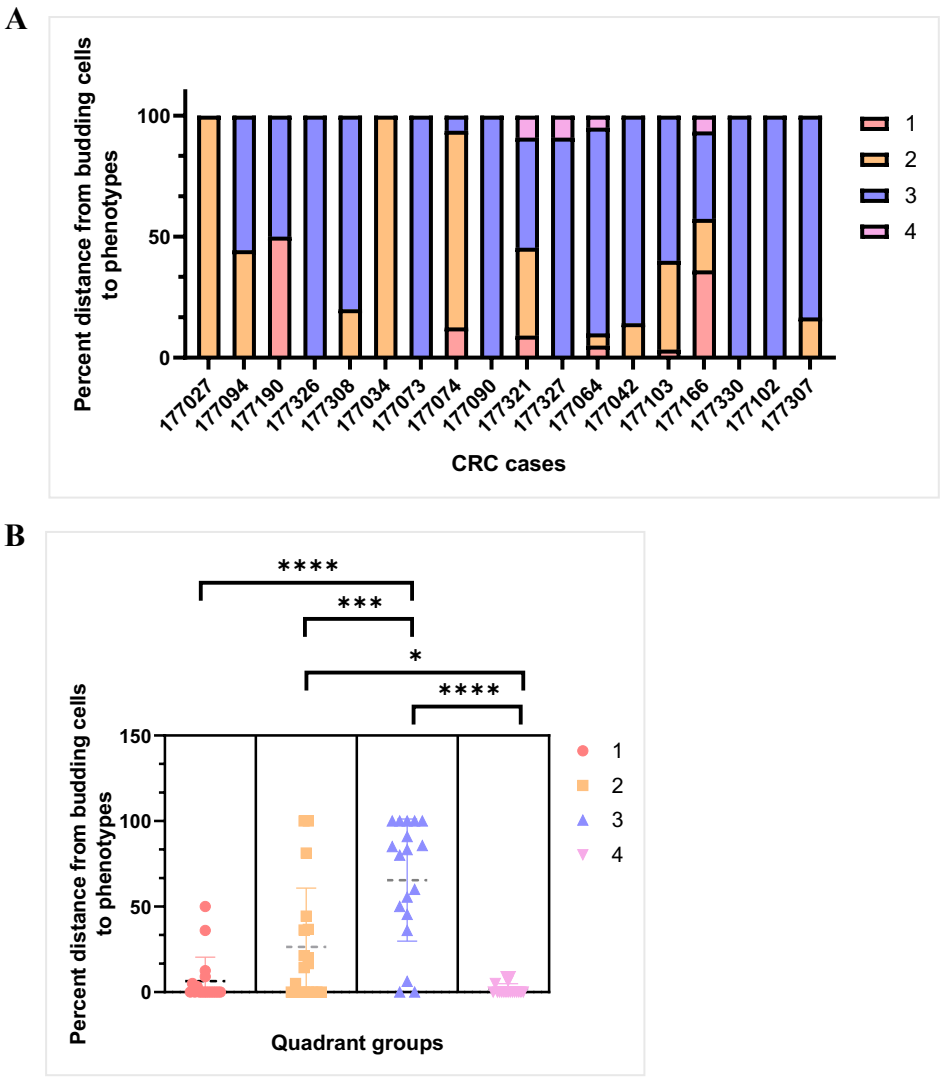

Figure 6.15 *(A) Bar plot showed the percentage of TB cluster in each CRC cases grouped in four quadrant categories. (B) The nested plot classifies budding clusters in each of the quadrant groups.*

6.6.2. Myeloid cells

The relationship between budding cells and myeloid cells was observed using the multiplex panel for CD68+, CD163+, and CD66b+ markers. CD68+ cells are significantly closer to budding clusters than CD68+CD163+ ($p<0.0001$) and CD66b+ ($p<0.001$) cells. In addition, when comparing the distance between neutrophils (CD66b+) and pro-inflammatory macrophages (CD68+CD163+), the budding clusters are significantly closer to neutrophils than CD68+CD163+ macrophages ($p=0.028$). It can be concluded that, budding clusters are closer in distance to pan-macrophages, neutrophils, and pro-inflammatory macrophages

respectively. Of the three phenotypes, pro-inflammatory macrophages were the farthest away from buds (Figure 6.16).

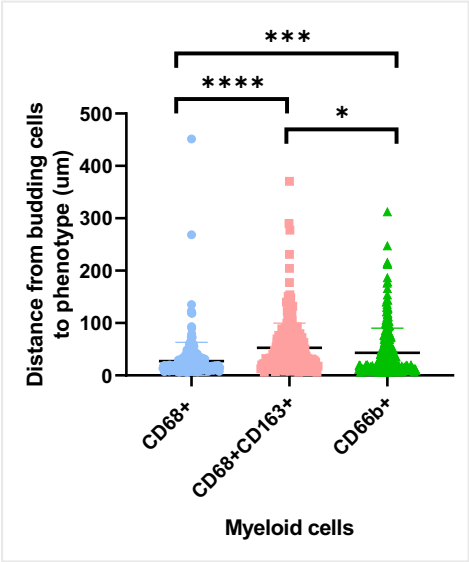

Figure 6.16 *The comparison between distances from budding cluster to pan (CD68+), pro-inflammatory (CD68+CD163+) macrophages and neutrophil (CD66b+).*

To determine the spatial interaction of individual buds, the distances from individual budding clusters to phenotypes were studied (Figure 6.17).

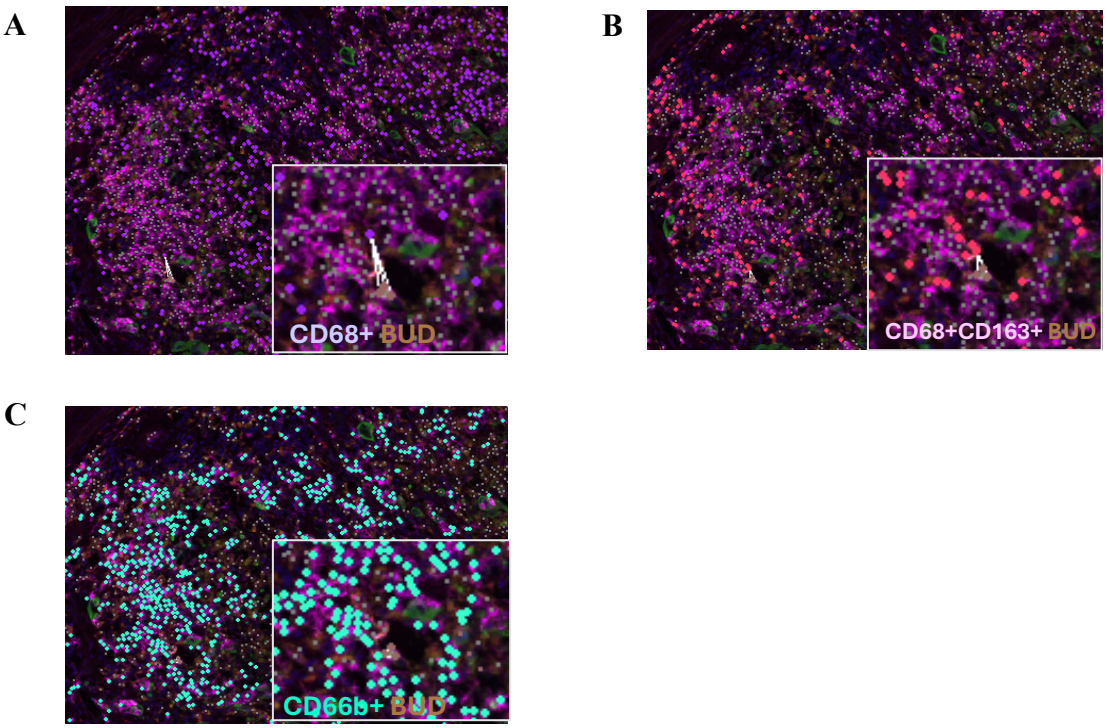

Figure 6.17 *Images showing the distance of bud cluster (brown) to (A) pan-macrophage (CD68+) (B) pro-inflammatory macrophages(CD68+CD163+) and (C) neutrophils (CD66b+) cells performed by nearest neighbour analysis.*

The budding clusters were identified in each of the CRC cases (n=16), two cases with low budding phenotype were excluded as no budding cluster was found. There was heterogeneity regarding the percentage distance from budding clusters to phenotypes in the same CRC cases, thus they were classified into four quadrant groups to determine the prominent budding clusters among the four groups (Figure 6.18A) (Supplementary figure 6.2). The results revealed that, although there was no significant difference, a close interaction with budding clusters to both pan (CD68+) and pro-inflammatory (CD68+CD163+) macrophages was found (Figure 6.18B).

A

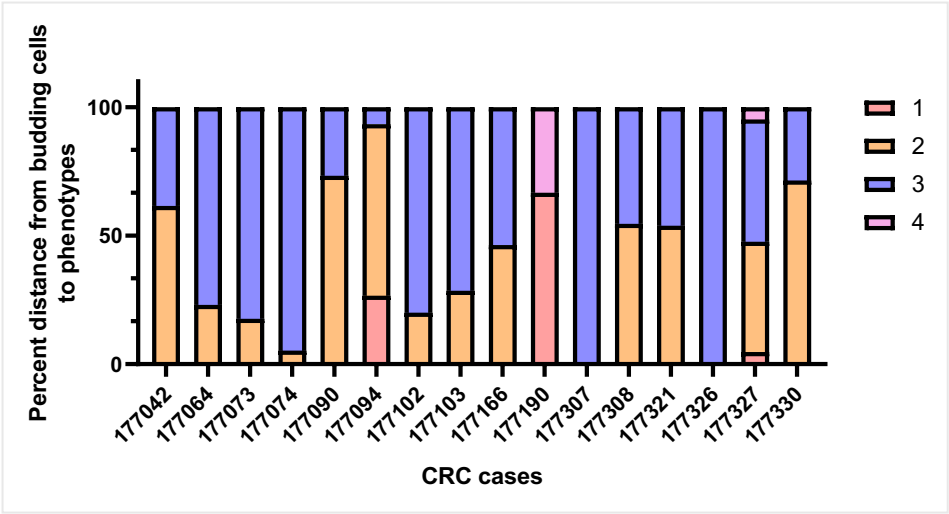

B

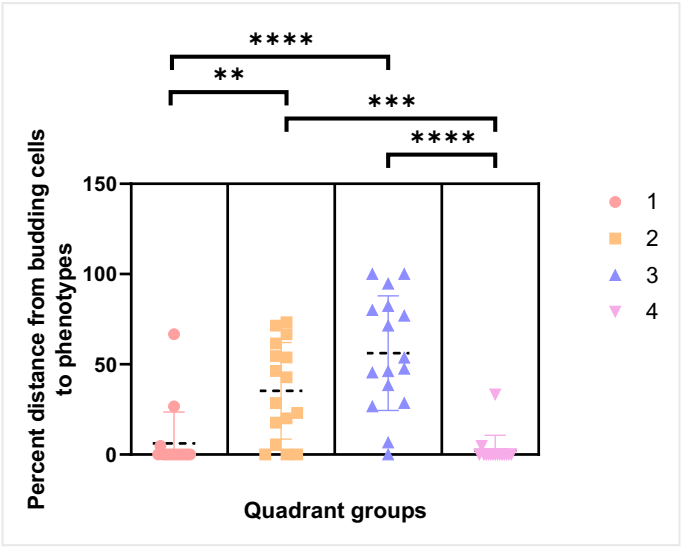

Figure 6.18 *(A) Bar plot showed the percentage of TB cluster in each CRC cases grouped in four quadrant categories. (B) The nested plot classifies budding clusters in each of the quadrant groups.*

In addition to the interaction with macrophage populations, budding clusters were classified into quadrant groups to determine the distance to CD66b+ (neutrophil) and CD68+ (pan-macrophage) cells (n=15) (Figure 6.19A) (Supplementary figure 6.3). Three CRC cases were excluded due to unavailable data. Interestingly, it was shown that budding clusters are significantly found in group three suggesting the close proximity of budding cells to both neutrophils and pan-macrophages (Figure 6.19B).

A

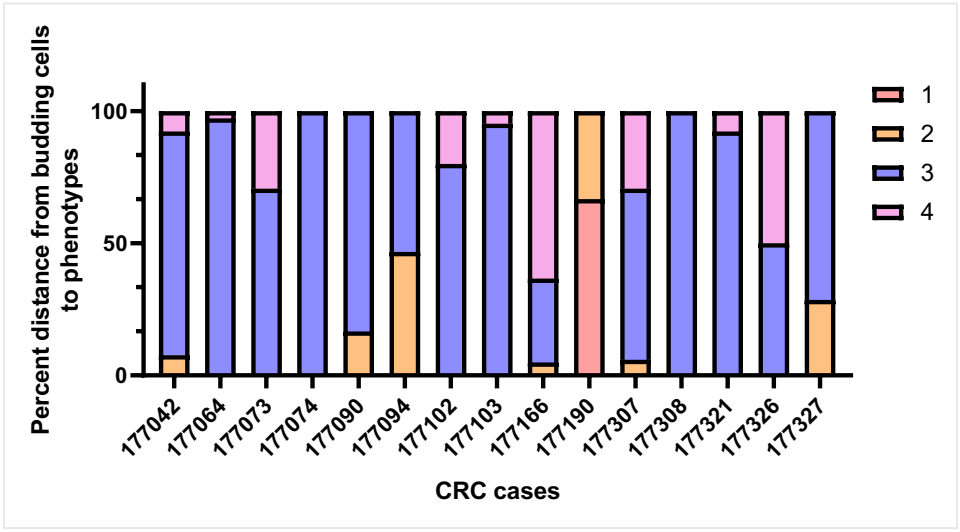

B

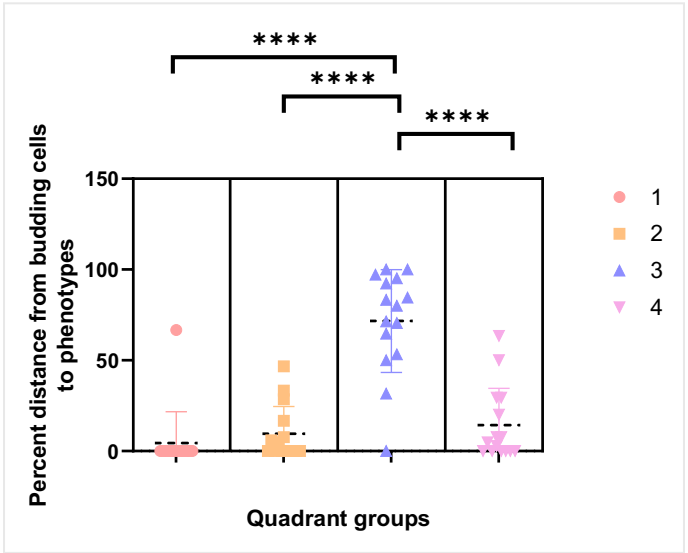

Figure 6.19 *(A) Bar plot showed the percentage of TB cluster in each CRC cases grouped in four quadrant categories. (B) The nested plot classifies budding clusters in each of the quadrant groups.*

The distances from budding cells to CD68+CD163+ and CD66b+ cells were also studied. A mixed population of buds, regarding the distance to phenotypes, was found in most of the CRC cases (Figure 6.20A) (Supplementary figure 6.4). However, budding clusters were mostly found in group three indicating the nearest distance of both phenotypes to budding cells (Figure 6.20B). Additionally, budding clusters closer to CD66b+ but not CD68+CD163+ cells, from quadrant two, were also frequently found.

A

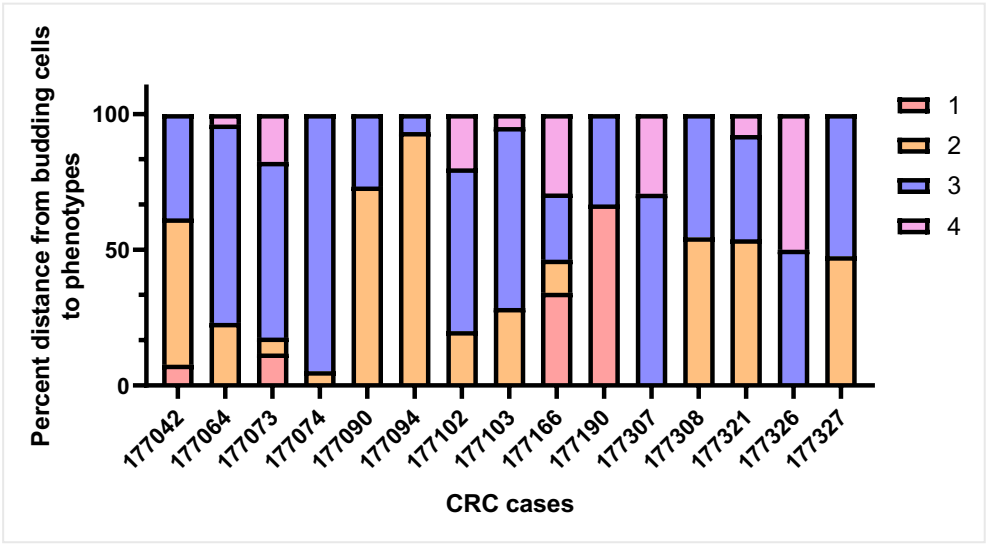

B

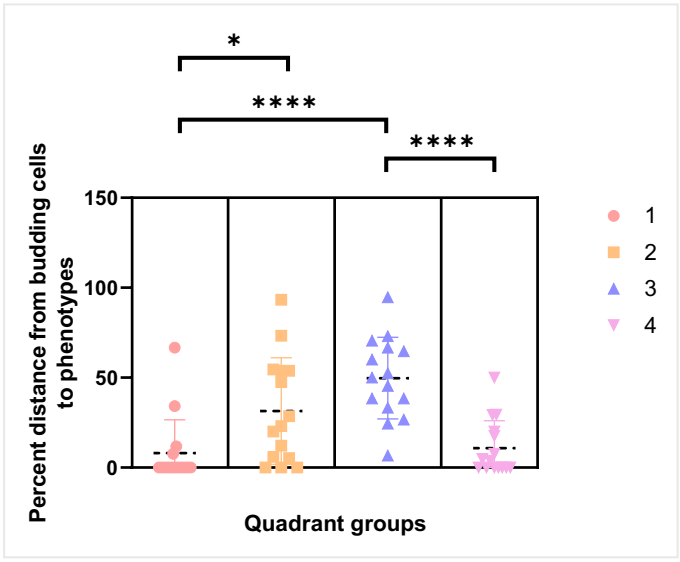

Figure 6.20 *(A) Bar plot showed the percentage of TB cluster in each CRC cases grouped in four quadrant categories. (B) The nested plot classifies budding clusters in each of the quadrant groups.*

6.7. Discussion

It has been reported that tumour core and invasive cells have a distinct gene expression which could contribute to identifying potential targets for tumour invasion and metastasis (285-287). The finding from Digital Spatial Profiling (DSP) provided evidence that tumours with high budding expressed a significant number of STAT-related genes at the invasive compared to the tumour area (n=6). The results were further validated using a previously made TMAs at of the invasive tumour budding area (n=180), total STAT1 protein expression was investigated as it had the highest significance from the DSP results. The survival analysis showed that, when accessing STAT1 at the invasive tumour, patients with high STAT1 tend to have a poorer outcome compared to those with low STAT1. However, statistical significance was not reached although the KM plots had wide separation of the curves, it was concluded that this was due to the cohort being underpowered. A power analysis was carried out suggesting a cohort size of 385 (see appendix for further calculation). This study included only 180 cases, some samples were also lost during the analysis with only 82 samples remaining, this would require more samples for results to reach significance. Evidence in support of a role for STAT proteins in tumour development has been reported (295). In CRC, the underlying mechanism of tumour progression is also related to increased STATs signalling and this influences tumour infiltrating immune cells. The downstream target genes of this signalling are known to provide tumours with the capability to thrive in hard conditions (296). Therefore, it could be that while the tumour core tends to be the original source of tumour progression, the acquisition of other signalling may occur to increase invasion at the invasive front.

The interaction between tumour cells and their microenvironment may result in tumour development and progression (192, 297-299). The DSP findings demonstrated that, when tumours exhibit a high budding phenotype, there is a profound loss of immune activation at the invasive compared to the distant stromal area. The relationship between tumour buds and the

infiltrating immune cells has been reported (13, 18, 160). These results suggest that budding cells may perhaps be associated with immunosuppression allowing them to evade the immune system and start to metastasise to another part of the body.

To validate DSP results, multiplex staining was conducted using the panel of lymphocytes and myeloid cell markers to represent the microenvironment at the invasive stromal area. The results showed that there is a significantly higher number of regulatory (CD3FOXP3+) and a lower number of cytotoxic (CD3+CD8+) cells at the invasive compared to the stromal area. Similarly, Lin et al. reported that the vast majority of immune suppressive, while partially cytotoxic, cells were found in the invasive CRC tumour area (182). Moreover, a significantly high number of CD68+ and fewer CD68+CD163+ cells were found at the invasive compared to distant stromal areas in tumours with both low and high budding. A high number of CD66b+ cells were also found at the invasive tumour area in low budding tumours, although only 9 CRC cases per phenotype were studied and outliers were found in cases with high budding. Although fewer studies focus on the microenvironment of the invasive CRC tumour, these results could suggest that the invasive tumour with budding cells is likely to influence the activity of immune cells.

The use of spatial transcriptomic focusing on cell-cell interaction has been emerging to unravel the spatial relationship in tumour biology (300). Nearest neighbour analysis was conducted to identify the spatial relationship and determine how budding cells interact with their own microenvironment. Overall, the findings demonstrated that there is a heterogeneity among budding cells as individual buds seem to have different interactions between the immune phenotypes when investigated in the same CRC sample. In relation to the T cells, budding clusters tend to have a closer interaction with regulatory cells than cytotoxic cells. However, when investigating the interaction between budding cells and T lymphocytes, most bud clusters tend to have a closer interaction with both cytotoxic (CD3+CD8+) and regulatory

(CD3+FOXP3+). The regulatory cells are known as immunosuppressive cells, and studies reported their role in the secretion of molecules promoting progression and metastasis (301, 302). When regulatory cells are near budding clusters, they may recruit molecules that might help budding cell progress leading to a poor outcome in CRC patients. Regulatory T cells can also exert pro-tumour functions through suppression of cytotoxic T cell responses. Furthermore, a recent study on single-cell spatial transcriptomics suggested that CD8+ T cells became more exhausted as they moved inwards in the tumour (303). The finding that budding cells are mostly found in close proximity to cytotoxic cells may be explained by this. These small cluster of tumour cells may induce T cell exhaustion resulting in immune suppressive activity at the invasive area.

Although the role of T cells is well reported, there are fewer studies that report the correlation between tumour buds and macrophages. One study suggested that perhaps pro-inflammatory macrophages may have a role in budding formation (304). To identify the possible correlation between budding cells and macrophages, nearest neighbour analysis was performed. The results showed that most bud clusters are close to both CD68+ and CD68+CD163+ macrophages. Tumour-associated macrophages (TAMs) have been shown to have a crucial role in immunosuppression (305). Moreover, studies have shown that CD68+ macrophages could express PD-1 which can interact with PD-L1 leading to a poor prognostic phenotype in cancer patients (306-308). In CRC, the interaction between PD-L1 and PD-1 has been shown to be enriched near budding cells (182). Although the expression of CD68+ expressed PD-1 was not investigated, the close interaction between budding clusters and CD68+ cells could perhaps indicate this regulation and its role in budding cell progression and metastasis. Further studies are required to confirm this hypothesis.

In addition to T cells and macrophages, tumour-associated neutrophils (TANs) are consistently reported as an immunosuppressive phenotype that promotes carcinogenesis and

immune invasion (309). The comparison of the distance from budding clusters to three phenotypes demonstrated that budding cells tend to have the closest distance to CD68+, CD66b+, and CD68+CD163+ respectively. Moreover, when determining the distance from the same budding clusters to CD68+ and CD66b+, the individual clusters were mostly found close to both phenotypes. Similar results were found with CD68+CD163+ and CD66b+. There are many budding clusters that are closer to CD66b+ but not CD68+CD163+. These could suggest a crucial interaction of budding cells with both macrophages and neutrophils. These two immune cells may be a key target for budding cells to alter their surrounding environment. These results were supported by Kersten et al. who reported that a high number of macrophages could stimulate T cell exhaustion, therefore, leading to an increase in tumour progression and metastasis (303). Moreover, an increased number of TAMs was reported to promote regulatory cells which was shown to predict poor survival in ovarian cancer (310).

Overall, these results mainly focus on the differential gene expression in tumours with high budding to increase an understanding of the high budding phenotype in CRC. While STAT1 showed no significance in predicting patient survival, there was a trend towards worse outcomes in patients who exhibited high budding with high STAT1 phenotype. Future studies focusing on STATs signalling in budding formation could reveal a potential biomarker in CRC. In addition, the findings showed that there is a promising interaction between budding cells and their microenvironment especially T lymphocytes and macrophages. Clearly, more work is required to validate these results. The use of a single cell approach, such as Nanostring CosMx should be used to identify the underlying mechanism of budding cells and their interaction with the TME in CRC.

Chapter 7. *In vitro* study investigating the formation of tumour budding in CRC.

7.1. Introduction

In vitro studies are an essential step in the translation of lab-based finding into clinical application (311). Although cells grown as a monolayer are a convenient and affordable method of investigating simple mechanisms in tumour cells, the results obtained often do not translate into the results obtained from *in vivo* animal models (312). Studies have shown that the expression profiles of cells cultured in a monolayer can change over time, therefore, a three dimensional model of cancer cells called spheroids was introduced in an attempt to closer mimic the biology of the original tumour (313-315). Having said that, spheroids consist of clusters of cells which do not replicate the complexity of the specific organ (316, 317). Another 3D model derived from the stem cells or tissue-specific progenitor cells which resembles the tissue organ is the organoid (318). Organoid studies have had a huge impact on the direction of cancer research (319). Although the maintenance of organoid cultures is more complicated, the similarity between organoids and the tumour mass could improve the knowledge of tumour development in cancer patients (320, 321).

In the previous chapters, transcriptomic analysis from GeoMx DSP identified a possible gene related to the budding phenotype in CRC. Several studies have reported possible signalling pathways that could regulate budding formation in CRC (21). However, no studies have reported if these signalling pathways can be targeted, or that budding formation could be stimulated by activation of these pathways *in vitro*.

Tumour necrosis factor-alpha (TNF-α) is a well-known pro-inflammatory cytokine associated with CRC metastasis (322, 323). It can induce cancer cell migration leading to the regulation of downstream targets related to CRC development (324). To our knowledge no study to date has demonstrated a correlation between the regulation of TNF- α and budding formation in CRC. In this thesis a correlation between inflammatory-related STATs signalling and budding phenotype in CRC was observed. The study of the TNF- α pathway may help

determine whether inflammation has an impact on TB in CRC. In addition to TNF-α, the transforming growth factor-beta (TGF-β) pathway is one of the main mechanisms in CRC development (325, 326). The pathway is involved in downstream targets thought to induce disease progression and metastasis (327-329). One major downstream target of TGF-β is epithelial-mesenchymal transition (EMT), reported to be involved in disease metastasis (234). TB has been reported to undergo partial EMT, although studies suggest that other downstream signalling targets of TGF-β could also be important for budding phenotype in CRC (16, 21)

The synergistic role of TNF-α and TGF-β has been used as a model to study tumour progression and metastasis (330). Epithelial organoids (IEOs), treated with TNF-α and TGF-β, underwent a mesenchymal phenotypic change with an induction of cell proliferation (331). Other studies also report the interaction between TNF-α and TGF-β in correlation with tumour-related signalling such as cell proliferation (332, 333), apoptosis (334), invasion (335) and inflammation (336). Interestingly, using laser microdissection, potential EMT biomarkers captured from tissue areas with TB and its surrounding microenvironment were reported in CRC patients. Li and colleagues suggested an integration between TNF-α and TGF-β pathways in the development of invasive CRC tumours (156). An EMT-related genes signature was also reported in another study; however, only bulk gene expression of the tumour-invasive front was captured (337).

In previous chapters, *CCND1* was reportedly expressed within TB suggesting its prognostic role in CRC patients. *CCND1*, which encodes cyclinD1, is associated with cell cycle activity (338). The meta-analysis reported a significant prognostic value of cyclinD1 expression in CRC patients (271). However, no study investigated the role of cyclinD1 within TB in CRC. Thus, this chapter will investigate the dual activity of TNF-α and TGF-β and the effect on TB formation *in vitro*. Additionally, the expression of cyclinD1 in cell line and spheroid models will be determined to explore the potential association with TB phenotype.

7.2. The regulation of TNF-α and TGF-β signalling and the formation of tumour budding in CRC

7.2.1. Monolayer CRC cell lines

To characterise the suitable cell lines for an invasive budding phenotype, CRC cell lines (HT29, HCT116, SW480 and SW620) were cultured. Cell culture media supplemented with TNF-α and TGF-β were used to study the effect of two signalling pathways on TB formation *in vitro*. Additionally, cyclinD1 expression may have an association with TB formation (Chapter5, section 5.7.2), thus, the expression of cyclinD1 was investigated.

7.2.1.1. Protein expression of cyclinD1 in CRC cell lines.

CRC cell lines (HT29, HCT116, SW480 and SW620) were used to represent the different subtypes of CRC. Cell culture media conditions: Normal complete media (positive control), complete media with 0.01%HCL (negative control) and supplemented media (TNF-α (20ng/ml) with TGF-β (10ng/ml)), were set up to determine the effect of two compounds (TNF-α and TGF-β) in an aggressive budding phenotype. Cells were seeded in 2-dimension (2D) and cultured according to the protocol (Chapter2, section 2.8.2). Briefly, cells were seeded and allowed to attached overnight (24 hours), then pre-treated with TNF-α for 24 hours then the combination of the two compounds was added to the culture media for another 24 hours (72 hours in total). The media was changed every 24 hours.

Cell lysates were collected and used to determine the protein expression in each of the CRC lines using western blot analysis. cyclinD1 expression was measured as a possible protein correlated with budding characteristics in CRC.

The protein expression of cyclinD1 was quantified using ImageJ image analysis program to compare the expression between control and supplemented (TNF-α and TGF-β) media conditions (n=3). The results demonstrated no significant difference in expression of cyclinD1 following treatment with TNF-α and TGF-β in any of the cell lines, except for HT29

(Figure 7.1A). An upregulation of cyclinD1 protein expression was observed in HT29 cultured in media supplemented with TNF-α /TGF-β compared to the control cells (p=0.07) (Figure 7.1B).

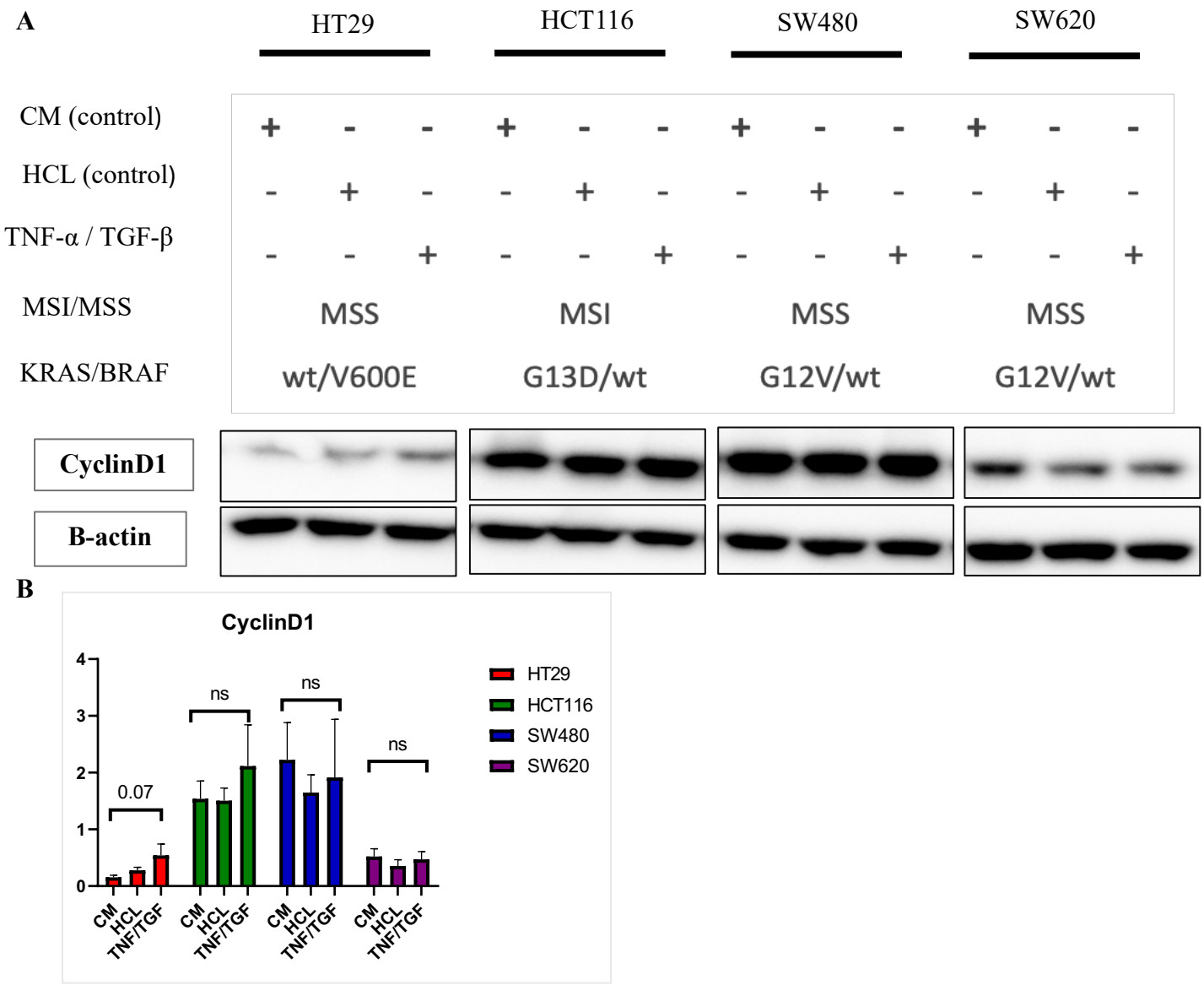

Figure 7.1 *(A) Protein expression of cyclinD1 in each CRC cell line for each condition using western blot analysis. (B) The bar plot shows a quantitative expression of cyclinD1 for each condition of CRC cell lines (n=3).*

To study the formation of TB, a 3D model was required, therefore the CRC cell lines were grown as spheroids. The same culture conditions as in the 2D experiment were used to determine if budding was induced and if expression of cyclinD1 within the budding area could be identified using immunofluorescence staining (IF).

7.2.2. Spheroids CRC

Previous results (section7.2.1) demonstrated an increased expression, though not statistically significant (p=0.07), of cyclinD1 when HT-29 cells were cultured with media supplemented with TNF-α/TGF-β comparing to the control group. To further investigate this in 3D model for TB phenotype, HT-29 cells were grown in 100% Matrigel domes to induce spheroid formation and if TB can be formed when regulated by TNF-α/TGF-β. The spheroids were cultured until the optimal size was reached before doing any experiments (Chapter2, section 2.8.3.1).

After 72 hours of incubation, a morphological change was observed. There was an increase in budding-like structures in spheroids cultured with media supplemented TNF-α/TGF-β (Figure 7.2B) when compared to the normal control media (Figure 7.2A).

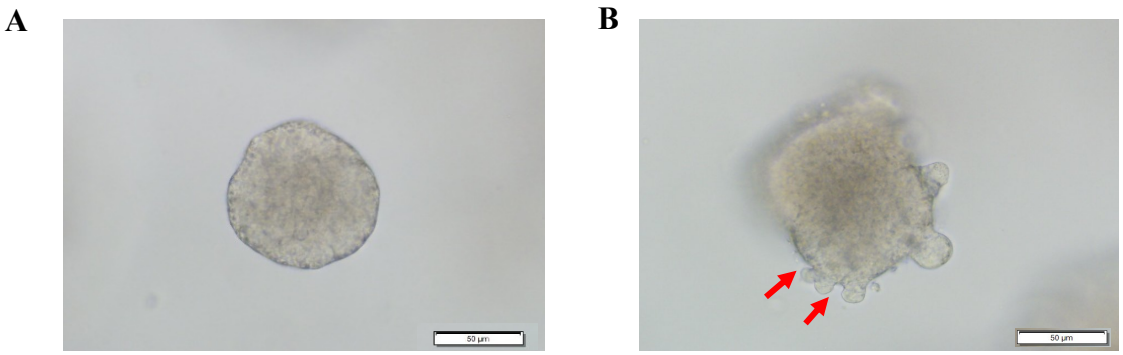

Figure 7.2 *The brightfield images of HT-29 spheroids cultured in (A) normal and (B) supplemented TNF-α / TGF- β media.*

7.2.2.1. Protein expression of cyclinD1 in budding-like structure CRC spheroids.

To investigate cyclinD1 expression within the budding-like structure, spheroids were cultured on cover slips and IF staining (n=3) performed according to the protocol (Chapter2, section 2.8.3.2). The budding-like area was studied to determine the expression of cyclinD1 with and without the supplemented (TNF-α/TGF-β) media (Figure 7.3). Florescence signals

were visualised and captured using the same setting to ensure the signal baseline levels are the same across different sample conditions (Supplementary table 7.1).

Using ImageJ software to quantify the intensity, a significant increase of cyclinD1 expression within the budding region of spheroids cultured in supplemented (TNF-α/TGF-β) media compared to control groups (p=0.014) (n=3) (Figure 7.4) was observed.

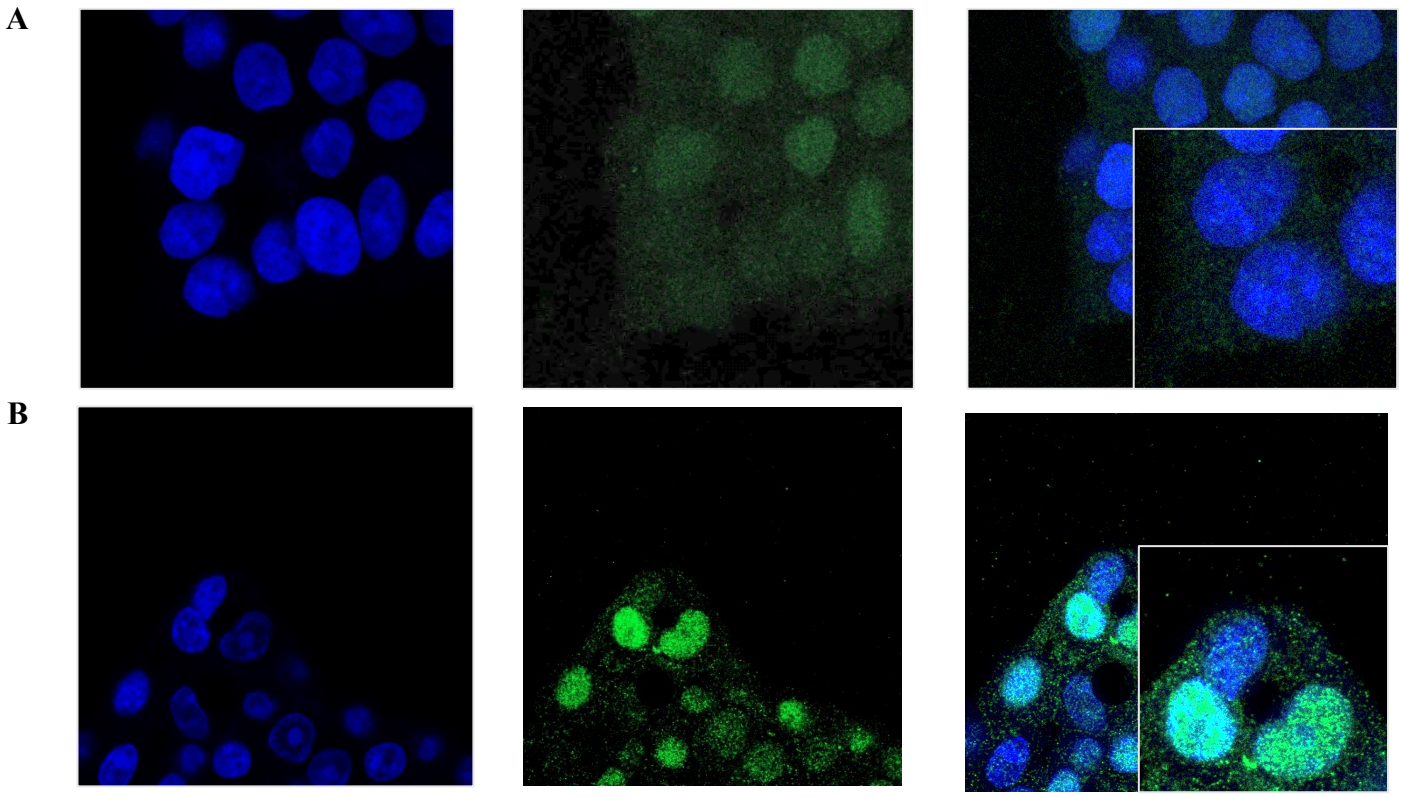

Figure 7.3 *CyclinD1 staining (green color) in the budding region of the HT-29 spheroids (A) cultured in normal and (B) supplemented with TNF-α / TGF-β media (n=3)*

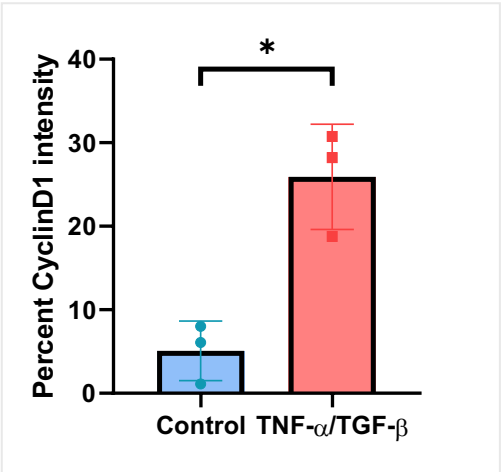

Figure 7.4 *Bar plots showed the percent intensity of cyclinD1 compared between control and supplemented (TNF-α / TGF-β) groups (n=3).*

7.2.3. Mouse CRC organoids

The mouse organoid lines extracted from the developed mouse CRC model was kindly provided by the Sansom group. The model was developed with well-known CRC common mutated genes (AKPT; *villin*Cre^{ER}*Apc*$^{fl/fl}$ *Kras*$^{G12D/+}$ *Trp53*$^{fl/fl}$ *Trgfbr1*$^{fl/fl}$) to study CRC development in murine animals. Therefore, the AKPT line was selected to investigate the formation of TB *in vitro*.

The AKPT lines were cultured in 100% Matrigel domes to promote organoid formation. To investigate the impact of TNF-α and TGF-β on organoids, a WST-1 assay was performed to identify if media supplemented with TNF-α and TGF-β could have an effect on the viability of the AKPT-organoids. The results revealed that AKPT-organoids cultured with TNF-α and TGF-β tend to have a higher percent viability, though there is no significant found, when compared to control groups (n=3) (Figure 7.5).

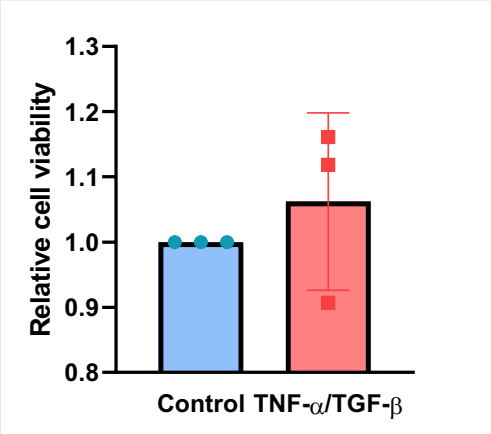

Figure 7.5 *The WST assay of AKPT mouse organoid viability compared between control and supplemented (TNF-α /TGF-β) groups (n=3).*

Live cell imaging was performed using Incucyte® to monitor budding formation in AKPT-organoids comparing those cultured in control and supplemented (TNF-α and TGF-β) conditions (n=3). The organoids were set up in 96-wells plate according to the protocol in chapter2 section 2.8.4. The AKPT-organoids were pre-monitored for 24 hours, then pretreated with TNF-α for 24 hours and treated with both TNF-α and TGF-β for the final 24 hours, thus

72 hours in total. AKPT-organoids cultured with supplemented TNF-α and TGF-β media were observed to produce more budding-like structures after 72 hours of incubation (Figure 7.6).

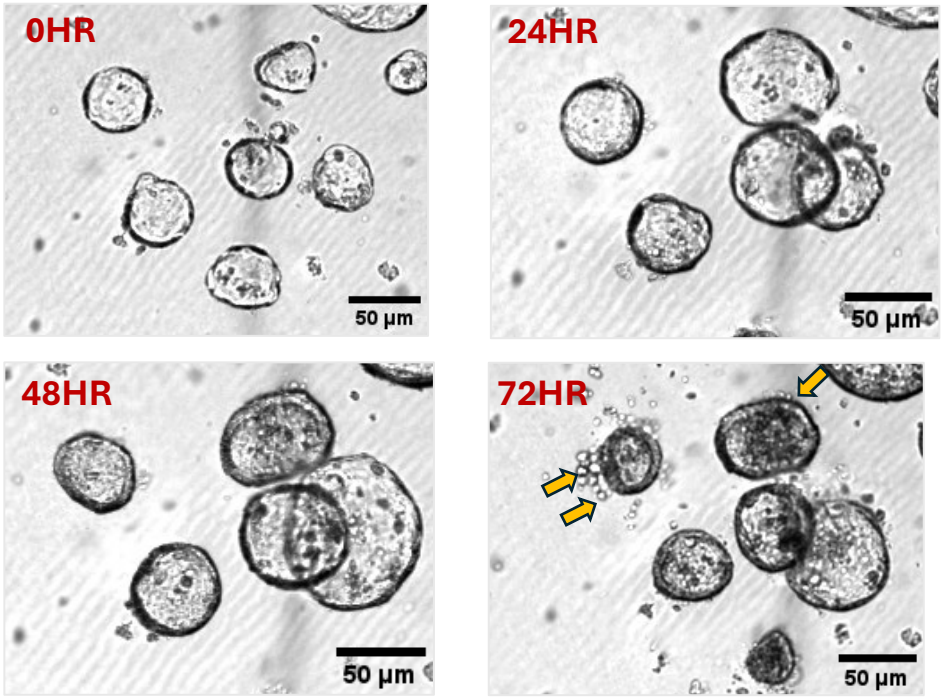

Figure 7.6 *AKPT mouse organoids in different timepoint 0, 24, 48 and 72 hours after cultured in media supplemented with TNF-α /TGF-β.*

To determine if there was a statistical difference in morphology between normal control and supplemented media, the roundness of individual AKPT-organoid was measured using the ImageJ program (Figure 7.7). Although some budding formation is observed in the control organoids it was observed that there is a less roundness signature of the AKPT-organoids supplemented with TNF-α and TGF-β when compared to those with control normal media at 72 hours incubation (Figure 7.8). A measure of less roundness correlates with increased budding and therefore provides evidence that TNF-α and TGF-β treatment is associated with budding formation.

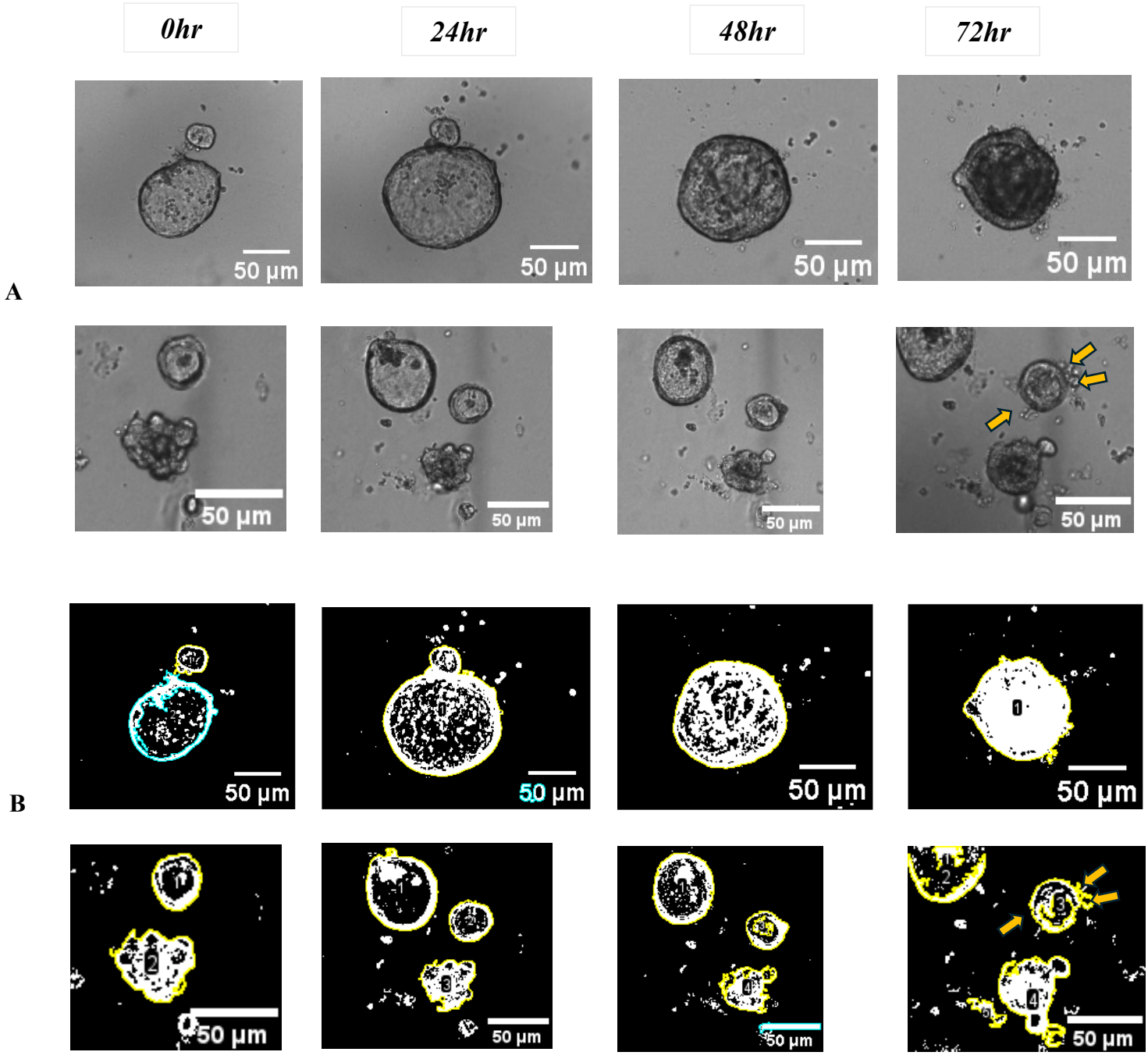

Figure 7.7 *(A) Brightfield and (B) Segmented images showed the morphology of organoids changed in 0-, 24-, 48- and 72-hours incubations. The top row presents an organoid cultured in control media and the 2nd row is an organoid cultured with TNF-α and TGF-β supplemented media. Amber arrow showed the bud-like structure in organoids.*

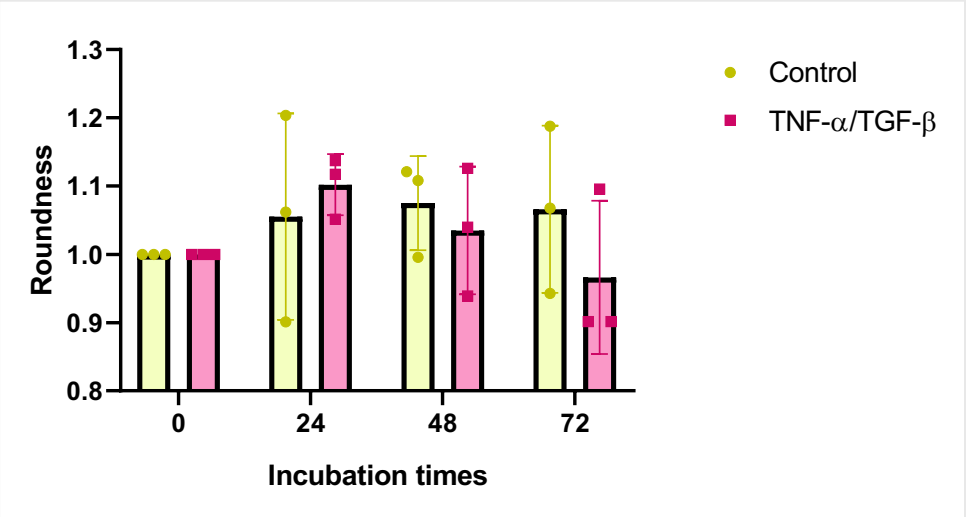

Figure 7.8 *Bar plot showed the quantified roundness of AKPT-organoids, across 72 incubation times, compared between organoids cultured in control (yellow) or supplemented (pink) media (n=3). Absolute roundness is 1.*

7.3. Discussion

In vitro tumour models have had an important impact on cancer research. The translation into clinical practise is reliant on good quality pre-clinical evidence gained from models to support novel cancer therapeutics (339). These models have been developed to provide insightful information for tumour development such as tumour growth and proliferation, metastasis, angiogenesis, and drug delivery (340, 341).

The role of tumour-related signalling has been shown to have an impact on tumour metastasis and progression in CRC (342). Tumour necrosis factor (TNF) signalling has been reported to play an important role in CRC development mainly in the control of inflammation and immune regulation (343). Its function is associated with an increase in immunosuppression in CRC development leading to progression and metastasis (344). Transforming growth factor-β (TGF-β) plays a crucial role in anti-tumorigenesis in normal colonic epithelial cells, however, it has also been shown to promote CRC development through cell proliferation, differentiation, apoptosis, and migration (326). Moreover, mutation of this signalling has been shown to increase the risk of disease development and metastasis in CRC (345).

Studies report a synergistic association between TNF-α and TGF-β to induce proliferation and metastasis (330, 331). Interestingly, one study proposed that potential EMT biomarkers expressed in TB are regulated through the dual activation of TNF-α and TGF-β signalling (156). Although the same results were not observed in bulk transcriptomic data (Chapter4), it is worth investigating if a combination of these compounds could induce the progressive characteristics of TB at the protein and phenotype level in CRC *in vitro* models. In addition, high expression of cyclinD1 in budding cells was observed and is hypothesised as a biomarker for budding in CRC patients (Chapter6 section 5.7.2). Therefore, the expression of cyclinD1 within budding cells *in vitro* was also studied.

Western blot protein analysis was employed to investigate if there was any differential cyclinD1 expression between cells cultured in normal and supplemented (TNF-α and TGF-β) media. In the HT-29 cell line, an increase in cyclinD1 protein expression in cells cultured in supplemented (TNF-α and TGF-β) compared to control normal media was observed. This protein is associated with cell cycle signalling and has previously been reported to be upregulated by either TGF- β or TNF- α (346-349). It may be suggested that there is a direct effect of these two signalling pathways in cell cycle regulation leading to the development of tumour aggressiveness and proliferation. However as budding formation could not be observed in 2D cell culture, this increase in cyclinD1 expression may not be associated with budding formation. Therefore, HT-29 spheroid cultures were used to investigate the role of cyclinD1 in budding formation.

HT-29 is a tumour-derived cell line with a proficient mismatch repair (pMMR) or microsatellite stable (MSS) type. Tumours with MSS status have consistently been reported to be associated with TB phenotype in CRC (154). Spheroids cultured in supplemented (TNF-α and TGF-β) media were observed under brightfield microscopy to have more budding-like structures when compared to those cultured with normal media. It has been reported that perhaps the dual activation of TNF-α and TGF-β signalling could be the key regulating pathway of the budding phenotype in CRC (156). However, further studies are required to support this hypothesis. Additionally, when investigating the budding area within the HT-29 spheroids, a significantly higher expression of cyclinD1 was found in spheroids cultured with supplemented TNF-α and TGF-β media than control groups. This could support the hypothesis that when budding is stimulated in MSS CRC spheroids cyclinD1 is a key regulator within the TB region. Although there are no peer reviewed studies in support of this finding, it may be that the aggressive behavior of spheroids as a result of the upregulation of TNF-α and TGF-β could be used as a model for invasive CRC in the future. One study reported that budding spheroids in

ovarian cancer were associated with the upregulation of vimentin and a lack of E-cadherin, suggesting the up-regulation of epithelial-mesenchymal transition (EMT) (350). Clearly, further work is needed to identify biomarkers for TB.

In addition to CRC spheroids, mouse CRC organoids have been employed to investigate the formation of TB in other 3D models. AKPT lines, mutated APC, KRAS, TP53 and TGF-βR1, were utilised as these are common mutations found in human CRC (351). Due to the time limitation, only live cell imaging was performed to observe the formation of budding cells in AKPT organoids. Budding-like structures were observed growing out from organoids cultured in media supplemented with TNF-α and TGF-β. Higher viability of cells in organoids cultured with supplemented TNF-α and TGF-β was also reported when compared to the control group. These results indicate the possible synergistic effect between TNF-α and TGF-β that may trigger the pro-tumourigenic downstream signalling in mouse organoids. Additionally, image analysis was performed to measure the roundness of the organoids cultured under control and supplemented (TNF-α and TGF-β) conditions. The organoids have a less round shape when cultured in TNF-α and TGF-β compared to control groups (n=3) after 72 hours of incubation although this was not statistically significant. As more budding-like cells are found when cultured with TNF-α and TGF-β compounds, the less round shape indicates more budding disturbing the roundness of organoids, therefore, increasing an induction of invasive capability.

The co-activation of TNF-α and TGF-β signalling has been reported to be involved in TB phenotype in CRC. Using a network construction analysis, genes associated with an invasive CRC phenotype were found to activate both pathways and were also reported to have a prognostic role in CRC (156). Having said that, studies are limited which investigate budding CRC formation *in vitro*. Studies have reported the budding crypt organoid expressing a stem cell-like characteristic. Although the original tissue used was normal intestine this could perhaps lead to another investigation into how the budding phenotype may acquire stem cell

properties (352, 353). Although there is little evidence in support of budding formation *in vitro*, one study has reported 'budding organoids' where cells branch their own body to initiate the progression (354). Interestingly, Serra and colleagues also found that the budding organoids remain proliferative after silencing of the Wnt pathway. A hyperactivation of Wnt signalling has been reported to play an important role in CRC development including initiation of the EMT process (355). The role of Wnt signalling in CRC TB formation may be worth investigation.

There are many gaps to be filled regarding the development of a robust model to study budding formation *in vitro*. Further evidence relating to the formation of TB is required. The use of a 3D model would be the most effective way to investigate the underlying mechanism of budding formation. The results in this chapter demonstrate a potential model to observe TB formation, however additional *in vitro* studies are required to better understand the TB phenotype. This could lead to the development of a model to test the effect of targeted therapeutics on TB in CRC.

Chapter 8. General Discussion

Discussion and future perspective

Colorectal cancer (CRC) is one of the most diagnosed cancers worldwide and within the UK (1). The disease heterogeneity, results in differences in prognostic and treatment responses and makes it very challenging to identify suitable therapeutic choices (356). Fortunately, the development of screening programs has improved patients' survival. However, some patients still have a poor prognosis due to metastatic disease (357).

Tumour budding (TB), one up to four tumour cells found at the invasive front of the tumour, has recently been reported as a promising prognostic marker in CRC (6, 8). Patients with a high budding phenotype experienced the worst clinical outcome and are associated with adverse features such as venous invasion, lymph node involvement, and higher tumour stages. The independent prognostic power of TB has been consistently reported in the literature (138, 358). This has resulted in an international consensus conference (ITBCC) on budding assessment, and it has been strongly suggested that TB status should be included in clinical reports in CRC (8, 175, 359, 360). In Glasgow, tumour budding is now included in routine pathology reporting of CRC.

Prognostic value of TB and the correlation between TB phenotype and clinical factors in CRC patients

To demonstrate the prognostic value of TB in Glasgow CRC cohort, TB was assessed according to the agreed method from ITBCC. In Chapter 3 the prognostic value of TB was reported. The survival analysis showed that patients with high TB had a worse outcome compared to those with low TB. Additionally, TB was found to be an independent prognostic factor as determined by multivariate analysis. This confirmed the prognostic value of TB in CRC as reported by other peer reviewed studies. Moreover, the statistical relationship between TB phenotype and adverse clinical factors in the CRC cohort, using Chi-square statistical analysis, was reported.

There is a possible correlation between key gene mutation and budding phenotype in CRC (356). *KRAS/BRAF* mutations are two of the common mutations found in CRC, tumours with these mutations usually present with an aggressive phenotype that potentially leads to disease metastasis (41, 361). In addition to *KRAS/BRAF* mutations, MMR status is known to classify patients based on their outcomes and response to treatment (362). Meta-analysis studies suggested a significant association between patients with mutated *KRAS*/ proficient MMR (pMMR) status and high TB phenotype (154). In the CRC cohort, no significant correlation was found between TB and mutational status (*KRAS/ BRAF* and MMR status). However, a higher number of TB was found in patients with mutated *KRAS* and in wild-type *BRAF* tumours. Interestingly, when patients were stratified by TB status, MMR deficient (dMMR) patients experienced poor survival compared to other groups. These findings contradict the previous meta-analysis (154), which indicated that tumours with pMMR were associated with high TB phenotype. However, different methods of assessing TB were used in the meta-analysis studies and this could affect the power of statistical significance. The finding reported in this thesis demonstrated no obvious correlation between TB and mutational profile, which suggests that the budding phenotype may not be driven by genetic events. However, the association between TB and CRC mutation warrants further studies to confirm this finding.

In addition to the mutational profile, TB status combined with tumour-infiltrating lymphocytes (TILs) was recently reported to stratify the outcomes of patients with stage II and III CRC (363). It has been suggested that, in patients with stage III tumours, responses to chemotherapy are associated with low TB/high TILs. Thus, if TB status is associated with an immune response, it could be employed to help customise CRC treatment. In the Glasgow CRC cohort, the modified-Glasgow Prognostic Score (mGPS) was used to measure systemic inflammation and Glasgow Microenvironment Score (GMS) for local inflammation. As detailed in Chapter 3, results showed no correlation between TB and mGPS, however, in

patients with high TB, only 43% of patients with mGPS2 survived after 10 years when compared to those with mGPS0 (67%). Interestingly, there is a significant inverse correlation between TB phenotype and inflammatory infiltration; Klintrup-Makinen score (KM). There is a significant association between tumours with high TB and GMS2 (low KM/high tumour stroma percentage). A higher number of budding cells was significantly observed in patients with GMS2 (p=0.034). Survival analysis also showed that, in patients with high TB, patients with GMS2 had the worst outcomes with only 46% compared to 100% survival in GMS0 patients after 10 years. Together, these results indicate the correlation between high TB and a decreased inflammatory response in CRC (mGPS2, low KM, and GMS2). Inadequate immune response commonly leads to a poorer outcome in CRC. This suggests that perhaps, when a tumour exhibits a high TB phenotype, it may alter the environment suppressing immune activation, therefore, allowing small TB cells to spread and metastasise to distant sites.

The association between TB and infiltrated immune cells was further studied. Multiplex staining was employed in a tissue microarray (TMA) previously constructed from the main tumour core. The markers of T lymphocytes; CD3 CD8 FOXP3, and Myeloid cells; CD68 CD163 CD66b were used to investigate the immune profile associated with TB status in CRC. As reported in Chapter 3, in patients with low TB, those who have a high density of CD3+ had a better outcome than those with a low density of CD3+ (p=0.017). Interestingly, a high percentage of cytotoxic CD3+CD8+ T cells were significantly found in tumours with low TB when compared to the high TB group (p=0.0062). Patients with high cytotoxic T cell infiltrating tumours with low TB had significantly better outcomes (p=0.013) which suggest a possible 'anti-tumour' effect. In addition to cytotoxic T cells, regulatory T cells have been reported to have a pro-tumourigenic role in CRC development. In low TB groups, those who exhibit a high number of CD3+FOXP3+ T regulatory cell infiltration have a significantly worst outcome (p=0.017). This is in agreement with other studies reporting an inverse correlation between TB

phenotype and the cytotoxic immune profile (20, 364). It also confirmed a possible correlation between TB and pro-tumourigenic T regulatory cells leading to a poor outcome in CRC patients. The prognostic role of these T cells is well-known in CRC, although few studies have reported their correlation with TB (18, 180, 364).

Additionally, the results in Chapter 3 demonstrated no significant differences between TB profile and infiltrating macrophages. However, when tumours exhibited high TB, there was significantly decreased survival in those with a high density of pan-macrophages CD68+ cells ($p<0.001$). Moreover, when determining the prognostic value of CD163+ cells in low TB patients, there was a significant increase in survival ($p=0.029$) in those with a high number of infiltrating CD163+ cells. These results suggest that pan-macrophages favour TB cells leading to a poorer outcome in CRC. This concurred with a study from Nearchou et al., that reported a weak positive correlation between TB and CD68+ cells in CRC using multiplex immunostaining (179). An *in vitro* study from Trumpi et al. also suggested that budding formation can be regulated by the presence of macrophages which represent the invasive characteristic of TB in CRC (304).

The relationship between TB and infiltrating neutrophils was also reported in Chapter 3. There was no significant association between TB and neutrophil status. However, in patients with a high TB phenotype, those with high infiltrating CD66b+ cells had a better outcome when compared to those with low CD66b+ infiltrating cells ($p=0.054$). Recently, a study from Markowski et al. reported a possible correlation between TB and the density of neutrophil infiltration (365). The finding reported in this thesis demonstrate a similar result, although further studies are required to confirm this finding.

To conclude, the prognostic value of TB in Glasgow cohort has been confirmed. However, there is an unmet need to investigate the underlying mechanism of TB that results in its prognostic role in CRC. Thus, different approaches were undertaken to identify tumour-

related pathways in relation to TB and the surrounding immune cells to further elucidate this phenotype.

Transcriptomic data

To understand the molecular mechanisms underlying the TB phenotype in CRC, Consensus Molecular Subtypes (CMS) were determined based on gene expression patterns obtained from tumour tissue in our CRC cohort (JH). As detailed in Chapter 4, a high number of TB was frequently found in the mesenchymal subtype (CMS4). Additionally, in high TB tumours, those with CMS4 showed poorer survival than other groups with only 44% passing 10 years of survival ($p=0.05$). CMS4 was shown to have strong activation of the common CRC developing signalling (TGF-β) as well as a reduction in an immune response. TB may correlate with decreased inflammation suggesting the possibility of TB-suppressed immune activation in CRC.

To further investigate the underlying mechanism of TB in Glasgow CRC cohort, bulk RNA transcriptomic analysis from the whole CRC tumour tissue ($n=787$) was performed. The differential gene expression profile between tumours with low and high budding phenotypes was determined. As reported in Chapter 4, there is no obvious differences in gene expression between the two groups. As TB is single tumour cells observed in the invasive tumour area, the use of whole tissue sequencing may not reflect the true biology of TB in CRC. Studies reported that specific tumour-related signalling could be the key regulator of TB formation (21). Using laser capture dissection within the TB area, studies have shown that budding cells express EMT signature genes indicating its aggressive phenotype in CRC (14, 156). Recently, transcriptomic data revealed that there is a difference in gene expression between true TB and the gland ruptures of small cluster of cells called pseudobudding (PsB) (158). Therefore, studies were undertaken using the GeoMx spatial profiler (DSP) to identify the region-specific gene expression related to TB phenotype in CRC.

GeoMx Digital Spatial Profiler (DSP)

In Chapters 5 and 6, the results from GeoMx DSP were reported. This technology can be used to identify gene expression in a specific area. The differential expression of genes related to TB in different tumour locations (tumour core, invasive and stromal area) was selected with an RNA panel of 96 immune-oncology genes utilised.

As shown in Chapter 5, when comparing differential genes expressed in tumour core of low (n=6) and high (n=6) TB, *CD44* was highly expressed in the tumour core area of high TB tumours. *CD44* is a gene related to stem cell markers, suggesting that perhaps TB could gain new functions by acquiring stemness properties to be able to thrive in a difficult environment. However, in an extended cohort (n=787) and another independent cohort (n=290), there was no significant association between high TB tumours and CD44 protein expression.

When comparing gene expression in the invasive tumour between low (n=6) and high (n=6) TB, the *CCND1* gene was found to be highly upregulated in the invasive tumour with high TB. *CCND1* encodes cyclinD1 which is a protein involved in cell cycle signalling (338). The prognostic value of cyclinD1 in CRC patients has been reported (271). However, no study has shown its correlation with TB in CRC. The validation of cyclinD1 expressed within TB was determined by its protein expression in the TMA previously constructed from the invasive budding area. Results outlined in Chapter 5 showed that patients with high expression of cyclinD1 within TB cells have poorer survival compared to those with TB-expressed low cyclinD1 (n=90). This finding is novel and also confirms the observation from 12 cases used in the GeoMx DSP studies.

GeoMx analysis also revealed that high expression of *CXCL9* and *CXCL10* was observed within the stromal invasive area of tumours with low TB compared to high TB tumours. Therefore, validation was carried out in the extended cohort (n=787). In Chapter 5,

the validation results showed that patients with high expression levels of these two chemokines had a better outcome. Although there is no significant correlation between TB and CXCL status, the finding is similar to other studies which report these two chemokines as favourable markers in CRC patients (366, 367). The high expression of CXCL9 and CXCL10 in an invasive area of tumours with low TB, suggests, again, that perhaps without the high density of TB cells, anti-inflammatory signalling could function leading to improve survival in CRC patients.

When comparing the stromal distant area between tumours with low and high TB, *STAT1* and *STAT2* were shown to have higher expression in tumours with low TB, whereas high expression of *IL6* and *CD68* was found in tumours with high TB. Tumour-relating signalling involved in an inflammatory response is STAT signalling (296). However, STAT1 is generally reported to be a tumour suppressor which is considered a favourable prognostic marker in CRC (282). Validation of protein expression using the TMA of the tumour core demonstrated that STAT1 was a good prognostic marker in the CRC cohort (p=0.016), confirming the results obtained from GeoMx DSP. The function of STAT proteins remains questionable in relation to its pro/anti-tumour development (368). Induction of STAT3/IL6 signalling was shown to relate to poor outcomes in CRC (369, 370). To validate the GeoMx DSP results, the interleukin-6 receptor (IL6R) was stained in a previously constructed TMA made from tumour core (n=787) (UH). Patients with high expression of IL6R in tumour cells had significantly poorer survival when compared to those with low IL6R expression (p=0.031). Interestingly, there is a significant correlation between TB and IL6R (p=0.02), a high number of budding cells is significantly associated with an increase of the protein expression (p=0.03). An increase in IL6 has been shown to be associated with poorer survival in CRC patients (371). Studies reported an important role between macrophages and IL6 as IL6 is secreted by macrophages to potentially induce tumour progression and metastasis. (372). However, regulation of IL6 signalling is required to activate the function of macrophages to induce

tumour destruction (373). The GeoMx DSP result revealed that high numbers of CD68 and IL6 were found together in tumours with high TB. The poorer outcomes of those patients with highly infiltrated macrophages in tumours with high TB were previously shown in Chapter 3. This suggested a possible relationship between IL6 and macrophages, which may be worth investigating in high TB in CRC.

To conclude, GeoMx DSP and the validation of target genes were shown to have a strongly correlative relationship with TB phenotype. Importantly, the expression of cyclinD1 found within the budding cells and whether cell cycle signalling could stimulate the production of TB leading to its prognostic value in CRC is worthy of further investigation.

Multiplex analysis

In Chapter 6, GeoMx DSP results showed that there is a decrease in anti-tumour immune activity in distant stromal compared to invasive stromal areas of tumours with high TB. This suggested a possible immunosuppressive role for TB which has been a consistent theme from the previous chapters. As previously described in Chapter 3, the immune profile showed no correlation with TB phenotype in the CRC cohort. However, studies reported the immunosuppressive activity at the invasive budding area, and that a high density of regulatory cells was found (182). To investigate the relationship between TB cells and their surrounding microenvironment, multiplex staining of T and myeloid cell markers was performed in whole CRC tissue sections. Eighteen CRC cases, including the twelve cases used in GeoMx DSP, were selected, invasive and distant stromal areas were investigated to identify differences in the immune profile. After image analysis, a decreased number of CD3+CD8+ cytotoxic cells were observed, whereas an increase in CD3+FOXP3+ regulatory cells was found in the invasive area surrounded by TB compared to the distant stromal area in high TB tumours. This finding indicates immunosuppressive activity when tumours exhibit high TB at the invasive tumour area, and that TB could alter their tumour microenvironment (TME) to stimulate

progression and metastasis in CRC. There are no differences in myeloid (macrophage and neutrophil) populations between invasive and distant stromal areas.

To unravel the spatial relationship between single TB cells and the surrounding TME, further advanced analysis; clustering, and nearest neighbour analysis, were conducted in the invasive tumour area. Albeit not statistically significant, CD3+FOXP3+ regulatory cells were observed to be closer in distance to budding cells when compared to the CD3+CD8+ cytotoxic cells. This suggested that TB recruit regulatory cells to stimulate pro-tumorigenic activity. Interestingly, there was a significant difference in the distances between macrophages and neutrophil populations from budding cells. CD68+ pan-macrophages, among the other two cell populations (CD66b+ and CD68+CD163+ respectively), were reported to have the closest distance to TB. It has been reported that macrophages might secrete the chemokines that induce the expression of PD-L1 which stimulates tumour development in CRC (374). The similar finding from Lin et al. also reported that, within the budding area, there is an increased immune cell expression of PD-L1 leading to immune invasion of budding cells (182). In the present study, a close distance between TB and macrophages was observed, which could support the above studies. However, there is a need to validate this data, especially the investigation in relation to PD-L1 expression as well as other immune cells in the invasive tumour area.

***In vitro* studies**

A study from Li et al. suggested a possible association between TB formation and integrated TNF-α and TGF-β pathways (156). As report in Chapter 4, there was no obvious signalling found associated with TB phenotype. Following the work from Li and colleagues, stimulating TNF-α and TGF-β signalling to observe TB formation *in vitro* was employed. As cyclinD1 was shown to have a poor prognostic outcome when expressed within the TB as reported in Chapter 5, investigation of cyclinD1 expression in TB *in vitro* was conducted.

In Chapter 7, the role of TNF-α and TGF-β signalling in promoting TB was characterised using different *in vitro* models. When HT-29 cells were grown as spheroids, there was an increase in TB formation when the medium was supplemented with TNF-α and TGF-β. Interestingly, there was also an increase in cyclinD1 expression within the budding-like structure in the spheroids cultured in media supplemented with TNF-α and TGF-β. The results suggested a possible effect of these two pathways towards a budding phenotype in CRC which could confirm previous report (156).

In addition, stimulation of TB by TNF-α and TGF-β was also studied in mouse organoid *villinCre*^{ER}*Apc*$^{fl/fl}$ *Kras*$^{G12D/+}$ *Trp53*$^{fl/fl}$ *Trgfbr1*$^{fl/fl}$ (AKPT) models. An increase in budding formation when organoids were cultured with TNF-α/TGF-β was observed. The organoid's roundness was measured to quantify any increase in budding-like structures, leading to less roundness of the organoids, compared to the control group. Results showed a decrease in the roundness when organoids were cultured with supplemented media compared to control groups suggesting the possible induction of TB when cells have been stimulated by both TNF-α and TGF-β. These results suggested a possible mechanism to regulate TB in CRC, however, more work is required to confirm these results.

Future Perspective

Future work from this thesis should exploit single-cell technology to capture the true biology of budding cells in CRC. Identifying potential TB biomarkers by investigating budding formation *in vitro* would increase the understanding of TB and its underlying mechanisms which could then have an impact on identifying alternative treatments in CRC.

CosMx™ spatial molecular imager

In this thesis, bulk RNA GeoMx revealed the possible underlying mechanism of TB and how this phenotype may be associated with immune suppression at the invasive tumour area. However, bulk RNA cannot differentiate between the bulk tumour and a

small cluster of TB, therefore provides only a limited insight into the TB mechanism. Recent advances in single-cells omic technology have allowed characterisation of gene expression from intact tissue sections, with single-cell resolution. Therefore, the investigation of spatial gene expression within the budding cells and its interaction with the surrounding TME should be studied. This will avoid the limitation of bulk RNA transcriptomics leading to the generation of deep single cell spatial gene profiling.

Protein staining validation

Any results obtained at the single-cell RNA level should be validated at the protein level on the TMA previously made from an invasive budding area (n=190) to investigate the protein expression within the TB cells on the patient CRC tissue. The prognostic value of those proteins should also be determined.

Explore TB formation *in vitro* studies.

In this thesis, *in vitro* studies were conducted, however, further validation is required to understand TB formation. Spheroid cultures successfully mimic the physical and biochemical features of CRC disease making this an excellent model for preclinical research. (375). Additionally, gene editing has been established as a useful tool for tissue engineering to disrupt cellular mechanisms and enhance the knowledge of tumour development (376). Therefore, cancer genes can be manipulated to investigate the underlying tumour mechanism (377). To evaluate the key genes of interest involved in TB formation, genome editing could also be facilitated to stimulate budding formation within the 3D spheroid model setting. Protein expression within the buds should be studied to determine budding-specific biomarkers. In addition to this, mouse organoid models could also be employed to expand the pipeline for future *in vivo* studies.

Identify TB characteristics.

TB is defined as one or up to four tumour cells at the invasive edge of the tumour tissue. However, a study from Haddad et al. reported the presence of pseudobudding (PsB), cell clusters surrounded with fragmented glands, found within the invasive tumour front. This group of cells cannot be distinguished from true TB by a standard H&E or PanCK staining. They suggested that true buds may not have a high proliferation rate while PsB showed higher proliferative (158). As TB is now suggested to be included in clinical reports, with the single cell technology, identifying the differences between the true TB and other budding-like structure could help classify the risk of patients and perhaps improve the treatment choices in CRC.

Conclusion

This thesis reported the promising role of TB and its independent prognostic value in CRC patients which confirmed reports from other studies. Using bulk GeoMx RNA, tumourigenic genes were identified to be associated with TB phenotype in different tumour areas (tumour core, invasive, distant stromal area) (n=12; 6 high TB and 6 low TB). The protein validation of these genes was then carried out in an extended full CRC cohort (n=787). Of these, cyclinD1 expressed within TB has shown to have a promising prognostic value suggesting a regulation of cell-cycle signalling in budding formation in CRC. In addition, tumour microenvironment surrounding TB has shown a decrease in immune activities indicating the suppressive role of TB and their ability to evade inflammation in CRC. This could support the association between TB and metastasis factors such as venous invasion and lymph node involvement as shown in the present study and consistently reported in other peer reviewed studies. Multiplex staining was then conducted to confirm the above hypothesis and to identify the spatial relationship between TB and the surrounding immune cells. This thesis reported that TB tend to have a closer proximity to macrophages as well as regulatory T cells

suggesting pro-tumourigenic activity therefore leading metastasis in CRC. However, the investigation into the underlying mechanism of TB is still required as the use of bulk RNA does not represent the true biology of a small cluster of budding cells. The preliminary results from this thesis showed that TB phenotype can perhaps be stimulated by the synergistic activation of TNF-α/TGF-β. Nevertheless, future studies are required to collect more data related to TB formation in CRC. This could lead to the use of an *in vitro* study models to target the genes and reverse the phenotype for future therapeutic approaches.

Appendix

Supplementary Figures

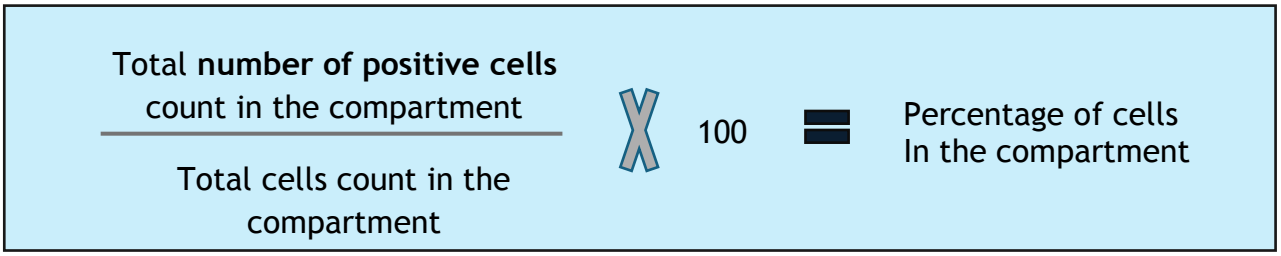

Supplementary Figure 2.1 *The calculation for number of positive cells in multiplex staining.*

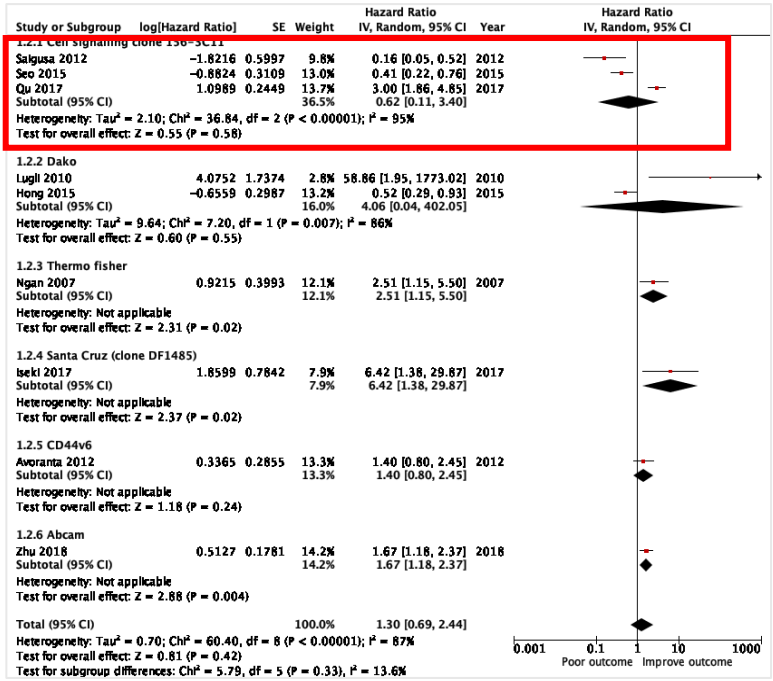

Supplementary Figure 5.1 *Meta-analysis of the used of CD44 antibodies in CRC patients.*

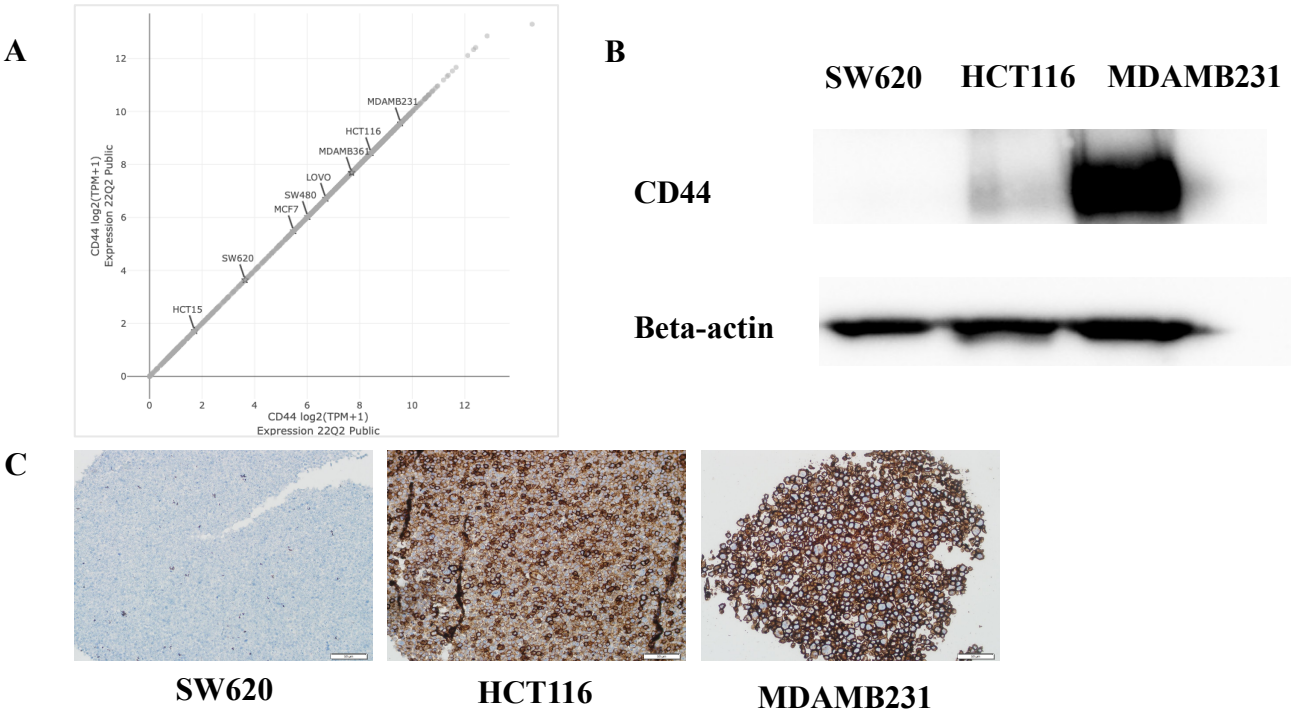

Supplementary Figure 5.2 *(A) CD44 expression in tumour cells from online database DepMap (B) Western blot analysis of the expression of CD44 and (C) CD44 expression, performed by IHC, of the cell pellet of SW620, HCT116 and MDAMB231. Three independent times were used for biological replicates.*

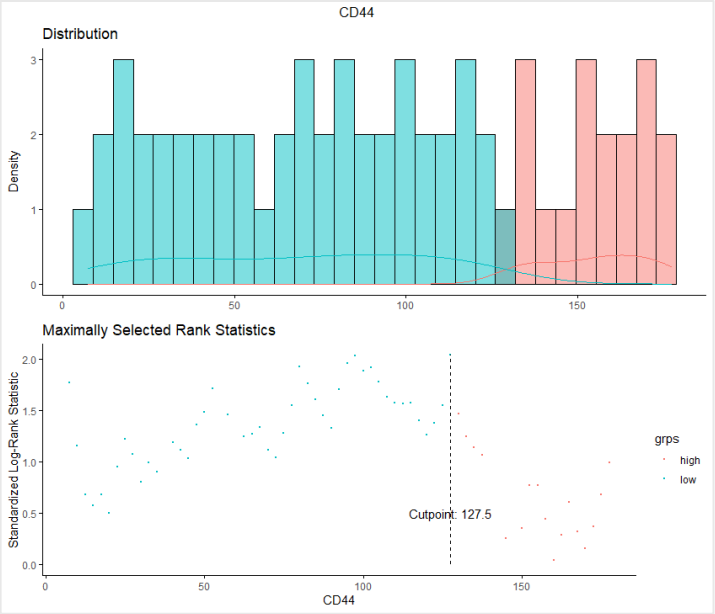

Supplementary Figure 5.3 *Cut off point based on cancer-specific survival of CRC patients with CD44 protein expression.*

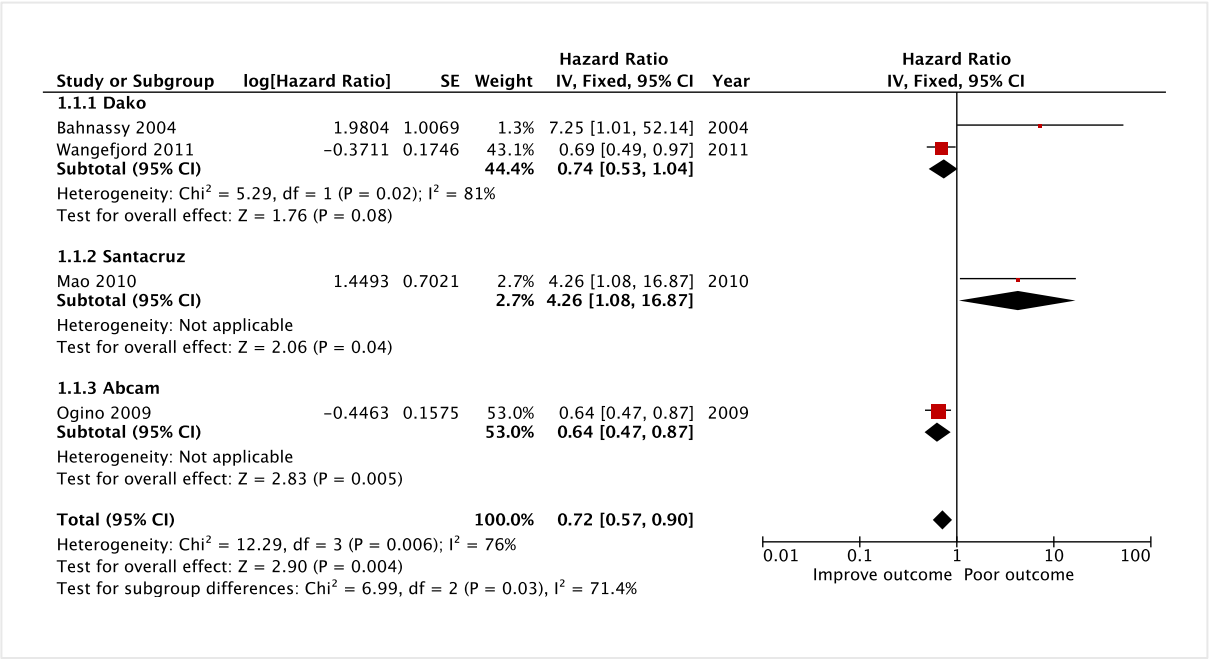

Supplementary Figure 5.4 *Meta-analysis of cyclinD1 antibodies in CRC patients*

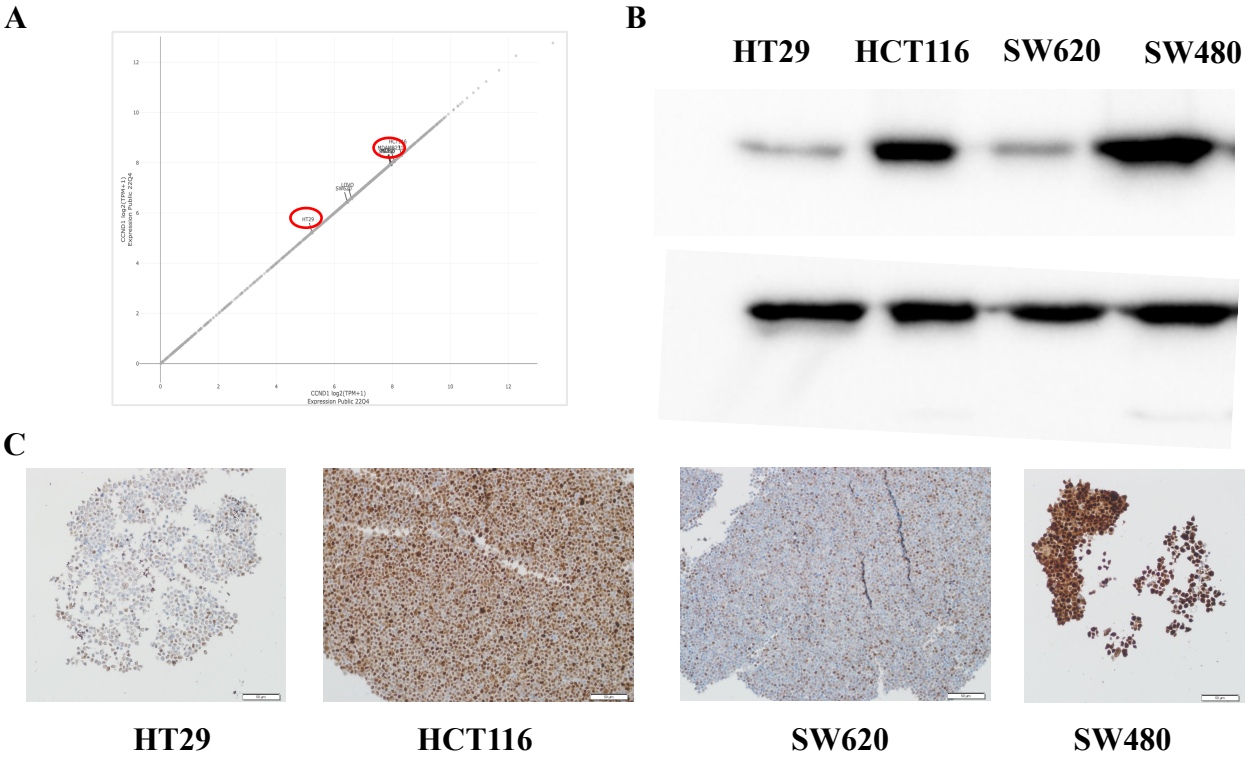

Supplementary Figure 5.5 *(A) CyclinD1 expression in tumour cells from online database Depmap (B) Western blot anlysis of the expression of cyclinD1 and (C) CyclinD1 expression, performed by IHC, of the cell pellet of HT29, HCT116, SW620 and SW480. Three executive times were used for biological replicates.*

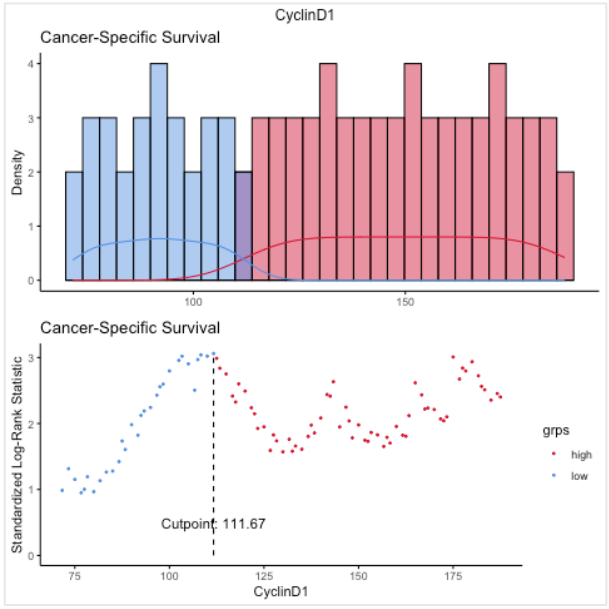

Supplementary Figure 5.6 *Cut off point based on cancer-specific survival of CRC patients with cyclinD1 expression.*

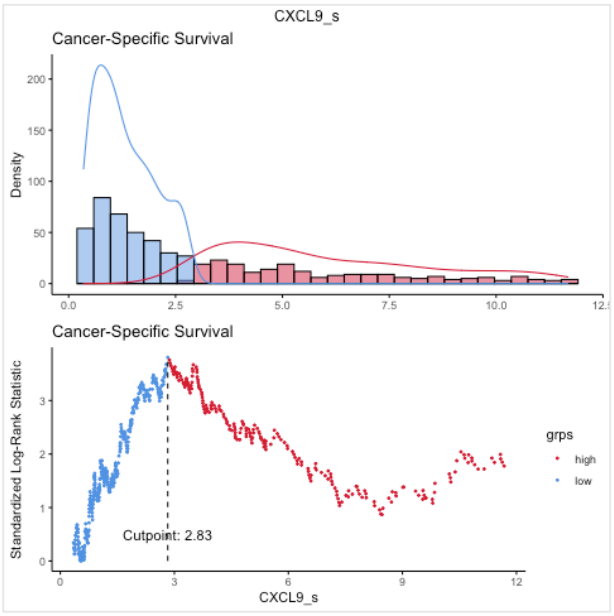

Supplementary Figure 5.7 *Cut off point based on cancer-specific survival of CRC patients with CXCL9 expression.*

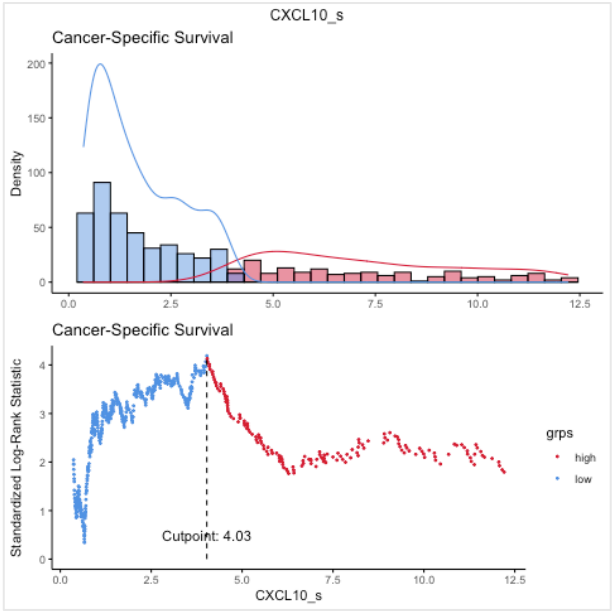

Supplementary Figure 5.8 *Cut off point based on cancer-specific survival of CRC patients with CXCL10 expression.*

Determine the sample size to estimate the proportion of patients used to determine the expression of cyclinD1 within TB with 95% confidence, and a margin of error of 5%. Assume a population proportion of 0.5, and unlimited population size.

$$n = \frac{z^2 \times \hat{p}(1-\hat{p})}{\varepsilon^2}$$

$$n = \frac{1.96^2 \times 0.5(1-0.5)}{0.05^2} = \boldsymbol{384.16 \sim 385}$$

where

z is the z score
ε is the margin of error
N is the population size
p̂ is the population proportion

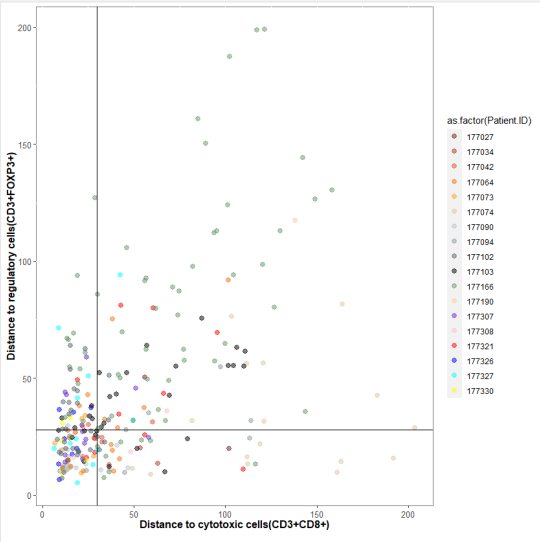

Supplementary Figure 6.1 *(A)Scatter plot shows the distribution of the distance from bud cluster to cytotoxic (x-axis) and regulatory (y-axis) cells.*

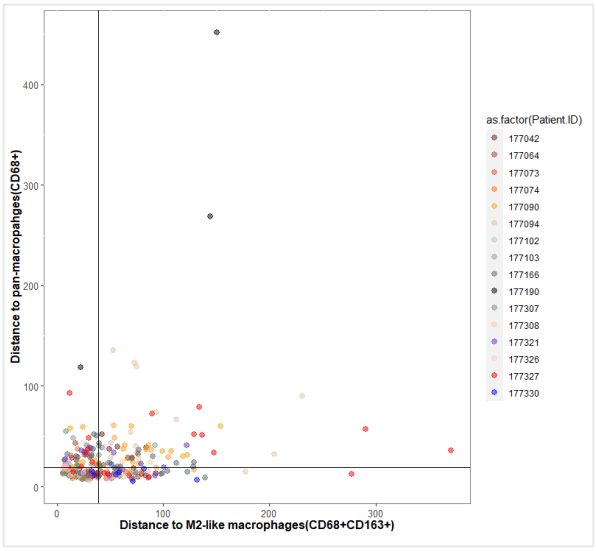

Supplementary Figure 6.2 *(A)Scatter plot shows the distribution of the distance from bud cluster to M2-like (x-axis) and pan (y-axis) macrophages.*

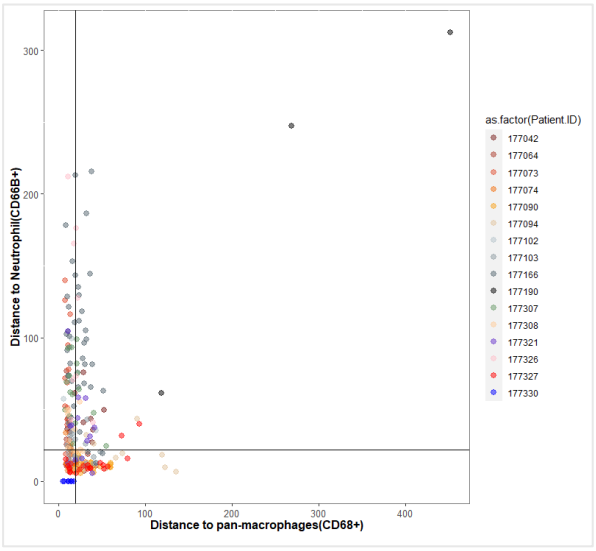

Supplementary Figure 6.3 *(A)Scatter plot shows the distribution of the distance from bud cluster to pan-macrophages (x-axis) and neutrophil (y-axis)*

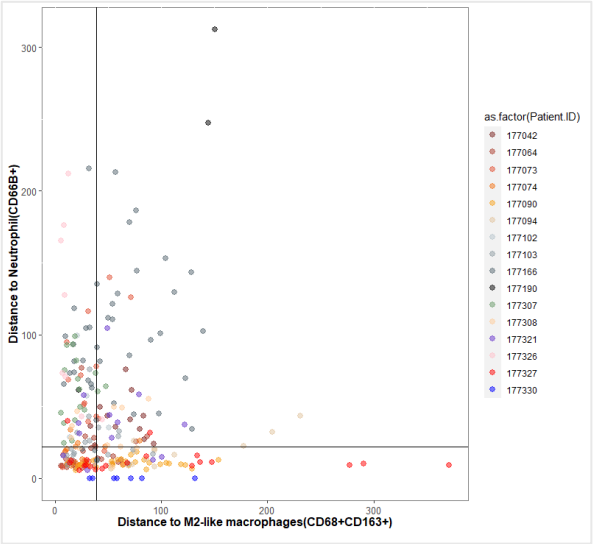

Supplementary Figure 6.4 *(A)Scatter plot shows the distribution of the distance from bud cluster to M2-like macrophages (x-axis) and neutrophil (y-axis)*

Supplementary Tables

Supplementary Table 2.1

Lymphocyte panel

	Exposure time	
	CRC1*	CRC2*
FOXP3	40	16
CD3	128	96
CD8	64	40
KI67	24	24
PanCK	64	128

**Control CRC tissue*

Myeloid panel

	Exposure time
CD68	256
CD163	112
CD66b	190

Supplementary Table 7.1

	Channel1 (488nm)	Channel2 (DAPI)
Pinhole	49um	49um
Excitation Wavelength	493	353
Emission Wavelength	517	465

References

1. Rawla P, Sunkara T, Barsouk A. Epidemiology of colorectal cancer: incidence, mortality, survival, and risk factors. Prz Gastroenterol. 2019;14(2):89-103.
2. Navarro M, Nicolas A, Ferrandez A, Lanas A. Colorectal cancer population screening programs worldwide in 2016: An update. World J Gastroenterol. 2017;23(20):3632-42.
3. Koo S, Neilson LJ, Von Wagner C, Rees CJ. The NHS Bowel Cancer Screening Program: current perspectives on strategies for improvement. Risk Manag Healthc Policy. 2017;10:177-87.
4. Cohen R, Platell CF. Metachronous colorectal cancer metastasis: Who, what, when and what to do about it. J Surg Oncol. 2024;129(1):71-7.
5. Chen W, Frankel WL. A practical guide to biomarkers for the evaluation of colorectal cancer. Mod Pathol. 2019;32(Suppl 1):1-15.
6. Lugli A, Zlobec I, Berger MD, Kirsch R, Nagtegaal ID. Tumour budding in solid cancers. Nat Rev Clin Oncol. 2021;18(2):101-15.
7. Mitrovic B, Handley K, Assarzadegan N, Chang HL, Dawson HAE, Grin A, et al. Prognostic and Predictive Value of Tumor Budding in Colorectal Cancer. Clin Colorectal Cancer. 2021;20(3):256-64.
8. Lugli A, Kirsch R, Ajioka Y, Bosman F, Cathomas G, Dawson H, et al. Recommendations for reporting tumor budding in colorectal cancer based on the International Tumor Budding Consensus Conference (ITBCC) 2016. Mod Pathol. 2017;30(9):1299-311.
9. Lawlor RT, Veronese N, Nottegar A, Malleo G, Smith L, Demurtas J, et al. Prognostic Role of High-Grade Tumor Budding in Pancreatic Ductal Adenocarcinoma: A Systematic Review and Meta-Analysis with a Focus on Epithelial to Mesenchymal Transition. Cancers (Basel). 2019;11(1).
10. Lloyd AJ, Ryan EJ, Boland MR, Elwahab SA, Malone C, Sweeney KJ, et al. The histopathological and molecular features of breast carcinoma with tumour budding-a systematic review and meta-analysis. Breast Cancer Res Treat. 2020;183(3):503-14.
11. Huang T, Bao H, Meng YH, Zhu JL, Chu XD, Chu XL, et al. Tumour budding is a novel marker in breast cancer: the clinical application and future prospects. Ann Med. 2022;54(1):1303-12.
12. Okuyama K, Suzuki K, Yanamoto S. Relationship between Tumor Budding and Partial Epithelial-Mesenchymal Transition in Head and Neck Cancer. Cancers (Basel). 2023;15(4).
13. Kadota K, Yeh YC, Villena-Vargas J, Cherkassky L, Drill EN, Sima CS, et al. Tumor Budding Correlates With the Protumor Immune Microenvironment and Is an Independent Prognostic Factor for Recurrence of Stage I Lung Adenocarcinoma. Chest. 2015;148(3):711-21.
14. De Smedt L, Palmans S, Andel D, Govaere O, Boeckx B, Smeets D, et al. Expression profiling of budding cells in colorectal cancer reveals an EMT-like phenotype and molecular subtype switching. Br J Cancer. 2017;116(1):58-65.
15. Kevans D, Wang LM, Sheahan K, Hyland J, O'Donoghue D, Mulcahy H, et al. Epithelial-mesenchymal transition (EMT) protein expression in a cohort of stage II colorectal cancer patients with characterized tumor budding and mismatch repair protein status. Int J Surg Pathol. 2011;19(6):751-60.

16. Grigore AD, Jolly MK, Jia D, Farach-Carson MC, Levine H. Tumor Budding: The Name is EMT. Partial EMT. J Clin Med. 2016;5(5).
17. Yamada N, Sugai T, Eizuka M, Tsuchida K, Sugimoto R, Mue Y, et al. Tumor budding at the invasive front of colorectal cancer may not be associated with the epithelial-mesenchymal transition. Hum Pathol. 2017;60:151-9.
18. Fujiyoshi K, Vayrynen JP, Borowsky J, Papke DJ, Jr., Arima K, Haruki K, et al. Tumour budding, poorly differentiated clusters, and T-cell response in colorectal cancer. EBioMedicine. 2020;57:102860.
19. van Wyk HC, Park JH, Edwards J, Horgan PG, McMillan DC, Going JJ. The relationship between tumour budding, the tumour microenvironment and survival in patients with primary operable colorectal cancer. Br J Cancer. 2016;115(2):156-63.
20. Lugli A, Karamitopoulou E, Panayiotides I, Karakitsos P, Rallis G, Peros G, et al. CD8+ lymphocytes/ tumour-budding index: an independent prognostic factor representing a 'pro-/anti-tumour' approach to tumour host interaction in colorectal cancer. Br J Cancer. 2009;101(8):1382-92.
21. Hatthakarnkul P, Quinn JA, Ammar A, Lynch G, Van Wyk H, McMillan DC, et al. Molecular mechanisms of tumour budding and its association with microenvironment in colorectal cancer. Clin Sci (Lond). 2022;136(8):521-35.
22. Kim SE, Paik HY, Yoon H, Lee JE, Kim N, Sung MK. Sex- and gender-specific disparities in colorectal cancer risk. World J Gastroenterol. 2015;21(17):5167-75.
23. Zhao Z, Feng Q, Yin Z, Shuang J, Bai B, Yu P, et al. Red and processed meat consumption and colorectal cancer risk: a systematic review and meta-analysis. Oncotarget. 2017;8(47):83306-14.
24. Histopathology. Canine and Feline Gastroenterology2013. p. 333-85.
25. Nagtegaal ID, Odze RD, Klimstra D, Paradis V, Rugge M, Schirmacher P, et al. The 2019 WHO classification of tumours of the digestive system. Histopathology. 2020;76(2):182-8.
26. Fleming M, Ravula S, Tatishchev SF, Wang HL. Colorectal carcinoma: Pathologic aspects. J Gastrointest Oncol. 2012;3(3):153-73.
27. Korphaisarn K, Morris V, Davis JS, Overman MJ, Fogelman DR, Kee BK, et al. Signet ring cell colorectal cancer: genomic insights into a rare subpopulation of colorectal adenocarcinoma. Br J Cancer. 2019;121(6):505-10.
28. Fadel MG, Malietzis G, Constantinides V, Pellino G, Tekkis P, Kontovounisios C. Clinicopathological factors and survival outcomes of signet-ring cell and mucinous carcinoma versus adenocarcinoma of the colon and rectum: a systematic review and meta-analysis. Discov Oncol. 2021;12(1):5.
29. Hyngstrom JR, Hu CY, Xing Y, You YN, Feig BW, Skibber JM, et al. Clinicopathology and outcomes for mucinous and signet ring colorectal adenocarcinoma: analysis from the National Cancer Data Base. Ann Surg Oncol. 2012;19(9):2814-21.
30. Yang LL, Wang M, He P. Clinicopathological characteristics and survival in colorectal signet ring cell carcinoma: a population-based study. Sci Rep. 2020;10(1):10460.
31. Tajiri K, Sudo T, Ishi K, Kawahara A, Nagasu S, Shimomura S, et al. Investigation of clinicopathological characters and gene expression features in colorectal signet-ring cell carcinoma utilizing CMS classification. Mol Clin Oncol. 2021;14(5):98.
32. Yao Y, Dai W. Genomic Instability and Cancer. J Carcinog Mutagen. 2014;5.

33. Pino MS, Chung DC. The chromosomal instability pathway in colon cancer. Gastroenterology. 2010;138(6):2059-72.
34. Yaeger R, Cercek A, Chou JF, Sylvester BE, Kemeny NE, Hechtman JF, et al. BRAF mutation predicts for poor outcomes after metastasectomy in patients with metastatic colorectal cancer. Cancer. 2014;120(15):2316-24.
35. Laszlo L, Kurilla A, Takacs T, Kudlik G, Koprivanacz K, Buday L, et al. Recent Updates on the Significance of KRAS Mutations in Colorectal Cancer Biology. Cells. 2021;10(3).
36. Cha PH, Hwang JH, Kwak DK, Koh E, Kim KS, Choi KY. APC loss induces Warburg effect via increased PKM2 transcription in colorectal cancer. Br J Cancer. 2021;124(3):634-44.
37. Mitani Y, Ohashi S, Kikuchi O, Nakai Y, Ida T, Mizumoto A, et al. HER2 G776S mutation promotes oncogenic potential in colorectal cancer cells when accompanied by loss of APC function. Sci Rep. 2022;12(1):9213.
38. Ye Q, Cai W, Zheng Y, Evers BM, She QB. ERK and AKT signaling cooperate to translationally regulate survivin expression for metastatic progression of colorectal cancer. Oncogene. 2014;33(14):1828-39.
39. Xu J, Attisano L. Mutations in the tumor suppressors Smad2 and Smad4 inactivate transforming growth factor beta signaling by targeting Smads to the ubiquitin-proteasome pathway. Proc Natl Acad Sci U S A. 2000;97(9):4820-5.
40. Lee H, Lee H, Chin H, Kim K, Lee D. ERBB3 knockdown induces cell cycle arrest and activation of Bak and Bax-dependent apoptosis in colon cancer cells. Oncotarget. 2014;5(13):5138-52.
41. Li ZN, Zhao L, Yu LF, Wei MJ. BRAF and KRAS mutations in metastatic colorectal cancer: future perspectives for personalized therapy. Gastroenterol Rep (Oxf). 2020;8(3):192-205.
42. Gonsalves WI, Mahoney MR, Sargent DJ, Nelson GD, Alberts SR, Sinicrope FA, et al. Patient and tumor characteristics and BRAF and KRAS mutations in colon cancer, NCCTG/Alliance N0147. J Natl Cancer Inst. 2014;106(7).
43. Pai RK, Bettington M, Srivastava A, Rosty C. An update on the morphology and molecular pathology of serrated colorectal polyps and associated carcinomas. Mod Pathol. 2019;32(10):1390-415.
44. Patai AV, Molnar B, Tulassay Z, Sipos F. Serrated pathway: alternative route to colorectal cancer. World J Gastroenterol. 2013;19(5):607-15.
45. De Palma FDE, D'Argenio V, Pol J, Kroemer G, Maiuri MC, Salvatore F. The Molecular Hallmarks of the Serrated Pathway in Colorectal Cancer. Cancers (Basel). 2019;11(7).
46. Trinh A, Ladrach C, Dawson HE, Ten Hoorn S, Kuppen PJK, Reimers MS, et al. Tumour budding is associated with the mesenchymal colon cancer subtype and RAS/RAF mutations: a study of 1320 colorectal cancers with Consensus Molecular Subgroup (CMS) data. Br J Cancer. 2018;119(10):1244-51.
47. Boland CR, Goel A. Microsatellite instability in colorectal cancer. Gastroenterology. 2010;138(6):2073-87 e3.
48. Imai K, Yamamoto H. Carcinogenesis and microsatellite instability: the interrelationship between genetics and epigenetics. Carcinogenesis. 2008;29(4):673-80.

49. Kim CG, Ahn JB, Jung M, Beom SH, Kim C, Kim JH, et al. Effects of microsatellite instability on recurrence patterns and outcomes in colorectal cancers. Br J Cancer. 2016;115(1):25-33.
50. Venderbosch S, Nagtegaal ID, Maughan TS, Smith CG, Cheadle JP, Fisher D, et al. Mismatch repair status and BRAF mutation status in metastatic colorectal cancer patients: a pooled analysis of the CAIRO, CAIRO2, COIN, and FOCUS studies. Clin Cancer Res. 2014;20(20):5322-30.
51. Aasebo KO, Dragomir A, Sundstrom M, Mezheyeuski A, Edqvist PH, Eide GE, et al. Consequences of a high incidence of microsatellite instability and BRAF-mutated tumors: A population-based cohort of metastatic colorectal cancer patients. Cancer Med. 2019;8(7):3623-35.
52. Katballe N, Christensen M, Wikman FP, Orntoft TF, Laurberg S. Frequency of hereditary non-polyposis colorectal cancer in Danish colorectal cancer patients. Gut. 2002;50(1):43-51.
53. Lee J, Xiao YY, Sun YY, Balderacchi J, Clark B, Desani J, et al. Prevalence and characteristics of hereditary non-polyposis colorectal cancer (HNPCC) syndrome in immigrant Asian colorectal cancer patients. BMC Cancer. 2017;17(1):843.
54. Porkka N, Lahtinen L, Ahtiainen M, Bohm JP, Kuopio T, Eldfors S, et al. Epidemiological, clinical and molecular characterization of Lynch-like syndrome: A population-based study. Int J Cancer. 2019;145(1):87-98.
55. Hampel H. Population Screening for Hereditary Colorectal Cancer. Surg Oncol Clin N Am. 2018;27(2):319-25.
56. Karstensen JG, Burisch J, Pommergaard HC, Aalling L, Hojen H, Jespersen N, et al. Colorectal Cancer in Individuals With Familial Adenomatous Polyposis, Based on Analysis of the Danish Polyposis Registry. Clin Gastroenterol Hepatol. 2019;17(11):2294-300 e1.
57. Baek SJ, Kim SH. Colitis-associated colorectal cancer in patients with inflammatory bowel disease. Minerva Chir. 2017;72(6):520-9.
58. Weiser MR. AJCC 8th Edition: Colorectal Cancer. Ann Surg Oncol. 2018;25(6):1454-5.
59. Puccini A, Berger MD, Zhang W, Lenz HJ. What We Know About Stage II and III Colon Cancer: It's Still Not Enough. Target Oncol. 2017;12(3):265-75.
60. Nelson H, Petrelli N, Carlin A, Couture J, Fleshman J, Guillem J, et al. Guidelines 2000 for colon and rectal cancer surgery. J Natl Cancer Inst. 2001;93(8):583-96.
61. Guinney J, Dienstmann R, Wang X, de Reynies A, Schlicker A, Soneson C, et al. The consensus molecular subtypes of colorectal cancer. Nat Med. 2015;21(11):1350-6.
62. Menter DG, Davis JS, Broom BM, Overman MJ, Morris J, Kopetz S. Back to the Colorectal Cancer Consensus Molecular Subtype Future. Curr Gastroenterol Rep. 2019;21(2):5.
63. Okita A, Takahashi S, Ouchi K, Inoue M, Watanabe M, Endo M, et al. Consensus molecular subtypes classification of colorectal cancer as a predictive factor for chemotherapeutic efficacy against metastatic colorectal cancer. Oncotarget. 2018;9(27):18698-711.
64. Ten Hoorn S, de Back TR, Sommeijer DW, Vermeulen L. Clinical Value of Consensus Molecular Subtypes in Colorectal Cancer: A Systematic Review and Meta-Analysis. J Natl Cancer Inst. 2022;114(4):503-16.

65. Buikhuisen JY, Torang A, Medema JP. Exploring and modelling colon cancer inter-tumour heterogeneity: opportunities and challenges. Oncogenesis. 2020;9(7):66.
66. Isella C, Terrasi A, Bellomo SE, Petti C, Galatola G, Muratore A, et al. Stromal contribution to the colorectal cancer transcriptome. Nat Genet. 2015;47(4):312-9.
67. Calon A, Lonardo E, Berenguer-Llergo A, Espinet E, Hernando-Momblona X, Iglesias M, et al. Stromal gene expression defines poor-prognosis subtypes in colorectal cancer. Nat Genet. 2015;47(4):320-9.
68. Isella C, Brundu F, Bellomo SE, Galimi F, Zanella E, Porporato R, et al. Selective analysis of cancer-cell intrinsic transcriptional traits defines novel clinically relevant subtypes of colorectal cancer. Nat Commun. 2017;8:15107.
69. Malla SB, Byrne RM, Lafarge MW, Corry SM, Fisher NC, Tsantoulis PK, et al. Pathway level subtyping identifies a slow-cycling biological phenotype associated with poor clinical outcomes in colorectal cancer. Nat Genet. 2024;56(3):458-72.
70. Pretzsch E, Bosch F, Neumann J, Ganschow P, Bazhin A, Guba M, et al. Mechanisms of Metastasis in Colorectal Cancer and Metastatic Organotropism: Hematogenous versus Peritoneal Spread. J Oncol. 2019;2019:7407190.
71. Waldman AD, Fritz JM, Lenardo MJ. A guide to cancer immunotherapy: from T cell basic science to clinical practice. Nat Rev Immunol. 2020;20(11):651-68.
72. Zhang Y, Zhang Z. The history and advances in cancer immunotherapy: understanding the characteristics of tumor-infiltrating immune cells and their therapeutic implications. Cell Mol Immunol. 2020;17(8):807-21.
73. Esfahani K, Roudaia L, Buhlaiga N, Del Rincon SV, Papneja N, Miller WH, Jr. A review of cancer immunotherapy: from the past, to the present, to the future. Curr Oncol. 2020;27(Suppl 2):S87-S97.
74. Farkona S, Diamandis EP, Blasutig IM. Cancer immunotherapy: the beginning of the end of cancer? BMC Med. 2016;14:73.
75. Eren T, Burcu B, Tombalak E, Ozdemir T, Leblebici M, Ozemir IA, et al. Clinical Significance of the Glasgow Prognostic Score for Survival after Colorectal Cancer Surgery. J Gastrointest Surg. 2016;20(6):1231-8.
76. Sugimoto K, Komiyama H, Kojima Y, Goto M, Tomiki Y, Sakamoto K. Glasgow prognostic score as a prognostic factor in patients undergoing curative surgery for colorectal cancer. Dig Surg. 2012;29(6):503-9.
77. McMillan DC. The systemic inflammation-based Glasgow Prognostic Score: a decade of experience in patients with cancer. Cancer Treat Rev. 2013;39(5):534-40.
78. Schmitt M, Greten FR. The inflammatory pathogenesis of colorectal cancer. Nat Rev Immunol. 2021;21(10):653-67.
79. Park JH, Watt DG, Roxburgh CS, Horgan PG, McMillan DC. Colorectal Cancer, Systemic Inflammation, and Outcome: Staging the Tumor and Staging the Host. Ann Surg. 2016;263(2):326-36.
80. Muthusami S, Ramachandran IK, Babu KN, Krishnamoorthy S, Guruswamy A, Queimado L, et al. Role of Inflammation in the Development of Colorectal Cancer. Endocr Metab Immune Disord Drug Targets. 2021;21(1):77-90.
81. Lu X, Guo W, Xu W, Zhang X, Shi Z, Zheng L, et al. Prognostic value of the Glasgow prognostic score in colorectal cancer: a meta-analysis of 9,839 patients. Cancer Manag Res. 2019;11:229-49.

82. Proctor MJ, Morrison DS, Talwar D, Balmer SM, O'Reilly DS, Foulis AK, et al. An inflammation-based prognostic score (mGPS) predicts cancer survival independent of tumour site: a Glasgow Inflammation Outcome Study. Br J Cancer. 2011;104(4):726-34.
83. Nozoe T, Iguchi T, Egashira A, Adachi E, Matsukuma A, Ezaki T. Significance of modified Glasgow prognostic score as a useful indicator for prognosis of patients with gastric carcinoma. Am J Surg. 2011;201(2):186-91.
84. Balkwill F, Mantovani A. Inflammation and cancer: back to Virchow? Lancet. 2001;357(9255):539-45.
85. Zhao H, Wu L, Yan G, Chen Y, Zhou M, Wu Y, et al. Inflammation and tumor progression: signaling pathways and targeted intervention. Signal Transduct Target Ther. 2021;6(1):263.
86. Mantovani A, Allavena P, Sica A, Balkwill F. Cancer-related inflammation. Nature. 2008;454(7203):436-44.
87. Greten FR, Grivennikov SI. Inflammation and Cancer: Triggers, Mechanisms, and Consequences. Immunity. 2019;51(1):27-41.
88. Mogoanta SS, Lungu C, Ilie C, Albu DF, Totolici B, Neamtu C, et al. Peritumoral inflammatory reaction in colon cancer. Histological and immunohistochemical study. Rom J Morphol Embryol. 2014;55(4):1429-35.
89. Sokolov M, Angelov K, Vasileva M, Atanasova MP, Vlahova A, Todorov G. Clinical and prognostic significance of pathological and inflammatory markers in the surgical treatment of locally advanced colorectal cancer. Onco Targets Ther. 2015;8:2329-37.
90. Alexander PG, van Wyk HC, Pennel KAF, Hay J, McMillan DC, Horgan PG, et al. The Glasgow Microenvironment Score and risk and site of recurrence in TNM I-III colorectal cancer. Br J Cancer. 2023;128(4):556-67.
91. Gonzalez H, Hagerling C, Werb Z. Roles of the immune system in cancer: from tumor initiation to metastatic progression. Genes Dev. 2018;32(19-20):1267-84.
92. Liu Y, Cheng L, Li C, Zhang C, Wang L, Zhang J. Identification of tumor microenvironment-related prognostic genes in colorectal cancer based on bioinformatic methods. Sci Rep. 2021;11(1):15040.
93. Idos GE, Kwok J, Bonthala N, Kysh L, Gruber SB, Qu C. The Prognostic Implications of Tumor Infiltrating Lymphocytes in Colorectal Cancer: A Systematic Review and Meta-Analysis. Sci Rep. 2020;10(1):3360.
94. Quail DF, Joyce JA. Microenvironmental regulation of tumor progression and metastasis. Nat Med. 2013;19(11):1423-37.
95. Pagès F, Mlecnik B, Marliot F, Bindea G, Ou F-S, Bifulco C, et al. International validation of the consensus Immunoscore for the classification of colon cancer: a prognostic and accuracy study. The Lancet. 2018;391(10135):2128-39.
96. Giraldo NA, Sanchez-Salas R, Peske JD, Vano Y, Becht E, Petitprez F, et al. The clinical role of the TME in solid cancer. Br J Cancer. 2019;120(1):45-53.
97. Pages F, Mlecnik B, Marliot F, Bindea G, Ou FS, Bifulco C, et al. International validation of the consensus Immunoscore for the classification of colon cancer: a prognostic and accuracy study. Lancet. 2018;391(10135):2128-39.
98. Domingo E, Kelly C, Hay J, Sansom O, Maka N, Oien K, et al. Prognostic and Predictive Value of Immunoscore in Stage III Colorectal Cancer: Pooled Analysis of Cases From the SCOT and IDEA-HORG Studies. J Clin Oncol. 2024:JCO2301648.

99. Sun G, Dong X, Tang X, Qu H, Zhang H, Zhao E. The prognostic value of immunoscore in patients with colorectal cancer: A systematic review and meta-analysis. Cancer Med. 2019;8(1):182-9.
100. Malka D, Lievre A, Andre T, Taieb J, Ducreux M, Bibeau F. Immune scores in colorectal cancer: Where are we? Eur J Cancer. 2020;140:105-18.
101. Zafari N, Khosravi F, Rezaee Z, Esfandyari S, Bahiraei M, Bahramy A, et al. The role of the tumor microenvironment in colorectal cancer and the potential therapeutic approaches. J Clin Lab Anal. 2022;36(8):e24585.
102. Zhao Y, Chen C, Xu X, Ge X, Ding K, Zheng S, et al. An Efficient Prognostic Immune Scoring System For Colorectal Cancer Patients With Peritoneal Metastasis. Oncoimmunology. 2021;10(1):1901464.
103. Liang Z, Sun R, Tu P, Liang Y, Liang L, Liu F, et al. Immune-related gene-based prognostic index for predicting survival and immunotherapy outcomes in colorectal carcinoma. Front Immunol. 2022;13:944286.
104. Cassetta L, Fragkogianni S, Sims AH, Swierczak A, Forrester LM, Zhang H, et al. Human Tumor-Associated Macrophage and Monocyte Transcriptional Landscapes Reveal Cancer-Specific Reprogramming, Biomarkers, and Therapeutic Targets. Cancer Cell. 2019;35(4):588-602 e10.
105. Bindea G, Mlecnik B, Tosolini M, Kirilovsky A, Waldner M, Obenauf AC, et al. Spatiotemporal dynamics of intratumoral immune cells reveal the immune landscape in human cancer. Immunity. 2013;39(4):782-95.
106. Li J, Li L, Li Y, Long Y, Zhao Q, Ouyang Y, et al. Tumor-associated macrophage infiltration and prognosis in colorectal cancer: systematic review and meta-analysis. Int J Colorectal Dis. 2020;35(7):1203-10.
107. Grossman JG, Nywening TM, Belt BA, Panni RZ, Krasnick BA, DeNardo DG, et al. Recruitment of CCR2(+) tumor associated macrophage to sites of liver metastasis confers a poor prognosis in human colorectal cancer. Oncoimmunology. 2018;7(9):e1470729.
108. Gazzillo A, Polidoro MA, Soldani C, Franceschini B, Lleo A, Donadon M. Relationship between Epithelial-to-Mesenchymal Transition and Tumor-Associated Macrophages in Colorectal Liver Metastases. Int J Mol Sci. 2022;23(24).
109. Zhou Q, Peng RQ, Wu XJ, Xia Q, Hou JH, Ding Y, et al. The density of macrophages in the invasive front is inversely correlated to liver metastasis in colon cancer. J Transl Med. 2010;8:13.
110. Yang C, Wei C, Wang S, Shi D, Zhang C, Lin X, et al. Elevated CD163(+)/CD68(+) Ratio at Tumor Invasive Front is Closely Associated with Aggressive Phenotype and Poor Prognosis in Colorectal Cancer. Int J Biol Sci. 2019;15(5):984-98.
111. Zheng W, Wu J, Peng Y, Sun J, Cheng P, Huang Q. Tumor-Associated Neutrophils in Colorectal Cancer Development, Progression and Immunotherapy. Cancers (Basel). 2022;14(19).
112. Jaillon S, Ponzetta A, Di Mitri D, Santoni A, Bonecchi R, Mantovani A. Neutrophil diversity and plasticity in tumour progression and therapy. Nat Rev Cancer. 2020;20(9):485-503.
113. Mukaida N, Sasaki SI, Baba T. Two-Faced Roles of Tumor-Associated Neutrophils in Cancer Development and Progression. Int J Mol Sci. 2020;21(10).

114. Kim JH, Lee JY, Kim HK, Lee JW, Jung SG, Jung K, et al. Prognostic significance of the neutrophil-to-lymphocyte ratio and platelet-to-lymphocyte ratio in patients with stage III and IV colorectal cancer. World J Gastroenterol. 2017;23(3):505-15.
115. Chen ZY, Raghav K, Lieu CH, Jiang ZQ, Eng C, Vauthey JN, et al. Cytokine profile and prognostic significance of high neutrophil-lymphocyte ratio in colorectal cancer. Br J Cancer. 2015;112(6):1088-97.
116. Naszai M, Kurjan A, Maughan TS. The prognostic utility of pre-treatment neutrophil-to-lymphocyte-ratio (NLR) in colorectal cancer: A systematic review and meta-analysis. Cancer Med. 2021;10(17):5983-97.
117. Markman JL, Shiao SL. Impact of the immune system and immunotherapy in colorectal cancer. J Gastrointest Oncol. 2015;6(2):208-23.
118. Kalyan A, Kircher S, Shah H, Mulcahy M, Benson A. Updates on immunotherapy for colorectal cancer. J Gastrointest Oncol. 2018;9(1):160-9.
119. Vayrynen V, Wirta EV, Seppala T, Sihvo E, Mecklin JP, Vasala K, et al. Incidence and management of patients with colorectal cancer and synchronous and metachronous colorectal metastases: a population-based study. BJS Open. 2020;4(4):685-92.
120. Biller LH, Schrag D. Diagnosis and Treatment of Metastatic Colorectal Cancer: A Review. JAMA. 2021;325(7):669-85.
121. Xie YH, Chen YX, Fang JY. Comprehensive review of targeted therapy for colorectal cancer. Signal Transduct Target Ther. 2020;5(1):22.
122. Zlobec I, Hädrich M, Dawson H, Koelzer VH, Borner M, Mallaev M, et al. Intratumoural budding (ITB) in preoperative biopsies predicts the presence of lymph node and distant metastases in colon and rectal cancer patients. British Journal of Cancer. 2013;110(4):1008-13.
123. Koelzer VH, Zlobec I, Lugli A. Tumor budding in colorectal cancer--ready for diagnostic practice? Hum Pathol. 2016;47(1):4-19.
124. Salhia B, Trippel M, Pfaltz K, Cihoric N, Grogg A, Ladrach C, et al. High tumor budding stratifies breast cancer with metastatic properties. Breast Cancer Res Treat. 2015;150(2):363-71.
125. Pai RK, Cheng YW, Jakubowski MA, Shadrach BL, Plesec TP, Pai RK. Colorectal carcinomas with submucosal invasion (pT1): analysis of histopathological and molecular factors predicting lymph node metastasis. Mod Pathol. 2017;30(1):113-22.
126. Slik K, Blom S, Turkki R, Välimäki K, Kurki S, Mustonen H, et al. Combined epithelial marker analysis of tumour budding in stage II colorectal cancer. The Journal of Pathology: Clinical Research. 2019;5(1):63-78.
127. Ho YY, Wu TY, Cheng HC, Yang CC, Wu CH. The significance of tumor budding in oral cancer survival and its relevance to the eighth edition of the American Joint Committee on Cancer staging system. Head Neck. 2019;41(9):2991-3001.
128. Zanoletti E, Daloiso A, Nicole L, Cazzador D, Mondello T, Franz L, et al. Tumor budding to investigate local invasion, metastasis, and prognosis of head and neck carcinoma: A systematic review. Head Neck. 2024;46(3):651-71.
129. Wei L, Delin Z, Kefei Y, Hong W, Jiwei H, Yange Z. A classification based on tumor budding and immune score for patients with hepatocellular carcinoma. Oncoimmunology. 2020;9(1):1672495.
130. Kairaluoma V, Kemi N, Pohjanen VM, Saarnio J, Helminen O. Tumour budding and tumour-stroma ratio in hepatocellular carcinoma. Br J Cancer. 2020;123(1):38-45.

131. Max N, Harbaum L, Pollheimer MJ, Lindtner RA, Kornprat P, Langner C. Tumour budding with and without admixed inflammation: two different sides of the same coin? Br J Cancer. 2016;114(4):368-71.
132. Li X, Wei B, Sonmez C, Li Z, Peng L. High tumor budding count is associated with adverse clinicopathologic features and poor prognosis in breast carcinoma. Hum Pathol. 2017;66:222-9.
133. Zlobec I, Dawson HE, Blank A, Bokhorst JM, Berger MD, Nagtegaal ID, et al. Are tumour grade and tumour budding equivalent in colorectal cancer? A retrospective analysis of 771 patients. Eur J Cancer. 2020;130:139-45.
134. Shinto E, Jass JR, Tsuda H, Sato T, Ueno H, Hase K, et al. Differential prognostic significance of morphologic invasive markers in colorectal cancer: tumor budding and cytoplasmic podia. Dis Colon Rectum. 2006;49(9):1422-30.
135. Choi HJ, Park KJ, Shin JS, Roh MS, Kwon HC, Lee HS. Tumor budding as a prognostic marker in stage-III rectal carcinoma. Int J Colorectal Dis. 2007;22(8):863-8.
136. Guzinska-Ustymowicz K. The role of tumour budding at the front of invasion and recurrence of rectal carcinoma. Anticancer Res. 2005;25(2B):1269-72.
137. Kanazawa H, Mitomi H, Nishiyama Y, Kishimoto I, Fukui N, Nakamura T, et al. Tumour budding at invasive margins and outcome in colorectal cancer. Colorectal Dis. 2008;10(1):41-7.
138. Rogers AC, Winter DC, Heeney A, Gibbons D, Lugli A, Puppa G, et al. Systematic review and meta-analysis of the impact of tumour budding in colorectal cancer. Br J Cancer. 2016;115(7):831-40.
139. Lino-Silva LS, Salcedo-Hernández RA, Gamboa-Domínguez A. Tumour budding in rectal cancer. A comprehensive review. Współczesna Onkologia. 2018;22(2):61-74.
140. Zlobec I, Lugli A. Tumour budding in colorectal cancer: molecular rationale for clinical translation. Nat Rev Cancer. 2018;18(4):203-4.
141. Garfinkle R, Lee L, Boutros M, Cardin M-J, Spatz A, Morin N. Tumour budding predicts increased recurrence after curative resection for T2N0 colorectal cancer. Canadian Journal of Surgery. 2019;6(5):334-9.
142. Cappellesso R, Luchini C, Veronese N, Lo Mele M, Rosa-Rizzotto E, Guido E, et al. Tumor budding as a risk factor for nodal metastasis in pT1 colorectal cancers: a meta-analysis. Hum Pathol. 2017;65:62-70.
143. Lugli A, Karamitopoulou E, Zlobec I. Tumour budding: a promising parameter in colorectal cancer. Br J Cancer. 2012;106(11):1713-7.
144. Mitrovic B, Schaeffer DF, Riddell RH, Kirsch R. Tumor budding in colorectal carcinoma: time to take notice. Mod Pathol. 2012;25(10):1315-25.
145. Betge J, Kornprat P, Pollheimer MJ, Lindtner RA, Schlemmer A, Rehak P, et al. Tumor budding is an independent predictor of outcome in AJCC/UICC stage II colorectal cancer. Ann Surg Oncol. 2012;19(12):3706-12.
146. Petrelli F, Pezzica E, Cabiddu M, Coinu A, Borgonovo K, Ghilardi M, et al. Tumour Budding and Survival in Stage II Colorectal Cancer: a Systematic Review and Pooled Analysis. J Gastrointest Cancer. 2015;46(3):212-8.
147. Nakamura T, Mitomi H, Kanazawa H, Ohkura Y, Watanabe M. Tumor budding as an index to identify high-risk patients with stage II colon cancer. Dis Colon Rectum. 2008;51(5):568-72.
148. Ueno H, Ishiguro M, Nakatani E, Ishikawa T, Uetake H, Matsuda C, et al. Prospective Multicenter Study on the Prognostic and Predictive Impact of Tumor

Budding in Stage II Colon Cancer: Results From the SACURA Trial. J Clin Oncol. 2019;37(22):1886-94.
149. Nozawa H, Kawai K, Hata K, Tanaka T, Nishikawa T, Otani K, et al. High-risk Stage II Colorectal Cancers Carry an Equivalent Risk of Peritoneal Recurrence to Stage III. In Vivo. 2018;32(5):1235-40.
150. Quirke P, West NP, Nagtegaal ID. EURECCA consensus conference highlights about colorectal cancer clinical management: the pathologists expert review. Virchows Arch. 2014;464(2):129-34.
151. van de Velde CJ, Boelens PG, Borras JM, Coebergh JW, Cervantes A, Blomqvist L, et al. EURECCA colorectal: multidisciplinary management: European consensus conference colon & rectum. Eur J Cancer. 2014;50(1):1 e- e34.
152. Nagata K, Shinto E, Yamadera M, Shiraishi T, Kajiwara Y, Okamoto K, et al. Prognostic and predictive values of tumour budding in stage IV colorectal cancer. BJS Open. 2020;4(4):693-703.
153. Fonseca GM, de Mello ES, Faraj SF, Kruger JAP, Coelho FF, Jeismann VB, et al. Prognostic significance of poorly differentiated clusters and tumor budding in colorectal liver metastases. J Surg Oncol. 2018;117(7):1364-75.
154. Hatthakarnkul P, Quinn JA, Matly AAM, Ammar A, van Wyk HC, McMillan DC, et al. Systematic review of tumour budding and association with common mutations in patients with colorectal cancer. Crit Rev Oncol Hematol. 2021;167:103490.
155. Jensen DH, Dabelsteen E, Specht L, Fiehn AM, Therkildsen MH, Jonson L, et al. Molecular profiling of tumour budding implicates TGFbeta-mediated epithelial-mesenchymal transition as a therapeutic target in oral squamous cell carcinoma. J Pathol. 2015;236(4):505-16.
156. Li H, Zhong A, Li S, Meng X, Wang X, Xu F, et al. The integrated pathway of TGFbeta/Snail with TNFalpha/NFkappaB may facilitate the tumor-stroma interaction in the EMT process and colorectal cancer prognosis. Sci Rep. 2017;7(1):4915.
157. Steinbichler TB, Savic D, Dudas J, Kvitsaridze I, Skvortsov S, Riechelmann H, et al. Cancer stem cells and their unique role in metastatic spread. Semin Cancer Biol. 2020;60:148-56.
158. Haddad TS, van den Dobbelsteen L, Ozturk SK, Geene R, Nijman IJ, Verrijp K, et al. Pseudobudding: ruptured glands do not represent true tumor buds. J Pathol. 2023;261(1):19-27.
159. van Wyk HC, Roseweir A, Alexander P, Park JH, Horgan PG, McMillan DC, et al. The Relationship Between Tumor Budding, Tumor Microenvironment, and Survival in Patients with Primary Operable Colorectal Cancer. Ann Surg Oncol. 2019;26(13):4397-404.
160. Nearchou IP, Lillard K, Gavriel CG, Ueno H, Harrison DJ, Caie PD. Automated Analysis of Lymphocytic Infiltration, Tumor Budding, and Their Spatial Relationship Improves Prognostic Accuracy in Colorectal Cancer. Cancer Immunol Res. 2019;7(4):609-20.
161. Hatthakarnkul P, Pennel K, Alexander P, van Wyk H, Roseweir A, Inthagard J, et al. Histopathological tumour microenvironment score independently predicts outcome in primary operable colorectal cancer. J Pathol Clin Res. 2024;10(3):e12374.
162. Mitrovic B, Schaeffer DF, Riddell RH, Kirsch R. Tumor budding in colorectal carcinoma: time to take notice. Modern Pathology. 2012;25(10):1315-25.

163. Lugli A, Zlobec I. The battle for prognosis at the invasive front of colorectal cancer. EBioMedicine. 2020;58:102918.
164. Noone AM, Schussler N, Negoita S, Adamo M, Cronin K, Cyr J, et al. Availability of TNM Staging Data Elements in the Medical Record and Training Needs Assessment: Results from the 2014 SEER Training Needs Assessment for TNM Study. J Registry Manag. 2015;42(2):40-7.
165. Yeakley JM, Shepard PJ, Goyena DE, VanSteenhouse HC, McComb JD, Seligmann BE. A trichostatin A expression signature identified by TempO-Seq targeted whole transcriptome profiling. PLoS One. 2017;12(5):e0178302.
166. Dobin A, Davis CA, Schlesinger F, Drenkow J, Zaleski C, Jha S, et al. STAR: ultrafast universal RNA-seq aligner. Bioinformatics. 2013;29(1):15-21.
167. Subramanian A, Tamayo P, Mootha VK, Mukherjee S, Ebert BL, Gillette MA, et al. Gene set enrichment analysis: a knowledge-based approach for interpreting genome-wide expression profiles. Proc Natl Acad Sci U S A. 2005;102(43):15545-50.
168. Liberzon A, Birger C, Thorvaldsdottir H, Ghandi M, Mesirov JP, Tamayo P. The Molecular Signatures Database (MSigDB) hallmark gene set collection. Cell Syst. 2015;1(6):417-25.
169. Szklarczyk D, Franceschini A, Wyder S, Forslund K, Heller D, Huerta-Cepas J, et al. STRING v10: protein-protein interaction networks, integrated over the tree of life. Nucleic Acids Res. 2015;43(Database issue):D447-52.
170. Hernandez S, Lazcano R, Serrano A, Powell S, Kostousov L, Mehta J, et al. Challenges and Opportunities for Immunoprofiling Using a Spatial High-Plex Technology: The NanoString GeoMx((R)) Digital Spatial Profiler. Front Oncol. 2022;12:890410.
171. Arnold M, Sierra MS, Laversanne M, Soerjomataram I, Jemal A, Bray F. Global patterns and trends in colorectal cancer incidence and mortality. Gut. 2017;66(4):683-91.
172. Garfinkle R, Lee L, Boutros M, Cardin MJ, Spatz A, Morin N. Tumour budding predicts increased recurrence after curative resection for T2N0 colorectal cancer. Can J Surg. 2019;62(5):334-9.
173. Chen L, Yang F, Qi Z, Tai J. Predicting lymph node metastasis and recurrence in patients with early stage colorectal cancer. Front Med (Lausanne). 2022;9:991785.
174. Demir A, Alan O, Oruc E. Tumor budding for predicting prognosis of resected rectum cancer after neoadjuvant treatment. World J Surg Oncol. 2019;17(1):50.
175. Zlobec I, Berger MD, Lugli A. Tumour budding and its clinical implications in gastrointestinal cancers. Br J Cancer. 2020;123(5):700-8.
176. Cangucu AL, Valerio E, Peixoto RBP, Felismino TC, de Mello CAL, Neotti T, et al. The prognostic influence of tumour budding in Western patients with stage II colorectal cancer. Ecancermedicalscience. 2020;14:1130.
177. Syk E, Lenander C, Nilsson PJ, Rubio CA, Glimelius B. Tumour budding correlates with local recurrence of rectal cancer. Colorectal Dis. 2011;13(3):255-62.
178. Salemme V, Centonze G, Cavallo F, Defilippi P, Conti L. The Crosstalk Between Tumor Cells and the Immune Microenvironment in Breast Cancer: Implications for Immunotherapy. Front Oncol. 2021;11:610303.
179. Nearchou IP, Gwyther BM, Georgiakakis ECT, Gavriel CG, Lillard K, Kajiwara Y, et al. Spatial immune profiling of the colorectal tumor microenvironment predicts good outcome in stage II patients. NPJ Digit Med. 2020;3:71.

180. Dawson H, Christe L, Eichmann M, Reinhard S, Zlobec I, Blank A, et al. Tumour budding/T cell infiltrates in colorectal cancer: proposal of a novel combined score. Histopathology. 2020;76(4):572-80.
181. Tan WCC, Nerurkar SN, Cai HY, Ng HHM, Wu D, Wee YTF, et al. Overview of multiplex immunohistochemistry/immunofluorescence techniques in the era of cancer immunotherapy. Cancer Commun (Lond). 2020;40(4):135-53.
182. Lin JR, Wang S, Coy S, Chen YA, Yapp C, Tyler M, et al. Multiplexed 3D atlas of state transitions and immune interaction in colorectal cancer. Cell. 2023;186(2):363-81 e19.
183. Puppa G, Sonzogni A, Colombari R, Pelosi G. TNM staging system of colorectal carcinoma: a critical appraisal of challenging issues. Arch Pathol Lab Med. 2010;134(6):837-52.
184. Lopes-Ramos CM, Quackenbush J, DeMeo DL. Genome-Wide Sex and Gender Differences in Cancer. Front Oncol. 2020;10:597788.
185. Tsai YJ, Huang SC, Lin HH, Lin CC, Lan YT, Wang HS, et al. Differences in gene mutations according to gender among patients with colorectal cancer. World J Surg Oncol. 2018;16(1):128.
186. Hases L, Ibrahim A, Chen X, Liu Y, Hartman J, Williams C. The Importance of Sex in the Discovery of Colorectal Cancer Prognostic Biomarkers. Int J Mol Sci. 2021;22(3).
187. Huang D, Sun W, Zhou Y, Li P, Chen F, Chen H, et al. Mutations of key driver genes in colorectal cancer progression and metastasis. Cancer Metastasis Rev. 2018;37(1):173-87.
188. Lavacchi D, Fancelli S, Roviello G, Castiglione F, Caliman E, Rossi G, et al. Mutations matter: An observational study of the prognostic and predictive value of KRAS mutations in metastatic colorectal cancer. Front Oncol. 2022;12:1055019.
189. Kawakami H, Zaanan A, Sinicrope FA. Implications of mismatch repair-deficient status on management of early stage colorectal cancer. J Gastrointest Oncol. 2015;6(6):676-84.
190. Ju SY, Ma SJ. High C-reactive protein to albumin ratio and the short-term survival prognosis within 30 days in terminal cancer patients receiving palliative care in a hospital setting: A retrospective analysis. Medicine (Baltimore). 2020;99(9):e19350.
191. Forrest LM, McMillan DC, McArdle CS, Angerson WJ, Dunlop DJ. Evaluation of cumulative prognostic scores based on the systemic inflammatory response in patients with inoperable non-small-cell lung cancer. Br J Cancer. 2003;89(6):1028-30.
192. Alexander PG, Roseweir AK, Pennel KAF, van Wyk HC, Powell A, McMillan DC, et al. The Glasgow Microenvironment Score associates with prognosis and adjuvant chemotherapy response in colorectal cancer. Br J Cancer. 2021;124(4):786-96.
193. Lu X, Wang Y, He M, Gou Z. Prognostic value and tumour microenvironment characteristics of the Glasgow Microenvironment Score in primary triple-negative breast cancer. J Clin Pathol. 2022.
194. Park JH, McMillan DC, Powell AG, Richards CH, Horgan PG, Edwards J, et al. Evaluation of a tumor microenvironment-based prognostic score in primary operable colorectal cancer. Clin Cancer Res. 2015;21(4):882-8.
195. Li J, Chen D, Shen M. Tumor Microenvironment Shapes Colorectal Cancer Progression, Metastasis, and Treatment Responses. Front Med (Lausanne). 2022;9:869010.

196. Ruiz-Patino A, Arrieta O, Cardona AF, Martin C, Raez LE, Zatarain-Barron ZL, et al. Immunotherapy at any line of treatment improves survival in patients with advanced metastatic non-small cell lung cancer (NSCLC) compared with chemotherapy (Quijote-CLICaP). Thorac Cancer. 2020;11(2):353-61.
197. Kasurinen J, Hagstrom J, Kaprio T, Beilmann-Lehtonen I, Haglund C, Bockelman C. Tumor-associated CD3- and CD8-positive immune cells in colorectal cancer: The additional prognostic value of CD8+-to-CD3+ ratio remains debatable. Tumour Biol. 2022;44(1):37-52.
198. Yin C, Okugawa Y, Yamamoto A, Kitajima T, Shimura T, Kawamura M, et al. Prognostic significance of CD8(+) tumor-infiltrating lymphocytes and CD66b(+) tumor-associated neutrophils in the invasive margins of stages I-III colorectal cancer. Oncol Lett. 2022;24(1):212.
199. Ling A, Edin S, Wikberg ML, Oberg A, Palmqvist R. The intratumoural subsite and relation of CD8(+) and FOXP3(+) T lymphocytes in colorectal cancer provide important prognostic clues. Br J Cancer. 2014;110(10):2551-9.
200. Salama P, Phillips M, Grieu F, Morris M, Zeps N, Joseph D, et al. Tumor-infiltrating FOXP3+ T regulatory cells show strong prognostic significance in colorectal cancer. J Clin Oncol. 2009;27(2):186-92.
201. Sinicrope FA, Rego RL, Ansell SM, Knutson KL, Foster NR, Sargent DJ. Intraepithelial effector (CD3+)/regulatory (FoxP3+) T-cell ratio predicts a clinical outcome of human colon carcinoma. Gastroenterology. 2009;137(4):1270-9.
202. Zlobec I, Minoo P, Terracciano L, Baker K, Lugli A. Characterization of the immunological microenvironment of tumour buds and its impact on prognosis in mismatch repair-proficient and -deficient colorectal cancers. Histopathology. 2011;59(3):482-95.
203. Lu L, Liu YJ, Cheng PQ, Hu D, Xu HC, Ji G. Macrophages play a role in inflammatory transformation of colorectal cancer. World J Gastrointest Oncol. 2021;13(12):2013-28.
204. Wang H, Tian T, Zhang J. Tumor-Associated Macrophages (TAMs) in Colorectal Cancer (CRC): From Mechanism to Therapy and Prognosis. Int J Mol Sci. 2021;22(16).
205. Pinto ML, Rios E, Duraes C, Ribeiro R, Machado JC, Mantovani A, et al. The Two Faces of Tumor-Associated Macrophages and Their Clinical Significance in Colorectal Cancer. Front Immunol. 2019;10:1875.
206. Trumpi K, Frenkel N, Peters T, Korthagen NM, Jongen JM, Raats D, et al. Macrophages induce “budding” in aggressive human colon cancer subtypes by protease-mediated disruption of tight junctions. Oncotarget. 2018;9(28):19490-507.
207. da Silva KD, Caldeira PC, Alves AM, Vasconcelos ACU, Gomes APN, de Aguiar MCF, et al. High CD3(+) lymphocytes, low CD66b(+) neutrophils, and scarce tumor budding in the invasive front of lip squamous cell carcinomas. Arch Oral Biol. 2019;104:46-51.
208. Mizuno R, Kawada K, Itatani Y, Ogawa R, Kiyasu Y, Sakai Y. The Role of Tumor-Associated Neutrophils in Colorectal Cancer. Int J Mol Sci. 2019;20(3).
209. Singh MP, Rai S, Singh NK, Srivastava S. Transcriptomic landscape of early age onset of colorectal cancer identifies novel genes and pathways in Indian CRC patients. Sci Rep. 2021;11(1):11765.
210. Cieslik M, Chinnaiyan AM. Cancer transcriptome profiling at the juncture of clinical translation. Nat Rev Genet. 2018;19(2):93-109.

211. Netea MG, Schlitzer A, Placek K, Joosten LAB, Schultze JL. Innate and Adaptive Immune Memory: an Evolutionary Continuum in the Host's Response to Pathogens. Cell Host Microbe. 2019;25(1):13-26.
212. Bruck O, Lee MH, Turkki R, Uski I, Penttila P, Paavolainen L, et al. Spatial immunoprofiling of the intratumoral and peritumoral tissue of renal cell carcinoma patients. Mod Pathol. 2021;34(12):2229-41.
213. Fan J, Slowikowski K, Zhang F. Single-cell transcriptomics in cancer: computational challenges and opportunities. Exp Mol Med. 2020;52(9):1452-65.
214. Chawla S, Rockstroh A, Lehman M, Ratther E, Jain A, Anand A, et al. Gene expression based inference of cancer drug sensitivity. Nat Commun. 2022;13(1):5680.
215. Hoadley KA, Yau C, Wolf DM, Cherniack AD, Tamborero D, Ng S, et al. Multiplatform analysis of 12 cancer types reveals molecular classification within and across tissues of origin. Cell. 2014;158(4):929-44.
216. Picard E, Verschoor CP, Ma GW, Pawelec G. Relationships Between Immune Landscapes, Genetic Subtypes and Responses to Immunotherapy in Colorectal Cancer. Front Immunol. 2020;11:369.
217. Rebersek M. Consensus molecular subtypes (CMS) in metastatic colorectal cancer - personalized medicine decision. Radiol Oncol. 2020;54(3):272-7.
218. Lenz HJ, Ou FS, Venook AP, Hochster HS, Niedzwiecki D, Goldberg RM, et al. Impact of Consensus Molecular Subtype on Survival in Patients With Metastatic Colorectal Cancer: Results From CALGB/SWOG 80405 (Alliance). J Clin Oncol. 2019;37(22):1876-85.
219. Aderka D, Stintzing S, Heinemann V. Explaining the unexplainable: discrepancies in results from the CALGB/SWOG 80405 and FIRE-3 studies. Lancet Oncol. 2019;20(5):e274-e83.
220. Pavlic A, Bostjancic E, Kavalar R, Ilijevec B, Bonin S, Zanconati F, et al. Tumour budding and poorly differentiated clusters in colon cancer - different manifestations of partial epithelial-mesenchymal transition. J Pathol. 2022;258(3):278-88.
221. Zlobec I, Lugli A. Epithelial mesenchymal transition and tumor budding in aggressive colorectal cancer: tumor budding as oncotarget. Oncotarget. 2010;1(7):651-61.
222. Mooi JK, Wirapati P, Asher R, Lee CK, Savas P, Price TJ, et al. The prognostic impact of consensus molecular subtypes (CMS) and its predictive effects for bevacizumab benefit in metastatic colorectal cancer: molecular analysis of the AGITG MAX clinical trial. Ann Oncol. 2018;29(11):2240-6.
223. Guil-Luna S, Mena R, Navarrete-Sirvent C, Lopez-Sanchez LM, Khouadri K, Toledano-Fonseca M, et al. Association of Tumor Budding With Immune Evasion Pathways in Primary Colorectal Cancer and Patient-Derived Xenografts. Front Med (Lausanne). 2020;7:264.
224. Coebergh van den Braak RRJ, Ten Hoorn S, Sieuwerts AM, Tuynman JB, Smid M, Wilting SM, et al. Interconnectivity between molecular subtypes and tumor stage in colorectal cancer. BMC Cancer. 2020;20(1):850.
225. Pleasance E, Bohm A, Williamson LM, Nelson JMT, Shen Y, Bonakdar M, et al. Whole-genome and transcriptome analysis enhances precision cancer treatment options. Ann Oncol. 2022;33(9):939-49.

226. Young LC, Hartig N, Munoz-Alegre M, Oses-Prieto JA, Durdu S, Bender S, et al. An MRAS, SHOC2, and SCRIB complex coordinates ERK pathway activation with polarity and tumorigenic growth. Mol Cell. 2013;52(5):679-92.
227. Mathieu ME, Faucheux C, Saucourt C, Soulet F, Gauthereau X, Fedou S, et al. MRAS GTPase is a novel stemness marker that impacts mouse embryonic stem cell plasticity and Xenopus embryonic cell fate. Development. 2013;140(16):3311-22.
228. Dolatkhah R, Dastgiri S, Eftekhar Sadat AT, Farassati F, Nezamdoust M, Somi MH. Impact of RAS/RAF mutations on clinical and prognostic outcomes in metastatic colorectal cancer. Bioimpacts. 2021;11(1):5-14.
229. Witte I, Foerstermann U, Devarajan A, Reddy ST, Horke S. Protectors or Traitors: The Roles of PON2 and PON3 in Atherosclerosis and Cancer. J Lipids. 2012;2012:342806.
230. Campagna R, Pozzi V, Salvucci A, Togni L, Mascitti M, Sartini D, et al. Paraoxonase-2 expression in oral squamous cell carcinoma. Hum Cell. 2023;36(3):1211-3.
231. Zhou Z, Xie X, Wang X, Zhang X, Li W, Sun T, et al. Correlations Between Tumor Mutation Burden and Immunocyte Infiltration and Their Prognostic Value in Colon Cancer. Frontiers in Genetics. 2021;12.
232. Uribe ML, Marrocco I, Yarden Y. EGFR in Cancer: Signaling Mechanisms, Drugs, and Acquired Resistance. Cancers (Basel). 2021;13(11).
233. Schinke H, Shi E, Lin Z, Quadt T, Kranz G, Zhou J, et al. A transcriptomic map of EGFR-induced epithelial-to-mesenchymal transition identifies prognostic and therapeutic targets for head and neck cancer. Mol Cancer. 2022;21(1):178.
234. Vu T, Datta PK. Regulation of EMT in Colorectal Cancer: A Culprit in Metastasis. Cancers (Basel). 2017;9(12).
235. Matsuyama T, Ishikawa T, Takahashi N, Yamada Y, Yasuno M, Kawano T, et al. Transcriptomic expression profiling identifies ITGBL1, an epithelial to mesenchymal transition (EMT)-associated gene, is a promising recurrence prediction biomarker in colorectal cancer. Mol Cancer. 2019;18(1):19.
236. Hur K, Toiyama Y, Takahashi M, Balaguer F, Nagasaka T, Koike J, et al. MicroRNA-200c modulates epithelial-to-mesenchymal transition (EMT) in human colorectal cancer metastasis. Gut. 2013;62(9):1315-26.
237. An G, Liu Y, Hou Y, Lei Y, Bai J, He L, et al. RRP12 suppresses cell migration and invasion in colorectal cancer cell via regulation of epithelial-mesenchymal transition. J Gastrointest Oncol. 2023;14(5):2111-23.
238. Otrock ZK, Mahfouz RA, Makarem JA, Shamseddine AI. Understanding the biology of angiogenesis: review of the most important molecular mechanisms. Blood Cells Mol Dis. 2007;39(2):212-20.
239. Lugano R, Ramachandran M, Dimberg A. Tumor angiogenesis: causes, consequences, challenges and opportunities. Cell Mol Life Sci. 2020;77(9):1745-70.
240. Liu ZL, Chen HH, Zheng LL, Sun LP, Shi L. Angiogenic signaling pathways and anti-angiogenic therapy for cancer. Signal Transduct Target Ther. 2023;8(1):198.
241. Gasparini G, Longo R, Toi M, Ferrara N. Angiogenic inhibitors: a new therapeutic strategy in oncology. Nat Clin Pract Oncol. 2005;2(11):562-77.
242. Gao LF, Zhong Y, Long T, Wang X, Zhu JX, Wang XY, et al. Tumor bud-derived CCL5 recruits fibroblasts and promotes colorectal cancer progression via CCR5-SLC25A24 signaling. J Exp Clin Cancer Res. 2022;41(1):81.

243. Righi A, Sarotto I, Casorzo L, Cavalchini S, Frangipane E, Risio M. Tumour budding is associated with hypoxia at the advancing front of colorectal cancer. Histopathology. 2015;66(7):982-90.
244. Xu CJ, Mikami T, Nakamura T, Tsuruta T, Nakada N, Yanagisawa N, et al. Tumor budding, myofibroblast proliferation, and fibrosis in obstructing colon carcinoma: the roles of Hsp47 and basic fibroblast growth factor. Pathol Res Pract. 2013;209(2):69-74.
245. McNab F, Mayer-Barber K, Sher A, Wack A, O'Garra A. Type I interferons in infectious disease. Nat Rev Immunol. 2015;15(2):87-103.
246. Vidal P. Interferon alpha in cancer immunoediting: From elimination to escape. Scand J Immunol. 2020;91(5):e12863.
247. Masaki T, Matsuoka H, Sugiyama M, Abe N, Goto A, Sakamoto A, et al. Matrilysin (MMP-7) as a significant determinant of malignant potential of early invasive colorectal carcinomas. Br J Cancer. 2001;84(10):1317-21.
248. Guzinska-Ustymowicz K. MMP-9 and cathepsin B expression in tumor budding as an indicator of a more aggressive phenotype of colorectal cancer (CRC). Anticancer Res. 2006;26(2B):1589-94.
249. Nascimento G, Silva LPD, Matos FR, Silva TAD, Medeiros SRB, Souza LB, et al. Polymorphisms of matrix metalloproteinase-7 and -9 are associated with oral tongue squamous cell carcinoma. Braz Oral Res. 2020;35:e019.
250. Marei HE, Althani A, Afifi N, Hasan A, Caceci T, Pozzoli G, et al. p53 signaling in cancer progression and therapy. Cancer Cell Int. 2021;21(1):703.
251. Li K, Guo Q, Yang J, Chen H, Hu K, Zhao J, et al. FOXD3 is a tumor suppressor of colon cancer by inhibiting EGFR-Ras-Raf-MEK-ERK signal pathway. Oncotarget. 2017;8(3):5048-56.
252. Lei Y, Tang R, Xu J, Wang W, Zhang B, Liu J, et al. Applications of single-cell sequencing in cancer research: progress and perspectives. J Hematol Oncol. 2021;14(1):91.
253. Zhuang X. Spatially resolved single-cell genomics and transcriptomics by imaging. Nat Methods. 2021;18(1):18-22.
254. Ramazzotti D, Lal A, Wang B, Batzoglou S, Sidow A. Multi-omic tumor data reveal diversity of molecular mechanisms that correlate with survival. Nat Commun. 2018;9(1):4453.
255. Trajanoska K, Bherer C, Taliun D, Zhou S, Richards JB, Mooser V. From target discovery to clinical drug development with human genetics. Nature. 2023;620(7975):737-45.
256. Heo YJ, Hwa C, Lee GH, Park JM, An JY. Integrative Multi-Omics Approaches in Cancer Research: From Biological Networks to Clinical Subtypes. Mol Cells. 2021;44(7):433-43.
257. Xu F, Jiang L, Zhao Q, Zhang Z, Liu Y, Yang S, et al. Whole-transcriptome and proteome analyses identify key differentially expressed mRNAs, miRNAs, lncRNAs and circRNAs associated with HCC. Oncogene. 2021;40(29):4820-31.
258. Gambardella G, Viscido G, Tumaini B, Isacchi A, Bosotti R, di Bernardo D. A single-cell analysis of breast cancer cell lines to study tumour heterogeneity and drug response. Nat Commun. 2022;13(1):1714.
259. Joanito I, Wirapati P, Zhao N, Nawaz Z, Yeo G, Lee F, et al. Single-cell and bulk transcriptome sequencing identifies two epithelial tumor cell states and refines the

consensus molecular classification of colorectal cancer. Nat Genet. 2022;54(7):963-75.
260. Landry AP, Balas M, Alli S, Spears J, Zador Z. Distinct regional ontogeny and activation of tumor associated macrophages in human glioblastoma. Sci Rep. 2020;10(1):19542.
261. Lewis SM, Asselin-Labat ML, Nguyen Q, Berthelet J, Tan X, Wimmer VC, et al. Spatial omics and multiplexed imaging to explore cancer biology. Nat Methods. 2021;18(9):997-1012.
262. Merritt CR, Ong GT, Church SE, Barker K, Danaher P, Geiss G, et al. Multiplex digital spatial profiling of proteins and RNA in fixed tissue. Nat Biotechnol. 2020;38(5):586-99.
263. Oh T, Kim G, Baek SH, Woo Y, Koo BS, Hwang EH, et al. Spatial transcriptome atlas reveals pulmonary microstructure-specific COVID-19 gene signatures in cynomolgus macaques. Commun Biol. 2023;6(1):879.
264. Li W, Li T, Sun C, Du Y, Chen L, Du C, et al. Identification and prognostic analysis of biomarkers to predict the progression of pancreatic cancer patients. Mol Med. 2022;28(1):43.
265. Liu HT, Chen SY, Peng LL, Zhong L, Zhou L, Liao SQ, et al. Spatially resolved transcriptomics revealed local invasion-related genes in colorectal cancer. Front Oncol. 2023;13:1089090.
266. Beechem JM. High-Plex Spatially Resolved RNA and Protein Detection Using Digital Spatial Profiling: A Technology Designed for Immuno-oncology Biomarker Discovery and Translational Research. Methods Mol Biol. 2020;2055:563-83.
267. Voutsadakis IA. Proteasome expression and activity in cancer and cancer stem cells. Tumour Biol. 2017;39(3):1010428317692248.
268. Wang L, Zuo X, Xie K, Wei D. The Role of CD44 and Cancer Stem Cells. Methods Mol Biol. 2018;1692:31-42.
269. Mohamed SY, Kaf RM, Ahmed MM, Elwan A, Ashour HR, Ibrahim A. The Prognostic Value of Cancer Stem Cell Markers (Notch1, ALDH1, and CD44) in Primary Colorectal Carcinoma. J Gastrointest Cancer. 2019;50(4):824-37.
270. Walcher L, Kistenmacher AK, Suo H, Kitte R, Dluczek S, Strauss A, et al. Cancer Stem Cells-Origins and Biomarkers: Perspectives for Targeted Personalized Therapies. Front Immunol. 2020;11:1280.
271. Li Y, Wei J, Xu C, Zhao Z, You T. Prognostic significance of cyclin D1 expression in colorectal cancer: a meta-analysis of observational studies. PLoS One. 2014;9(4):e94508.
272. Matthews HK, Bertoli C, de Bruin RAM. Cell cycle control in cancer. Nat Rev Mol Cell Biol. 2022;23(1):74-88.
273. Dawson H, Koelzer VH, Karamitopoulou E, Economou M, Hammer C, Muller DE, et al. The apoptotic and proliferation rate of tumour budding cells in colorectal cancer outlines a heterogeneous population of cells with various impacts on clinical outcome. Histopathology. 2014;64(4):577-84.
274. Chen J, Ye X, Pitmon E, Lu M, Wan J, Jellison ER, et al. IL-17 inhibits CXCL9/10-mediated recruitment of CD8(+) cytotoxic T cells and regulatory T cells to colorectal tumors. J Immunother Cancer. 2019;7(1):324.

275. Mlecnik B, Tosolini M, Charoentong P, Kirilovsky A, Bindea G, Berger A, et al. Biomolecular network reconstruction identifies T-cell homing factors associated with survival in colorectal cancer. Gastroenterology. 2010;138(4):1429-40.
276. Zhang J, Tao J, Gao RN, Wei ZY, He YS, Ren CY, et al. Cytotoxic T-Cell Trafficking Chemokine Profiles Correlate With Defined Mucosal Microbial Communities in Colorectal Cancer. Front Immunol. 2021;12:715559.
277. Kistner L, Doll D, Holtorf A, Nitsche U, Janssen KP. Interferon-inducible CXC-chemokines are crucial immune modulators and survival predictors in colorectal cancer. Oncotarget. 2017;8(52):89998-90012.
278. Altin JG, Sloan EK. The role of CD45 and CD45-associated molecules in T cell activation. Immunol Cell Biol. 1997;75(5):430-45.
279. Roxburgh CS, Salmond JM, Horgan PG, Oien KA, McMillan DC. Tumour inflammatory infiltrate predicts survival following curative resection for node-negative colorectal cancer. Eur J Cancer. 2009;45(12):2138-45.
280. Zhou J, Tang Z, Gao S, Li C, Feng Y, Zhou X. Tumor-Associated Macrophages: Recent Insights and Therapies. Front Oncol. 2020;10:188.
281. Kumari N, Dwarakanath BS, Das A, Bhatt AN. Role of interleukin-6 in cancer progression and therapeutic resistance. Tumour Biol. 2016;37(9):11553-72.
282. Gordziel C, Bratsch J, Moriggl R, Knosel T, Friedrich K. Both STAT1 and STAT3 are favourable prognostic determinants in colorectal carcinoma. Br J Cancer. 2013;109(1):138-46.
283. Dagogo-Jack I, Shaw AT. Tumour heterogeneity and resistance to cancer therapies. Nat Rev Clin Oncol. 2018;15(2):81-94.
284. Uhlen M, Zhang C, Lee S, Sjostedt E, Fagerberg L, Bidkhori G, et al. A pathology atlas of the human cancer transcriptome. Science. 2017;357(6352).
285. Gillies RJ. Cancer heterogeneity and metastasis: life at the edge. Clin Exp Metastasis. 2022;39(1):15-9.
286. Huang Y, Qi L, Kogiso M, Du Y, Braun FK, Zhang H, et al. Spatial Dissection of Invasive Front from Tumor Mass Enables Discovery of Novel microRNA Drivers of Glioblastoma Invasion. Adv Sci (Weinh). 2021;8(23):e2101923.
287. Arora R, Cao C, Kumar M, Sinha S, Chanda A, McNeil R, et al. Spatial transcriptomics reveals distinct and conserved tumor core and edge architectures that predict survival and targeted therapy response. Nat Commun. 2023;14(1):5029.
288. Bastola S, Pavlyukov MS, Yamashita D, Ghosh S, Cho H, Kagaya N, et al. Glioma-initiating cells at tumor edge gain signals from tumor core cells to promote their malignancy. Nat Commun. 2020;11(1):4660.
289. Palla G, Fischer DS, Regev A, Theis FJ. Spatial components of molecular tissue biology. Nat Biotechnol. 2022;40(3):308-18.
290. Wu Y, Cheng Y, Wang X, Fan J, Gao Q. Spatial omics: Navigating to the golden era of cancer research. Clin Transl Med. 2022;12(1):e696.
291. Van TM, Blank CU. A user's perspective on GeoMx(TM) digital spatial profiling. Immunooncol Technol. 2019;1:11-8.
292. Taliano RJ, LeGolvan M, Resnick MB. Immunohistochemistry of colorectal carcinoma: current practice and evolving applications. Hum Pathol. 2013;44(2):151-63.
293. Sheng W, Zhang C, Mohiuddin TM, Al-Rawe M, Zeppernick F, Falcone FH, et al. Multiplex Immunofluorescence: A Powerful Tool in Cancer Immunotherapy. Int J Mol Sci. 2023;24(4).

294. Im K, Mareninov S, Diaz MFP, Yong WH. An Introduction to Performing Immunofluorescence Staining. Methods Mol Biol. 2019;1897:299-311.
295. Thomas SJ, Snowden JA, Zeidler MP, Danson SJ. The role of JAK/STAT signalling in the pathogenesis, prognosis and treatment of solid tumours. Br J Cancer. 2015;113(3):365-71.
296. Lin Y, He Z, Ye J, Liu Z, She X, Gao X, et al. Progress in Understanding the IL-6/STAT3 Pathway in Colorectal Cancer. Onco Targets Ther. 2020;13:13023-32.
297. Baghban R, Roshangar L, Jahanban-Esfahlan R, Seidi K, Ebrahimi-Kalan A, Jaymand M, et al. Tumor microenvironment complexity and therapeutic implications at a glance. Cell Commun Signal. 2020;18(1):59.
298. Galon J, Costes A, Sanchez-Cabo F, Kirilovsky A, Mlecnik B, Lagorce-Pages C, et al. Type, density, and location of immune cells within human colorectal tumors predict clinical outcome. Science. 2006;313(5795):1960-4.
299. Fridman WH, Zitvogel L, Sautes-Fridman C, Kroemer G. The immune contexture in cancer prognosis and treatment. Nat Rev Clin Oncol. 2017;14(12):717-34.
300. Kaminska K, Szczylik C, Bielecka ZF, Bartnik E, Porta C, Lian F, et al. The role of the cell-cell interactions in cancer progression. J Cell Mol Med. 2015;19(2):283-96.
301. Mougiakakos D. Regulatory T cells in colorectal cancer: from biology to prognostic relevance. Cancers (Basel). 2011;3(2):1708-31.
302. Halvorsen EC, Mahmoud SM, Bennewith KL. Emerging roles of regulatory T cells in tumour progression and metastasis. Cancer Metastasis Rev. 2014;33(4):1025-41.
303. Kersten K, Hu KH, Combes AJ, Samad B, Harwin T, Ray A, et al. Spatiotemporal co-dependency between macrophages and exhausted CD8(+) T cells in cancer. Cancer Cell. 2022;40(6):624-38 e9.
304. Trumpi K, Frenkel N, Peters T, Korthagen NM, Jongen JMJ, Raats D, et al. Macrophages induce "budding" in aggressive human colon cancer subtypes by protease-mediated disruption of tight junctions. Oncotarget. 2018;9(28):19490-507.
305. DeNardo DG, Ruffell B. Macrophages as regulators of tumour immunity and immunotherapy. Nat Rev Immunol. 2019;19(6):369-82.
306. Jiang LR, Zhang N, Chen ST, He J, Liu YH, Han YQ, et al. PD-1-Positive Tumor-Associated Macrophages Define Poor Clinical Outcomes in Patients With Muscle Invasive Bladder Cancer Through Potential CD68/PD-1 Complex Interactions. Front Oncol. 2021;11:679928.
307. Homicsko K, Zygoura P, Norkin M, Tissot S, Shakarishvili N, Popat S, et al. PD-1-expressing macrophages and CD8 T cells are independent predictors of clinical benefit from PD-1 inhibition in advanced mesothelioma. J Immunother Cancer. 2023;11(10).
308. Teramoto K, Igarashi T, Kataoka Y, Ishida M, Hanaoka J, Sumimoto H, et al. Prognostic impact of soluble PD-L1 derived from tumor-associated macrophages in non-small-cell lung cancer. Cancer Immunol Immunother. 2023;72(11):3755-64.
309. Coffelt SB, Wellenstein MD, de Visser KE. Neutrophils in cancer: neutral no more. Nat Rev Cancer. 2016;16(7):431-46.
310. Curiel TJ, Coukos G, Zou L, Alvarez X, Cheng P, Mottram P, et al. Specific recruitment of regulatory T cells in ovarian carcinoma fosters immune privilege and predicts reduced survival. Nat Med. 2004;10(9):942-9.
311. Niu N, Wang L. In vitro human cell line models to predict clinical response to anticancer drugs. Pharmacogenomics. 2015;16(3):273-85.

312. Van Zundert I, Fortuni B, Rocha S. From 2D to 3D Cancer Cell Models-The Enigmas of Drug Delivery Research. Nanomaterials (Basel). 2020;10(11).
313. Kilian KA, Bugarija B, Lahn BT, Mrksich M. Geometric cues for directing the differentiation of mesenchymal stem cells. Proc Natl Acad Sci U S A. 2010;107(11):4872-7.
314. Petersen OW, Ronnov-Jessen L, Howlett AR, Bissell MJ. Interaction with basement membrane serves to rapidly distinguish growth and differentiation pattern of normal and malignant human breast epithelial cells. Proc Natl Acad Sci U S A. 1992;89(19):9064-8.
315. Abbas ZN, Al-Saffar AZ, Jasim SM, Sulaiman GM. Comparative analysis between 2D and 3D colorectal cancer culture models for insights into cellular morphological and transcriptomic variations. Sci Rep. 2023;13(1):18380.
316. Zanoni M, Cortesi M, Zamagni A, Arienti C, Pignatta S, Tesei A. Modeling neoplastic disease with spheroids and organoids. J Hematol Oncol. 2020;13(1):97.
317. Gunti S, Hoke ATK, Vu KP, London NR, Jr. Organoid and Spheroid Tumor Models: Techniques and Applications. Cancers (Basel). 2021;13(4).
318. Zhao Z, Chen X, Dowbaj AM, Sljukic A, Bratlie K, Lin L, et al. Organoids. Nat Rev Methods Primers. 2022;2.
319. Drost J, Clevers H. Organoids in cancer research. Nat Rev Cancer. 2018;18(7):407-18.
320. Wang R, Mao Y, Wang W, Zhou X, Wang W, Gao S, et al. Systematic evaluation of colorectal cancer organoid system by single-cell RNA-Seq analysis. Genome Biol. 2022;23(1):106.
321. Zhao H, Yan C, Hu Y, Mu L, Huang K, Li Q, et al. Sphere-forming assay vs. organoid culture: Determining long-term stemness and the chemoresistant capacity of primary colorectal cancer cells. Int J Oncol. 2019;54(3):893-904.
322. Alotaibi AG, Li JV, Gooderham NJ. Tumour Necrosis Factor-Alpha (TNF-alpha)-Induced Metastatic Phenotype in Colorectal Cancer Epithelial Cells: Mechanistic Support for the Role of MicroRNA-21. Cancers (Basel). 2023;15(3).
323. Wei W, Wang J, Huang P, Gou S, Yu D, Zong L. Tumor necrosis factor-alpha induces proliferation and reduces apoptosis of colorectal cancer cells through STAT3 activation. Immunogenetics. 2023;75(2):161-9.
324. Zhao P, Zhang Z. TNF-alpha promotes colon cancer cell migration and invasion by upregulating TROP-2. Oncol Lett. 2018;15(3):3820-7.
325. Yip HYK, Papa A. Signaling Pathways in Cancer: Therapeutic Targets, Combinatorial Treatments, and New Developments. Cells. 2021;10(3).
326. Xu Y, Pasche B. TGF-beta signaling alterations and susceptibility to colorectal cancer. Hum Mol Genet. 2007;16 Spec No 1(SPEC):R14-20.
327. Yue B, Qiu S, Zhao S, Liu C, Zhang D, Yu F, et al. LncRNA-ATB mediated E-cadherin repression promotes the progression of colon cancer and predicts poor prognosis. J Gastroenterol Hepatol. 2016;31(3):595-603.
328. Xiong J, Liu Y, Jiang L, Zeng Y, Tang W. High expression of long non-coding RNA lncRNA-ATB is correlated with metastases and promotes cell migration and invasion in renal cell carcinoma. Jpn J Clin Oncol. 2016;46(4):378-84.
329. Flum M, Dicks S, Teng YH, Schrempp M, Nystrom A, Boerries M, et al. Canonical TGFbeta signaling induces collective invasion in colorectal carcinogenesis through a Snail1- and Zeb1-independent partial EMT. Oncogene. 2022;41(10):1492-506.

330. Liu ZW, Zhang YM, Zhang LY, Zhou T, Li YY, Zhou GC, et al. Duality of Interactions Between TGF-beta and TNF-alpha During Tumor Formation. Front Immunol. 2021;12:810286.
331. Hahn S, Nam MO, Noh JH, Lee DH, Han HW, Kim DH, et al. Organoid-based epithelial to mesenchymal transition (OEMT) model: from an intestinal fibrosis perspective. Sci Rep. 2017;7(1):2435.
332. Kitasato H, Noda M, Akahoshi T, Okamoto R, Koshino T, Murakami Y, et al. Activated Ras modifies the proliferative response of rheumatoid synovial cells to TNF-alpha and TGF-alpha. Inflamm Res. 2001;50(12):592-7.
333. Martino RB, Coelho AM, Kubrusly MS, Leitao R, Sampietre SN, Machado MC, et al. Pentoxifylline improves liver regeneration through down-regulation of TNF-alpha synthesis and TGF-beta1 gene expression. World J Gastrointest Surg. 2012;4(6):146-51.
334. Saile B, Matthes N, El Armouche H, Neubauer K, Ramadori G. The bcl, NFkappaB and p53/p21WAF1 systems are involved in spontaneous apoptosis and in the anti-apoptotic effect of TGF-beta or TNF-alpha on activated hepatic stellate cells. Eur J Cell Biol. 2001;80(8):554-61.
335. Takahashi E, Nagano O, Ishimoto T, Yae T, Suzuki Y, Shinoda T, et al. Tumor necrosis factor-alpha regulates transforming growth factor-beta-dependent epithelial-mesenchymal transition by promoting hyaluronan-CD44-moesin interaction. J Biol Chem. 2010;285(6):4060-73.
336. Lerrer S, Liubomirski Y, Bott A, Abnaof K, Oren N, Yousaf A, et al. Co-Inflammatory Roles of TGFbeta1 in the Presence of TNFalpha Drive a Pro-inflammatory Fate in Mesenchymal Stem Cells. Front Immunol. 2017;8:479.
337. Kobayashi T, Masaki T, Nozaki E, Sugiyama M, Nagashima F, Furuse J, et al. Microarray Analysis of Gene Expression at the Tumor Front of Colon Cancer. Anticancer Res. 2015;35(12):6577-81.
338. Montalto FI, De Amicis F. Cyclin D1 in Cancer: A Molecular Connection for Cell Cycle Control, Adhesion and Invasion in Tumor and Stroma. Cells. 2020;9(12).
339. Katt ME, Placone AL, Wong AD, Xu ZS, Searson PC. In Vitro Tumor Models: Advantages, Disadvantages, Variables, and Selecting the Right Platform. Front Bioeng Biotechnol. 2016;4:12.
340. Hulkower KI, Herber RL. Cell migration and invasion assays as tools for drug discovery. Pharmaceutics. 2011;3(1):107-24.
341. Wirtz D, Konstantopoulos K, Searson PC. The physics of cancer: the role of physical interactions and mechanical forces in metastasis. Nat Rev Cancer. 2011;11(7):512-22.
342. Koveitypour Z, Panahi F, Vakilian M, Peymani M, Seyed Forootan F, Nasr Esfahani MH, et al. Signaling pathways involved in colorectal cancer progression. Cell Biosci. 2019;9:97.
343. Kalliolias GD, Ivashkiv LB. TNF biology, pathogenic mechanisms and emerging therapeutic strategies. Nat Rev Rheumatol. 2016;12(1):49-62.
344. Mohd Salim NH, Mussa A, Ahmed N, Ahmad S, Yean Yean C, Hassan R, et al. The Immunosuppressive Effect of TNFR2 Expression in the Colorectal Cancer Microenvironment. Biomedicines. 2023;11(1).
345. Villalba M, Evans SR, Vidal-Vanaclocha F, Calvo A. Role of TGF-beta in metastatic colon cancer: it is finally time for targeted therapy. Cell Tissue Res. 2017;370(1):29-39.

346. Dai M, Al-Odaini AA, Fils-Aime N, Villatoro MA, Guo J, Arakelian A, et al. Cyclin D1 cooperates with p21 to regulate TGFbeta-mediated breast cancer cell migration and tumor local invasion. Breast Cancer Res. 2013;15(3):R49.
347. Jin Y, Cui Z, Li X, Jin X, Peng J. Correction: Upregulation of long non-coding RNA PlncRNA-1 promotes proliferation and induces epithelial-mesenchymal transition in prostate cancer. Oncotarget. 2019;10(50):5253.
348. Zhang C, Chen Z, Meng X, Li M, Zhang L, Huang A. The involvement and possible mechanism of pro-inflammatory tumor necrosis factor alpha (TNF-alpha) in thoracic ossification of the ligamentum flavum. PLoS One. 2017;12(6):e0178986.
349. Kriegel C, Amiji MM. Dual TNF-alpha/Cyclin D1 Gene Silencing With an Oral Polymeric Microparticle System as a Novel Strategy for the Treatment of Inflammatory Bowel Disease. Clin Transl Gastroenterol. 2011;2(3):e2.
350. Pease JC, Brewer M, Tirnauer JS. Spontaneous spheroid budding from monolayers: a potential contribution to ovarian cancer dissemination. Biol Open. 2012;1(7):622-8.
351. Chan DKH, Buczacki SJA. Tumour heterogeneity and evolutionary dynamics in colorectal cancer. Oncogenesis. 2021;10(7):53.
352. Chen CL, Yu X, James IO, Zhang HY, Yang J, Radulescu A, et al. Heparin-binding EGF-like growth factor protects intestinal stem cells from injury in a rat model of necrotizing enterocolitis. Lab Invest. 2012;92(3):331-44.
353. Rodriguez-Colman MJ, Schewe M, Meerlo M, Stigter E, Gerrits J, Pras-Raves M, et al. Interplay between metabolic identities in the intestinal crypt supports stem cell function. Nature. 2017;543(7645):424-7.
354. Serra D, Mayr U, Boni A, Lukonin I, Rempfler M, Challet Meylan L, et al. Self-organization and symmetry breaking in intestinal organoid development. Nature. 2019;569(7754):66-72.
355. Gonzalez DM, Medici D. Signaling mechanisms of the epithelial-mesenchymal transition. Sci Signal. 2014;7(344):re8.
356. Testa U, Pelosi E, Castelli G. Colorectal cancer: genetic abnormalities, tumor progression, tumor heterogeneity, clonal evolution and tumor-initiating cells. Med Sci (Basel). 2018;6(2).
357. Zeineddine FA, Zeineddine MA, Yousef A, Gu Y, Chowdhury S, Dasari A, et al. Survival improvement for patients with metastatic colorectal cancer over twenty years. NPJ Precis Oncol. 2023;7(1):16.
358. Sirin AH, Sokmen S, Unlu SM, Ellidokuz H, Sarioglu S. The prognostic value of tumor budding in patients who had surgery for rectal cancer with and without neoadjuvant therapy. Tech Coloproctol. 2019;23(4):333-42.
359. Haddad TS, Lugli A, Aherne S, Barresi V, Terris B, Bokhorst JM, et al. Improving tumor budding reporting in colorectal cancer: a Delphi consensus study. Virchows Arch. 2021;479(3):459-69.
360. Graham RP, Vierkant RA, Tillmans LS, Wang AH, Laird PW, Weisenberger DJ, et al. Tumor Budding in Colorectal Carcinoma: Confirmation of Prognostic Significance and Histologic Cutoff in a Population-based Cohort. Am J Surg Pathol. 2015;39(10):1340-6.
361. Meng M, Zhong K, Jiang T, Liu Z, Kwan HY, Su T. The current understanding on the impact of KRAS on colorectal cancer. Biomed Pharmacother. 2021;140:111717.

362. Sinicrope FA, Foster NR, Thibodeau SN, Marsoni S, Monges G, Labianca R, et al. DNA mismatch repair status and colon cancer recurrence and survival in clinical trials of 5-fluorouracil-based adjuvant therapy. J Natl Cancer Inst. 2011;103(11):863-75.
363. Lang-Schwarz C, Melcher B, Dregelies T, Norouzzadeh Z, Rund-Kuffner S, Lang-Schwarz K, et al. Adjuvant chemotherapy in stage II and III colon cancer: the role of the "budding and TILs-(tumor-infiltrating lymphocytes) combination" as tumor-host antagonists. Int J Colorectal Dis. 2021;36(8):1765-79.
364. Georges NDF, Oberli B, Rau TT, Galvan JA, Nagtegaal ID, Dawson H, et al. Tumour budding and CD8(+) T cells: 'attackers' and 'defenders' in rectal cancer with and without neoadjuvant chemoradiotherapy. Histopathology. 2021;78(7):1009-18.
365. Markowski AR, Markowska AJ, Ustymowicz W, Pryczynicz A, Guzinska-Ustymowicz K. Simultaneous analysis of tumor-infiltrating immune cells density, tumor budding status, and presence of lymphoid follicles in CRC tissue. Sci Rep. 2022;12(1):21732.
366. Jiang Z, Xu Y, Cai S. CXCL10 expression and prognostic significance in stage II and III colorectal cancer. Mol Biol Rep. 2010;37(6):3029-36.
367. Wu Z, Huang X, Han X, Li Z, Zhu Q, Yan J, et al. The chemokine CXCL9 expression is associated with better prognosis for colorectal carcinoma patients. Biomed Pharmacother. 2016;78:8-13.
368. Li YJ, Zhang C, Martincuks A, Herrmann A, Yu H. STAT proteins in cancer: orchestration of metabolism. Nat Rev Cancer. 2023;23(3):115-34.
369. Heichler C, Scheibe K, Schmied A, Geppert CI, Schmid B, Wirtz S, et al. STAT3 activation through IL-6/IL-11 in cancer-associated fibroblasts promotes colorectal tumour development and correlates with poor prognosis. Gut. 2020;69(7):1269-82.
370. Bhat AA, Nisar S, Singh M, Ashraf B, Masoodi T, Prasad CP, et al. Cytokine- and chemokine-induced inflammatory colorectal tumor microenvironment: Emerging avenue for targeted therapy. Cancer Commun (Lond). 2022;42(8):689-715.
371. Waldner MJ, Foersch S, Neurath MF. Interleukin-6--a key regulator of colorectal cancer development. Int J Biol Sci. 2012;8(9):1248-53.
372. Jedinak A, Dudhgaonkar S, Sliva D. Activated macrophages induce metastatic behavior of colon cancer cells. Immunobiology. 2010;215(3):242-9.
373. Beyranvand Nejad E, Labrie C, van Elsas MJ, Kleinovink JW, Mittrucker HW, Franken K, et al. IL-6 signaling in macrophages is required for immunotherapy-driven regression of tumors. J Immunother Cancer. 2021;9(4).
374. Yin Y, Liu B, Cao Y, Yao S, Liu Y, Jin G, et al. Colorectal Cancer-Derived Small Extracellular Vesicles Promote Tumor Immune Evasion by Upregulating PD-L1 Expression in Tumor-Associated Macrophages. Adv Sci (Weinh). 2022;9(9):2102620.
375. Pampaloni F, Reynaud EG, Stelzer EH. The third dimension bridges the gap between cell culture and live tissue. Nat Rev Mol Cell Biol. 2007;8(10):839-45.
376. Jiang Z, Xu Y, Fu M, Zhu D, Li N, Yang G. Genetically modified cell spheroids for tissue engineering and regenerative medicine. J Control Release. 2023;354:588-605.
377. Chira S, Nutu A, Isacescu E, Bica C, Pop L, Ciocan C, et al. Genome Editing Approaches with CRISPR/Cas9 for Cancer Treatment: Critical Appraisal of Preclinical and Clinical Utility, Challenges, and Future Research. Cells. 2022;11(18).